Fall 10-25-2018

Optical Wireless Data Center Networks

Abdelbaset S. Hamza
University of Nebraska - Lincoln, ahamza@huskers.unl.edu

OPTICAL WIRELESS DATA CENTER NETWORKS

by

Abdelbaset S. Hamza

A DISSERTATION

Presented to the Faculty of

The Graduate College at the University of Nebraska

In Partial Fulfillment of Requirements

For the Degree of Doctoral of Philosophy

Major: Engineering

Under the Supervision of Professors Jitender S. Deogun and Dennis R. Alexander

Lincoln, Nebraska

December, 2018

OPTICAL WIRELESS DATA CENTER NETWORKS

Abdelbaset S. Hamza, Ph.D.

University of Nebraska, 2018

Advisors: Jitender S. Deogun and Dennis R. Alexander

Bandwidth and computation-intensive Big Data applications in disciplines like social media, bio- and nano-informatics, Internet-of-Things (IoT), and real-time analytics, are pushing existing access and core (backbone) networks as well as Data Center Networks (DCNs) to their limits. Next generation DCNs must support continuously increasing network traffic while satisfying minimum performance requirements of latency, reliability, flexibility and scalability. Therefore, a larger number of cables (i.e., copper-cables and fiber optics) may be required in conventional wired DCNs. In addition to limiting the possible topologies, large number of cables may result into design and development problems related to wire ducting and maintenance, heat dissipation, and power consumption.

To address the cabling complexity in wired DCNs, we propose OWCells, a class of optical wireless cellular data center network architectures in which fixed line of sight (LOS) optical wireless communication (OWC) links are used to connect the racks arranged in regular polygonal topologies. We present the OWCell DCN architecture, develop its theoretical underpinnings, and investigate routing protocols and OWC transceiver design. To realize a fully wireless DCN, servers in racks must also be connected using OWC links. There is, however, a difficulty of connecting multiple adjacent network components, such as servers in a rack, using point-to-point LOS links. To overcome this problem, we propose and validate the feasibility of an FSO-Bus to connect multiple adjacent network components using NLOS point-to-point

OWC links.

To complete the design of the OWC transceiver, we develop a new class of strictly and rearrangeably non-blocking multicast optical switches in which multicast is performed efficiently at the physical optical (lower) layer rather than upper layers (e.g., application layer).

I dedicate this to my parents, five brothers, and my wife.

Acknowledgements

First and foremost, I would like to thank my parents for their endless support, love, and sincere prayers. Without their love and support, this dissertation would not have been completed. I heartily thank Mohammed, Haitham, Kamal, Faisal, and Abdelrahman for their love and support. They are not only great brothers, but also my true friends.

Special thanks to my advisors Prof. Jitender Deogun and Prof. Dennis Alexander. Their keen insights, support, patience, and the strong belief in my capability played a key role in building this work.

I would like to thank Prof. Lily Wang and Prof. Lisong Xu for serving on my Ph.D. committee.

Special thanks to Prof. Jerry L. Hudgins and Prof. Sohrab Asgarpoor for offering me the exciting opportunity of teaching the ELEC 370/CSCE 335 and ELEC 211 courses. This experience was crucial for shaping my teaching skills and philosophy.

I would like to thank my dear and best friends Ahmed Abdelraheem and Beligh Ben Taleb for their continuous support. They taught me the true meaning of friendship.

Finally, I would like to convey my appreciation to the Makkawy's for their support during my stay in Lincoln. Special thanks to Karim Makkawy, Amin Makkawy, and Hatem Kittana.

Contents

List of Figures

List of Tables

Chapter 1

Introduction

Big Data is a term used to describe high volume, high velocity, and/or high variety data sets [17]. Big Data applications can be found in disciplines like, Internet-of-Things (IoT) [18], Bioinformatics [19], Social media [20], and Nanoinformatics [21]. For example, it is expected that the Large Synoptic Survey Telescope (LSST), which will be deployed in Chile in 2016, will acquire around 10 Gbps for ten years resulting in a final disk storage and database size of 400 Exabytes and 15 Petabytes, respectively [22]. According to the International Data Corporation (IDC), the IoT market is expected to grow from 9.1 billion devices and objects connected to the Internet in 2013 to 28.1 billion by 2020 [23]. As the portfolio of bandwidth and computation intensive Big Data applications continues to grow, so does the demand for efficient *Data Centers (DCs)* that support 100,000 servers and beyond [24].

A *DC Network (DCN)* is the networking infrastructure that provides the intra- and inter-DC networking services. It is, therefore, essential to design an efficient high-speed/high-bandwidth DCN to meet the high computing and communication demands in DC. The design of a DCN must also satisfy several requirements such as scalability, low latency, availability, and cost effectiveness. Other practical con-

cerns, including cabling complexity, power consumption, and cooling, must also be considered in the design [9, 25].

The design space of DCNs is witnessing an accelerated evolution vis-à-vis academia and industry are advancing new technologies for DCNs as the portfolio of bandwidth and computation-intensive Big Data applications continues to expand. Thus, the design and development of highly efficient high-speed/high-bandwidth DCNs is critical to maximize total aggregated computing and communication capacities of future DCs. For the rest of this chapter, we use Figure 1.1 to pictorially depict our understanding of how the design space of DCNs is reshaping. Each box in Figure 1.1 represents a design philosophy. Links between boxes represent the challenges faced by each design and the arrow points to the proposed solution.

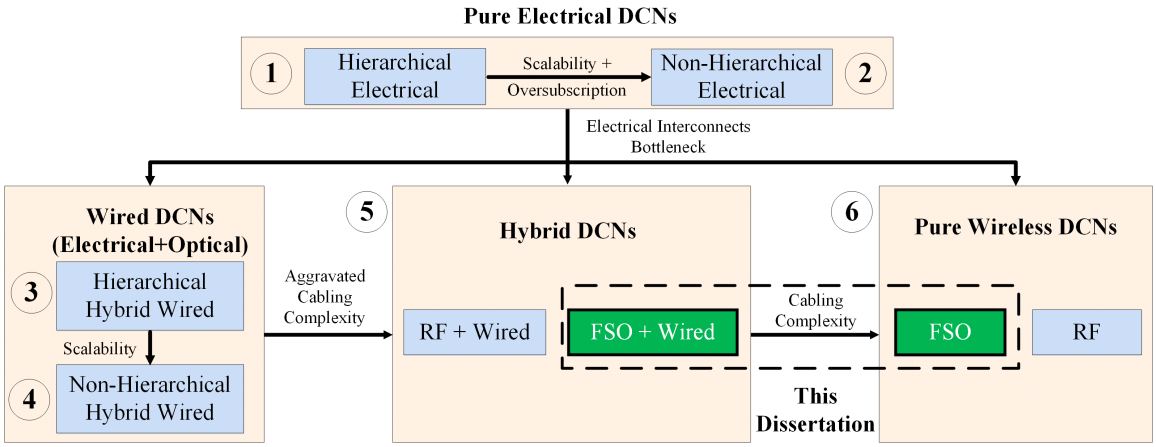

Figure 1.1: DCN design space roadmap.

In a widely used conventional hierarchical *tree-based DCN* architecture, servers are stacked in racks that are arranged in rows. A Top-of-Rack (ToR) switch is used to perform intra- and inter-rack communications [see Figure 1.2]. A gateway router is used to connect the front end of the content and load balancing switches with the internet. At the back end, the content and load balancing switches are connected to servers using two (core-ToR) or three (core-aggregate-ToR) layers of switches.

Electrical cables are mostly used for intra- and inter-rack communication links [Box 1 in Fig. 1.1]. As we move up in the tree, more powerful links and switches must be used with over-subscription factors of 1:2 or more at higher levels in the tree. High oversubscription ratios, however, adversely impact inter-rack communications [26].

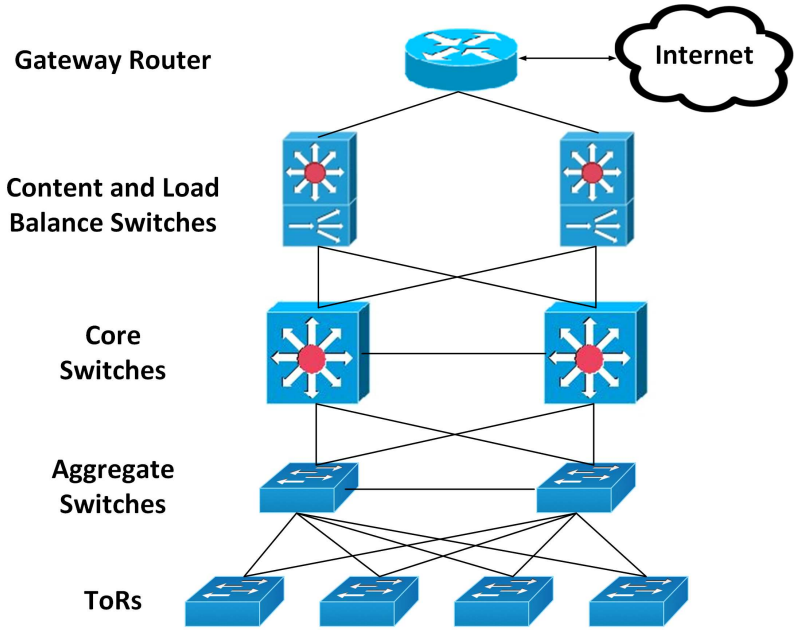

Figure 1.2: Conventional hierarchical tree-based DCN architecture.

Analysis of real world DC traffic statistics shows that some applications do have unpredictable traffic patterns and unbalanced traffic distributions [27–32] that can lead to temporary ***hotspots***. It is difficult for hierarchical DCN architectures to support or adapt to unpredictable changes in traffic patterns. Therefor, the performance of the network may degrade due to inadequate network capacity and flow congestions [31, 32]. Current trends in high-speed/high-bandwidth DC applications show that the hotspot problem is likely to worsen in the future [6, 33, 34]. Moreover, hierarchical DCN architecture may have low scalability and performance [35–39], and may also require expensive switches for supporting large number of servers [29].

To appease the oversubscription problem encountered by hierarchical DCNs, re-

searchers improved existing hierarchical topologies (e.g., Fat-Tree [40], VL_2 [41], and PortLand [42]), and developed new non-hierarchical, mostly recursive, topologies (e.g., BCube [35], DCell [36], FiConn [39], DPillar [37], and BCN [38]). In non-hierarchical DCNs [Box 2 in Fig. 1.1], large number of links and switches with variants of multipath routing are used such that the core of the network is not over-subscribed [27]. At any point in the network, full bisection bandwidth is available to forward all incoming traffic. Non-hierarchical DCN architectures demonstrate better scalability and fault tolerance attributes as compared to the conventional hierarchical architectures [27], however, the performance improvement is achieved at the cost of larger number of wires leading to increased ***cabling complexity*** problems (e.g., cable management, maintenance, and heat dissipation).

Electrical interconnects used by most existing DCNs (hierarchical/non-hierarchical are increasingly becoming a bottleneck as optical-electrical-optical (O-E-O) conversion is required at every port. Moreover, recent real world DC traffic traces show that more than 95% of the data are being transferred by the top 10% largest flows. Thus, interconnects that can support elephant flows (i.e., flows with large amount of data) may be more favorable than guaranteeing full bisection bandwidth between large number of pairs of servers across the DCN. This in turn has motivated researchers to investigate the use of optical interconnects in DCNs [18, 19, 21-28], especially for transferring the elephant flows.

Another approach to tackle the hotspot problem is to realize a "flexible" network to establish on-demand links between nodes that are susceptible to the hotspot problem. The on-demand links can be based on a wired [Box 3 and 4 in Fig. 1.1] or a wireless [Box 5 in Fig. 1.1] technology. In case of wired technologies, commodity switches are deployed to connect a subset of nodes and provide on-demand wired links when needed. The advantage of the wired solution is that the flexible wired

network realized is consistent with the original DCN especially that most DCNs deployed today can be classified as wired DCNs that use copper-cables and fiber optics for communication. For the wired flexible network to operate efficiently, the network must interconnect the nodes that are susceptible to the hotspot problem. However, prediction of such nodes is a difficult problem. Thus, a wired solution may not be able to provide the required flexibility. Moreover, a wired flexible network requires the deployment of a larger number of cables escalating problems related to cabling complexity.

The potential capability of establishing flexible on-demand wireless links have motivated the researchers to investigate wireless communication as a possible solution for hotspot and cabling-complexity problems, simultaneously. A wireless technology can be used either to augment a wired DCN; leading to hybrid DCN [Box 5 in Fig. 1.1] or to develop a pure wireless DCN [Box 6 in Fig. 1.1]. There are two candidate wireless technologies, radio frequency (RF) and optical wireless communication (OWC), also known as free space optics (FSO). The difference between the two terms will be explained in detail in Chapter 2. For the sake of brevity, we use the terms OWC and FSO interchangeably in this dissertation. In case of RF, researchers focus on 60 GHz RF technology since it stands out from other RF technologies due to its short range and high bandwidth. In FSO communication, a modulated light beam propagates in free space with no fibers involved. Therefore, FSO combines the flexibility of wireless communication and the high-speed/high-bandwidth of the optical communication.

Ramachandran et al. propagated the idea of using 60 GHz RF technology in DCN design [4]. Following their work, considerable research has been devoted to investigating the feasibility of deploying 60 GHz RF technology in DCNs [6, 43–49]. Although promising, 60 GHz technology has its limitations as it has lower practical bandwidth, and suffers from high attenuation and propagation loss [4,9,50]. Radiation

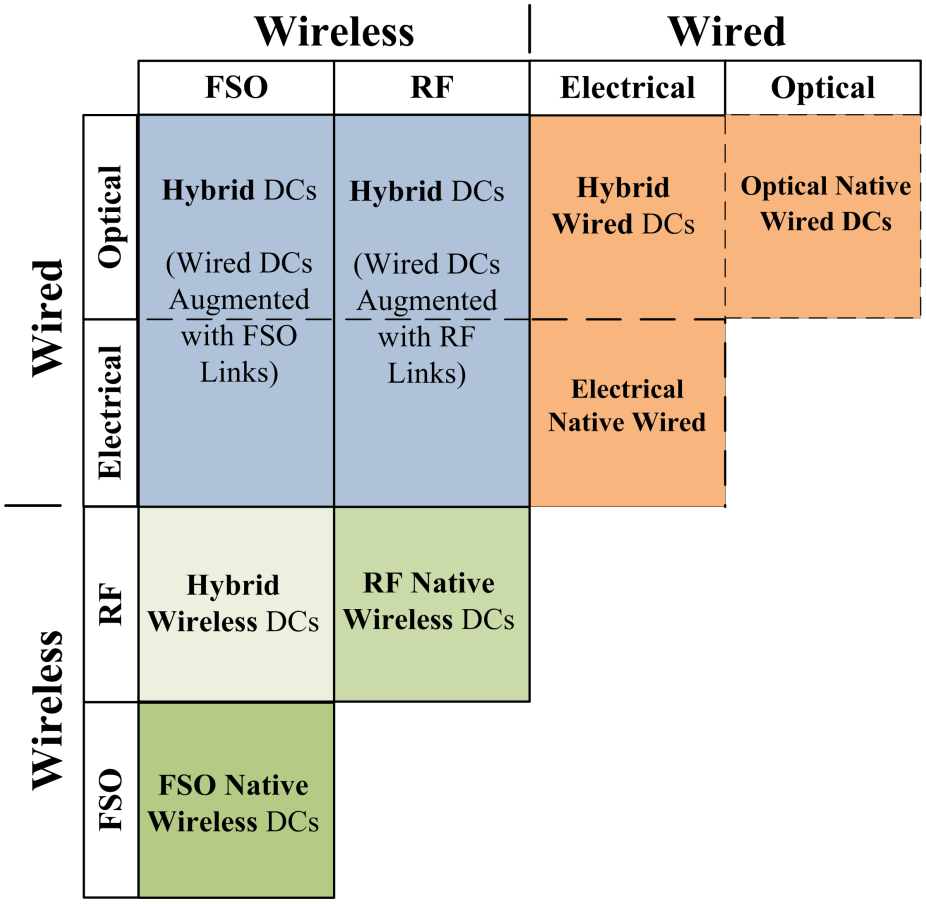

Figure 1.3: DCN design space.

patterns of 60 GHz impose additional restrictions on the activity of wireless modules in close proximity because of interference. This increases the complexity of routing and network management, and reduces the throughput [6].

Recent advances in FSO/OWC technology have narrowed the gap between FSO and RF technologies to the point that FSO is now seen as a complement technology for RF in next-generation communication systems, such as 5G wireless networks. RF technology can offer high data rates when high carrier frequencies are used, however, RF propagation becomes more LOS dependent. Thus, key features of RF technologies, such as, mobility, coverage, and receiver sensitivity, become unclear [51]. Both 60 GHz and FSO technologies are comparable as they operate in an unregulated, yet

standardized band of the spectrum. Moreover, both technologies have short range and potentially low cost making them strong candidates for networking in DCNs. In case of FSO, the very high carrier frequency and the relatively large detector area provide spatial diversity that averts multipath fading. On the other hand, RF links experience signal magnitude and phase fluctuations. Therefore, the design of FSO links can be simpler than that of RF [1].

The advantages of FSO technology and its successful deployment in a wide range of applications has motivated researchers to investigate the use of FSO in the design of DCNs [9, 11, 50, 52]. Examples of applications in which FSO has already found its place are, mobile networks backhaul, space communications, and underwater sensing. The notable increasing use of FSO technology in different applications is due to the advantages presented by FSO technology, such as, high data rate, low interference, and high speed of light that is approximately 1.5 times faster than that of fiber optics, which mean less latency.

Figure 1.1 is an evident that DCN design space is reshaping and there is a current need to rethink the design philosophy of DCNs [52, 53]. There are four technologies that can be used for communication in DCNs, wired electrical cables, wired optical fiber, wireless RF technology, and wireless FSO technology. Figure 1.3 depicts the resulting DCN design space. Each of these four technologies can be used individually, leading to a pure (electrical/optical/RF/FSO) DCN. On the other hand, different technologies can be integrated leading to wired (electrical + optical), wireless (FSO + RF), or a hybrid DCN; (FSO + wired) or (RF + wired).

Since the deployment of 60 GHz and FSO technologies in DCNs has not yet been fully investigated, we focus our research on *pure FSO*, and *hybrid (FSO + wired) DCN designs*. It is not yet known which of these two types of DCNs provides a better solution. In this dissertation, we address the problem of cabling complexity in wired

DCNs. To this end, we propose OWCells, a class of optical wireless cellular data center network architectures in which fixed line of sight (LOS) optical wireless communication (OWC) links are used to connect the racks arranged in *regular polygonal topologies*. We present the OWCell DCN architecture, develop its theoretical underpinnings, and investigate routing protocols and OWC transceiver design. To realize a fully wireless DCN, servers in racks must also be connected using OWC links. There is, however, a difficulty of connecting multiple adjacent network components, such as servers in a rack, using point-to-point LOS links. To overcome this problem, we propose and validate the feasibility of an FSO-Bus to connect multiple adjacent network components using NLOS point-to-point OWC links.

In DCNs, a rack requires a combination of local (intra-rack) and remote (inter-rack) data access to complete a task. Therefore, applications hosted by DCNs generate large demands for bandwidth with different communication patterns involving a combination of unicast, multicast, in-cast, and all-to-all-cast traffics [24, 54].

For example, Hadoop is one of the widely used implementations of MapReduce [55], which is a distributed processing framework for large datasets. Distributed systems use data replication to offer scalability and availability of data. For example, a file written to Hadoop Distributed File System (HDFS) is split into smaller data blocks that have configurable size. To ensure availability and scalability, Hadoop randomly distributes three replicas of each data block among distinct nodes housed in different servers, in the network [56], two of which are on the same rack to reduce inter-rack communication. Therefore, Hadoop requires in-cast traffic delivery during the shuffle stage of MapReduce, and requires multicast for data replication, parallel database join operation, as well as data dissemination in virtual machine (VM) provisioning [54]. As part of the design of the OWC transceiver, we develop a new class of strictly and rearrangeably non-blocking multicast optical switches in which multicast

is performed efficiently at the physical optical (lower) layer rather than upper layers (e.g., application layer).

The main contributions of this dissertation are as following.

1. We present a multi-level classification for FSO technology applications in four different communication environments, namely: *indoor*, *atmospheric*, *space*, and *underwater*. To the best of our knowledge, there exists no classification/survey that addresses the variety of the FSO technology applications in all four environments.

2. We propose a classification that can be used to classify existing and emerging wired and wireless DCNs. The proposed classification leads to a nearly complete picture of the design space for DCNs. This help us to identify potential unexplored solutions for next-generation DCNs.

3. We present, *OWC-Bus*, a communication scheme used to connect multiple adjacent network components using OWC links..

4. We develop, OWCells, a family of cellular optical wireless DCN architectures. OWCells utilize line-of-sight (LOS) OWC links to connect racks that are arranged in regular polygonal shapes.

5. We propose a new class of strictly non-blocking (SNB) and rearrangeably non-blocking (RNB) FSO multicast switches that utilizes *tri-state switching elements (T-SEs)* and is optimal with respect to hardware complexity.

1.1 Dissertation Outline

In this section, we give an outline of the dissertation organization.

In Chapter 2, we present a classification scheme for FSO technology and use the classification to review both; the research and standardization literature of the FSO technology. In Chapter 3, we propose a classification that can be used to classify any DC, including existing wired and emerging wireless DCs. We use the classification to review and highlight the challenges faced by DCNs in the literature which motivates to our work. In Chapter 4, we present an OWC-DC that is based on OWC-Bus.

Although the design proposed in Chapter 4 present a useful design for OWC rack of servers, the conventional row-based DCN arrangement forms a great impairment for wireless connectivity in DCNs. We dedicate Chapter 5 to discuss the proposed cellular optical wireless DCN architectures, OWCells, that can overcome the problems encountered by conventional row-based DCNs.

In Chapters 6 and Chapter 7, we propose a new class of strictly non-blocking (SNB) and rearrangeable non-blocking (RNB) FSO multicast switches using tri-state switching elements (T-SEs).

Finally, Conclusions and Future Research directions are presented in Chapter 12.

Chapter 2

Optical Wireless Communication (OWC) Technology

Free Space Optical (FSO) communication technology, also known as *Optical Wireless Communications (OWC)*, has regained a great interest over the last few years. In some cases, FSO is seen as an alternative to existing technologies, such as radio frequency. In other cases, FSO is considered as a strong candidate to complement and integrate with next-generation technologies, such as 5G wireless networks. Accordingly, FSO technology is being widely deployed in various indoor (e.g., data centers), terrestrial (e.g., mobile networks), space (e.g., inter-satellite and deep space communication), and underwater systems (e.g., underwater sensing). As the application portfolio of FSO technology grows, so does the need for a clear classification for FSO link configurations. Most existing surveys and classifications are single-level classifications, and thus not inclusive enough to accommodate recent and emerging changes and developments of different FSO link configurations and systems. In this chapter, we propose a multi-level classification framework to classify existing and future indoor, terrestrial, space, underwater, and heterogenous FSO links and systems using

common and simple unified notation. We use the proposed classification to review and summarize major experimental work and systems in the area until 2017. Using the proposed classification and survey, we aim to give researchers a jump-start to tap into the growing and expanding realm of the FSO technology in different environments. The proposed classification can also help organize and systematically present the progress in the research on FSO technology. This makes the identification of the market needs for standards an easier task. Moreover, different entities involved in the standardization process including academic, industry, and regulatory organizations can use the proposed classification as a unified language to communicate during the early stages of standard development which require ambiguity-free discussions and exchange of ideas between different standardization entities. We use the proposed classification to review existing standards and recommendations in the field of FSO. It is also envisioned that the proposed classification can be used as a unified framework to define different FSO channel models for simulation tools.

2.1 Introduction

Emerging Big Data applications and systems found in disciplines like social media and Internet-of-Things (IoT), are characterized by being bandwidth-intensive and performance-sensitive. The IoT market is expected to grow from 9.1 billion devices and objects connected to the Internet in 2013 to 28.1 billion by 2020 [23], that is more than three times the global population expected by 2020. As such applications and systems rapidly move closer to end users, wireless communication systems, are the favored communication technologies as they allow for user mobility. Moreover, wireless technologies avoid most of the inherent complexity that wired technologies suffer from, such as, long setup time, right of the way for digging, and the sunk cost

once the cables are laid [57]. It is expected that two-thirds of total IP traffic by 2020 will be generated by wireless and mobile devices [58].

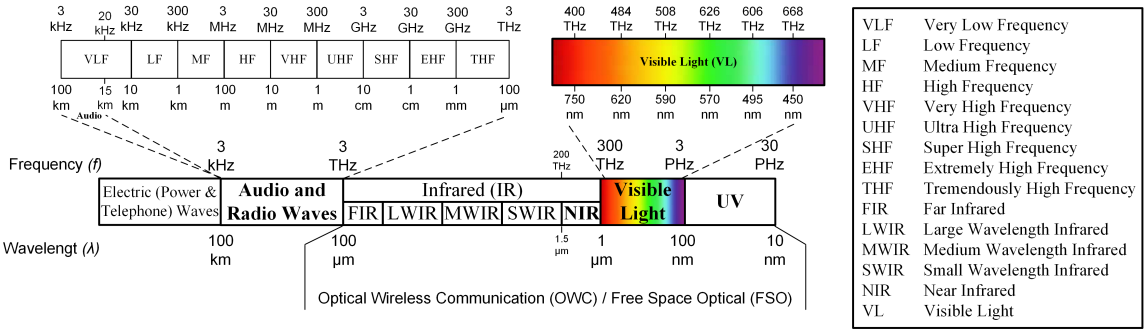

Figure 2.1: Part of the electromagnetic (EM) spectrum showing the frequency (and wavelength) ranges for each band.

Figure 2.1 depicts part of the electromagnetic (EM) spectrum and the frequency (and wavelength) ranges for each band of the spectrum. As the frequency increases, the wavelength and effective area of an antenna decrease. The carrier frequency is selected based on the application. For example, ground-to-submarine communications utilize audio waves due to its very long wavelengths (i.e., very low frequency and very large antenna) and the limited propagation capability of RF signals in electrical conductors such as salt water due to absorption. On the other hand, radio frequencies in the Ultra High Frequency (UHF) and Super High Frequency (SHF) band range are capable of penetrating windows, walls, and ceils. Therefore, the IEEE 802.11b/g/n (WiFi) networks utilize the unlicensed 2.4 GHz UHF and 5 GHz SHF radio bands.

RF is a mature technology and is being widely deployed in many indoor, terrestrial, and space communication systems. However, the propagation nature of the RF communication systems raises a problem of interference, which in turn affects the usability of frequencies, and hence, the capacity. Therefore, the RF spectrum is regulated by the local and international authorities to limit the interference, and guarantee proper operation and coexistence of systems relying on RF. As the appli-

cations of RF communication are progressively increasing, the RF spectrum becomes more congested, scarce and thus expensive to acquire. Several efforts are put from research and industry to stretch the capability of existing wireless technologies (e.g., alleviating interference) and to develop new ones to fulfill the emerging needs [59,60].

Free Space Optical (FSO) communication, also known as *Optical Wireless Communication (OWC)* as discussed later in Section 2.2.1, is being extensively investigated over the last few decades as an attractive alternative technology to RF. Similar to fiber optics, data are used to modulate a light beam in FSO. The light beam then propagates from one point to another, however, in a wireless manner. The recent spike in interest in FSO technology stems from the fact that FSO combines high-bandwidth of optical communication systems and the flexibility of wireless technologies.

FSO technology operates in a broad spectrum (see Figure 2.1) including Near Infrared (NIR), Visible Light (VL), and Ultraviolet (UV) bands. Conventionally, terrestrial and space FSO links operate in the NIR band similar to fibre-optic systems [61]. As will be shown in subsequent sections, terrestrial systems can also operate in the VL [62] and UV [63] bands. On the other hand, Indoor FSO links commonly operate in the NIR [64] and VL [65] bands, whereas, underwater OWC systems operate in the NIR [66] and VL [67] bands. The extremely short wavelengths (i.e., high frequencies) at which FSO systems operate make FSO detectors immune to multipath fading (i.e., large fluctuations in received signal magnitude and phase) as opposed to RF links, which are highly susceptible to multipath fading. This can be attributed to the spatial diversity resulting from the fact that FSO detector areas are extremely large compared to the wavelengths [1]. In addition to the unregulated spectrum, most of the optical components used in FSO links are cheaper, smaller, lighter and have lower power consumption as compared to that of RF components leading to cost and energy saving [3, 68–71]. Although most of the FSO components

are cheaper, lighter, and smaller than that of RF links, one must keep in mind that FSO networking solutions are not as mature and commercially available as their RF counterpart. We believe that this is a main contributor to the fact that FSO commercial solutions can be sometimes more expensive and bulkier especially in the case of terrestrial FSO links [72]. As the technology becomes more popular and with the expected increase in the market competition, the price of FSO solutions is expected to drop. On the other hand, as the technology matures, designer of FSO solutions will be able to develop the best design practices which will influence the size of the modules used in the FSO systems.

FSO technology has also been considered as a complementary technology to existing RF systems since FSO and RFs do not interfere [2]. This property is very important for applications in which interference with RF systems must be avoided such as in hospitals and in personal entertainment systems on commercial aircrafts to mitigate the interference with the RF-sensitive navigation and avionics electronic systems [73]. Moreover, the next generations of wireless communication systems (e.g., 5G) incorporate several complementary access technologies along with the RF technology, including FSO [74, 75].

A preliminary optical communication experiment was among the secondary objectives of the mission Gemini 7 conducted by NASA in 1965 [76]. The experiment was only partially completed due to the cloud obscuration and the spacecraft altitude restrictions [77]. Three years later, Erhard Kube published the original FSO communications white paper "*Information transmission by light beams through the atmosphere*" [78]. In this chapter, E. Kube explained the possibility of transmitting data through the atmosphere using green (0.6 μm) and red (0.8 μm) laser sources. Continued development of lasers led to the development of a small and continuous-beam semiconductor light sources that work at room temperature by Zhores Alferov

in 1970. This invention opened new horizons for the development of OWC systems. In 1979, Gfeller and Bapst introduced the first indoor OWC system in which the diffuse emissions in the infrared (IR) band were used [79]. The continued research and development by academic institutions, industry and military organizations, enabled the FSO communication to find its place in many applications, such as, mobile networks backhaul [80,81], space communication [82], underwater (UW) sensing [83,84], wireless sensor networks (WSNs) [63], indoor local area networks [85,86], data center networks (DCNs) [64] and many other applications.

2.1.1 Motivation and Contribution

Advantages of the FSO technology have been known for a long time. However, utilization of these advantages was facilitated by recent development and advances in FSO enabling technologies. As a result, a large number of research papers on new FSO applications has been published recently. Given that most of the FSO technology classification efforts were made in the late 90s, we believe that existing classifications of FSO technologies are outdated [1,2,87].

Most of the old classification efforts simply review and differentiate FSO systems without taking into consideration development of new/future FSO links. Therefore, it may be difficult, if not impossible, to fit some of the emerging and future configuration classes into existing *single-level* classification schemes. Accordingly, many survey papers have to introduce additional classes, which makes the overall classification scheme inconsistent and nonsystematic in its expansion. For an example, consider the quasi (multi-spot) diffuse system [88, 89] propagated as a sperate class despite its similarities to diffuse systems [1, 73, 90, 91]. Furthermore, a large number of new developments in FSO result in several inconsistencies, and sometimes, contradictions between various classifications and definitions such as in their naming conventions

or operational principles. For example, the three notations *LOS/Directed*, *LOS*, and *Point-to-Point* all refer to the same FSO link configuration [1, 2, 73, 87, 90–95].

We believe that there is a need for a classification that can express the existing, emerging, and future FSO link configurations and applications in a systematic way. Accordingly, in this chapter, we have the following three major objectives.

- Develop a rigorous multi-level classification based on a set of notation that can be systematically used to express various present and emerging FSO link configurations to help reduce ambiguity. To show the effectiveness of the proposed classification, we use it to classify different link configurations listed in various existing classifications. We also use the proposed classification to classify FSO link configurations that could not be classified before. Furthermore, we show how the proposed classification can evolve to include any future FSO link configurations.

- Survey FSO technology applications in different communication environments, namely: *indoor*, *atmospheric*, *space*, *underwater*, and *heterogenous*. To the best of our knowledge, there exists no classification/survey that addresses the variety of the FSO technology applications in all environments. For each environment type, we summarize recent research efforts and provide a list of selected references for applications on each link configuration. We also discuss the typical impairments encountered by each link configuration and possible solutions for these impairments. Finally, we classify and review existing standards and recommendations for FSO technology in each environment.

- Put the proposed classification into action and use it to describe different existing FSO systems. We review *heterogenous FSO systems* in which different types of FSO links are combined to realize an efficient system. We also review *hybrid*

FSO systems in which FSO is combined with a different technology (e.g., RF). In addition to classifying FSO systems, we envision that the unified framework presented here can also be used to develop modular and consistent FSO channel models for FSO simulation tools.

It should be noted that the development of FSO in each of the four environments (or a subfield thereof) represents a broad research area in its own right. Thus developing a single comprehensive survey to cover all the developments, impairments, and solutions in detail is infeasible. That being said, in this chapter, we aim to give researchers a jump-start to tap into the growing and expanding realm of the FSO technology in different environments. To this end, we present a novel classification scheme for FSO links. To demonstrate the effectiveness of the proposed classification, we bring recent advances in all fields of FSO in a single place saving researchers the time and effort to capture the big picture. Therefore, our contribution is a comprehensive breadth-focused survey and we acknowledge that, focused and dedicated survey papers based on our proposed classification may be needed to cover a particular domain in detail in the future.

2.1.2 Chapter Organization

The remainder of this chapter is organized as follows. In Section 2.2, we discuss the generic FSO link components, including light sources, photodetectors, and modulation schemes. We dedicate Section 2.3 to discuss related work. In Section 2.4, the proposed classification of *FSO link configurations* is presented and various schemes are explained. Sections 2.5 - 2.9 demonstrate the use of the proposed classification scheme to classify FSO applications and related standards/recommendations in indoor, terrestrial, space, underwater, and heterogenous environments, respectively. We then use the proposed classification to review different FSO systems in Section 2.10.

Research directions and open problems for FSO systems are discussed in Section 8.1.1. Summary is given in Section 2.11.

2.2 Preliminaries and Basic Concepts

In this section, we discuss preliminaries and basic concepts related to optical wireless communication. We discuss the naming convention of the optical wireless technology since it has been observed that researchers use different names to refer to the optical wireless technology in the literature. We also briefly discuss the preliminaries and basic components of a generic FSO link, such as light sources, photodetectors, and modulation schemes. The details of the components used in optical communication systems and the advances in the research related to these components are, however, beyond the scope of this chapter. Interested readers can refer to the papers and books discussing the theory of operation, variations and advancement of different types of light sources and photodetectors [96–104]. Discussion on eye safety and existing regulations can be found in [105–108]. Moreover, excellent summaries and taxonomy of modulation schemes in OWC are available in [51, 81, 90].

2.2.1 Naming Convention - FSO vis-à-vis OWC

Optical wireless and fiber-optic communication systems operate in the same band of the spectrum and have similar transmission bandwidth capabilities, therefore, optical wireless communication is used to be referred to as *fiber-less optics*. As the fiber-less optics technology continued to advance and used in new domains, new names for the technology emerged in the literature, such as; *Lasercom*, *Optical Wireless Communication (OWC)*, and *Free Space Optics (FSO)*. Over the last few decades, the notations "OWC" and "FSO" became widely used whereas "fiber-less optics" and

"lasercom" are considered archaic [109].

It has been noticed that the term OWC is used in the literature to refer to indoor and outdoor fiber-less optical systems, whereas, the term FSO is mostly used to refer to outdoor fiber-less optical systems. In a recent classification and survey [3], Kaushal and Kaddoum use the notation OWC to refer to the fiber-less optics technology. The authors then classify OWC technology into Indoor Systems and Outdoor Systems (FSO). The FSO system is further classified into Terrestrial Links and Space Links. The use of FSO to refer to outdoor links is because the technology utilizes an unguided channel in both the terrestrial atmosphere and the vacuum (outer space). However, this is also true for indoor and underwater environments where the fiber-less optical systems are utilizing unguided channels. This led many researchers to refer to the fiber-less optical systems using the notation FSO in indoor [71, 110] and underwater [111–113] environments.

Since FSO and OWC refer to the fiber-less communication with unconfined medium disregard the environment in which the link is established, and taking into consideration the fact that both terms have been widely used in the literature, we use both terms interchangeably in this chapter to refer to the *fiber-less technology* in *any environment*. It is found that the OWC in the underwater (UW) environment is widely referred to as Underwater Optical Wireless Communication (UOWC). Therefore, for research related to UW OWC, we use the term UOWC to maintain the consistency with the literature.

2.2.2 Light Sources

The most commonly used light sources in FSO systems are *Laser Diodes (LDs)* and *Light Emitting Diodes (LEDs)*. LDs are preferred in applications with high data rate requirements due to their high optical power outputs and broader modulation

bandwidths. There are, however, standards and power restrictions controlling the usage of the LDs to mitigate potential eye and skin safety hazard [51].

LEDs, on the other hand, are preferred in low/medium data rate indoor applications. This is because LEDs are cheaper than LDs and more reliable. Moreover, LEDs are extended sources with large-area emitters. Therefore, LEDs can be operated safely even at relatively high powers. Compared to LDs, LEDs support lower data rates [93,114]. However, data rates up to 1 Gpbs using LEDs and rate-adaptive discrete multitone modulation are achieved [115]. In [116], Tsonev et al. present a 3 Gbps FSO link operating in the visible light band using a single 50-μm gallium nitride LED and Orthogonal frequency division multiplexing (OFDM) modulation scheme.

2.2.3 Photodetectors

Positive-Intrinsic-Negative (PIN) photodetectors and Avalanche Photodetectors (APDs) are the most commonly used types of photodetectors in FSO systems [1, 51]. PIN photodetectors are preferred in low cost and low data rates FSO links. This is because they are cheap, can operate at low-bias, and have tolerance to wide temperature fluctuations [1, 93]. APDs are PIN photodetectors operating at very high reverse bias. This leads to high internal electrical gain that increases the SNR at the receiver [1,2]. Compared to PIN photodetectors, APDs have superior performance especially in systems with limited ambient light noise. Therefore, APDs are favored in high data rates and high-performance FSO systems. On the other hand, APDs are more expensive and their gain is temperature-dependent. Analysis of different noise sources related to PINs and APDs are discussed in [51].

Recent advances in the field of graphene, two-dimensional materials, and nanomaterials, such as plasmonic nanoparticles, semiconductors, quantum dots have paved the way to the development of ultrafast photodetectors that work over a broad range

of wavelengths [117–119]. These photodetectors facilitate ultrahigh bandwidth optical communication systems supporting higher data rates.

2.2.4 Modulation

Different modulation schemes have different transmission reliability, energy, and spectral efficiencies. A modulation scheme is selected based on the type of the application. For example, the simplicity of On-Off keying (OOK) modulation makes it the most commonly used modulation scheme in FSO systems. However, OOK can be inefficient in more complex systems that require high data rate such as deep space communication. For such applications, Pulse Position Modulation (PPM) or one of its variations, e.g., Variable-PPM (VPM), is usually preferred [51, 84, 120].

Both OOK and PPM are considered as single-carrier pulsed modulation. As the data rate increases, single-carrier modulation schemes become inefficient due to the increase ISI [121]. Moreover, PPM requires complex time-domain equalization which can be problematic for FSO links with severe channel conditions and impairments [90]. In this case, Subcarrier Intensity Modulation (MSIM) and Multiple SIM (MSIM) such as Orthogonal Frequency-Division Multiplexing (OFDM) are used. In SIM-based approaches, an optical source is driven by a pre-modulated RF signal carrying the data. A DC bias is added to the signal before it is used to drive the optical source to maintain an all positive amplitude because the input of the LD must be non-negative [122]. Compared to single-carrier modulation schemes, SIM techniques help mitigate channel impairments and provide a simpler and cost-effective implementation [123]. Moreover, SIM improves bandwidth efficiency as compared to that of PPM techniques [124].

The addition of the DC bias (non-information signal) to the pre-modulated RF signal to avoid non-negative amplitudes leads to poor power efficiency. As the number

of carriers increase, such as in MSIM techniques, the DC bias required may become very large to prevent clipping and nonlinear distortion in the optical domain. This, in turn, leads to high peak-to-average power ratio (PAPR) and worsens the power efficiency [124]. The nonlinearity of light source is another challenge in MSIM techniques [122, 125]. The nonlinearity at the light source leads to interference among the subcarriers and broadening of the signal spectrum resulting in mixed signals and Inter-Modulation Distortion (IMD). To limit the transmit power and reduce the IMD, MSIM techniques need to employ small number of carriers. However, this limits the transmission data rate. Another approach to eliminate the IMD is to transmit each subcarrier using a separate optical source [126].

To improve the performance of the MSIM techniques, a PAPR reduction technique can be used to make the signal less vulnerable to the nonlinear distortion [127]. Another approach is to have the nonlinearities compensated for by predistortion or postdistortion [128, 129]. In [124], Hassan et al. present a detailed survey of SIM techniques. They discuss the advantages and challenges of SIM/MSIM.

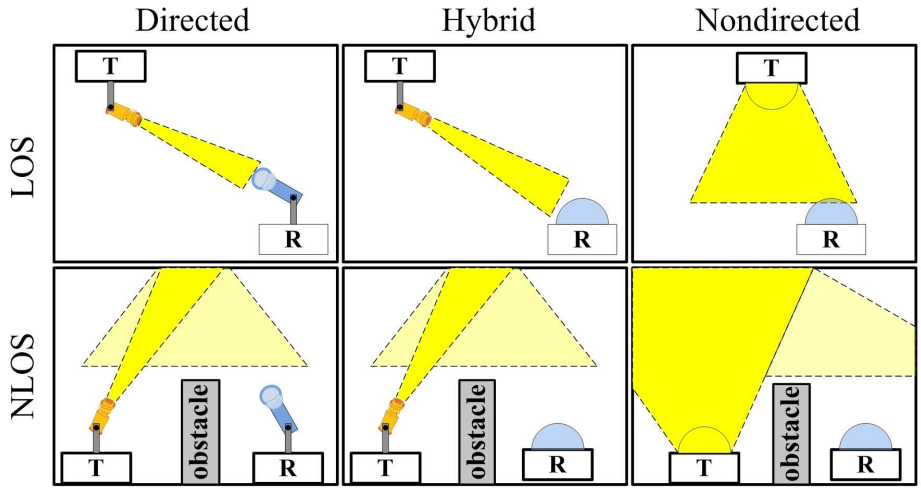

Figure 2.2: Classification of Indoor FSO communication links by Kahn and Barry [1].

2.3 Existing Classifications and Surveys of FSO Links

We briefly review main classifications of FSO communication technology. FSO technology can be deployed in four different environments: indoor, atmospheric, space, and UW. Out of the four different scenarios, indoor FSO has the largest share of surveys and classifications [1, 2, 73, 87, 90–95]. The last few decades have witnessed the development of various FSO communication schemes. Therefore, it is important to develop a classification that accommodates current and future FSO link configurations in different environments.

In [1], Kahn and Barry proposed one of the most popular and widely used classifications of indoor FSO communication systems in the literature to date. Therefore, it is reasonable to present a little-detailed discussion of this classification.

The classification by Kahn and Barry is based on two criteria: the directionality of the transmitter and receiver (i.e., directed, non-directed or hybrid), and whether the link is a line-of-sight (LOS) or non-line-of-sight (NLOS) link. These two criteria result in a total of six different FSO link configurations (see Figure 2.2).

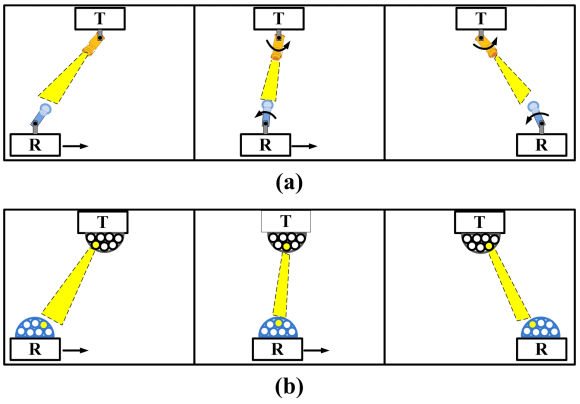

Figure 2.3: Tracked systems (a) steerable optics. (b) arrays of emitters and detectors.

In directed links, transmitted beam is directional and the receiver has a narrow

field of view (FOV). Directed links maximize power efficiency since it experiences low path loss and ambient light noise. However, this comes at the expense of the added complexity of aligning the transmitter and receiver due to their directionality. Contrary to directed links, undirected links utilize wide transmitters and receivers with wide FOV. This rules out the aligning constraint allowing a degree of receiver mobility. However, the performance of the undirected link is reduced due to the distribution of the source power on a large beam spot size. In hybrid links, the transmitter and receiver have a different degree of directionality.

LOS links are realized using an uninterrupted path between the transmitter and receiver. This maximizes the power efficiency and minimizes multipath distortion. On the other hand, NLOS links utilize the reflection of light from *diffusely* reflecting surface such as ceiling or walls, which improves the robustness of the FSO link especially with the existence of barriers. Apart from increasing robustness and ease of use, Nondirected/NLOS link, which is often referred to as a *diffuse* link, allows user's mobility.

During the same year (1997), Street et al. presented a tutorial review of indoor FSO systems [87]. Four different link configurations were used to classify FSO links, namely: LOS, wide-LOS (WLOS or cellular), diffuse and tracked. It might be noted that LOS, cellular and diffuse links are similar to the Directed/LOS, Nondirected/LOS and Nondirected/NLOS links presented by Kahn and Barry in [1], respectively.

In a tracked system, a narrow down-beam (spotlight) from the base station is used to illuminate only a single user station. A base station produces several narrow spotlights simultaneously. Each spotlight establishes a LOS link with one of several user stations, offering high bit rate links to multiple users within the same cell. Moreover, the spotlights produced by the base station are steerable [see Figure 2.3-(a)],

therefore, they can track the mobile user stations as they move around and between cells. Similarly, for a high data rate uplink (from user to base stations), the steerable spotlight at the mobile user station would be required. In addition to supporting high bit rates, tracked systems integrate the high power flux densities and low losses inherent in LOS links with the extended coverage provided by the WLOS (cellular) systems.

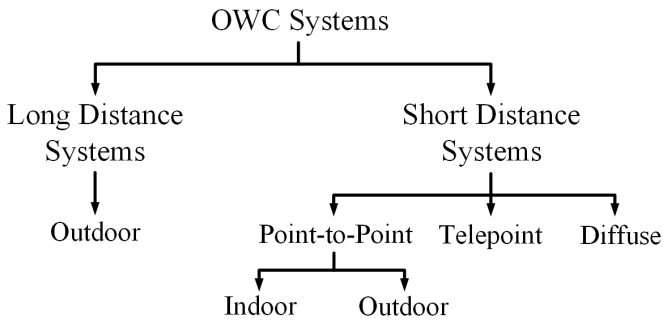

Figure 2.4: Classification of OWC systems by Heatley et al. [2].

In [130, 131], Wisely et al. proposed tracked FSO links in which spotlights are steered using mechanically steerable optics. The authors also discussed realizing solid-state tracking functionality using multi-element transmitter and receiver arrays. Using a tracking algorithm, appropriate array element depending on the position and user station is activated. As the user station moves within the cell, the activated beams would migrate from one PIN to the adjacent one in the array such that the LOS link is maintained [see Figure 2.3-(b)]. This process continues until the user station becomes again stationary or leaves the cell.

In 1998, Heatley et al. (including Wisely), published a paper which can be considered as the first attempt to present a classification that is not limited to the indoor FSO communication systems [2]. In this classification, FSO systems are classified as *long distance systems* and *short distance systems*.

Long distance systems are outdoor point-to-point links, whereas, short distance systems are further classified into four categories, namely, point-to-point, telepoint (similar to Nondirected/LOS in [1] or cellular in [87]) and diffuse. The point-to-point class includes short distance point-to-point outdoor links, and indoor point-to-point links. Moreover, Heatley et al. discussed the tracking architecture for indoor systems in a separate section, however, they showed no attempt to classify it. We summarize the classification presented by Heatley et al. in Figure 2.4.

In [81], Khalighi and Uysal classify an FSO link based on its range into five categories, ultra-short, short, medium, long and ultra-long range OWC. The authors focus on long-range links used in outdoor terrestrial OWC links. The paper is divided into two parts. In the first part of the paper, the authors describe the channel model of an FSO terrestrial link. In the second part, the authors discuss information theoretical limits of FSO channels. Moreover, they review system design research to approach these limits.

In [132], Ghassemlooy et al. (including Khalighi and Uysal) extend their previous work [81] and present an overview of FSO applications in the four environments using the link distance as a classification attribute. It is worth pointing that, classifying FSO links merely based on distance overlooks several crucial factors and attributes such as environment properties, LOS/NLOS nature of the link, coverage, and mobility.

The remaining survey papers can be divided into two groups: one group directly refers to one of the three main classifications [70,92–95], the other group [73,91] uses a subset of previous classifications which best indicate the most practical types of FSO links according to the authors point of view. For example, in [91], Elgala et al. chose Directed/LOS, Nondirected/LOS, and diffuse links from previous classifications and added the quasi diffuse links as a separate, fourth class, whereas, Borah et al. picked point-to-point and diffuse links from previous classifications and added multi-spot

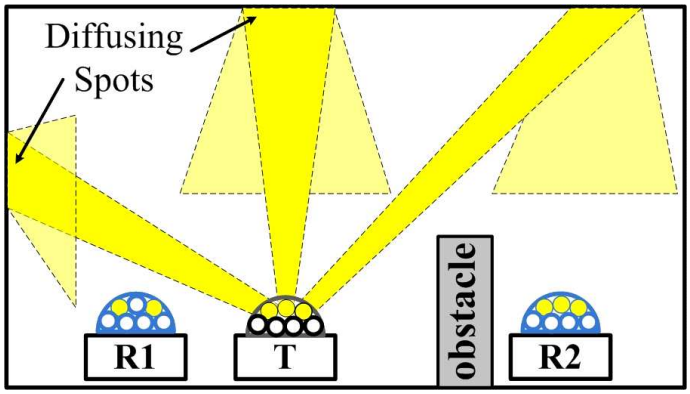

Figure 2.5: Quasi (multispot) diffuse FSO links.

diffuse as separate class [73].

In [88,89], Yun and Kavehard proposed the *quasi (multi-spot) diffuse* indoor optical wireless link. In multi-spot diffusing links, a transmitter sends more than one IR narrow beams to geographically separated diffusing spots. The use of narrow beams in quasi-diffuse FSO links help to reduce the channel power loss as compared to that of indoor diffuse systems, in which the transmitted power is distributed over a single wide beam.

At the receiver, multiple receivers aimed at different diffusing spots can be used. The added redundancy promotes the robustness of the system as compared to a single wide diffusing spot in diffuse systems.

Figure 2.5 depicts a quasi diffuse link. The transmitter is creating three diffusing spots. Receiver $R1$ is capable of receiving two out of the three diffusely reflected beams, whereas $R2$ can be illuminated by one of the beams. More diffusing spots can be created and their positions can be changed by steering the beams [89].

It might be noted that quasi-diffuse links can be considered as a set of Directed/NLOS communication links, however, the function performed is very similar to the Nondirected/NLOS links. Even though Kahn and Barry have mentioned multi-spot diffusing systems in [1], they showed no attempt at classifying the multi-spot

diffusing system using their proposed classification in that paper. Moreover, recent classification attempts result in considering quasi/multi-spot diffuse as a separate class of indoor FSO links [1, 73, 90, 91].

In [133], Johnson et al. present a brief survey and classification of UOWC. Similar to [90, 91], Johnson et al. classify UOWC links into four link configurations, namely; LOS, non-directed LOS, non-LOS, and retro-reflector. More recent and comprehensive surveys on UOWC are presented in [67, 134]. The authors survey the progress in the field of UOWC and present detailed discussions on the impairments of UOWC. However, similar to the work by Johnson et al. in [133], Kaushal et al. [134] and Zeng et al. [67] also use the classification with four configurations; LOS, non-directed LOS, non-LOS, and retro-reflector.

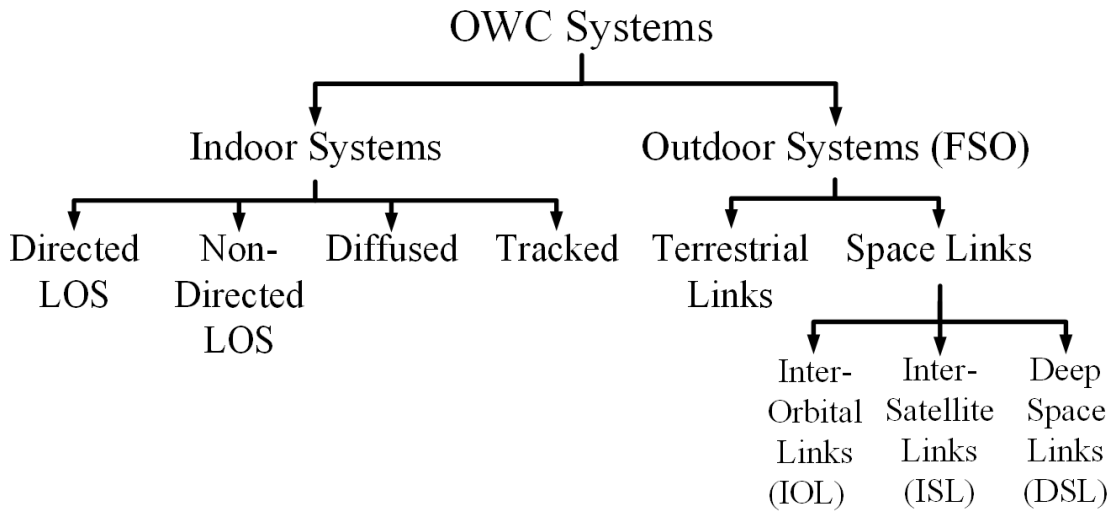

Figure 2.6: Classification of OWC systems by Kaushal and Kaddoum [3].

In [3], Kaushal and Kaddoum present a comprehensive survey of FSO in space environment. The authors adopt the classification depicted in Figure 2.6. In this classification, the notation OWC is used to refer to the optical wireless technology in general. The authors then classify OWC technology into Indoor Systems and

Outdoor Systems (FSO). Similar to existing surveys on indoor OWC, Kaushal and Kaddoum use the classification of Street et al. [87]. On the other hand, Kaushal and Kaddoum classify the Outdoor System (FSO) into Terrestrial Links and Space Links (see Figure 2.6). According to their classification, Space Links include Inter-Orbital, Inter-Satellite, and Deep Space links. It is noted, however, that the classification by Kaushal and Kaddoum completely disregards the classification of OWC in the Underwater environment.

In [135], Chowdhury et al. present a general overview and a comparative survey of OWC-based technologies. The survey, however, adopts the distance-based classification developed by Khalighi and Uysal [81].

Table 2.1 summarizes the classifications of FSO communication systems appeared in the literature. We use the notation used in [1] as a reference in the literature summary. A check mark indicates the presence of a certain FSO link configuration in the classification of the referenced paper. We also include the name of the configuration if it is different from that of in [1]. A closer look at Table 2.1 reveals the following:

- In [1], Kahn and Barry present an interesting classification, however, we notice the following:

    1. The classification limits NLOS links to diffusely reflected links, and thus Directed/NLOS link configuration is not used by any practical system in the literature. However, as we will discuss later in Section 2.4, some applications use FSO link configurations similar to the Directed/NLOS FSO links by replacing the diffuse reflecting surfaces, such as walls and ceils, with specularly reflecting surfaces such as mirrors.

    2. Out of the six possible FSO link configuration classes presented based on their classification, only three classes are used to describe configurations

Table 2.1: Summary of OWC/FSO Link Classifications in Literature.

Link Configuration	**[1, 92, 93, 95]**	**[87, 94]**	**[2]**	**[90, 91]**	**[73]**	**[81]**	**[67, 133, 134, 136]**	**[3]**
Environment	Indoor	Indoor	Indoor/ Terrestrial	Indoor	Indoor	Terrestrial	Underwater	Indoor/ Terrestrial/ Space
Directed/LOS	✓	✓ LOS	✓ Point-to-Point	✓	✓ Point-to-Point	✓	✓ LOS	✓
Hybrid/LOS	✓	✗	✗	✗	✗	✗	✗	✗
Nondirected/LOS	✓	✓ Wide-LOS or Cellular	✓ Telepoint	✓	✗	✗	✓	✓
Directed/NLOS	✓	✗	✗	✗	✗	✗	✗	✗
Hybrid/NLOS	✓	✗	✗	✗	✗	✗	✗	✗
Nondirected/NLOS (Diffuse)	✓	✓	✓	✓	✓	✗	✓	✓
Additional Classes	✗	Tracked		Quasi/Multi-spot Diffuse		✗	Retro-Reflector	Outdoor (Terrestrial and Space)

reported during the period 1997-2017. Therefore, there is a need for a more inclusive classification that can accommodate existing and emerging classes of FSO link configurations.

- A limited number of surveys show an attempt to classify terrestrial FSO systems in addition to the typical indoor systems. However, most of the existing classifications consider only Directed/LOS link configuration and thus is not sufficient for accommodating other configurations that have been recently developed.

- Several existing classifications refer to the same FSO link configuration using different names. This leads to more confusion in the FSO community and hinders the integration of knowledge reported in the various survey and classification papers reported in the literature.

- Most of the classifications reported are developed to simply review and differentiate existing FSO systems without taking into consideration future development of new FSO links. Therefore, it may be difficult, if not impossible, to fit some of the emerging and future configuration classes into existing classification schemes. Accordingly, many survey papers needed to introduce additional separate classes, which makes the overall classification scheme inconsistent and nonsystematic in its expansion.

2.4 Proposed Framework for FSO Link Classification

After analyzing various existing classification schemes for OWC link configurations discussed in Section 2.3, we observe that one of the main issues that led to ambiguity in previous classifications is that OWC link configurations are classified based on the

nature of their implementation rather than their functionalities. To this end, in this section, we develop and introduce a new function-based (scenario-oriented) classification model for OWC link configurations. The proposed classification abstracts the implementation details of various configurations, such that configurations with different implementation details but perform the same function are combined into a single class. For example, using the proposed classification, it is now possible to combine diffuse and quasi (multi-spot) diffuse systems under the same link configuration since they are similar in function, but different in implementation as pointed earlier.

2.4.1 Elements of the Proposed Classification

In our proposed classification, we use five criteria, namely: *Environment*, *Coverage Type*, *LOS Availability*, *Mobility*, and *Link Distance*, in order to classify any OWC link. In the following, we first discuss the five criteria, their variations, and used notation, and then we present the general structure of the proposed classification.

- **Environment (ε):** OWC technology can be used in four different environments, namely: *Indoor (I)*, *Terrestrial (T)*, *Space (S)* and *Underwater (UW)*. An indoor OWC link established in a confined space such as a chip, room or building. On the other hand, *Terrestrial (T)* OWC link is used to refer to OWC links realized in the outdoor environment where atmospheric factors affect the quality of the link. Contrary to Terrestrial OWC link, a Space link refers to the outdoor links that do not experience atmospheric effects such as in outer space inter-satellite communication. Finally, an Underwater OWC link is the link that is realized under any water surface. An FSO link may traverse a *set* of environments in some applications. We refer to this link as a *heterogenous FSO link*.

- **Coverage Type (κ):** An OWC link can be either a *Point Coverage (PC)* or a *Cellular Coverage (CC)* link. In *PC* configuration, an OWC link is established between a single transmitter and a single receiver such that the data transmitted cannot be received except by the intended receiver. A *PC* system usually deploys a narrow transmitter (NT), whereas, the receiver can be either a narrow receiver (NR), or wide receiver (WR). On the other hand, a *CC* link utilizes a wide transmitter (WT) or an array of NTs. This allows multiple receivers (NRs or WRs) to simultaneously receive the beam of the transmitter. WTs spread the transmitted light over a large coverage area, reducing the density of the light per unit area. Using a single NR is not practical since it may not collect enough light, and thus, WR or angle-diversity receiver which utilizes multiple NR elements is preferred.

- **LOS Availability (α):** An OWC link can be achieved using *LOS* or *NLOS* link configuration. In case of LOS, an uninterrupted line between the transmitter and receiver exists. LOS systems do not suffer the negative effects of a multipath. Also, the receiver in a LOS system does not require a large FOV or a concentrator. Therefore, LOS links are used for higher data rates. NLOS links, on the other hand, are used when a direct view of the transmitter and receiver does not exist or blocked by obstacles. In *NLOS* links, an active repeater or a passive reflector is used to connect the transmitter and the receiver. An active repeater receives a signal from the transmitter and retransmits the signal to the intended receiver. This is similar to relays used in wireless communication to extend the coverage or to boost the performance. On the other hand, a passive reflector can be a *diffuse* surface (e.g., walls, ceils, etc.) or a *specular* surface (e.g., mirrors, beam splitters, etc.). In our classification, we consider links with passive reflectors as the NLOS links. On the other hand, a NLOS system with

active repeater is discussed as a relayed system in Section 8.1.1 since there is a discontinuity in the propagation of the original light beam and a different link budget calculation is used each time the link is regenerated at one of the active repeaters used.

- **Mobility (μ):** An OWC link can be either a *fixed (F)* or *mobile (M)* link. For the F links, once installed, both transmitter and receiver remain fixed and aligned. If mobility is required, a mobile link is used, where transmitter and receiver are configured such that the link is maintained at the expense of complexity. Mobility can be realized using mechanically steerable optics or solid-state multi-element transmitter and receiver arrays.

  By mobility, we strictly mean the intended motion of the transmitter/receiver. As we will discuss later, it is possible that FSO links undergo unintentional displacements that may affect the link existence and quality. For example, an FSO link on top of a building can be affected by the continuous sway of the buildings. Another example is a UOWC that may be affected by the unstable hovering of two terminals due to water streams.

- **Link Distance (δ):** For the distance criterion, we adopt the classes proposed by Khalighi et al. [81]. Depending on the environment and the application, OWC links can be one of five different link distances (ranges): Ultra-short range [e.g., chip-to-chip communications], Short range [e.g., underwater communications], Medium range [e.g., indoor wireless local area networks (WLANs)], Long range [e.g., terrestrial connections], and Ultra-long range [e.g., deep space links].

2.4.2 The Proposed Classification

Based on the above discussion, an OWC link configuration can be expressed using the tuple $(\varepsilon/\kappa/\alpha/\mu/\delta)$, where:

$\varepsilon \in \mathcal{P}\left(\{\ I, T, S, UW\ \}\right) \setminus \{\emptyset\}$, where $\mathcal{P}(.)$ is the power set.

$\kappa \in \{\ PC, CC\ \}$

$\alpha \in \{\ LOS, NLOS\ \}$

$\mu \in \{\ F, M\ \}$

$\delta \in \{\ UShort, Short, Medium, Long, ULong\ \}$

Combinations of first four criteria are more cohesive than any combination that includes the fifth criterion. Therefore, in our proposed classification, we divide the five criteria into two dimensions (groups). First four criteria form the first dimension, and link distance represents the second dimension.

Any combination of criteria in the first dimension yields an OWC link configuration. A total of 32 different OWC link configurations can be expressed. However, there are clear dependencies and relations among the various criteria in the first dimension. In the following, we highlight these dependencies and discuss various link configurations and their implications.

A *CC* link differs from a *PC* link in that a CC link inherently supports mobility. This is because, in a *CC* link, the transmitter has a large coverage area (cell), and hence, a receiver can be either fixed or mobile within the cell. Since, *CC* OWC links inherently support mobility, we do not use F or M in our notation in case of *CC* systems. Therefore, the number of possible OWC link combinations expressed using the first four criteria becomes 24 different configurations.

Table 2.2: Proposed classification framework and notation of FSO communication link configurations. Grayed cells indicate infeasible link environment-range combinations. We use No Application (NA) to indicate that an application for the specific environment-range combination has not been reported in the literature yet.

					Link Distance				
					UShort $\leq$ 5 cm	Short 5 cm - 50 m	Medium 50 m - 500 m	Long 500 m - 500 km	ULong $\geq$ 500 km
Indoor (I)	Point Coverage (PC)	LOS	F	I / PC / LOS / F	[137–140]	[141–146]	[85, 86, 147, 148]		
			M	I / PC / LOS / M	NA	NA	[130, 131, 149, 150, 150–157]		
		NLOS	F	I / PC / NLOS / F	[16, 53, 158–165]	[52]	[9, 50, 166]		
			M	I / PC / NLOS / M	NA	NA	NA		
	Cellular Coverage (CC)	LOS		I / CC / LOS	NA	[167]	[10, 168]		
		NLOS		I / CC / NLOS	NA	NA	[10, 51, 65, 79, 88, 89, 169–171]		
Terrestrial (T)	Point Coverage (PC)	LOS	F	T / PC / LOS / F		NA	NA	[81, 106, 108, 172–176]	
			M	T / PC / LOS / M		NA	NA	[177–185]	
		NLOS	F	T / PC / NLOS / F		NA	[186]	[186]	
			M	T / PC / NLOS / M		NA	NA	NA	
	Cellular Coverage (CC)	LOS		T / CC / LOS		[62]	[187]	[187–190]	
		NLOS		T / CC / NLOS		NA	NA	[63, 191–213]	
Space (S)	Point Coverage (PC)	LOS	F	S / PC / LOS / F					NA
			M	S / PC / LOS / M					[214–217]
		NLOS	F	S / PC / NLOS / F					NA
			M	S / PC / NLOS / M					[217]
	Cellular Coverage (CC)	LOS		S / CC / LOS					NA
		NLOS		S / CC / NLOS					NA
Underwater (UW)	Point Coverage (PC)	LOS	F	UW / PC / LOS / F	[66]	[218–232]	[233–238]		
			M	UW / PC / LOS / M	NA	[239–242]	NA		
		NLOS	F	UW / PC / NLOS / F	NA	NA	NA		
			M	UW / PC / NLOS / M	NA	NA	NA		
	Cellular Coverage (CC)	LOS		UW / CC / LOS	NA	[243]	[244]		
		NLOS		UW / CC / NLOS	NA	[245–247]	[248]		
Heterogenous FSO Links				{S-T} / PC / LOS / F					[82, 109, 249–262]
				{S-T} / PC / LOS / M					[109,251]
				{I-T} / PC / LOS / F		NA	NA	[263]	

It is possible that few of these link configurations are not populated with practical OWC systems today, however, the main aim of the proposed classification is to accommodate any new OWC link configuration that can be developed as the OWC technology continues to develop and advance.

In (x/PC/LOS/F) link, transmitter and receiver are connected using a LOS, fixed link forming a point coverage form of communication. This class refer to Directed/LOS [1], LOS [87] and point-to-point [2] in indoor environment, while it is equivalent to long distance systems [81] in atmospheric environment. On the other hand, an (x/PC/LOS/M) is similar to (x/PC/LOS/F) except that the receiver is mobile. This class describes all kinds of tracked systems (i.e., systems based on mechanical steerable or solid multi-element transmitters) [2, 87, 130, 131].

A *NLOS* FSO link can be realized using relayed systems utilizing active repeaters, or a passive reflector that diffusely/specularly reflects light beams. Both, relays and passive reflectors can be used to realize (x/PC/NLOS/F) links since the link does not change once aligned and established. To establish NLOS link with mobility, relay systems can be used such that the uplink and/or the downlink are (x/PC/LOS/M). On the other hand, realizing an (x/PC/LOS/M) link using a specular passive reflector can be very difficult. This is because both transmitter and receiver will need a synchronized motion to maintain the link, which in turn adds to the complexity of the link.

An (x/CC/LOS/x) link is similar to the (x/PC/LOS/F/x) except that the narrow beam used in the (x/PC/LOS/F/x) is replaced with a wide diverging beam. A common configuration used as (x/CC/LOS/x) is a base station with a wide beam forming a *cell*, which is the coverage area of the base station. Any user outside this cell cannot receive the data transmitted by this base station. Depending on the area that must be covered, single or multiple cells can be used, and inter-cell mobility via

handover means can be supported. Nondirected/LOS [1], Wide-LOS (cellular) [87] and telepoint [2] refer to the same class (I/CC/LOS).

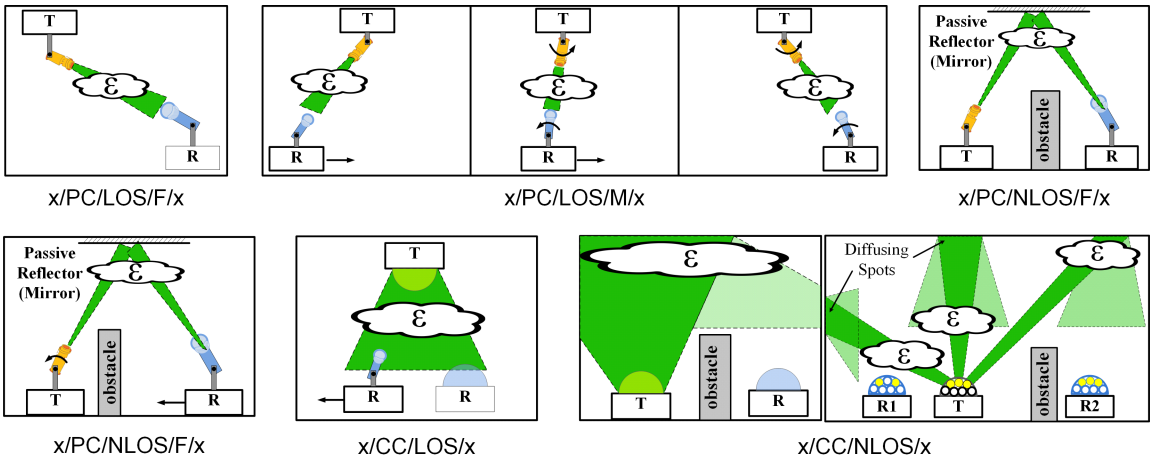

Figure 2.7: Different FSO link configurations in the proposed classification. The link configurations are consistent across different environments, and therefore we use the cloud symbol to represent the environment (ϵ).

Unlike specular reflection, NLOS links with mobility can be easily realized using diffuse passive reflectors. In (x/CC/NLOS) links, wide beams or a set of narrow beams are diffusely reflected off of surrounding surfaces such as the ceiling, walls, floor, and furniture. Receivers deployed have a wide FOV or multiple receivers with narrow FOV in order to capture the reflected beams from the different angles in addition to the LOS (if existed). Compared to previous classifications, the proposed (I/CC/NLOS) link configuration captures both diffuse and quasi-diffuse systems since both of them allow cellular coverage using NLOS links, yet using a different implementation.

Figure 2.7 shows the different link configurations in our proposed classification. We use the proposed classification in the following five sections to briefly review FSO applications in the different environments (indoor, terrestrial, space, underwater, and any combination of these environments). We also discuss the typical impairments encountered by each link configuration and review related standards and recommen-

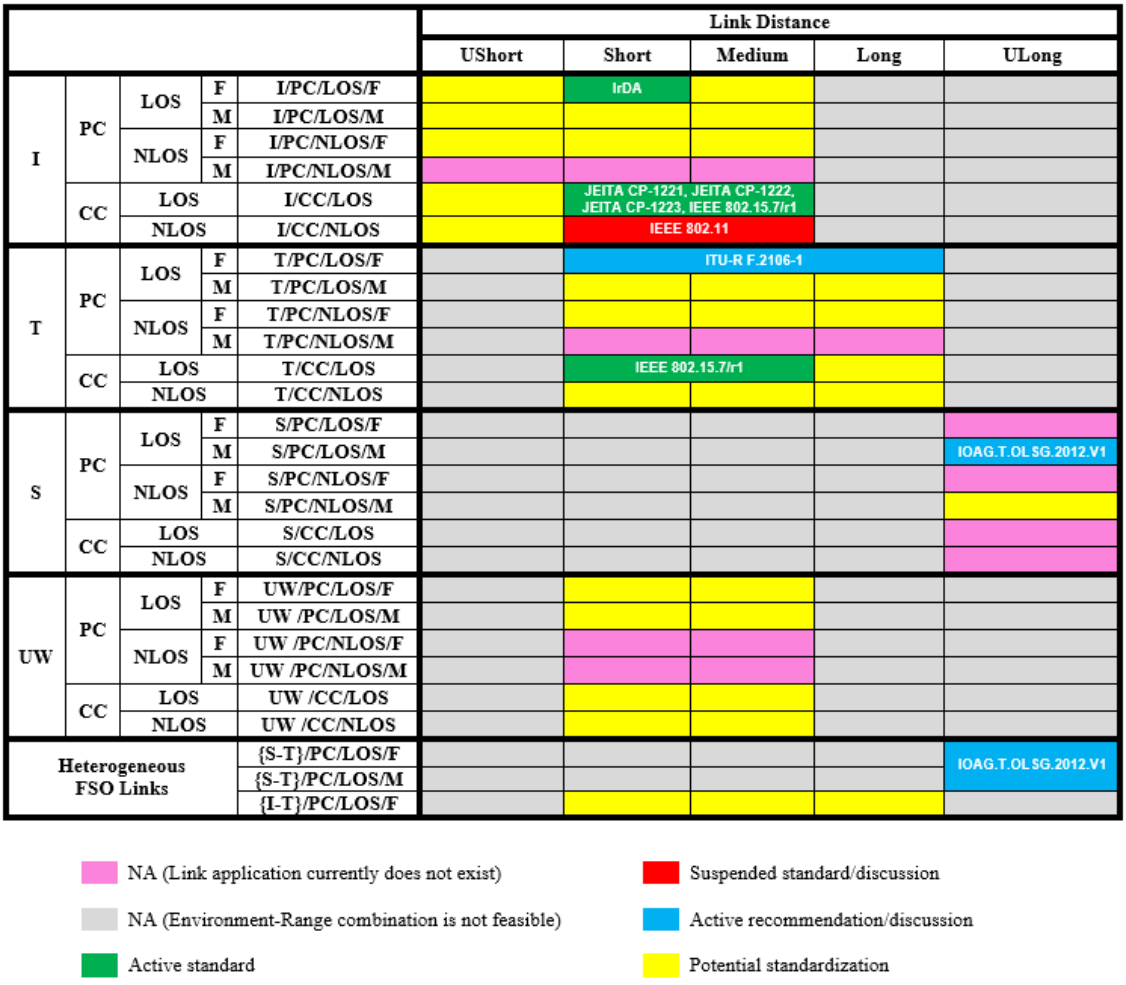

Figure 2.8: Classification of existing FSO standards and recommendations using the proposed FSO classification scheme.

dations. We focus on the physical layer of the standards and recommendations since the physical layer is directly related to the classification of different FSO link configurations. Table 2.2 summarizes the proposed classification with its 24 FSO link configurations in addition to few examples of heterogenous FSO links and a list of selected references for each. Figure 2.8 depicts a classification of existing standards and recommendations using the proposed classification.

As mentioned earlier, it is possible that few of the link configurations in the proposed classification may not be populated with practical OWC systems today. One of the possible reasons is that the environment-range combination of an OWC link is infeasible. For example, an ultrashort OWC link can only be realized in an indoor environment, whereas an ultra long link can only be realized in space communication. Infeasible environment-range combinations are grayed out in both Table 2.2 and Figure 2.8.

2.5 Indoor FSO Links

In this section, we discuss different indoor FSO link configurations and their recent research efforts.

2.5.1 Indoor FSO Link Configurations

I/PC/LOS/F/x

The I/PC/LOS/F/x FSO links deploy highly directional transmitters and receivers with narrow FOVs. The highly directional transmitters help eliminate the multipath dispersion effect and the receivers with narrow FOVs reject the majority of the ambient light. Therefore, I/PC/LOS/F/x links are capable of rejecting the majority of noise, and thus preferred in high data rate applications.

In [137], Rachmani and Arnon investigate the use of I/PC/LOS/F/UShort FSO link for card-to-card communication in a computer backplane. The authors study the impact of temperature and air turbulence caused by cooling air flow on the link. Wavelength-diversity is proposed to mitigate the scintillation and fading caused by the temperature and turbulence. A link using dual-wavelength transmitter (1550 and 670 nm) is deployed. Results indicate that wavelength-diversity can help reduce the link outage caused by temperature and turbulence. Following the work by Rachmani and Arnon multiple recent papers investigated the use of I/PC/LOS/F/UShort FSO links in computer backplanes [138–140].

I/PC/LOS/F/Short links have been used in low data rate remote control applications [141–143]. In 1998, Matsuda et al. demonstrated an IR multimedia home network based on the IEEE 1394 standard (FireWire) [144].

Since 1993, the Infrared Data Association (IrDA) group, has been using the I/PC/LOS/F/Short link configuration ($\leq 1m$) in its standards for applications that use the concept of point and shoot [145]. The links in IrDA standards provide data rates from 9.6 kbps to 512 Mbps [94, 145], and are mainly used to connect portable devices such as laptops, smart phones, and digital cameras. The details of different IrDA standards are discussed in Section 2.5.3.

In [147], Glushko et al. demonstrate a 1-10 Gbps I/PC/LOS/F/Medium (2-6 m) bidirectional FSO link with bit error rate better than 10^{-9}. The Person Area Network (PAN) system developed by Glushko et al. consists of a central station that serves up to 8 subscribers. On the other hand, Chowdhury et al. demonstrate an experiment involving a I/PC/LOS/F/Medium (15 m) link in the 1550-nm wavelength range directly modulated by the Cable Television (CATV) signal with data rates of 1 and 10 Gbps [85,86]. In [148], we propose OWCells, a class of optical wireless cellular data center network architectures in which I/PC/LOS/F/Medium links are used to

connect racks of servers arranged in regular polygonal topologies.

I/PC/LOS/M/x

As pointed our earlier, I/PC/LOS/F/x link is the preferred link configuration for high data rate applications. In some applications, it is desirable to provide a high data rate link for a mobile user. In I/PC/LOS/M/x links, narrow beams are steered to create high data rate FSO links with mobile terminals. The steering can be done using mechanical or passive solid state tracking systems [130, 131, 149, 150, 150–157].

Tracked systems presented by McCullagh et al. in [130, 149], and discussed in Section 2.3, can be classified as I/PC/LOS/M/Medium FSO links.

In [154, 155], Jungnickel et al. demonstrated electronic tracking system using I/PC/LOS/M/Short FSO links over a distance of 2 m and data rate of 155 Mbps. A transmitter with an array of LDs and a receiver with an array of wide FOV PDs are used. Tracking is achieved by activating the appropriate receiving element based on the location of the receiver with respect to the transmitter.

Despite the added complexity for tracking and handover, I/PC/LOS/M/x links have many advantages. Using I/PC/LOS/M/x links guarantees point coverage and LOS link, which means that reduced eye-safe power levels can be used for transmission to realize high data rate while covering large areas. Moreover, the use of a narrow FOV receiver means smaller transceiver which is suitable for mobile devices.

It is worth pointing, however, that I/PC/LOS/M/x links are not usually utilized independently. Instead, other FSO links are used for tracking the mobile terminal and pointing the I/PC/LOS/M/x links. We refer to the systems in which multiple FSO link configurations are used together as *Heterogenous FSO Systems* which we discuss in detail in Section .

I/PC/NLOS/F/x

This link configuration is widely used in applications where the delivery of point-to-point high bit rates are required between spatially distributed transmitters and receivers. Usually, the connecting terminals are distributed over the same plane, and thus any-to-any LOS links are unfeasible.

In 1988, Feldman et al. proposed the first intra- and inter-chip optical interconnect. The interconnect uses integrated optical signal transmitters, detectors, and a hologram to establish I/PC/NLOS/F/UShort links [158]. The authors presented a power and switching delay comparisons between the FSO interconnect and the conventional electrical interconnects. Results showed that the FSO intra-chip interconnects proposed by the authors are promising in high data rates and/or large fan-outs large area VLSI circuits.

Following the work by Feldman et al., many papers on the topic of intra- and inter-chip FSO interconnects using the I/PC/NLOS/F/UShort link model are published [159, 160, 162–164]. In [162], a 3D FSO interconnect (FSOI) that enables all-to-all direct communication links between processor cores with varying topological distances is introduced by Xue et al.

In [16,53,165,264], we propose a new class of non-blocking multicast FSO interconnect using non-moveable tri-state switching elements (T-SEs). A T-SE is a switching element that can be reconfigured in one of three states (Figure 2.9): *Reflective*, Transmissive, or *Splitting* state (half reflective/half transmissive). Any material similar to the one used in SMs can be used to realize T-SEs. Using the splitting state, a beam can split into any number of copies enabling multicast using I/PC/NLOS/F/UShort.

An FSO data bus for nanosatellites developed by NASA is proposed in [161]. The system model consists of multiple adjacent transceivers that are normally connected using a wired bus topology. Replacing the wired bus topology with a reflector surface

and FSO transceivers to establish I/PC/NLOS/F/UShort FSO links, the authors demonstrate a lighter communication system as well as significant power savings.

In [52], we propose a fully connected FSO rack of servers for FSO Data Center networks using what we refer to as *FSO bus* topology. The full connectivity is realized by steering I/PC/NLOS/F/Short FSO beams emitted by transmitters on one side of the rack, using mirrors, to the other side of the rack where beam splitters are used to distribute the optical beam to different servers.

Using a similar approach to the one used in [162] by Xue et al., however, at a different scale, Hamedazimi et al. develop *FireFly*, a configurable DC utilizing the FSO I/PC/NLOS/F/Medium links [9, 50]. In FireFly, the I/PC/NLOS/F/Medium FSO links are used for inter-rack communications, where top-of-rack (ToR) switches are connected using pre-configured FSO links that reflects off a reflector (mirror) mounted to the ceil.

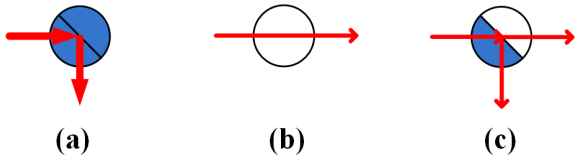

Figure 2.9: T-SE (a) R-State. (b) T-State. (c) S-State.

In [166], Bao et al. propose FlyCast FSO DCN. FlyCast is essentially a modification of FireFly using the concept of T-SEs used in our interconnects to provide multicast. In FlyCast, the authors utilize the splitting (referred to as mixed) state of the SMs to enable multicast without the need for a switch.

I/CC/LOS/x

The I/CC/LOS/x configuration represents three link types mentioned in the literature, namely; nondirected/LOS [1], Wide-LOS (cellular) [87], and *Telepoint* [2]. This

link configuration can be thought of as an I/PC/LOS/F/x link with wide angle transmitter. To realize the wide angle at the transmitter, I/CC/LOS/x links utilize LEDs, or LDs with diffusers. The I/CC/LOS/x link is designed such that the receiver detects the light from the LOS beam. It is possible, however, that the receiver will also collect beams that are reflected from walls which can be negligible as compared to the LOS component of the link [149, 265, 266].s

Visible Light Communication (VLC) is a form of OWC in which LEDs are utilized to transmit data. The main OWC link configuration used in VLC is I/CC/LOS/x. VLC represents an emerging mainstream research in its own right and has been well-surveyed in several recent survey papers [10, 75, 267]. VLC has also received great attention and wide range of standardization efforts as we will discuss in detail in Section 2.5.3. Although LEDs are usually used as transmitters in VLC, LEDs are limited in modulation bandwidth and efficiency. Therefore, researchers are investigating VLC systems that deploy LDs instead of LEDs [268].

One of the VLC applications that utilizes I/CC/LOS/Short FSO links is the passengers' entertainment systems in different vehicles such as cars and airplanes. The overhead light units associated with each passenger is used as a BS to transmit/receive entertainment and communication contents. In [167], Tagliaferri and Capsoni present an in-flight VLC I/CC/LOS/Short downlink that can provide each user a 10 Mbps link with uncoded BER of 10^{-6} along with an IR uplink. The downlink proposed takes into consideration the terminal misalignment due to the random movements of the passenger.

I/CC/LOS/Medium FSO links can be found in *Light fidelity (Li-Fi)* networks. Li-Fi is a high-speed bidirectional network in which mobile wireless communications using VLC is implemented. The LEDs in a network are used for illumination and data communication [10].

It should also be noted that VLC links can be deployed in outdoor terrestrial links as will be discuss in Section 2.6.

I/CC/NLOS/x

An I/CC/NLOS/Medium link configuration is realized by diffusely reflecting a single (diffuse) [79] or a set of narrow (quasi-diffuse) light beams [88, 89] off of diffuse reflecting surface, such as, a wall or a ceil. As pointed out in Section 2.3, in diffuse systems, the transmitted light is distributed over a single wide beam spot leading to reduced power and weaker received signal. On the other hand, using multiple narrow beams in quasi-diffuse links can help reduce the channel power loss, and hence the transmitted power. Moreover, quasi-diffuse links enables user mobility by covering the same area the single wide beam in a diffuse link would cover while reducing reflections and multipaths [91]. It is worth pointing that the advantages quasi-diffuse systems provide come at the expense of increased system complexity [91]. Multiple receivers can receive the diffusely reflected beams with different angles and positions. This type of links may appear even when I/CC/LOS/Medium links are used due to unintended reflection off of walls. In this case, each of the two channels will have its own model.

Depending on how the system is designed, it is possible to utilize the I/CC/NLOS links especially in case of shadowing during which an object or a human blocks the LOS link. In that case, it is important for the system to exploit the diffused light in a timely manner [65].

The estimation of the I/CC/NLOS channel has been investigated by Hashemi et al. in [170]. The performance and analysis of the I/CC/NLOS link has been well-investigated [51, 171]. Moreover, I/CC/NLOS can also be used in VLC as discussed by Bao et al. in [10]. On the other hand, an I/CC/NLOS link using multiple light

beams that can achieve a data rate of 70 Mbps has been reported by Carruther and Kahn in [169].

Optical Camera Communications (OCC) is another form of OWC in which flash, displays, and image sensor transceivers (or cameras) are used for data transmission, positioning/localization, and message broadcasting. Information is modulated in the pixels of the LED array at the transmitter. At the receiver, an image sensor or a camera captures the images of the LED array of the transmitter. The receiver then analyzes the intensity variation and extracts the transmitted signal [269, 270]. A camera can be operating in one of two modes; global-shutter and rolling-shutter modes [271].

The wide spread of smart devices with embedded LED flash lights and ever developing high quality cameras makes OCC a pragmatic form of OWC communication. Compared to other OWC technologies such as VLC, OCC operates at a wider spectrum that extends from IR to UV and including VL [269, 270]. Unlike conventional OWC link deploying a single PD at the receiver, a camera can be modeled as a 2D array of PDs [272]. The use of an image sensor allows the receiver in an OCC system to separate light signals both spatially and based on their wavelengths. Therefore, OCC system is convenient for spatial-division multiplexing (SDM), imaging Multiple-Input-Multiple-Output (MIMO), and Wavelength Division Multiplexing (WDM) modulation [270, 272].

Similar to I/CC/LOS, MIMO system can be used to improve the performance of the system, however, optical MIMO for I/CC/NLOS links has received little attention [65, 273, 274] and thus, optimizing MIMO performance for I/CC/NLOS channels should be investigated further [65].

2.5.2 Impairments of Indoor FSO Links

The most dominant noise source in indoor FSO systems is the shot noise due to ambient light from natural and artificial light sources [1, 51]. Natural light sources are classified as point sources (e.g., the Sun) and extended (e.g., the sky). Artificial Light sources are incandescent (tungsten), fluorescent lamps, and LEDs..

Although, optical filters can be used to minimize received background light, shot noise due to the background noise will still be existent. Shot noise is signal-independent and can be modeled as white Gaussian noise due to its high intensity [1]. On the other hand, in the absence of the ambient light, receiver preamplifier noise becomes the dominant noise source.

Sunlight and skylight represent unmodulated sources that have higher average power as compared to that of the desired signal [1]. In particular, sunlight extends over a broad spectral width with a background current that can reach 5 mA [51]. Artificial ambient light sources, on the other hand, are modulated.

Multipath induced dispersion (distortion) is another impairment for indoor FSO links. In particular, I/CC/NLOS/x in which a beam is allowed to diffusely reflect off of diffusing surfaces such as ceils and walls is the highly susceptible link configuration to the multipath induced dispersion. Multipath induced dispersion depends on the size of the room and the reflection coefficients of the reflecting surfaces. Moreover, the severity of the dispersion depends on the I/CC/NLOS/x implementation. For example, in diffuse (single-spot) I/CC/NLOS/x the transmitted wide beam can experience multiple reflections. Using a single wide FOV receiver will collect large number of reflections. This, in turn, leads to intersymbol interference (ISI), and thus, data rate reduction [73]. To overcome the multipath induced dispersion in diffuse systems, quasi-diffuse (multi-spot) I/CC/NLOS/x is used. Although quasi-diffuse links has the same theory of operation as diffuse systems, quasi-diffuse implementation has

the advantage of the spatial-diversity which helps limiting the ISI [73]. The use of multiple spots allows for a controlled projection of spots both in numbers and directions. Moreover, since the reflections are narrower, multiple narrow FOV receivers can be used. The narrow FOVs blocks most of the ambient light and rejects large number of undesired reflections. The main challenge of quasi-diffuse implementation is the complexity of the transmitter and the receiver with diversity combining [155]. For example, projecting multiple spots can lead to a complex and bulky transmitter with multiple sources. This can be avoided by using holograms [1, 73].

There are several challenges facing OCC systems. For example, the frame rate of the camera used as a receiver is an important factor to determine the achievable data rate of the system. Since the frame rate of a commercial camera is usually low, around 30 and 60 frames per second (fps), the total achievable data rate in an OCC system is usually low [269]. Using cameras with high fps can help improve the data rate [270, 271]. Such high speed cameras supporting hundreds of fps are already developed [270]. Furthermore, it is expected that the frame rates of commercial cameras will continue to increase as the image sensor nanotechnology continues to advance. Symbol synchronization is another challenge facing OCC systems. Since OCC is mostly used for broadcasting systems, a feedback channel is not available. With the absence of the feedback channel, the variable sampling rates, and the randomness of the sampling, it is possible to sample during a symbol and thus losing it. To solve the synchronization problem, reference signal or code embedded in the image can be used is most cases [269]. Detailed discussions on the advantages, limitations/challenges, and applications of OCC can be found in [269–272].

A summary of indoor FSO impairments, their causes, effects and solutions is tabulated in Table 2.3

Table 2.3: Indoor FSO Link Impairments.

Impairment	**Causes**	**Effects**	**Solutions**
Ambient light	Sunlight Skylight Incandescent lamps Fluorescent lamps LEDs	Reduced SNR	- High transmitted power - Highly directional links. - Using LEDs out-of-band of the light sources used in the FSO link.
Multipath induced dispersion	Reflection off of diffusing surfaces	-Reduced SNR - Intersymbol Interference (ISI)	- High transmitted power - Multi-spot diffusing - Spatial Diversity - Equalization - FEC

2.5.3 Indoor FSO Standards and Recommendations

IrDA

Infrared Data Association (IrDA) developed several layer-based standards for low cost half-duplex I/PC/LOS/F/Short FSO links ranging from 6 cm to 1 m and operating at wavelengths of 850-900 nm. Protocols are then implemented on different layers for applications such as contact information exchanges to ultra-fast file transfers. Table 2.4 summarizes different IrDA standards and data rates supported.

The next version of Giga-IR standard is expected to support data rate up to 10 Gbps. However, as the data rate increases so do the restrictions on the beam alignment. For example, in case of Giga-IR, a docking station is used which limits the link length to 6 cm.

JEITA VLC Standards

The recent development of highly-efficient LEDs, in addition to the inherent advantages of VLC over RF communications are the reasons that motivated academic and industrial communities to investigate the deployment of VLC in a broad spectrum of applications. In response to the advances in the VLC technology and its deployment in many applications, several standardization organizations, such as Japan Electronics and Information Technology Industries Association (JEITA) and IEEE, are developing standards for VLC technology. In the following, we discuss the efforts by JEITA and IEEE to standardize the VLC technology.

In November 2003, the Visible Light Communications Consortium (VLCC) [the predecessor of the Visible Light Communications Association (VLCA)] was established in Japan to explore different applications of VLC. In 2006, members of VLCC proposed the standards, CP-1221 (VLC System), and CP-1222 (Visible Light ID

Table 2.4: Summary of IrDA Standards.

Standard	**Data Rates**
Serial Infrared (SIR)	2.4-115.2 kbps
Medium Infrared (MIR)	0.576 and 1.152 Mbps
Fast Infrared (FIR)	4 Mbps
Very Fast Infrared (VFIR)	16 Mbps
Ultra Fast Infrared (UFIR)	96 Mbps
Gigabit Infrared (Giga-IR)	512 Mbps and 1.024 Gbps

System) [275] to avoid fragmentation and proprietary protocols, and to prevent interference between different optical communication equipments.

Light in the range of 380-750 nm is used for communication. Sub-carrier modulation is used instead of single-carrier modulation schemes to avoid ISI. Three major frequency ranges are defined in CP-1221 and CP-1222:

- Range 1 (15 kHz-40 kHz): Communication purposes and used by JEITA Visible Light ID System.
- Range 2 (40 kHz-1 MHz): In this range, the noise radiated from the inverter fluorescent lamp is fairly large, and thus fluorescent lights cannot use this range.
- Range 3 (>1 MHz): Dedicated to vast data transmission using special LEDs.

More recommendations regarding the PHY are proposed by JEITA CP-1222. The transmission frame consists of an ID (fixed data) and arbitrary data (non-fixed). It is recommended to use SC frequency of 28.8 kHz and SC-4PPM modulation scheme to avoid flickering. The transmission rate of 4.8 kbps is achieved using cyclic redundancy checks (CRC) for error detection/correction.

In 2013, JEITA proposed the CP-1223 (Visible Light Beacon System) to TC-100 of the International Electrotechnical Commission (IEC) and was approved as IEC 62943

in 2014 [276]. The standard CP-1223, which is a simplified and improved version of CP-1222, is designed to support single directional visible light beacon system. This type of links is particularly useful in applications such as identification of objects, providing positional information for localization, and the establishment of various guiding systems by transmitting simple identification (ID) information unique to the visible light source. Similar to CP-1222, visible light of peak wavelength in the range of 380 nm to 750 nm is used. Visible light is intensity modulated by 4PPM signals at 4.8 kbps. A data frame of 158 bits is used with a start of frame (SOF) and end of frame (EOF) data of 14 and 16 bits, respectively, and payload of 128 bits.

IEEE Standards

IEEE has demonstrated early efforts to standardize the FSO technology. However, as mentioned earlier, only recent development in FSO enabling technology has allowed the realization of products and systems that can be efficiently used. In the light of these recent advances, IEEE proceeds with developing new standards for emerging systems. In this section, we will discuss old and recent efforts by IEEE in the domain of standardizing the FSO technology.

IEEE 802.11

In 1997, IEEE released the standard IEEE 802.11 in which two data rates of 1 and 2 Mbps are specified. Transmission is specified to be using IR signals and the 2.4 GHz frequency in the Industrial, Scientific and Medical (ISM) band [146, 277].

The IEEE 802.11 specification was developed for I/CC/NLOS/Medium links (i.e., diffuse link) with a link range of 10 m and transmitting in the range of 850-950 nm [277]. Two modulation schemes, 16 and 4 PPM are used for the two data rates 1 and 2 Mbps, respectively.

Despite the advantages of the communication in the IR band, the drawbacks exhibited by indoor IR communications, discussed in Section 2.5.2, prevented the implementation of the infrared channels of IEEE 802.11. Therefore, IR channels remains a part of the standard IEEE 802.11, but has no actual implementations.

IEEE 802.15.7-2011

In 2011, the *IEEE 802.15.7* standard for VLC was released defining the PHY and medium access control (MAC) layers for $\{I,T\}/CC/LOS/\{Short,Medium\}$ links. Three classes of VLC devices are defined in IEEE 802.15.7:

- Infrastructure: Also called coordinator is a stationary device that has unconstrained form factor and power supply.
- Mobile: Movable devices with limited power supply and constrained form factor. Mobile VLC devices use weak light sources, and thus operates at short ranges and can transmit at high data rates.
- Vehicle: Mobile devices with unconstrained form factor and moderate power supply. Employs intense light source to communicate over long distances at low data rates.

The above VLC devices can be arranged in one of three network topologies; star, peer-to-peer, or broadcast.

- Star: Supports communication between several mobile devices and one coordinator.
- Peer-to-peer: Supports communication between two close devices, one of which acts as the coordinator.

- Broadcast: Uni-directional transmission from a coordinator to one or more devices.

The IEEE 802.15.7 standard supports three PHY operation mode [146, 278]:

- PHY I: Low data rate outdoor applications (11.6 to 266.6 kbps). Employs On-Off Keying (OOK) and variable pulse-position modulation (VPPM). Also supports concatenated coding with Reed-Solomon (RS) and convolutional codes.
- PHY II: High data rate outdoor/indoor applications (1.25-96 Mbps). Similar to PHY I, PHY II employs OOK, VPPM and supports RS coding, but does not support convolutional codes.
- PHY III: Designed to support systems with multiple light sources/detectors at different frequencies (colors). Employs Color-Shift Keying (CSK) and Reed-Solomon coding to achieve 12-96 Mbps.

The three physical layers supported by IEEE 802.15.7 are designed to co-exist but not to interoperate [146]. A VLC device compliant with IEEE 802.15.7 must implement PHY I and/or PHY II. Moreover, for co-existence purposes, PHY II must be implemented along with PHY III [146].

IEEE 802.15.7r1

In 2014, the IEEE 802.15 has formed a Short-Range Optical Wireless Communications Task Group to write a revision for IEEE 802.15.7-2011. The aim is to accommodate wider spectrum, IR and near UV in addition to VLC, [279] as well as developing new communication links and modes of operation such as Multiple Input/Multiple Output (MIMO). In particular, the task group works on accommodating the following communication techniques and networks:

- Optical Camera Communications (OCC)
- LED-ID: Wireless light Identification system.
- LiFi: LiFi is a high-speed bidirectional network in which mobile wireless communications using light is implemented.

In [269], Saha et al. present a survey discussing the key technology consideration in IEEE 802.15.7r1, impairments, and enhancements in application scenarios of the OCC systems. A detailed discussion on the reference channel models endorsed by the IEEE 802.15.7r1 Task Group for evaluation of VLC system proposals are discussed by Uysal et al. [280].

2.6 Terrestrial FSO Links

Terrestrial FSO link is finding its place in several applications including, metropolitan network extensions, last-mile access, enterprise connectivity, fiber backup, cellular network backhaul, service acceleration and network disaster recovery [263]. It is also expected that FSO links will have a great potential for applications in the fifth generation (5G) wireless systems and beyond [74,75]. Future wireless networks will be hybrid and will incorporate complementary access technologies with higher channel capacities, multiple antennas, and Gbps data rates [74]. For example, FSO links can be used to carry cellular traffic from base stations to the base station controller [263]. Terrestrial FSO links can also be used in wireless sensor networks where a large number of nodes are distributed over a wide area and need to communicate using NLOS links.

2.6.1 Terrestrial FSO Link Configurations

T/PC/LOS/F/x

The T/PC/LOS/F/x is the most commonly used configuration to realize a high data rate terrestrial FSO link. The performance of T/PC/LOS/F/x links has been investigated thoroughly in the literature [106, 172–176]. In [81], Khalighi and Uysal focus on the modeling and performance of the T/PC/LOS/F/x link configuration. T/PC/LOS/F/x FSO links are now a commercial reality [72] that is deployed in a wide range of applications. A list of 29 companies with T/PC/LOS/F/Long FSO link products can be found in [108].

T/PC/LOS/M/x

FSO T/PC/LOS/M/x link configurations are used for applications in which the stringent acquisition, pointing, and tracking requirements need to be relaxed due to the mobility of one (or both) communicating terminal such as in aircraft to ground communication [281]. In [177], Ortiz et al. present an experiment in which an Unmanned-Aerial-Vehicle (UAV), named Altair, is used to collect data and fly in a predefined circle around a ground station. Altair was designed to receive an optical beacon from the ground station, and using tracking systems, it sends the collected data using an T/PC/LOS/M/Long downlink to the ground station. In November 2013, the first experiment of an OWC link using jet platform was performed. A 60 km T/PC/LOS/M/Long link was established between a jet platform (i.e., Tornado) flying at 800 km/h and the ground. Data is transmitted at a rate of 1 Gbps using a ViaLight Communications laser terminal [184, 185].

During the late 1990s, the U.S. Naval Research Laboratory (NRL) started conducting experiments on modulating retroreflector (MRR) FSO communication links.

An MRR link provides a mean for limited duplex communication link with an interrogator at one end and a small passive optical retroreflector at the other end. The source housing the interrogator is assumed to have high power. The retroreflector can be corner cube or a cat's eye and is coupled to an optical modulator. The interrogator transmits a continuous wave beam towards the retroreflector which passively reflects the beam back after the optical modulator has imposed a signal on it. Shore-to-shore, boat-to-shore and sky-to-ground MRR FSO links were successfully realized [178, 179, 182, 183, 282]. In [181], Rabinovich et al. establish a 1 km MRR FSO link with a robot at data rate of 1.5 Mbps. A bidirectional 16 km MRR FSO link is established in [180]. One of the most recent experiments in the domain of T/PC/LOS/x/x was performed by Li et al. [282]. In their experiment, Li et al. test a T/PC/LOS/x/Medium link between a ground station that is used as an interrogator and a UAV equipped with a retro-reflector. The distance between the ground station and the UAV is 100 m roundtrip and thus we classify the link as terrestrial (T) and medium range (Medium). Two PC/LOS links are established with the UAV. The first link is established while the UAV is hovering (T/PC/LOS/F/Medium) and the other is with the UAV moving (T/PC/LOS/M/Medium). Using two Orbital Angular Momentum (OAM) multiplexed beams, Li et al. realize 80 Gbps with each beam carrying a 40-Gbps Quadrature Phase Shift Keying (QPSK) signal. As expected, the T/PC/LOS/F/Medium link provides better performance as compared to that of T/PC/LOS/M/Medium in terms of the power fluctuation of the on the desired mode and the crosstalk to the other mode.

T/PC/NLOS/F/x

As mentioned earlier, T/PC/LOS/F/x link configuration is used to establish point-to-point high bit rate communication link. However, finding a LOS between two points

may become infeasible, especially in urban cities with varying building heights, and thus T/PC/NLOS/F/x link is needed. In [186], Rahman et al. discuss FSONet, an FSO backhaul for multi-gigabit picocells using T/PC/LOS/F/Medium,Long steerable links. In FSONet, links are steered using reconfigurable mirrors. This is very similar to the FireFly Data Center Network developed by the same lab.

Due to beam divergence, which can be relatively big for long distance terrestrial links, using passive reflectors (mirrors or walls) may become impractical. Therefore, to establish T/PC/NLOS/F/x links, relay systems utilizing active repeaters with two or more T/PC/LOS/F/x link segments can be used. Such systems will be discussed in detail in Section 8.1.1.

T/CC/LOS/x

In addition to indoor deployment (discussed in Section 2.5.1), VLC communication deployment in Intelligent Transportation Systems (ITS) is being investigated [62]. This model aims to utilize the LEDs that are widely deployed for traffic lights, vehicular (head, tail, and brake) lights and street lights as transmitters. Traffic lights and vehicles are equipped with receivers such as high-speed cameras [62] in case of OCC (discussed in Section 2.5.1) to establish vehicle-to-infrastructure (V2I) and vehicle-to-vehicle (V2V) T/CC/LOS/Short OWC links. Traffic safety-related information along with infotainment applications are broadcasted using the LED array at the transmitter and the data captured by receiver's camera interacts with the computers in vehicles to enhance traffic flow and reduce accidents and fatalities.

Data Communications (Data Comm) is an essential module of the Next Generation (NextGen) framework being developed by Federal Aviation Administration (FAA). Data Comm aims to enable the exchange of digital information that can be visually displayed and interpreted between air traffic controllers (ATCs) and pilots.

Compared to the conventional audio communication currently used in the aviation field [283], Data Comm messages will require significantly less bandwidth. Moreover, Data Comm is expected to lead to safer operation as it will help improve the visual, auditory, and cognitive workload for controllers and pilots. Moreover, future versions of Data Comm will be designed such that the digital messages exchanged between the ATCs and aircrafts can interact with the computers on-board enforcing rules and safety measures [284, 285].

Delivering Data Comm traffic between ATCs and pilots requires a data communication networking infrastructure. Similar to the application of OWC in vehicular communications, we envision that aircraft-to-aircraft (A2A) and aircraft-to-infrastructure (A2I) can be achieved using T/CC/LOS/{Medium,Long} links serving as the infrastructure for Data Comm [187]. We envision that the airport's infrastructure of lights and signages along the taxiways and runways for Data Comm can be utilized for this purpose. Furthermore, OWC links can be used for aircrafts localization on the airport ground and help raise pilots' situational awareness.

High-speed trains (HSTs) traveling at speeds between 250 and 575 km/h are gaining popularity across the world especially in China, France, Germany, Japan, Spain, and potentially the United States [286]. Maintaining a reliable ground-to-train communication link is essential for delivering the signaling traffic of the train operation control system which is the system responsible for the safety of the HSR [286]. In addition to the train operation control system, there is an increasing demand by users aboard HSTs for high data rate internet access [188]. However, providing high data rate access to users aboard HSTs is another application that is testing the boundaries of RF-based communication systems. RF-based communication networks are not capable of meeting the high data rate demand on HSTs due to several technology limitations such as Doppler frequency shifts, penetration losses, and the frequent

handovers.

Initially, a dedicated narrow-band Global System for Mobile communications for railway (GSM-R) network was realized. GSM-R, however, utilizes the same frequency band used by the public land GSM network [286]. This poses a risk on the safety of the HSR's operation due to the potential co-channel interference. Moreover, GSM-R network is incapable of meeting the demands for the high data rate. To overcome the challenges facing GSM-R, the broadband Long Term Evolution for Railways (LTE-R) was developed to achieve high capacity, low latency, and high reliability. LTE-R networks features fast synchronization, channel estimation and equalization, Doppler shift estimation and correction, and MIMO technique. LTE-R, however, experiences frequent handovers which may lead to interrupted transmission of critical train control signals as well as call drops and spotty internet access. In addition to GSM-R and LTE-R, IEEE 802.11p and IEEE 802.15.4p are also being utilized for ground-to-train communication links.

Despite the recent advances in RF-based technologies for HST systems, the data rates RF-based technologies provide is limited and does not meet the increasing demands by HSTs and their passengers [287, 288]. This makes HST an application in which the FSO technology can be utilized [71]. In [188–190], the authors utilize T/CC/LOS/Long links to create overlapping coverage cells along the railroad of HSTs such that the an HST travels within the coverage area of the FSO beam eliminating the need for tracking systems. FSO transceivers mounted on top of the trains and directed towards the source of the FSO beams along the railroad are used to maintain a permanent communication link with handovers performed in the overlapping regions of adjacent base stations (BSs).

T/CC/NLOS/x

PC/LOS FSO communication links are usually preferred to achieve high data rate communication links between two points. This is notably true in the terrestrial environment due to the atmospheric impairments that can limit the performance of the FSO link. However, contrary to what was widely believed, FSO in the atmospheric scenario does not require PC/LOS setup for operation [289].

The solar radiation in the deep UV spectral region (i.e., 200-280 nm) is absorbed and scattered by ozone in the upper atmosphere (about 40 km away from the Earth's surface). This means that FSO links transmitting in this region do not encounter background noise, and thus this band is referred to as *solar-blind ultraviolet* [191].

Although the scattering of light by particles and aerosols is considered an impairment for most of the FSO links as it degrades the link quality, the unique propagation attributes of the solar blind ultraviolet wavelengths, such as being strongly scattered by particles and aerosols, facilitate the realization of T/CC/NLOS/Long FSO links. This type of communication is referred to as *optical scattering communication (OSC)* which can be very useful when a LOS link between the transmitter and the receiver is infeasible. In OSC, a transmitter emits a light beam with preselected divergence and elevation angels forming a cone. A receiver with large FOV pointing towards the formed cone of transmitted beam detects the scattered light from the atmosphere. To collect more backscattered optic power from the transmitter, receivers with large FOVs are needed. A possible application for OSC is to establish T/CC/NLOS/Long links between nodes in energy-constrained distributed WSNs [290].

In 1970, Lerner and Holland [291], and Kennedy [292] analyzed the characteristics of atmospheric optical scattering channel laying the foundation for OSC. In [293], Reilly proposes the single scattering model and investigates the pulse broadening effect of T/CC/NLOS/Long OSC. In [290], Shaw et al. develop a simulation model

Table 2.5: Terrestrial FSO Link Impairments.

Impairment	**Causes**	**Effects**	**Solutions**
Ambient Light	Sunlight	Reduced SNR	- Increase transmitted power - Highly directional links
Swaying Buildings	Winds and seismic activity	Loss of signal	- Beam diverging - Active tracking - Spatial diversity
Attenuation	Fog, rain, snow, dust or a combination of them.	Absorption, refraction and scattering	- Increase transmitted power. - Diversity. - Efficient modulation
Atmospheric Turbulence	Refractive index variations	Beam wandering and heat dependency.	- Adaptive optics. - Aperture averaging - Temporal and spatial diversity - Relay transmission - Hybrid Links - Reconfiguration and re-routing

to analyze the performance of the T/CC/NLOS/Long UV link and compare it to conventional RF links.

The last two decades have witnessed an upsurge of research on T/CC/NLOS/Long OSC [63, 191–213]. Modeling T/CC/NLOS/x OSC channel is more challenging than modeling traditional LOS links [194]. Therefore, most of the research in OSC is directed towards the modeling of OSC channels assuming single-scatter [210,212,294], multiple scattering [199,202,203] which is essential when the transmitter's beam axis and the receiver's FOV axis are not coplanar, and most recently, considering the inhomogeneity of the atmosphere to achieve a more accurate model [213]. Other researchers focus on deploying new modulation schemes to improve the performance and the bit rate of the link such as M-ary Spectral-Amplitude-Coding [207], and frequency-shift keying modulation scheme [211]. As a result of the evident interest in the OSC systems, recent survey papers [70, 295–297] summarize and survey major experimental and modeling research on OSC.

2.6.2 Impairments of Terrestrial FSO Links

The exposure of the terrestrial FSO links to the turbulence caused by atmospheric variations can lead to severe link performance degradation. Several publications have discussed the impairments of terrestrial FSO links in detail [3, 81, 106, 298], therefore, in this subsection, we only briefly discuss the different impairments, causes, and mitigation techniques.

A terrestrial FSO link can be affected by sunlight, beam misalignment due to building sway, attenuation (due to fog, rain, and snow) and atmospheric turbulence [263]. Fog, rain, snow, dust, or any various combination of them can lead to absorption, refraction, and scattering resulting in signal attenuation and link performance degradation [74, 106]. Atmospheric turbulence can be caused by scintillation,

beam wanders and beam spreading. Atmospheric scintillation is the spatiotemporal change of light intensities at the receiver due to variations of air index of refraction.

There is a wide range of atmospheric turbulence impairment techniques that can be applied at the physical layer, such as; aperture averaging, adaptive optics, diversity, relay transmission, and hybrid systems. Other recent approaches explore atmospheric turbulence mitigation at higher layers including retransmission and Reconfiguration and re-routing [3].

Aperture averaging relies on the idea that more light can be collected by a receiver with wider aperture and thus, it is possible to average out relatively fast fluctuations. However, increasing the aperture of the receiver has its limitations in terms the available real-state. Similar to RF wireless communication, space, spatial, and temporal diversity techniques can improve the link availability and help mitigate atmospheric impairments. In adaptive optics, the conjugate of atmospheric turbulence that is estimated to impact the beam to be transmitted is added before the transmission. Relay transmission is another form of spatial diversity in which the transmitters are distributed over a network instead of being co-located at the sending node location. This can help utilize links that are not undergoing the same impairments as the direct link between the source and destination nodes. Another approach to mitigate atmospheric turbulence is to switch to a technology that is not affected with such impairment (e.g., RF). Such a system is referred to as hybrid FSO/x system and we discuss it in detail in Section 2.10.2. Since RF is the most mature wireless technology in the terrestrial setting, FSO/RF hybrid systems are usually used. To overcome atmospheric turbulence, retransmission of data can also be used. In this approach, protocols that guarantees reliable delivery of messages, such as; automatic repeat request (ARQ), go-back-N ARQ, and selective repeat ARQ (SR-ARQ) are used. In case of FSO networks, reconfiguration and rerouting of the path that a signal takes can be

very useful to avoid links that are affected by severe atmospheric turbulence. This approach is also useful for avoiding node failures and building robust and fault-tolerant networks.

A possible approach to overcome the atmospheric scintillation is to operate at a higher wavelength (e.g., 2000-2200 nm) [299]. However, the development of optical components operating in this range are not as widely commercially available since this range is unsuitable for fiber optic technology which is more mature than the FSO technology. Recent attention, however, has been directed towards this band due to its advantages when used in FSO technology. Currently, sources operating in this range are available using Fabry-Perot and Discrete Mode Fabry-Perot (DFB) technologies [300].

Recent advances in the domain of Quantum Cascaded Laser (QCL) [301] have enabled the development of FSO links operating in the infrared ranges (2.5-10 μm). Nevertheless, most of these links are experimental [302] with an exception of a very few commercial products [303]. In [304, 305], a survey of recent advances in the domain of QCL and its use in the development of FSO systems.

Although most terrestrial FSO links may be affected by the same impairments, link distance, day, and time during the day may influence the severity of the impairment. For example, an FSO link is affected by the sunlight which induces a shot noise at the receiver reducing the SNR. This impact is the highest during the sunrise and dawn when the Sun is co-linear with the FSO link (also called solar conjunction) [106, 306, 307].

The sway of tall buildings due to wind or seismic activity can result in a link misalignment which in turn causes a reduction of received power. The effect of building sway and deviation can be compensated for by diverging the transmitted beam so that it covers a large area around the receiver and hence the beam is received.

However, this technique results in a lower SNR as the beam power is distributed over a larger beam spot size. On the other hand, for high capacity, long range links APT systems can be used to compensate for the effect of building sway [74, 263].

The major limitation of OSC is the intensity attenuation due to the scattering of the transmitted beam. Since the performance of an OSC link is dependant on the geometry of the transmitter and receiver beams [308], one of the approaches to improve the received intensity in OSC is to apply beam shaping techniques using freeform lens. In [308], Zou et al. investigate the use of elliptical and rectangular beam reshaping instead of the conventional cone-geometry. It is found that both shapes can significantly improve the received signal with different degrees depending on the Tx-Rx angle pair.

Table 2.5 tabulates different impairments of terrestrial FSO links, causes, effects and solutions.

2.6.3 Terrestrial FSO Standards and Recommendations

The standards by IrDA, IEEE (802.11 and 802.15.7), and JEITA are mainly designed to address indoor OWC links. On the other hand, the International Telecommunication Union (ITU) is interested in standards and recommendations related to terrestrial OWC links. In particular, the ITU has released the Recommendations ITU-R P.1814-0 [306], ITU-R P.1817-1 [307], and ITU-R F.2106-1 [299]. Recommendations ITU-R P.1814-0 and ITU-R P.1817-1 are related to the propagation prediction methods for planning terrestrial FSO links operating in VL and IR regions of the spectrum, whereas ITU-R F.2106-1 is more focused on the planning of fixed service terrestrial FSO link.

ITU-R P.1814-0 and ITU-R P.1817-1

In [306], the power budget of generic LOS FSO link and the means of calculating the terms forming the power budget equation. The recommendation emphasizes the importance of the location selection taking into consideration different factors such as the weather conditions, physical obstructions, surface type along the path, and the transceiver mounting arrangements. Several sections are dedicated to discuss different weather factors that must be taken into consideration as the FSO link is planned. One of the factors to be considered while calculating the FSO link margin is the impact of the solar conjunction which occurs when the Sun is parallel to the optical link and the Sun projects high power inside the receiver that can can override the transmitted signal of the link. To avoid this effect, the FSO link transceivers must be arranged such that the sun is always off-axis. Due to the significant importance of the weather impact and impairments on the terrestrial FSO links, the ITU discusses different weather factors in the Recommendation ITU-R P.1814-0 and also dedicates the Recommendation ITU-R P.1817-1 to discuss different weather impairments in detail.

ITU-R P.1817-1

Recommendation ITU-R P.1817-1 provides a comprehensive discussion regarding the methods for predicting the propagation parameters required for planning FSO links. First, basic definitions and causes of atmospheric impairments such as; frequency selective absorption, scattering, and scintillation are explained and discussed. These basics are then followed by the a detailed discussion including equations, parameters, and variables of different factors that must be taken into consideration during the design of an FSO link such as; Molecular absorption and scattering, aerosol absorption and scattering, scintillation, rain attenuation, snow (wet and dry) attenuation, and

ambient light effect. The recommendation also discusses the visibility measurement at the maximum intensity of the solar spectrum (i.e., around 550 nm).

Appendix 1 of the Recommendation ITU-R P.1817-1 lists available computer modeling programs that can be used to determine the atmospheric transmission coefficient useful for the planning of the terrestrial FSO links such as LOWTRAN from ONTAR [309] which contains models of optical signal attenuation by aerosols.

ITU-R F.2106-1

In [299], the ITU recommendation sector released the report number F.2106-1 (2010) in which recommendations related to the fixed service applications using T/PC/LOS/F/x FSO links are discussed. Link ranges can vary from a few tens of meters to several kilometers depending on the equipment used and other factors such as weather conditions; clear-sky propagation, the effect of fog, rain, snow attenuation, ambient light attenuation, and scintillation.

Table 2.6: Space FSO Link Impairments.

Impairment	**Causes**	**Effects**	**Solutions**
Ambient Light	- Sunlight - Sunlight reflection from planetary surfaces. - Integrated starlight. - Zodical light.	Reduced SNR	- Increasing transmitted power. - Using optical filters.
Link Misalignment	- Narrow beams - Moving terminals - Terminals disorientation.	Link loss	- Automatic tracking system - Using optical filters.

Laser diodes (LD) are used with transmission power in the order of 10 mW. Wavelengths in the 1300-1500 nm and 780-800 nm ranges are used for FSO applications. These ranges are selected due to their small atmospheric absorption and the commercial availability of the corresponding devices from the optical fiber technology.

The wavelength range 2000-2200 nm that is part of the Short-wavelength Infrared

(SWIR) band is another convenient FSO transmission window due to the minimal aerosol scattering and molecule absorption as well as the reduced sensitivity to optical beam bending caused by atmosphere temperature variation [299]. Unlike the 1300-1500 nm and 780-800 nm bands, transceivers in this range were not widely and commercially available at the time this recommendation was released. This can be attributed to the fact that the enabling technology used in FSO was mainly adopted from the mature optical fiber technology [310]. Therefore, researchers were inclined to use off-the-shelf and readily available components used in fiber optics. Due to the limitations of the 2000-2200 nm band in fiber optics technology with respect to fiber absorption, optical components operating in this band were not widely used. However, as discussed in Section 2.6.2, recent advances in the enabling technologies have allowed the development of FSO transceivers operating in the SWIR (2000-2200 nm), as well as MIR [310] and LWIR [311] using the QCL technology.

2.7 Space FSO Links

FSO is an attractive alternative to RF inter-satellite-link (ISL) including intra- (e.g., LEO-LEO) and inter-orbit (e.g., LEO-GEO) links. In addition to the wide bandwidth and high data rate an FSO system can provide, FSO systems have lower antenna weight and size especially in the absence of atmospheric effects in space. Most of the space FSO links are of the type S/PC/x/x/ULong with link distances ranging from 15,000 to 85,000 km [251].

2.7.1 Space FSO Link Configurations

S/PC/LOS/M/x

An example of an S/PC/LOS/M/ULong ISL link is the Semiconductor Inter-satellite Link Experiment (SILEX) conducted by the European Space Agency (ESA) [214]. The development phase of an FSO system for an in-orbit demonstration started in 1991. In 1998, an Optical link between two geostationary (GEO-GEO) satellites was established at 50 Mbps [215]. Moreover, since 2003, SILEX system has routinely used a 50 Mbps LEO-GEO S/PC/LOS/M/ULong link twice a day [215].

Another example is the project Laser Communication Terminal on Terra-SAR-X (LCTSX) conducted by Tesat-Spacecom with funding support from the German Space Agency (DLR) [217]. In this experiment, a LEO-LEO coherent optical inter-satellite link with data rate up to 5.65 Gbps was demonstrated.

S/PC/NLOS/M

A good candidate for this FSO link configuration is the deep-space communication. Instead of transmitting the data using a direct link that goes from the probe to the ground station, a link can be relayed from the deep space probes to the ground station through data relay satellite system using FSO links. This allows the systems to exploit the low mass, power consumption and volume of the FSO systems as compared to that of RF technology which is the dominant technology [250, 312].

2.7.2 Impairments of Space FSO Links

Compared to the terrestrial scenario, space FSO links experience lower noise and impairments (Table 2.6). However, the space links are still susceptible to shot noise due to ambient light interference. There are several sources of external light such

as the sunlight, sunlight reflected off of planetary surfaces, integrated starlight, and zodiacal light.

As mentioned earlier, ISL distances can vary from 15,000 km in case of LEO-LEO links to 85,000 km in case of GEO-MEO links [251]. The ultra long range of the links is another critical impairment for ISL FSO links. This is because the longer the range, the higher the transmission power, size, mass, and cost. Moreover, alignment of the transmit and receive antennas must be maintained within 1μrad despite the vibration and the continuous movement of satellites and probes [313]. To this end, tracking servo loop must be used at both ends of the FSO link for laser beam *Acquisition, Pointing, and Tracking (APT)*. Control loops maintain the alignment using optical beacons using a dedicated laser beam or using the communication signal. In [3], Kaushal and Kaddoum present a detailed discussion of the challenges and mitigation techniques for OWC in space.

2.7.3 Space FSO Standards and Recommendations

IOAG.T.OLSG.2012.V1A

An Optical Link Study Group (OLSG) was established by the Interagency Operations Advisory Group-14 (IOAG-14) to assess the viability of a cross support in the FSO space communication domain. Various mission scenarios, including, Low Earth Orbit (LEO), Moon, Lagrange, Mars Space-to-Earth, and Earth relay, are defined and analyzed taking into account the effect of weather (clouds, optical turbulence, and other atmospherics) and aviation interference using 1550 nm and 1064 nm wavelengths. The aim is to determine the requirements for the ground terminal solution that maximizes the data return for the mission. However, since the number of ground stations required can be a substantial cost burden for a single agency, OLSG recommended

the cross support among agencies.

The highest priority for standards development was given to the standards for core services under development, core services that will lead to significant benefits (operational and/or financial), and for capabilities or services that were planned to be committed to flight operations or tracking networks starting September 2015.

2.8 Underwater FSO Links

Propagation of mechanical waves in the acoustic frequency band experiences less absorption in the underwater environment compared to other frequencies on the spectrum [314]. Consequently, acoustic technology became the dominant communication technology for UW communication systems. Underwater acoustic (UWA) can be used to realize long-range communication links. Recent research efforts aim to improve UWA communication links [315–318]. Despite recent advances, UWA links can experience significant latency due to the slow speed of sound in water (approximately 1500 m/s) [319]. Moreover, the propagation of UWA experiences multipath fading that leads to long delay spreads (10-100 ms). The delay spread, in turn, leads to significant ISI and thus UWA links have very limited data rates (less than 100 Mbps).

The need for higher data rates has pushed the researchers to consider other technologies for underwater communication. Although it seems reasonable to turn to RF communications given its maturity and advances in the terrestrial and space applications, RF propagation in the UW environment is severely limited compared to that in air and space due to the opacity of water with respect to electromagnetic radiation. The most popular example of UW RF communication link is the link used to communicate with naval submarines. In this system, the link operates in the extremely low

frequency (ELF) band (30-300 Hz). Using RF in the ELF range makes it possible for the signal to penetrate the water. However, this system has a very limited functionality as the data rate is very low that it cannot modulate voice, moreover, it requires extremely high transmission power and large antenna that cannot be installed on a submarine for a full-duplex operation. Therefore, such system is usually used to transmit basic messages from terrestrial bases to submarines. On the other hand, for a submarine to establish a reliable terrestrial RF communication link, the submarine must surface to use frequencies in the High Frequency (HF), Very High Frequency (VHF), or UHF bands.

There has been, however, a pressing need for even higher data rate UW communication links to fulfill the performance requirements by emerging applications such as UW wireless sensor network (UWSN). In UWSN, a network of distributed sensor nodes that can perform real-time spatiotemporal sampling and monitoring of climate change, biological, and ecological processes. The huge amount of data sampled and stored by the distributed nodes are then collected using unmanned UW vehicles [320, 321]. Data acquisition by the unmanned vehicles must be fast beyond the capabilities of acoustic and RF communication technologies.

On the other hand, the visible spectrum is less affected by the opacity of the water as compared to other EM frequencies. Moreover, recent advances in the OWC enabling technologies have triggered the re-evaluation of OWC as a solution for UW applications. This, in turn, led to the development of underwater OWC links at data rates up to 4.8 Gbps [225, 226, 230, 231]. This technology is widely referred to as *Underwater Optical Wireless Communication (UOWC)*. In this section, we discuss existing and recent research efforts in the UOWC domain.

2.8.1 Underwater FSO Link Configurations

It is found that, different water bodies have different turbidity levels, and thus different characteristics and impact on the light beam. There are different water bodies with different turbidity level. Therefore, it is crucial to investigate the properties of the water in which an UOWC system is to be deployed. This helps in the selection of the link parameters, including light source wavelength, modulation scheme, transmit power and link configuration. Good overviews of the properties of UOWC channels can be found in [134, 322–326].

In the following, we discuss different UOWC link configuration and summarize corresponding experiments. For each experiment, we highlight the type of water used.

UW/PC/LOS/F/x

Even though visible spectrum is less affected by the opacity of the water as compared to other EM frequencies, light penetration in the visible band is limited to a few hundreds of meters in clear waters (e.g., deep water) and even less in turbid water. Fixed LOS links can help overcome this limitation by avoiding losses and allowing maximum collection of incident light by the PDs resulting in high data rate transmissions. Therefore, UW/PC/LOS/F/UShort [66], UW/PC/LOS/F/Short [218–232], and UW/PC/LOS/F/Medium [233–238] are the most common UOWC link configurations.

We chronologically summarize the major UW/PC/LOS/F/x UOWC studies in Table 2.7. We summarize the highlight for each study, the type of light source and modulation technique used. We also list the type of water in which the experiment is conducted and the achieved data rate and link length.

Table 2.7: Summary of Major UW/PC/LOS/F/x UOWC Link Experiments.

Reference	Year	Experiment Highlights	Light Source	Modulation	Data Rate	Link Length (m)
Snow et al. [233]	1992	Lab experiments to measure the spatiotemporal properties of the laser pulses using large freshwater tanks, natural ponds, and coastal seawater.	LD	-	50 Mbps	18
Bales and Chrissotomidis [234]	1995	Two FSO communication links in clear dark waters. The first is between an Autonomous UW vehicle (AUV) and its docking station. The two units are mechanically attached facilitating an aligned (UW/PC/LOS/F) FSO link. The second link is established between two AUVs in the water.	LED (450 nm and 660 nm)	-	10 Mbps	20
Farr et al. [235]	2005	A 91 m link is realized in a 15 m deep pool using mirrors. And a dock experiment that is performed at night to minimize ambient light in slightly turbid water is performed to realize a 10 m vertical link.	LD	-	10 Mbps	100
Hanson and Radic [218]	2008	Error-free UOWC link in a laboratory water pipe with up to 36 dB of extinction.	LD (532 nm)	IM/DD	1 Gbps	2
Simpson et al. [222]	2010	A small, low-cost platform for UWSN is used in a lab experiment in which Maalox is used to vary the turbidity of the water.	LED	RS RZ	5 Mbps	3-7
Nakamura et al. [225]	2015	A lab experiment that involves an acrylic water tank and tap water.	LD (405 nm)	IM/DD-OFDM	1.45 Gbps	4.8
Oubei et al. [226]	2015	A $1m \times 6cm \times 6cm$ water tank is used. A link of 7m is realized using mirrors. High sensitivity Si APD is used to realize high data rate.	LD (520 nm)	16-QAM-OFDM	2.3 Gbps	7
Ren et al. [229]	2016	Orbital Angular Momentum (OAM) is employed to spatially multiplex optical channels.	LD (520 nm)	-	4 Gbps	
Xu et al. [230]	2016	Orbital Angular Momentum (OAM)	LD (red)	128-QAM-OFDM 32-QAM OFDM	1.324 Gbps (PIN) 4.883 Gbps (APD)	6
Kong et al. [238]	2017	WDM experiment in which RGB LD sources are used for transmission. The RGB sources achieved data rates of 4.17, 4.17 and 1.17 Gbps, respectively.	RGB LDs	32-QAM	9.51 Gbps	10
Al-Halafi et al. [232]	2017	A series of lab experiments to stream a high-quality video using a 5 m link in different water qualities.	LD (520 nm)	PSK and QAM	1.2 Gbps	5

Table 2.8: UOWC Link Impairments.

Impairment	**Causes**	**Effects**	**Solutions**
Ambient Light	The Sun near water surface	Reduced SNR	- Increase transmitted power - Using optical filters
Attenuation	intrinsic absorption and scattering	- Reduced SNR - Intersymbol Interference (ISI)	- Experimentally select appropriate wavelength for minimum absorption. - Higher transmitted power - Spatial Diversity - Equalization - FEC
Scintillation	Water turbulence and temperature variation	NA	NA

UW/PC/LOS/M/x

The success of the terrestrial modulating retro-reflectors (MRR) T/PC/LOS/M links have motivated researchers to consider deploying the technology in the UW environment [239–242]. As mentioned earlier in Section 2.6.1, MRR can help relax the pointing and tracking requirements which is essential for a link with a mobile transmitter and/or receiver. Moreover, MRR helps reduce the payload and power requirements at one of the link ends. This can be utilized in UW applications such as UWSN where SNs are of limited power, or in UW exploration with moving divers to communicate with a submarine.

Similar to all UOWC links, the quality (range and capacity) of an MRR link depends mainly on the type of water in which the link is deployed. In clear water, the link quality depends on the number of photons collected by the detector. To maximize the link range and capacity, relatively finer pointing and tracking is required. On the other hand, in case of turbid water, backscattering is the major limitation of the link quality. In [239] and [240], Mullen et al. present polarization discrimination technique to alleviate the impact of backscatter on UW/PC/LOS/M/Short MRR links. Experimental results show significant reduction in the backscatter component in an MRR channel.

A MEMS-based blue/green Fabry-Perot modulator for MRR link is proposed by Cox et al. [241]. Experiments are performed in a 7.7 meters long water tank. The turbidity of the water is varied by adding Maalox. UW/PC/LOS/M/Short MMR links at 1 Mbps and 500 kbps data rates are achieved at 2.7 and 5 attenuation lengths, respectively. On the other hand, error-free MRR links are realized at 6.5 and 3.8 attenuation lengths for 500 kbps and 1 Mbps, respectively, after deploying Reed Solomon error control code (ECC).

In [242], Rabinovich et al. present a theoretical UOWC MRR link budget in

natural waters. The authors also perform experimental tank measurements to verify the theoretical model.

UW/CC/LOS/x

As mentioned earlier, to achieve high data rate in UOWC, UW/PC/LOS are preferred. Therefore, less attention has been directed towards UW/CC/LOS as compared to UW/PC/LOS UOWC links.

In [243], Cochenour et al. present an experiment in which a diffuser is used to diffuse the light of a 532 nm LD to establish a UW/CC/LOS/Short link. A 20° full angle beam in 7.72 meters long water tank was realized and impulse response measurement at different modulation frequencies up to 1 GHz are performed. It is found that, in clear waters, the diffuse link requires > 30 dB more optical power than the collimated source to achieve a similar signal level at the receiver. Although, they used a single receiver, the experiment description suggests that other receivers can be deployed in the coverage area of the diffused transmitted beam allowing a cellular coverage link.

In [244], Pontbriand et al. demonstrate one-way broadcasting UW/CC/LOS/Medium UOWC links. Two different receiver configurations are used; large omnidirectional and small with flat window. Multiple experiments are performed in deep clear water (in Bermuda at depths of 1-2 km) and in the shallow turbid water off a dock. For the experiments in Bermuda, only the large receiver arrangement is used. Link distance is varied from 75 m to 200 m. The clarity of the water resulted in a clear channel with high SNR and a 5 Mbps is established despite the background light from bioluminescence and Cerenkov Radiation. Links with data rates ranging from 1 to 4 Mbps are realized during dock tests.

UW/CC/NLOS/x

An UW/CC/NLOS/x link can be used to establish a link in the absence of a LOS link due to obstructions, misalignment, or random orientation of the transceivers. In UW/CC/NLOS/x, a transmitter emits a wide beam in the upward direction. As the light reaches the water-air surface, an annular area is illuminated and the light partially bounces off of the water surface. A careful selection of the incidence angle along with the fact that the refractive index of water is higher than that of air can lead to total internal reflection. A turbulent sea surface forms a challenge for this link model since light can reflect back to the transmitter instead of the intended receivers.

UW/CC/NLOS/x UOWC links can be used for underwater ranging and imaging [245–247]. For example, a transmitter can detect the water quality by detecting the backscattered light from its own transmission without the need for a back-channel [246] enabling the transmitter to change its operating parameters such as transmit power, data and code rates.

In [245], Alley et al. propose an UW/CC/NLOS/Short imaging system. In the proposed system, a 7.7 m diameter water tank is used. An LD illuminator (488 nm or 530 nm) is placed close to the target object to eliminate the majority of the forward and backscatter that occurs on the way to the target. Water turbidity is varied from very clear water to most turbid by adding Maalox to the tank. Images from both LDs have high contrast and SNR in case of clear water. As the turbidity increases, the contrast and SNR degrades. In the most turbid water, images based on both LDs maintained the resolution. However, the 530 nm images have better contract and SNR as compared to those of 488 nm. This is because the tank water had a higher attenuation coefficient at 488 nm. Compared to conventional LOS imaging systems, the UW/CC/NLOS imaging system proposed by Alley et al. demonstrated improvements with respect to the SNR.

UW/CC/NLOS/x links can also be used to establish communication between separate transmitters and receivers. In [248], Arnon et al. analyze the use of UW/CC/NLOS/Medium links in the context of UWSNs. In this scenario, the LOS links between a transmitter and a set of distributed WSN nodes are not available.

2.8.2 Impairments of UOWC Links

An UOWC link is affected by three main impairments, namely; ambient light, attenuation (due to intrinsic absorption and scattering), and turbulence [81,327–331]. The impairments of UOWC links are summarized in Table 2.8. Near the surface, sunlight can result in a strong background signal that needs to be filtered [314]. Moreover, the amount of wave action can have significant effects on the performance of the UOWC link.

UW environment imposes some constraints on the used wavelength. For example, it is found that red and IR parts of the spectrum suffer higher light absorption in *clear* water, whereas blue light (400-450 nm) experience minimal absorption. However, this is not necessarily true in all cases since aquatic particles like chlorophyll, algae, or plankton can alter the absorption patterns leading to minimal absorption at different wavelengths. Therefore, experiments must be conducted to determine the optimal wavelength for the given application [332].

A light beam in the UW environment suffers *Attenuation* when it loses its intensity due to intrinsic *absorption* and *scattering* [328]. Attenuation in shallow water can be severe as compared to that of deep clear ocean water. In pure seawater, attenuation is dominated by absorption. Closer to land, scattering dominates the attenuation coefficients due to the organic matters. Scattering is the redirection of incident photons into new directions preventing the forward on-axis transmission. This in turn, reduces the light intensity and leads to reduced SNR and inter-symbol-interference

(ISI) [327].

Similar to atmospheric OWC links, UOWC links require the development of efficient transmission techniques to overcome environmental challenges such as turbidity. Therefore, the physical and data link layers must be equipped with energy-efficient modulations and powerful channel codes [81]. Moreover, localization and beam alignment can be challenging in the UW scenario and require careful design consideration.

From the above discussion, it is obvious that the limitation of the acoustic and FSO technologies does not qualify any of them as an efficient standalone technology. Therefore, and as we will discuss in Section 2.10, FSO, and acoustic communication technologies are usually operated in a complementary (or hybrid) fashion.

2.8.3 Underwater FSO Standards and Recommendations

There are no initiatives or standardization efforts related to the FSO technology in the underwater environment, to the best of our knowledge. In 2015, Yeong Jang, the chairman of IEEE 802.15.7r1, presented a discussion with the title: "Current Status of IEEE 802.15.7r1 OWC Standardization" in the "International Conference and Exhibition on Visible Light Communications 2015" [333]. In this discussion, Jang discusses the different aspects of the OWC Technology and different related applications/use cases including; A5-Underwater Communication using image sensor communications and C1-Underwater/Seaside Communication using low-rate PD communications.

2.9 Heterogenous FSO Links

An FSO communication link may traverse multiple environments in some applications. In this case, we refer to this optical link as a *heterogenous FSO link*. In a

heterogenous FSO link, different segments of the link experience different impairments based on the environment, however, the overall link is affected by all of these impairments. In the following, we discuss few examples of hybrid FSO Links:

2.9.1 Inter-Buildings Links $(\{I-T\}/PC/LOS/F/x)$

The transceivers of a terrestrial FSO link connecting two buildings can be mounted either on rooftops or behind windows [263]. There are additional costs to rent or acquire a permit to place links on top of buildings. Moreover, directing received signals on top of the building to the desired floor can be a tedious process. However, the small-sized and light weights of FSO system components as compared to that of equivalent RF technology allows for housing the transceivers in buildings.

In the case of the rooftop, the link is considered purely terrestrial. On the other hand, placing FSO transceivers behind windows means that a small segment of the link is indoor while the main part of the link is terrestrial. Therefore, in addition to the atmospheric impairments, the indoor part of the link may have an impact on the overall link performance. For example, the receiver might be affected by artificial ambient light or losses due to the propagation through the windows.

2.9.2 Space-Air/Ground Links $(\{S-T\}/PC/LOS/x/ULong)$

FSO communication links between earth stations and spacecraft or satellites in the space is one of the most popular FSO link configurations. A chronological summary of successful heterogenous (space-ground) FSO demonstrations between 1992 and 2016 is listed in Table 2.9.

Most existing ground-space FSO demonstrations utilize ground-based transceivers. Therefore, a portion of the link must propagate through the atmospheric channel and the designers of the link must take this into consideration [251]. Communication sys-

Table 2.9: Summary of Major Space and Heterogenous (Ground-Space) FSO Link Experiments.

Program's Name	**Year**	**Performing Organization(s)**	**Experiment Summary**
Semiconductor Inter-satellite Link Experiment (SILEX)	1991	European Space Agency (ESA).	Started the development phase of an optical communication system for an in-orbit demonstration [214].
Galileo Optical Experiment (GOPEX)	1992	California Institute of Technology Jet Propulsion Laboratory (JPL).	Uplink optical communication to Galileo spacecraft by Earth-based transmitters. A 532 nm laser was used [257].
Laser Communication Experiment (LCE)	1995	CRL and JPL	A space-to-earth bi-directional link was established from the GEO ETS-VI and a ground station outside of Tokyo [109, 258].
Semiconductor Inter-satellite Link Experiment (SILEX)	1998	ESA	LEO-LEO and GEO-LEO FSO links were established. 800-850 nm wavelength range, 2 Mbps modulation capability on forward link 50 Mbps data rate on return link [214].
Geosynchronous Lightweight Technology Experiment (GeoLITE)	2001	U.S. DoD	A successful Multi-Gbps link from GEO orbit [258]. GeoLlTE mission details are classified [109].
Mars Laser Communication Demonstration	2004	NASA's Goddard Space Flight Center (GSFC), JPL, and Massachusetts Institute of Technology Lincoln Laboratory (MITLL)	The project demonstrated at rates in the order of 1 to 80 Mbps [258]. This proves that FSO can improve NASA's ability to communicate with astronauts and planetary sensors, in the future, at high data rates [216].
Lunar Reconnaissance Orbiter (LRO)	2013	NASA	The first one-way laser planetary distance communication demonstrated by NASA to beam an image of the Mona Lisa to the LRO over a 385,000 km FSO link. The Lunar Orbiter Laser Altimeter (LOLA) instrument on the LRO received and reconstructed the image. Reed-Solomon error correction code is used to overcome the atmospheric impairments [259].
Optical PAyload for Lasercomm Science (OPALS)	2014	JPL	NASA transmitted "Hello, World!" high-definition video from the International Space Station (ISS) using FSO on Thursday, June 5. The transmission was at rate of 175-megabit [261, 262].
Laser Communications Relay Demonstration (LCRD)	2016	GSFC, JPL, and MITLL	NASAs first, long-duration FSO mission. The aim of the mission is to mature concepts and technologies for future near-Earth and deep space communication network missions [82]

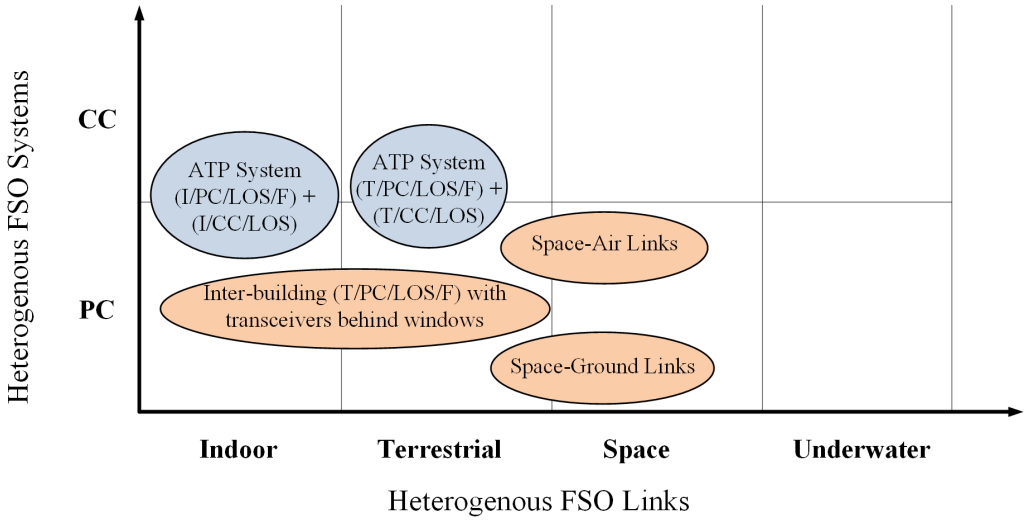

Figure 2.10: Difference between heterogenous FSO links and heterogenous FSO systems.

tem from low earth orbit (LEO) military satellite to mobile troops using Acquisition, Pointing, and Tracking (APT) systems are discussed in [249].

It might be noted that there are different considerations and design requirements for the uplink (i.e., ground-to-space) as compared to that of in downlink (i.e., space-to-ground). For example, similar to RF systems, a power on a space terminal is limited, whereas, a power on the ground is relatively unlimited. Another example that is more specific to the FSO systems is that in the downlink, a beam starts in a space environment where there are no impairments until the last 30 km where the beam is affected by the terrestrial impairments. On the other hand, in uplink, a beam starts in terrestrial (or atmospheric) environment which affects the beam until it cuts the first 30 km. This distorted beam will cut the longer distance in the space to get to the station [334]. The turbulence and the quality of the wavefront that is propagating in the atmosphere is characterized by the atmospheric coherence length [251]. The atmospheric coherence length depends on several factors, including, aperture area and resolution of the telescope, location, time during the day (nighttime is preferred).

Analysis shows that in a space-ground FSO link the satellite (uplink) experiences large atmospheric coherence length whereas ground station receiver (downlink) has smaller atmospheric coherence length and severe phase distortion [251]. The smaller coherence length and severe phase distortion experienced by the downlink beam can lead to large received signal spot size at the focal plane of the ground receiver. To be able to capture most of the signal photons, large surface photodetector must be used. However, using large photodetector limits the electrical bandwidth of the receiver, and thus, the ability to detect high data rate signals. To overcome this problem, adaptive optics or array detectors [3, 251].

Currently, many commercial airlines started to equip their fleets with real-time high-speed Internet access using RF communication systems. Most of these services are provided using ground-based access network. For example, US provider GoGo [252] has built a network of 3G ground stations all across the US, and planes communicate with these stations as they fly over. Although GOGO's system is simple to implements, the system has a very limited bandwidth of 3.1 Mbps per plane. Since most aircrafts have cruise altitude above the cloud layer, it is possible that FSO links from satellites provide high-speed service avoiding severe atmospheric impairments [250]. The legacy L-band technology is slow and relatively expensive. On the other hand, higher-frequency Ku-band (12-18GHz) satellites are relatively economical and more efficient. Lufthansa's FlyNet system [253], for instance, claims download speeds to the aircraft of up to 50 Mbps.

Table 2.10: Classification of Heterogenous and Hybrid FSO Systems Using the Proposed Framework.

Application	FSO System Type	Classification of Links	
		FSO Link	Non-FSO Link
Indoor Tracking Systems	Heterogenous	I/CC/LOS/Short I/PC/LOS/M/Short	-
Outdoor Tracking Systems for HSTs [335]	Heterogenous	T/CC/LOS/Long T/PC/LOS/M/Long	-
Relay-assisted network using UAVs [336]	Heterogenous	T/PC/LOS/F/Long T/PC/LOS/M/Long	-
card-to-card FSO/optical [337]	Hybrid	T/PC/LOS/F/UShort	Fiber
Backhaul RF/FSO Links	Hybrid	T/PC/LOS/Long	RF
Underwater Sensing	Hybrid	UW/CC/LOS/Short	Acoustic
Loon [338]	Hybrid	T/CC/LOS/Long T/PC/LOS/M/Long	RF
Internet.org [339]	Hybrid	T/PC/LOS/M/Long	RF

2.10 Classification of FSO Systems Using the Proposed Framework

In previous five sections, we discuss indoor, terrestrial, space, and underwater FSO links. We also discuss "heterogenous FSO links" in Section 2.9. In this section, we focus our discussion on two types of FSO systems, namely; *Heterogenous* FSO systems, and *Hybrid FSO/x* Systems.

Before we discuss FSO systems in details, we need to understand the difference between "heterogenous FSO links", "heterogenous FSO systems", and "hybrid FSO systems". We use Figure 2.10 to understand the difference between heterogenous FSO systems and links.

In heterogenous FSO links, a single FSO link spans multiple environments. For example, in case of Space-Air/Ground FSO links discussed in Section 2.9.2, a single transmitted FSO beam will propagate through a terrestrial channel, and then propagate through a space channel (or vice versa). In Figure 2.10, horizontal axis represents the different environments an FSO link can propagate through, whereas the vertical axis shows different configurations of FSO links in the four environments. We can see several examples of heterogenous FSO links that span two environments.

A heterogenous FSO system is a system that operates in a single environment, however, utilizes multiple link configurations to realize a more efficient system that could not be achieved using only one of the link configurations. Figure 2.10 depicts an example of a heterogenous FSO system which we will discuss in more details in the next section. As we can see, there is a system that operates entirely in the indoor environment. However, the system utilizes two link configurations; I/PC/LOS/F and I/CC/LOS.

It is important to note that although the environment is consistent, and the link

configurations are different, the heterogenous FSO system employs only FSO technology. Unlike heterogenous FSO systems, hybrid FSO/x systems are systems in which FSO is used with another technology (x) together to realize an improved communication system.

Table 2.10 summarizes the examples of the FSO systems to be discussed in this section.

2.10.1 Heterogenous FSO Systems

As mentioned earlier, x/PC/LOS/F/x FSO links provide high bit rate links for fixed users. If a high bit rate link is to be established for a mobile user x/PC/LOS/M/x links are used. However, establishing and maintaining a PC/LOS link with a mobile user can be challenging. On the other hand, x/CC/LOS/x links utilize wider beams and can cover a wide area which can help to relax the pointing and tracking requirements. However, this usually comes at the cost of reduced bit rate.

One of the most common examples of heterogenous FSO systems is the use of x/PC/LOS/M/x and x/CC/LOS/x together to establish a high bit rate link with a mobile user. This approach is one of the Acquisition, Tracking, and Pointing (ATP) mechanisms used to establish FSO link with mobile users [71]. ATP can be used for indoor, terrestrial, space, and can also be used for heterogenous FSO links.

In [340], Wang et al. have utilized an I/CC/LOS/Short link for user localization and I/PC/LOS/F/Short link for high bit rate with the user. In particular, when a user moves, localization steers the mirror and high bit rate is maintained.

In Section 2.6.1, we discuss the application high speed trains (HSTs) in which OWC-enabled BSs along the side of the railway tracks are used to provide the coverage and Internet access for passengers onboard the HST. The BSs are deploying wide beams that cover a long distance of the railway tracks leading to a simple im-

plementation of the system that does not require sophisticated pointing and tracking mechanisms. A different approach to achieve the same objective is to employ ATP to maintain the LOS link between the BSs and the transceivers on the train. In [335], Urabe et al. present an OWC heterogenous system in which I/CC/LOS/Long and I/PC/LOS/M/Long links are used to achieve 1 Gbps links to HSTs with a handover time in the order of 100 ms.

In [336], Fawaz et al. present relay-assisted network using UAVs equipped with buffers. In the proposed network, in addition to existing regular T/PC/LOS/F/Long relayed links, a UAV that is either stationary or flying between the sender and receiver can be used to establish T/PC/LOS/F/Long or T/PC/LOS/M/Long sender-UAV and UAV-receiver links. The links range from 1.5 and 3 km. The results showed the improvement in the performance with respect to packet delivery.

2.10.2 Hybrid FSO Systems

Different communication systems can be integrated together yielding an improved system that utilizes the advantages of both integrated systems. For example, in [341–343], Wang et al. incorporate high bandwidth I/PC/LOS/M/Short FSO links with RF system that is mainly used for user localization within the room.

In [337], Wang et al. demonstrate a high-speed reconfigurable card-to-card optical interconnect architecture that utilizes an I/PC/NLOS/F/UShort FSO links along with multi-mode fiber (MMF). The authors realized 3×10 Gbps optical interconnects despite the air turbulence from the fans cooling the board.

FSO links can be independently deployed in several terrestrial applications including last-mile access and back-haul networks [344]. Combining FSO and RF technologies to realize heterogeneous RF/FSO links can lead to higher-rate and more reliable communication. Single-hop RF/FSO systems consisting of two separate RF and FSO

links are widely investigated [345,346]. In this type of systems, A T/PC/LOS/F/Long FSO link is used for high-bit rate transmission as long as the weather permits, in case of severe weather, RF link acts as a backup. In other cases, both links can operate simultaneously to improve the overall performance of the system and in case of severe weather, the system performance degrades to the lower-bound of single RF link system. Similarly, multi-hop RF/FSO systems are also being investigated [347].

Acoustic communication system dominates the UW communication, therefore, it is possible that acoustic systems are used along with FSO in order to utilize the outreach of the acoustic system, and high bit rate of the optical systems. For example, since acoustic signals are capable of long-range low data rate communication, they can be used in UWSNs for localizing sensor nodes. Moreover, distance between nodes can be accurately determined due to the slow speed of sound which leads to accurate signal timing. Several experiments in the literature demonstrate heterogeneous communication systems where acoustic communication is used side by side to FSO communication systems [348, 349]. Short-range LOS FSO link is usually used for data transfer at high data rates, whereas, the acoustic signal is used for signalling and transmission of short messages. In [350], Vasilescu et al. presented a heterogeneous system with mobility along the transmitters LOS. UW/CC/LOS/Short FSO communication link is realized within a 90° cone with a range of 2-8 m. The acoustic link used for broadcast at lower data rates of 330 kbps and distances over 400 m.

Other examples of hybrid FSO/RF systems are the Loon project by Google [351] and Facebook's Internet.org project [339]. The objective of both projects is to provide Internet connectivity to people having no (or limited) Internet connectivity in unreachable and underdeveloped regions [71]. To this end, High Altitude Platforms (HAP) located 20 km above the earth's surface on the stratosphere are to be used. At this altitude, LOS connections can be established. Moreover, the atmospheric

impairments at this altitude are minimal.

In case of Loon project, the HAPs are balloons. The balloons are designed to endure the harsh conditions in the stratosphere [338]. At the stratosphere, winds can blow over 100 km/hr, the balloons are not protected against UV radiation and must endure temperature swings of 150° and temperature going as low as -90° [352]. Balloons are launched using a special launcher capable of launching a balloon every 30 minutes [352]. To control the balloons movement, the altitude of the balloon is controlled to utilize the stratified winds in the stratosphere. As the balloon enters different strata, the balloon will be carried at different speed and direction as desired and designed using specialized algorithms that can navigate the balloons. For the communication purposes, each balloon is equipped with three modules; an LTE module and two FSO modules. The LTE modules is used to communicate with the terrestrial base station that is connected to the internet. The LTE module is also used to connect with and carry the data to/from the mobile users in the unreachable and underdeveloped regions. To relay the data to/from the balloon that is connected to the base station, balloons utilize the FSO modules to communicate with each other. Loon system deploys a heterogenous FSO system in which a wide beacon beam T/CC/LOS/Long along with T/PC/LOS/M/Long are used for the realization of ATP for the moving balloons.

Unlike Loon project, Internet.org project deploys high-altitude solar-powered drones, LEO, and GEO satellites. All terminals are equipped with RF and FSO transceivers. Similar to Loon project, RF modules are used to communicate with the terrestrial base station, and communicate with the mobile users. FSO T/PC/LOS/M/Long links are used for inter-drone links that relays the data between the base stations and the mobile users. LEO and GEO satellite serve the same purpose of covering unreachable regions.

2.10.3 Case Study: LiFi-Based Systems

Hybrid FSO system is expected to be the working model of the 5G and next-generation wireless systems since RF is falling short in fulfilling the requirements of such next-generation networks alone. LiFi is a network that is based on VLC communication. LiFi offers dual-functionality to transmit data using optical sources (illumination concurrent with data communication) [168].

In [353], Ayyash et al. present general characteristics of heterogeneous (LiFi + WiFi) network and develop a framework in which LiFi and WiFi technologies coexist. The network consists RF macrocells, RF small cells (RF-SCs), and optical small cells (O-SCs). The system discussed in [353] is a *hybrid FSO/RF* system. Each of the LiFi luminaires (lights) is an *I/CC/LOS/Short* link model. It may be noted that *I/PC/LOS/F/Medium* FSO links can be used to form the backhaul network and connect different BSs in a large room instead of wires. A network of nodes equipped with the LiFi receivers can be supported by this network which makes this network very suitable for the IoT model.

2.11 Summary

FSO communication links can be deployed in indoor, terrestrial, space, or underwater environments. Depending on the environment, an FSO link experiences different impairments that impact its performance. Even for the same environment, different link configurations can be affected differently by the noise and impairment source, therefore, it is crucial to be able to differentiate link configurations.

This chapter presents a simple, yet powerful classification scheme of FSO technology. In this scheme, an FSO link can be classified as a combination of four different criteria, namely: Environment (ε), Coverage Type (κ), LOS Availability (α), Mobil-

ity (μ), and link distance (δ). An FSO link can be deployed in an indoor, terrestrial, space, or UW scenario. The link can be either a point or cellular coverage which can be realized using a LOS or NLOS link. Furthermore, a link can be fixed or mobile. Using the discussed four criteria, we were able to develop a generic classification that can be used to categorize different FSO links including recently evolving schemes in which other classifications in the literature fall short. In particular, the proposed classification scheme describes any FSO link configuration as a tuple ($\varepsilon/\kappa/\alpha/\mu/\delta$).

We discuss all possible FSO link configurations in the four different environments. We provide examples for each FSO link configuration by listing selected recent references and related research efforts. Moreover, we briefly discuss the impairments experienced by each link type and their possible solutions.

We also discuss heterogenous FSO link that spans multiple environments. Several examples including the earth-space communication links have been discussed. A heterogenous FSO link experiences a combinatorial effect due to the different environments.

Unlike heterogenous FSO *link*, a heterogenous FSO *system* might incorporate two or more FSO link configurations in order to improve the system performance combining different links advantages. On the other hand, a hybrid FSO system is a system in which one or more different communication technologies are used along with FSO systems. Examples of each type of systems are provided and discussed.

We use the proposed classification scheme to review existing FSO standards and recommendations. IrDA has produced a set of standards aiming for high data rate short FSO links. JEITA CP-1221, CP-1222, CP-1223, IEEE 802.15.7, and IEEE 802.15.7r1 standards are designed for short/medium range VLC supporting low data rate links. On the other hand, limited efforts are directed towards standardizing terrestrial, space, and underwater FSO links. For example, a single recommendation

for terrestrial FSO links, ITU-R F.2106-1, was proposed by ITU.

We can conclude that the FSO is increasingly becoming an attractive technology for emerging and future communication systems and applications. This holds true for either FSO as a stand-alone technology (as envisioned by NASA in its future space applications), or as a complementary technology (future wireless systems and in UW applications). This chapter presents an attempt to use a simple and powerful classification system to jump-start researchers to tap into the growing and expanding the realm of the FSO technology in indoor, terrestrial, space and UW environments.

Chapter 3

Wireless Data Center Networks

In this chapter, we compare the free space optical (FSO) communication and the 60 GHz radio frequency (RF), the two key candidate technologies for implementing wireless links in DCNs. We present a generic classification scheme that can be used to classify current and future DCNs based on the communication technology used in the network. The proposed classification is then used to review and summarize major research in the area of wireless DCNs.

3.0.1 Motivation and Scope

Most existing DCNs can be classified as wired DCNs in which copper and fiber cables are used for networking. Wired DCNs received an increasing attention in the DCN research community evident by the increasing number of papers and surveys that discuss, analyze, and motivate new developments in wired DCNs (see for example [34, 354–356]).

As discussed earlier, the need for developing adaptive DCNs has motivated the research community to investigate the feasibility of incorporating wireless technologies in DCNs. As a result, several research papers on wireless DCNs have been published.

A few recent survey papers on wired DCNs only briefly discuss the deployment of 60 GHz RF technology in DCNs [34, 354–356]. On the other hand, a recent survey paper that exclusively focuses on the topic of wireless DCNs was published early 2015 [357]. Similar to the survey papers on wired DCNs [34, 354–356], Baccour et al. [357] focus their discussion only on deploying the 60 GHz RF technology in DCNs. In [358], we focus our discussion on DCNs using FSO. We analyze existing indoor FSO standards and the challenges that may face the DCN designers. We also identify standardization needs and opportunities to help accelerate the development of FSO links for DCNs.

From the above discussion, we make the following observations:

1. DCN design space is reshaping as new technologies for networking are deployed, and there is a current need to rethink the design philosophy of DCNs. Therefore, a classification scheme that can formally express the changes in the DCN design space is required to help identify new DCN designs.

2. Deploying 60 GHz and FSO technologies in DCNs encounter different design requirements and challenges. However, as we will show in Section 3.1, there are many similarities between the two wireless technologies. Therefore, we believe that the development of DCNs using one of the technologies can significantly benefit from the other.

In the absence of a systematic description of the DCN design space evolution, it can be difficult for researchers to fully explore the DCN design space and identify potential designs. This motivates us to develop a new survey to collate and present current advances in wireless DCNs in a systematic fashion to facilitate the sharing of knowledge among researchers using different wireless technologies to develop wireless DCNs. We propose a classification that can be used to classify existing and emerging

wired and wireless DCNs. Based on this classification, we survey current state of the art of wireless DCNs. We review the requirements, challenges, and trends using 60 GHz RF and FSO technologies. The proposed classification leads to a nearly complete picture of the design space for DCNs. This help us to identify potential unexplored solutions for next-generation DCNs.

3.1 Potential Wireless Technologies in DCNs

In this section, we discuss two candidate wireless technologies, 60 GHz RF and FSO, that can be used in wireless DCNs. We compare their attributes, advantages, and disadvantages. We also compare FSO and optical fiber since they both are optical technologies. For the sake of completeness, we first give a brief introduction on wireless communication systems.

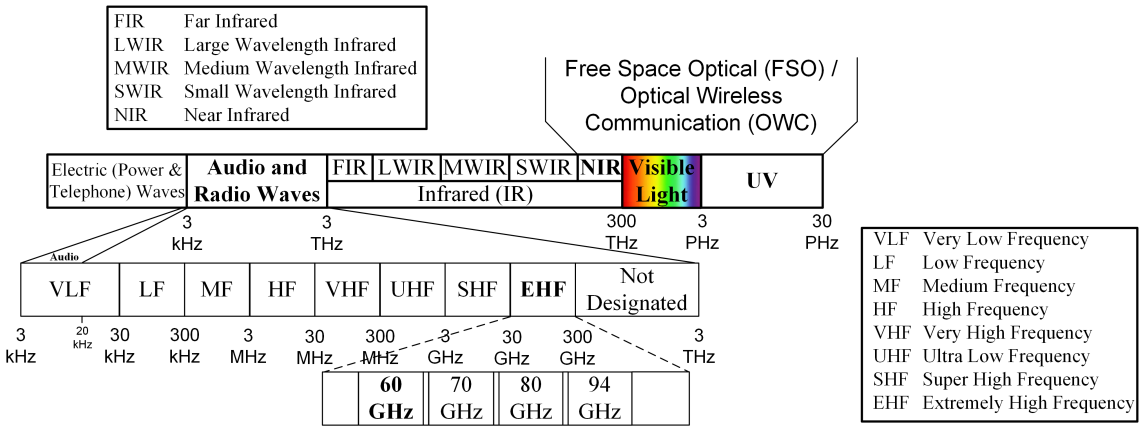

Figure 3.1: Electromagnetic Spectrum.

3.1.1 Basics of Wireless Communication

Wireless communication is one of the active areas of research in the communication field today. In wireless communication, information is transferred from the trans-

mitter to the receiver without the need for a confined medium (e.g., cable). Figure 3.1 depicts part of the electromagnetic (EM) spectrum. The wavelength of a signal decreases as the frequency increases and different frequencies across the EM spectrum have different propagation properties. According to Friis law, the effective area of an antenna decreases as frequency squared.

Audio frequencies extend from 3 kHz to 20 kHz in the very low frequency (VLF) band, whereas radio frequency (RF) occupies a very wide range of spectrum (20 kHz - 3 THz). Depending on the nature and requirements of the application, a suitable carrier RF frequency is selected. For example, radio waves have limited propagation capability in electrical conductors such as salt water due to absorption, and thus very long wavelengths (i.e., very low frequency and very large antenna) is required. Therefore, ground-to-submarine communications utilize audio waves, or RF in the VLF band which can penetrate only up to 20 meters below sea surface. On the other hand, IEEE 802.11b/g/n (WiFi) wireless local area networks require worldwide compatibility and moderate capability of penetrating windows, walls, and ceils. Therefore, the unlicensed 2.4 GHz UHF and 5 GHz SHF industrial, scientific, and medical (ISM) radio bands are utilized to realize short and medium range links in homes and offices.

When the term wireless communication is mentioned, conventionally, RF technology is the first to come to mind since it is a well-developed mature technology. However, recent advances in FSO technology have narrowed the gap between FSO and RF technologies. FSO technology can operate in a wide range of spectrum, including invisible infrared spectrum (used by optical fiber technology), visible light, and ultraviolet [359]. This helped FSO to be successfully used in a wide range of applications. Examples of applications in which FSO technology has already found its place are, mobile networks backhaul [81], space communication [82], underwater

sensing [84], and wireless sensor networks [211]. Moreover, it is envisioned that the 5G wireless communication systems will incorporate several complementary access technologies along with the RF technology, including FSO [75].

3.1.2 60 GHz RF Technology

Millimeter wave (mmWave) RF communications operating in the millimeter band (30-300 GHz) is rapidly advancing. Most of the current research is focused on the 60 GHz band and the E-band (71-76 GHz and 81-86 GHz) [27, 41, 360, 361]. The unlicensed spectrum of the mmWave communications makes it possible to launch products world-wide. Moreover, the extremely high frequency and the large spectrum of the mmWave band allow for high bandwidth short range links. The characteristics of the mmWave communications urged the researchers to consider the mmWave RF technology in the next generations of wireless communication systems (e.g., 5G) to provide multi-gigabit communication links [362].

The 60 GHz band is a 7 GHz wide unlicensed band of spectrum (57-64 GHz). Although unlicensed, recent standards, such as IEEE 802.11ad are developed to standardize very high data rate transmission at 60 GHz. Operating at 60 GHz has unique characteristics compared to other RF technologies, such as the ISM band at 2.4 GHz and ultra wide-band (UWB), for providing link connectivity in DCNs [4, 27, 41]. For example, the bandwidth of the 60 GHz band is 88× that of the ISM band at 2.4 GHz (80 MHz wide) which supports the IEEE 802.11b/g/n (WiFi) networks [27].

The large available spectrum in the 60 GHz range allows for a large number of independently operating directional links. Moreover, advances in modulation and coding techniques help improve spectral efficiency, and thus, even larger number of links can be provided using the same bandwidth. For example, a 1 Gbps link can be achieved using 100 MHz channel and spectral efficiency of 10, that is 70 orthogonal

Table 3.1: Comparison Between 60 GHz RF and FSO Wireless Technologies for DC Application.

Property of Medium	**60 GHz RF**	**Indoor FSO**	**Implications & Comments**
Bandwidth Regulated?	No	No	• Approval not required. • Worldwide compatibility.
Obstacle Penetration?	Yes (very limited)	No	• Good security attributes for FSO and 60 GHz technologies. • Limited coverage, and thus LOS point-to-point links are required.
Radio Frequency Interference	Yes	No	• FSO has better frequency reuse • Higher Overall System Capacity using FSO.
Path Loss[a]	High $\approx$ 68 dB for 1 m $\approx$ 91.5 dB for 15 m	Low $\approx$ 0 dB for 15 m	
Range/Coverage	Short ($\leq$ 15 m)	Medium [b] ($\leq$ 100 m)	Suitable for DC's confined space
Dominant Noise	Interference and thermal noise	Ambient artificial light	
SNR Proportional to	Signal amplitude	Signal power	High transmitter power requirement by FSO systems.
Technology Cost	Potentially Low	Potentially Low	

[a]Path loss is calculated for point-to-point LOS link.

[b]Longer FSO links can be realized using higher transmitted power and more sophisticated transceivers such as in outdoor and space FSO links.

channels using the 7 GHz bandwidth of the 60 GHz technology. This large number of channels, along with careful design can provide the level of scalability required for wireless mega DCN.

The high frequency of 60 GHz facilitates compact antennas with high gain. For example, a one-square inch (6.5 cm^2) antenna can provide a gain of 25 dBi at 60 GHz. Moreover, short wavelength of 60 GHz enables the design of sophisticated interfaces and the use of phase array antennas with a large number of elements of very small form factors [4]. Increased number of antenna elements in a phased array helps achieve highly directional beams with small footprints, thereby increasing the number of simultaneous transmissions.

3.1.3 FSO Technology

The absence of atmospheric impairments in addition to other attractive attributes of indoor FSO links make FSO a strong candidate wireless technology to be used in future wireless DCNs. A simple FSO link consists of a light source at the transmitter, and a photodetector (PD) at the receiver to detect the received light.

Light Emitting Diodes (LEDs) and Laser Diodes (LDs) are the most commonly used light sources in FSO links [51]. LDs are highly directional sources that have high optical power outputs and broader modulation bandwidths [114], and therefore, can support high data rate transmission. On the other hand, LEDs are large-area emitters and are considered as extended sources that can be operated safely even at relatively high powers. LEDs are cheaper and more reliable as compared to LDs, and thus, are preferred in some indoor applications. In general, LEDs support lower data rates as compared to that of LDs [114], however, recent research demonstrations show relatively high achievable data rate (up to 3 Gpbs) using LEDs [115, 116].

Positive-intrinsic-negative (PIN) or avalanche photodetectors (APDs) are widely

used to detect the light beam at the receiver [51]. PIN photodetectors are cheaper, operates at low-bias, and can tolerate wide temperature fluctuations [51]. Therefore, PIN photodetectors are used in many commercial infrared links that requires FSO links of low cost, and low data rates. APDs are essentially PIN photodetectors that are operated at very high reverse bias resulting in internal electrical gain [1]. APDs are favorable and have superior performance compared to PIN PDs when the ambient light noise is little. APDs are used in systems that require high data rates and high performance in general. Extensive research effort is being exerted in the field of quantum dot, Nano-particle and graphene-based PDs to develop ultrafast PDs that operate over a broad range of wavelengths [117, 363–368].

Although On-Off keying (OOK) is the most commonly used modulation scheme due to its simplicity, wide range of digital modulation schemes can be used in FSO systems. Pulse Position Modulation (PPM) or one of its variations, such as Variable-PPM (VPM), is usually used in high data rate applications (e.g., deep space communication) [51, 84, 120]. Both OOK and PPM are classified as single-carrier pulsed modulation. Multiple-subcarrier modulation, such as Orthogonal frequency-division multiplexing (OFDM), can also be used in severe channel conditions since it does not require complex time-domain equalization as compared to PPM [90].

3.1.4 60 GHz versus FSO

A comparison of indoor 60 GHz RF and FSO technologies is presented in Table 3.1. Both technologies occupy unregulated band of the spectrum. Therefore, operating using FSO or 60 GHz does not require approval allowing manufacturers to develop worldwide compatible components.

It is expected that the components of the 60 GHz technology will be inexpensive since standard 90nm CMOS technology is used for developing components of the 60

GHz technology with small form factors. On the other hand, most exiting commercial FSO devices are developed for outdoor long range FSO links. Therefore, FSO transceivers are housed in bulky packaging and are sophisticated to endure atmospheric impairments, including rain, fog, wind, and building sway. In indoor FSO links, however, this level of complexity is not required. It is possible to realize an indoor FSO link by using the output light from a single-mode fiber (SMF) or multimode fiber (MMF) and collimator. At the receiver, a collimator is used to couple the received light to the receiver SMF (or MMF) [50, 85, 86, 369].

RF technologies can offer high data rates when high carrier frequencies are used. At high-frequencies (i.e., short wavelengths) [370], diffraction and reflection barely apply. However, non-line of sight (NLOS) RF communications highly depend on the diffraction and reflection of signals. Therefore, 60 GHz links become line-of-sight (LOS) links, and the key features of RF technologies, such as coverage, ability to penetrate obstacles, and receiver sensitivity, become less clear [51]. Although this can be considered as a limitation for RF technologies operating at high carrier frequencies, that is not necessarily the case for 60 GHz technology in DCNs. In fact, having limited coverage and being unable to penetrate obstacles are among the factors that motivated researchers to consider 60 GHz for DCNs. In DCNs, racks are arranged in close proximity, therefore, short range links are required. Moreover, the inability to penetrate obstacles can help reduce the complexity of dealing with interference and security issues. Similarly, in indoor applications, FSO link is confined to the room in which the system is installed due to the inability to penetrate physical objects so it can not be detected outside, securing transmissions against eavesdropping. Accordingly, the complexity of security measures and data encryption needed for using FSO and 60 GHz technologies can be reduced leading to simpler design process and less overhead.

The channels in 60 GHz technology are wider than that at 5 GHz, and thus, for

a given link distance, the path loss is 20 dB higher than that at 5 GHz. Moreover, the 60 GHz band includes the absorption frequency of the oxygen atom. At 60 GHz, the signal-to-noise ratio (SNR) is roughly 55 dB worse than that of links at 2.4 GHz [44]. Therefore, 60 GHz technology has lower practical bandwidth than what is theoretically achievable. High path loss and link instability in 60 GHz technology can be alleviated using highly directional beams which can be realized using beamforming [4, 371]. Compared to RF, FSO inherently provide significantly higher bandwidth as compared to that of current RF technologies due to the large band of unregulated frequency. Moreover, FSO exhibit lower power attenuation, and thus, can offer higher data rates at short, medium, and long distances [51].

Radiation patterns of RF communication impose additional restrictions on the activity of wireless modules in close proximity to avoid interference [52]. Although it is less significant in 60 GHz technology, especially if beamforming is used, interference can increase the complexity of routing and network management schemes, and may thus reduce the overall throughput of the network. Moreover, using 60 GHz in a DCN full of metal structures can make the problem of interference more challenging [41, 372]. On the other hand, interference does not form a serious problem in case of FSO technology since point-to-point FSO links are used to achieve higher data rates [137]. This, however, means that FSO link requires accurate and stable alignment to maintain the link. As we will discuss in Section 3.5, vibrations due to server fans, discs, HVAC and UPS units may cause link misalignment adding more challenges to the design of FSO links in DCNs.

Intensity modulation with direct detection (IM/DD) is usually employed in FSO links. The high carrier frequency and the relatively large detector area provide spatial diversity that averts multipath fading. On the other hand, RF links experience signal magnitude and phase fluctuations due to reflections. Therefore, the design of FSO

links can be simpler than that of RF. However, FSO receivers have lower sensitivity as compared to that of RF due to the speed limitations of the photo-electric conversion mechanisms [73].

The advantages of the 60 GHz RF technology motivated Ramachandran et al. to propagate the idea of using 60 GHz RF technology in DCN design [4]. Following their work, considerable research has been devoted to investigating the feasibility of deploying 60 GHz RF technology in DCNs [6, 43–49]. Similarly, the advantages of FSO technology and its successful use in a wide range of applications has motivated researchers to investigate the use of FSO in the design of DCNs [9–11, 50, 52].

3.1.5 FSO versus Fiber Optics

FSO and optical fiber are two optical technologies providing comparable transmission bandwidth. Considering the similarities between FSO and optical fiber, we believe that it is important to compare the two technologies.

It might be noted that the advantages (disadvantages) of a technology may become less or more significant depending on the scenario in which the technology is deployed. For example, since we focus our discussion on the indoor DCN application, the capability of extending optical fibers for long distances becomes insignificant. On the other hand, complexities associated with laying fiber cables in an outdoor network, including permissions and digging, is absent in DCNs. Similarly, environment impairment, that is considered a major challenge for outdoor FSO links, becomes negligible in environmentally controlled mediums such as in DCNs.

Optical fiber technology uses a confined medium (i.e., fiber cable) for transmission, and thus optical fiber technology is immune to interference. However, according to optics and laser physics, light beam propagating in an optical fiber can suffer from chromatic and polarization mode dispersions, birefringence, scattering, and absorp-

tion [373].

In an FSO link, the light propagates through an unconfined medium (i.e., air). The absence of the confined transmission medium in FSO makes it, unlike optical fiber, insusceptible to chromatic and polarization mode dispersions, and birefringence. Moreover, light in fiber cables propagate by the mean of total internal reflection. Therefore, light beam in FSO can be around 1.5 times faster than that of in optical fiber resulting in lower propagation delay for FSO [52]. Nonetheless, unconfined mediums lead to beam divergence and make FSO links vulnerable to interference.

Fiber cables can be extended in overhead or under raised floor between any two racks in DCNs regardless of the physical arrangement of racks in the DC. Although this implies that there are no restrictions on the physical layout of a DCN, extending fiber cables require careful planning and time to ensure that installation standards are met. Specialized manpower is needed to adhere to installation recommendations, such as maximum bend radius and vertical rise, planning of cable routes, protection against impacts, and maximum tensile loading during the pull of the cable [374]. Unlike fiber optics, FSO links are point-to-point LOS/NLOS links, and thus require careful layout design to ensure feasible link alignment. This can lead to network layout design complexity. Once designed, FSO links do not require extensive setup planning or specialized personnel for installation as compared to fiber optics, and thus FSO links can be installed in a shorter time [57]. However, as discussed earlier, careful alignment and stability are required to maintain the FSO link.

In case of damage or failure, replacement or repair of a damaged fiber cable can be time consuming since cables are usually bundled. On the other hand, if an FSO transceiver fails it can be replaced as quickly as it was originally installed.

3.2 Proposed Classification of DCN Architectures

DCN architectures are broadly classified into *switch-centric* [40, 42, 375] and *server-centric* [35, 37–39] architectures. In switch-centric DCNs, servers operate only as computing nodes and switches are used for data routing. In server-centric DCNs, servers perform both, computation and data routing.

Wired DCNs are commonly classified based on switching schemes into three classes (see Figure 3.2); namely, electrical (circuit or packet switching), optical (packet, circuit, or burst switching), and hybrid [34, 356, 376, 377].

Wireless communication is a promising flexible approach that can help addressing the nondeterministic unbalanced traffic distribution of DCN applications and help alleviate congested hot spots [9,41]. Wireless communication technologies can be used in DCNs by either *augmenting* already existing wired infrastructure with additional inter-rack wireless links, or by completely replacing the wired infrastructure by a *pure* wireless network. In the latter, wireless communication links are used to perform intra and inter-rack communications.

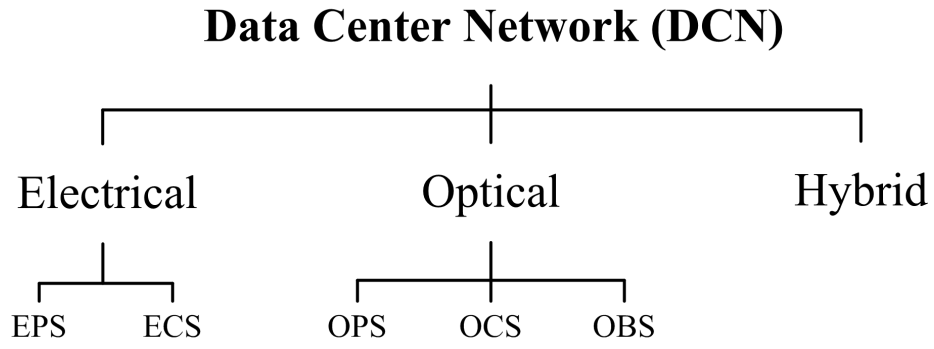

Figure 3.2: Classification of conventional wired DCNs.

Augmenting wired DCNs with wireless links can solve the problem of hotspots; however, the wiring complexity problem remains unsolved. On the other hand, realizing a pure wireless DCN is expected to solve the hot spot and wiring complexity

problems.

As wireless communication is finding its place in DCNs, we believe that a new classification is needed in order to include the emerging new DCN models. We identify four types of communication technologies that can be used in DCNs, wired (electrical cables and optical fiber) and wireless (RF and FSO). We classify DCNs based on the used communication technologies. Figure 3.3 depicts the proposed classification with all possible DCN design schemes based on the four communication technologies.

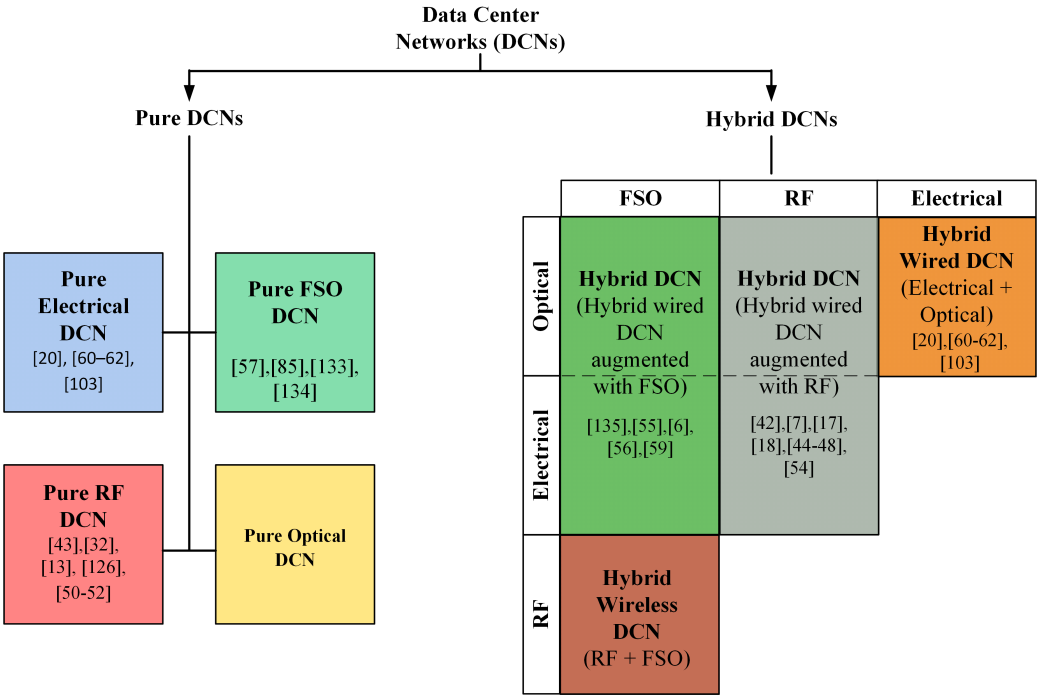

Figure 3.3: Proposed data center network (DCN) classification.

From Figure 3.3, DCNs can be broadly classified as Pure or Hybrid. Several DCN designs can fall under the broad hybrid class. In the following we formally define different types of DCN designs:

- **Pure Wired/Wireless DCN:** refers to a DCN in which a single (wired or wireless) communication technology is used for intra and inter-rack communication. This can result in a pure electrical/optical/RF/FSO DCN.

- **Hybrid DCN:** refers to a DCN that utilizes two or more technologies.
- **Hybrid Wired DCN:** is a DCN that deploys two or more wired technologies. This refers to a DCN in which electrical cables and optical fibers are used.
- **Hybrid Wireless DCN:** a DCN that uses two or more wireless technologies. A hybrid wireless DCN refers to a DCN in which RF and FSO are used for communication.
- **Hybrid (wired + wireless) DCN:** Refers to a DCN that deploys at least one wired technology and augmented with at least one wireless technology. This can lead to six types of hybrid DCNs:

    1. Pure Electrical + RF
    2. Pure Optical + RF
    3. Hybrid wired + RF
    4. Pure Electrical + FSO
    5. Pure Optical + FSO
    6. Hybrid wired + FSO

In Figure 3.3, for the sake of brevity, we only show Hybrid wired augmented with RF and Hybrid wired augmented with FSO DCNs. Dashed line indicates that we can further break it down to more categories as discussed above.

It might be noted that, using the proposed classification, an electrical/optical DCN in conventional classification can be classified as a pure electrical/optical DCN, respectively. On the other hand, a hybrid DCN in conventional DCN classification falls under the hybrid wired DCN class.

For the sake of completeness, in this section, we briefly discuss wired-based DCNs. However, since wired DCNs are not the main focus of this chapter, we refer interested readers to a selected list of recent comprehensive surveys that investigate research and development in the field of wired DCNs. Figure 3.3 is also populated with selected references.

Pure electrical DCN or simply *conventional DCN* is the most commonly deployed type of DCNs [34, 356, 376, 377]. Conventional DCN was first known as *server room*, which is a small room owned by a company. In a server room, a collection of servers are co-located and connected via an electrical network to serve the computational and storage needs of the company. Having large number of machines co-located in the same room requires good management and operation to guarantee their functionality. For example, it requires proper temperature and humidity control. Also, specialized personnel are needed in order to monitor and maintain the server room.

As companies increased in size, bigger rooms were needed. Fulfilling the requirements of expanding the server room requires large investment to cover the replacement of old networking components (servers, switches, etc.). A few companies were able to perform these changes, while for others it was an overhead too big to handle. The buildings equipped with a large network of servers in big companies started to be known as DCs. Small companies begun to outsource their computational and storage needs by using the DCs of big companies. This helped them avoid the huge costs of maintaining server rooms.

As mentioned earlier, it has been widely believed that to appease the ever increasing demand of high-bandwidth communication in DCs, DCN architectures must guarantee full bisection bandwidth between a significant number of servers [378–380]. However, according to empirical studies of DC traffic, it has been shown that 80% of the flows are mice flows (smaller than 10 KB in size) and 95% of the bytes trans-

ferred in a DC are in the top 10% of the elephant flows (flows with large amount of data) [28–30, 381]. Thus, full bisection bandwidth between more than a few pairs of servers at any instant is rarely required in a DCN [266, 378, 380, 382].

The limitations on electrical interconnects [383, 384] along with the existence of elephant flows have motivated researchers to consider *Hybrid wired DCNs*, where electrical and optical networks are utilized to perform inter-rack communication. In this scenario, optical networks are used to provide high-speed, on-demand, high bandwidth inter-rack communication in DCNs [266, 378–380, 382, 385]. Existing hybrid wired DCNs (e.g., c-Through and Helios) employ Electrical Packet Switching (EPS) and Optical Circuit Switching (OCS) technologies, respectively, for supporting bursty and long duration large flows in DCNs [127, 266, 378, 379, 383].

The need for EPS in DCNs is driven by the high switching time involved in OCS technologies [379]. However, the use of EPS may somewhat restrain the exploitation of the advantages of photonics in DCNs [380]. EPS already started to become a bottleneck in large scale DCNs, especially with the increasing demand for high-speed, high-bandwidth links. With the recent progress in optical technologies [386–388], Optical Burst Switching (OBS) has been propagated as a good candidate for burst communications in data-intensive cloud applications [24, 384, 389–395]. The use of OBS technologies in DCNs, however, has not yet received much attention.

Recent papers suggested the use of all-optical inter-rack communication instead of combining electrical and optical components [383,385,396–400]. It might be noted, however, that intra-rack communication is realized using electrical switching. This is because, traditional electrical cables (e.g., 10 GigE) are viable for distances below 10 meters (i.e., intra-rack communication) [399]. Moreover, the prices of the enabling technologies of optical communications are relatively high as compared to that of commodity electrical networking elements. Therefore, the concept of a pure wired

DCNs using optical fibers did not attract the designers of DCNs, yet.

In case of wireless communication, a wireless technology can be used for inter-rack communication only (augmenting links) or to replace the whole network (pure wireless DCN) including intra-rack communication. Therefore, we believe that it is important to distinguish between the all-optical inter-rack communication and all-optical DCNs (*pure optical DCNs*). According to this definition, pure optical DCNs do not exist, and DCNs that use all-optical inter-rack communication can be classified as *hybrid wired DCNs*.

It is also worth pointing that in most existing DCNs racks are arranged in row-based physical topology. Therefore, research is mainly concerned with changing the logical topology (i.e., connection of servers and switches). Using wired communication, it is possible to realize different logical topology over the standard row-based physical topology. On the other hand, due to the requirements and constraints imposed by wireless communication technologies, it is possible that both physical and logical topologies can be changed to realize new efficient DCNs.

3.3 Summary of Techniques for Adopting 60 GHz in DCNs

In 2008, Ramachandran et al. nurtured the idea of using 60 GHz technology in DCNs [4]. The authors identify the requirements of a DCN and the problems encountered due to wires. They discuss the suitability and the challenges of the use of 60 GHz inside DCNs. Ramachandran et al. envision three complementary deployment scenarios for both intra and inter-rack communications (see Figure 3.4). An array of antennas is used in order to create directional beam with small beam width. For intra-rack communication, Ramachandran et al. suggest using a reflector to cre-

ate indirect LOS links, whereas for inter-rack communication, LOS, indirect LOS, or multi-hop links can be used.

Following the proposal by Ramachandran et al., researchers have been investigating the effectiveness of 60 GHz RF links in DCNs [5,6,27,32,41,43,44,46–49,401–406].

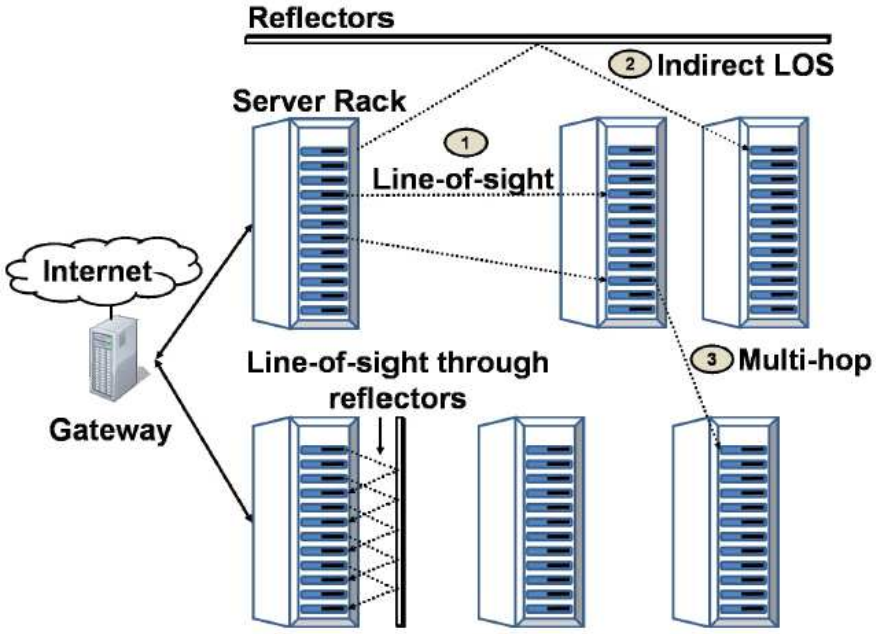

Figure 3.4: Intra and inter-rack communications in 60 GHz wireless DCs as envisioned by Ramachandran et al. [4].

3.3.1 Hybrid RF DCNs

In [27], Kandula et al. propose the concept of *flyways* to tackle the hot spot problem. Flyways are on-demand stable multi-Gbps additional links (wired or wireless), added to wired DCN to provide additional capacity and alleviate the problem of hot spots at a fraction of the cost required to over-provision the DCN.

In case of wired flyways, additional switches are used to inter-connect random subsets of the ToR switches. On the other hand, wireless flyways can be achieved

by placing one or more wireless transceivers atop each rack in the DCN. Wireless flyways provide more flexibility as compared to wired flyways. The authors formulate the wireless flyways placement problem and present a suboptimal algorithm in which a single flyway is added at a time. Preliminary results indicate that, using flyways can achieve a substantial improvement in the performance of the DCN with respect to the completion time of the demands (CTD). It is worth pointing that more wired flyways are needed as compared to wireless flyways in order to achieve the same overall improvement.

The work by Kandula et al. is preliminary and aim to understand the viability of adding on-demand links to solve the hot spot problem. Therefore, several assumptions made by the authors simplify the problem and overlook important aspects of the problem. For example, it is assumed that a 60 GHz module can communicate with other modules within its range of 10 m. Moreover, it is assumed that all flyways have the same capacity and the impact of interference is ignored.

In [44], the work on flyways by Kandula et al. [27] is extended. In this work, 60 GHz devices prototype is used. Performance measurement and simulation for 60 GHz link hardware, signal propagation, stability, interference, and TCP throughput are performed. Results indicate that directional 60 GHz links, are necessary for good link stability, interference avoidance and channel reuse, and higher throughput. The authors discuss three different models for establishing the flyways, namely, Straggler, Transit, and Greedy. In Straggler, a link is established between the pair of ToRs taking the longest time to complete. In transit model, indirect transit traffic is allowed using the room spared on a flyway in the Straggler model. Greedy model improves Transit model by picking the flyway that offloads the most traffic from bottleneck link. The proposed design is found to speed up DCN applications with predictable traffic workloads by 45% in 95% of the cases.

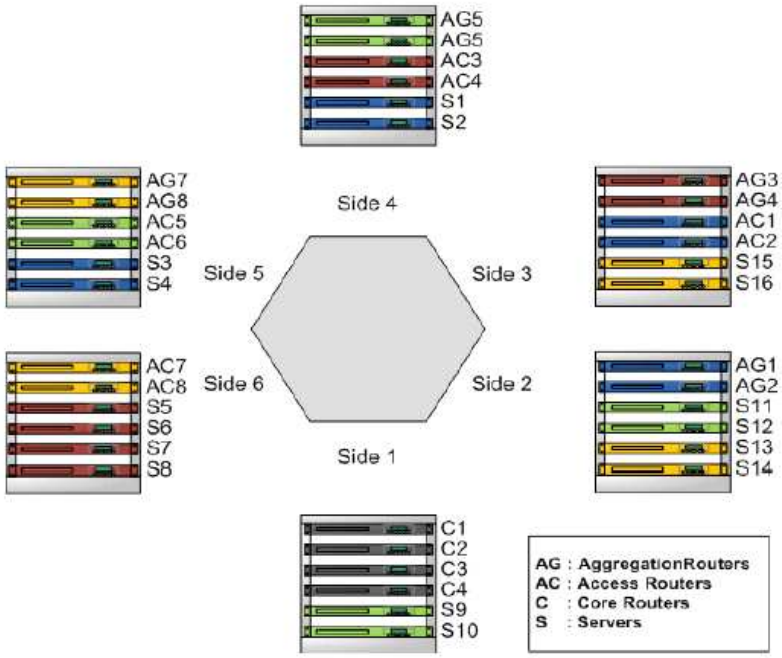

Figure 3.5: Design by Vardhan et al. [5].

Compared to their preliminary work in [27], the authors have improved several aspects regarding their model and assumptions. However, the discussion still topology-independent and it is not clear how links will be realized between racks. Moreover, we believe that the model does not fully utilize the flexibility of the wireless communication to create configurable and agile links.

The work by Kandula et al. is classified as hybrid RF DCN since they adopt the 60 GHz wireless technology to implement wireless flyways. However, it is worth pointing that it is one of the major motivator for researchers to investigate the feasibility of wireless DCNs in general.

Wireless Channel Allocation

Cui et al. investigate the wireless channel allocation problem in hybrid 60 GHz DCNs [41, 401, 402, 407]. In their analysis, Cui et al. consider a wired DCN with

hot spots. A separate 60 GHz wireless network is used to provide additional links and relieve the network. A rack is considered as a wireless transmission unit (WTU) with 60 GHz transceiver mounted on top of it. A wireless link is allocated to carry inter-rack traffic. Total transmission links form a wireless transmission graph. The authors adopt interference range model, in which a sender causes interference on the nodes inside its interference range. The problem of provisioning wireless links is formulated as an optimization problem with the objective function of maximizing the total utility of the wireless transmission. The utility of a link is defined in terms of the contribution to the global performance made by transmitting the traffic via wireless links. Genetic algorithm (GA) and greedy heuristic algorithm proposed by Cui et al. are used to solve the formulated optimization problem. Results show that using the wireless links improves the performance of the network with respect throughput and job completion.

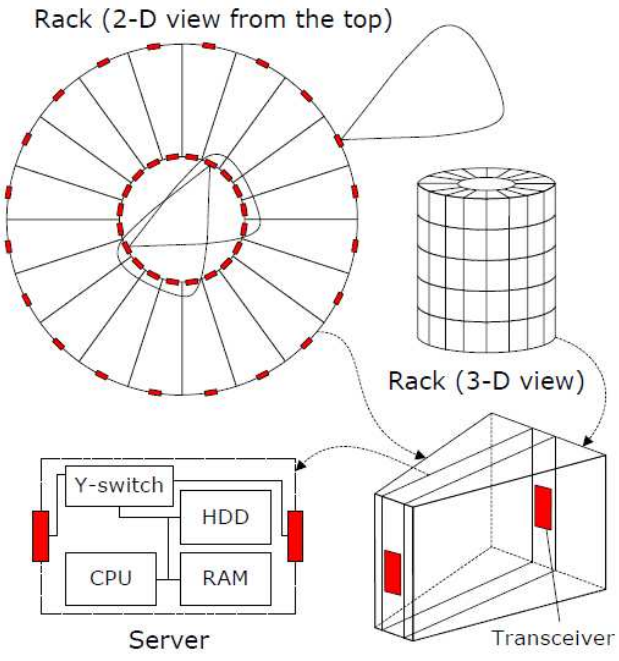

Figure 3.6: Rack and server design in Cayley DCN [6].

Results by Cui et al. confirm the effectiveness of using wireless communication to realize hybrid DCNs. However, the theoretical model used by the authors simplifies the problem and does not give a solid sense of the wireless channel allocation problem in real wireless DCN. For example, the model is topology-independent, in the sense that it is assumed that a WTU can communicate with any WTU in its range. This, however, is not true and great efforts are exerted by researchers to facilitate wireless communication in DCNs. Moreover, the used model ignores several aspects including the impact of reflections and metal structures on link interference.

Beamforming

Katayama et al. propose wireless packet-switching networking in DCs using steered-beam mmWave links [403]. Wireless transceivers are placed atop racks and LOS links between adjacent rows of racks are realized. Wireless transmission is limited to the adjacent row. Data packets are relayed via adjacent rows of racks wirelessly eliminating the need for long cables and additional switches, and without using long wireless links. Each node has a local routing table that stores routing information. The routing table is responsible of determining the next hop for the packet until the packet reaches its destination. A preliminary prototype of a mmWave steered-beam link combined with IEEE 802.11 control plane is demonstrated.

Katayama et al. do not carry out experiments to evaluate the proposed packet-switching DCN. However, since the proposed DCN is a short-range multi-hope network, one can expect that the DCN will show poor performance with respect to packet delivery latency.

Even though links realized using beamforming can help reduce interference, they still experience signal leakage. In packed small proximities such as in DCNs, this can significantly increase interference, and thus impact throughput.

In [43], Zhang et al. explore the feasibility of using 3D beamforming. They propose the use of 60 GHz wireless links that reflects off of a reflector mounted to the ceil of the DC as proposed by Ramachandran et al. [4]. The authors envision that this design is capable of addressing both link blockage and interference, thus improving overall transmission performance in DCNs.

A small 3D beamforming testbed is built by Zhou et al. [47] to demonstrate the ability of 3D beamforming in addressing both link blockage and link interference. Moreover, the authors propose a link scheduler. Using simulations, the authors show that wireless capacity and reach of 60 GHz links can be expanded using 3D beamforming as compared to that of 2D beamforming. A testbed is implemented.

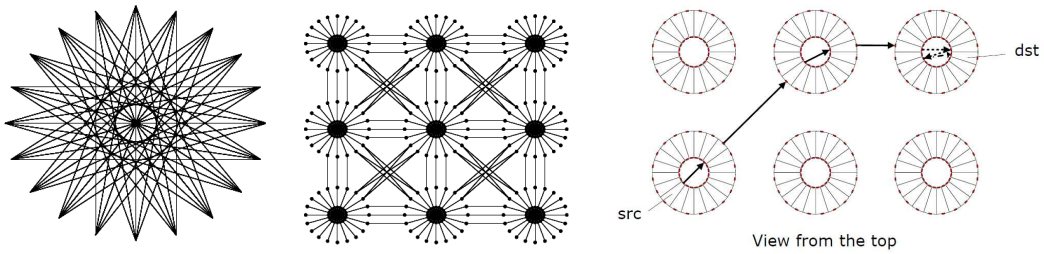

(a) (b) (c)

Figure 3.7: Cayley DC [6] (a) Intra-rack topology. (b) Inter-rack topology. (c) Diagonal XYZ routing.

Measurements confirm that using 3D beamforming, it is possible to realize 60 GHz links with zero reflection energy loss, reduced interference, and capability of avoiding obstacle that can block the beam. However, this comes at the cost of complexity of establishing the link. Moreover, the received signal strength (RSS) can vary with the curvature of the reflector. For example, a convex reflector leads to a drop in the RSS, whereas concave surface increases the RSS. Finally, careful design of the server floor is required to avoid obstacles such as cooling and cable ducts or columns.

3.3.2 Pure RF DCNs

In this section, we discuss the designs of pure RF DCNs. There are two main research directions to develop pure RF DCNs, emulation of well-known topologies, and the design of a completely new topology. In the following, we discuss these two research directions.

Emulation of Existing Topologies

Vardhan et al. discuss the possibility of realizing a pure 60 GHz DCN [5,32,48,49,404]. The authors discuss the emulation of two well-known DCN topologies, 3-tier layered and fat-tree architectures. In order to do that, the authors arrange the servers and switches in racks forming a hexagonal arrangement (see Figure 3.5) to facilitate direct LOS wireless links. Each rack is equipped with two transceivers mounted to the top of the rack. A transceiver utilize beanforming with phased array to achieve highly directional links. Phase rotator is utilized to steer the beam, and thus communicate with different servers.

In wired hierarchial and Fat-tree DCNs, adding new servers may require rewiring of a large number of existing servers. This can be time-consuming and may affect the availability of the DCN. Vardhan et al., however, present flexible wireless hierarchial and Fat-tree DCNs using 60 GHz technology. Therefore, adding new servers does not interrupt the DCN operation and can be done in a short time. Nevertheless, the work by Vardhan et al. lacks experimental analysis to fully evaluate the feasibility of the proposed design with respect to link capacities and packet delivery latency.

Influenced by mobile networks [60], we refer to DCN physical topologies that breaks down a network into uniform shapes as cellular DCNs. Foe example, the DCN design proposed by Vardhan et al. can be referred to as a cellular DCN with a single cell. Although modular and can be easily expanded, a cell in cellular DCN topologies

encloses unused space leading to DC floor underutilization. Moreover, using a single-cell topology leads to scalability issues.

Flexibility provided by the wireless links can be further utilized to go beyond just emulating the already existing topologies. For example, it can be interesting to investigate the possibility of realizing additional RF on-demand links similar to Flyways [27]. The design by Vardhan et al. can make implementing such links very easy. We believe that this can be an interesting merge that can lead to efficient easy to implement small to medium Fat-tree DCNs.

Design of New Physical Topologies

Although Vardhan et al. propose a pure wireless DCN using 60 GHz technology [5], their proposal aims to emulating well-known topologies such as hierarchial and Fat-tree topologies using wireless links. On the other hand, Shin et al. introduce a novel pure wireless DCN design using 60 GHz RF technology [6]. The novelty of the DCN proposed by Shin et al. stems from the fact that the DCN utilizes the properties of the wireless 60 GHz links to realize a physical topology that is different from the standard row-based topology. As a result, the network logical topology is also different from the well-known wired topologies.

The proposed design by Shin et al. features novel cylindrical rack design [see Figure 3.6]. A rack consists of S stories and each story holds C prism-shaped containers in which servers are stored. Racks are arranged in a semi-regular mesh topology resulting in a densely connected subgraph that is a member of *Cayley Graphs (CG)*. Two wireless transceivers are mounted on both ends of each server node. One is used for intra-rack communication, and the other is used for inter-rack communication. Figures 3.7-(a) and (b) depict the intra and inter-rack topology in Cayley DCN, respectively. A Y-switch connects the transceivers of a server to its system bus and a

routing protocol is used to direct packets within the Y-switch.

Figure 3.7-(c) depicts the diagonal XYZ Routing algorithm used in Cayley DCN. The algorithm is a two-level geographical routing algorithm used to route intra and inter-rack data exploiting the uniform topology of the Cayley DCN. A server is identified by a composition of three values: the coordinates of the rack, the story that contains the server within the rack and the index of the server in the story. A server uses three routing tables to forward package from source to destination using a shortest path route.

A set of experiments is conducted to evaluate the performance (packet delivery latency), failure tolerance, and cost of Cayley DCN. The authors assume a 10×10 grid with $S = 5$ stories and $C = 20$ servers/story. A custom packet level simulator is used to evaluate and measure the average and maximum packet delivery latency of Cayley DCN. Results show that, Cayley DCN exhibits better or comparable performance as compared to Fat-tree DCN, different oversubscription rates. Moreover, Cayley perform better under the assumption that the applications hosted by the DCN generate traffic patterns with small packet numbers and hops. However, this is not always the case in large scale DCNs.

The dense connectivity and the switch-less design leads to high fault tolerance allowing Cayley DCN to withstand up to 59% of node failure before two nodes become disconnected. However, since Cayley DCN relies on multi-hop communication, the maximum latency worsen as the traffic load increases.

In [408], Camelo et al. present a low space and time complexity routing algorithm for any interconnection network where its underlying graph is a CG of some finite group. The proposed algorithm is based on the fact that finite groups are Automatics and have a *Shortlex Automatic Structure (SAS)*. In [409], Camelo et al. extend their work to evaluates the required space to keep such structures and the several

intermediate finite state automata that arise during the process of constructing such AS. The authors evaluate six well-known families of CG to determine which structures are space-efficient to implement the scheme based on the so-called *k-fellow traveler* property. Results show that a CG with both low and constant k-fellow traveler property, needs very small routing tables. This was verified in the cases of the CG families Hypercube, Bubble-Sort and Transposition graphs. Other graph families, such as Butterfly and Star, also have a small tables with respect to a general-purpose algorithm for the same kind of graphs. However, the reduction of the routing table size only is effective when the number of vertices is very large.

According to Suto et al., Cayley DCN is not fault-tolerant enough to satisfy the requirements of hosting MapReduce. The authors attribute this limitation in Cayley graph to the cylindrical design of the rack. In cylindrical racks, servers are stacked on top of each other forming vertical columns and thus, servers are isolated. This in turn limits the performance of MapReduce. A possible solution to overcome this problem is to increase the degree of all servers in the cylindrical rack. This way, each server can reach more servers in the rack promoting fault tolerance. Nevertheless, this increases interference, and thus reduces spectrum efficiency and increases packet delivery latency.

Therefore, in [7], Suto et al. attempt to design a wireless 60 GHz DCN that satisfies the communication requirements of MapReduce (i.e., better fault-tolerance and better spectrum efficiency). To this end, the authors propose a two-part solution. First, the authors use bimodal degree distribution. This leads to two types of servers, where the majority of servers are non-hub with low degree, and a few become hub servers with higher degree. Hub servers makes the network more fault-tolerant to mechanical faults, whereas using only two types of servers makes the network more fault-tolerant to software faults (e.g., computer viruses).

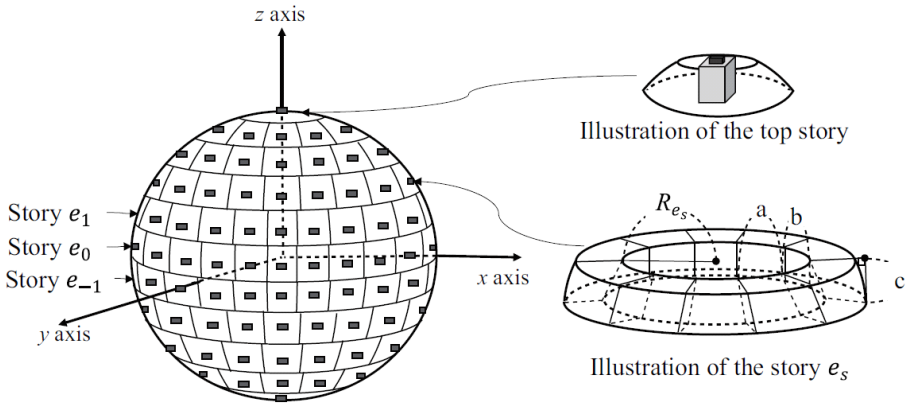

Figure 3.8: Design proposed by Suto et al. [7]

Hub servers are capable of connecting to multiple servers, however, as pointed out earlier, the cylindrical rack design hinders the connectivity between servers. Therefore, Suto et al. propose a new design of a spherical rack, in which a story forms a disc of servers (see Figure 3.8). The advantages of the proposed rack architecture are twofold, reduces the hop count for intra-rack communication as compared to that of cylindrical rack and reduces the distance of the intra-rack link, and thus the path power loss.

Results show that as the difference between the transmitter and receiver stories increase, so does the path loss for cylindrical rack design, whereas a spherical rack experiences reduction in path loss. Simulations also show that the spherical rack design leads to lower delivery latency as compared to that of in cylindrical rack in case of hardware faults. On the other hand, the performance of both racks is comparable in case of computer viruses.

It is worth pointing out, however, that the reduction in path loss due to the spherical rack is $< 7\%$, whereas, the reduction in data transmission time is $< 13\%$. We believe that there are several design complexities associated with the spherical rack design. For example, server containers are not homogenous. This may lead to the

management overhead to deal with non-uniform components and parts. Moreover, as we move towards the top, container size decreases. This could be limited by the dimensions of the server contents. It is also not clear how inter-rack communication links will be established or what type of challenges will be faced by racks near the top of the rack. Given that spherical rack leads to limited improvement over the cylindrical rack, extensive analysis and studies are needed to ensure that this is an effective tradeoff.

3.3.3 Control Networks and Enabling Technologies

It is worth pointing that the research on wireless DCNs using 60 GHz started to branch out and include techniques adopted from conventional wireless communication systems. Moreover, a few research efforts investigate the use of wireless 60 GHz links to realize control network in DCN [405,410] instead of using it for data traffic network. In the following we briefly discuss the two topics.

Enabling Technologies

In [46], Yamane et al. discuss a method for interference cancelation in distributed MIMO systems. The method is a geometric iterative optimization of signal to interference ratio (SIR) by natural gradients on matrix manifolds. Partial linear zero-forcing is applied to obtain more interference-suppressive initial points that can improve convergence property of the iterative algorithm. Yamane et al. applied their method to a channel model for a typical DC and the simulation results show that this method can improve SIR and achieve higher sum rate at high SNR.

Yu et al. study multicast data delivery problem in [411]. Multicast tree problem is defined, and the objective is to minimize the total multicast data traffic. Yu et al. prove that the problem is NP-hard. An efficient heuristic algorithm is proposed,

and results show that the proposed algorithm is effective, compared with an optimal solution designed for traditional wired DCs.

Control and Facilities Networks

In [405], Zhu et al. investigate the design of a dedicated facilities network for DCs using wireless communication. A facilities network is a network orthogonal to the data plane and is used to manage DCN. The facilities network is responsible for multiple critical jobs, such as, working as a control plane, and installs and brings up hardware devices.

Control traffic has tighter latency performance requirement as compared to the data traffic which mandates that the facilities plan is isolated from the data plane. Facilities network is different from traditional data plane networks in the sense that it requires lower bandwidth, higher availability, and long-term survivability as compared to those of a data plane. Moreover, the rate at which the bandwidth demands grows is slower.

Zhu et al. propose *Angora*, a low-latency facilities network in which 60 GHz technology with 3D beamforming is used. A testbed used to evaluate Angora, using both experimental measurements and simulations, is developed taking into account link coordination, link interference, and network failures. Results show that Angora can enable large number of concurrent low-latency control channels with high fault-tolerance and flexibility to adapt to workloads and network dynamics.

3.4 Approaches for Deploying FSO in DCNs

Recent research efforts demonstrate the possibility of implementing high capacity indoor FSO links [85, 86, 369]. In [86], Chowdhury et al. experimentally demonstrate

the transmission of a 15 m LOS point-to-point indoor FSO link. The link comprises three channels, uni-directional Cable Television (CATV) signal, and a bi-directional link comprised of two 10 Gbps data links. The authors use LD source that operates in the 1550-nm wavelength range. Direct detection using a PD with active area diameter of 0.5 mm is used at the receiver. To avoid link obstruction due to human movements, the system is placed at a height of 2 m. Results show that the FSO link realized is almost lossless. As expected, for a fixed received power, a better alignment of transmitter and receiver collimators results in more collected and collimated light, and thus received power. This leads to higher SNR and improved bit error rate (BER). The indoor FSO link demonstrated by Chowdhury et al. can be useful for several applications including inter-rack communication in DCNs.

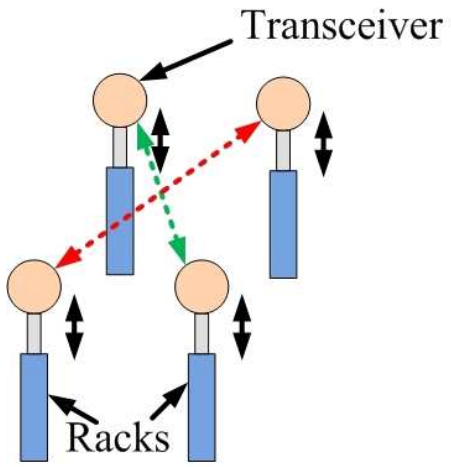

Figure 3.9: Design proposed by Riza et al. [8]

The research on deploying wireless technologies in DCNs is novice, and thus only a few papers [8–11, 50, 52, 412–414] and patents [12, 415, 416] discuss the deployment of FSO in DCNs. In the following, we discuss the efforts exerted by researchers to realize hybrid and pure FSO DCNs.

3.4.1 Hybrid FSO DCNs

Research efforts on hybrid FSO DCNs can be broken down into two types based on the approach used to configure the links used: mechanically steerable or electronically configurable links. In the following, we discuss both types.

Mechanically Steerable Links

In [8, 417], Marraccini and Riza experimentally demonstrate a power smart indoor FSO link that utilizes an electronically controlled variable focus lens (ECVFL). The link is designed to adaptively realize self-imaging effect at the receiver, and thus zero propagation loss via changing the properties of the Gaussian beam propagation. The authors use ABCD matrix analysis of Gaussian beams to theoretically analyze the link performance. A proof-of-concept is realized using an unmodulated 10 mW He-Ne laser operating at 632.8 nm and has a beam divergence of 0.62 mrad. A laser beam profiler is used to receive and measure the signal at different distances from the transmitter (up to 15 m). Depending on the length of the link, L, the duty cycle of the pulsed wave drive signal is varied to change the focal length of the ECVFL.

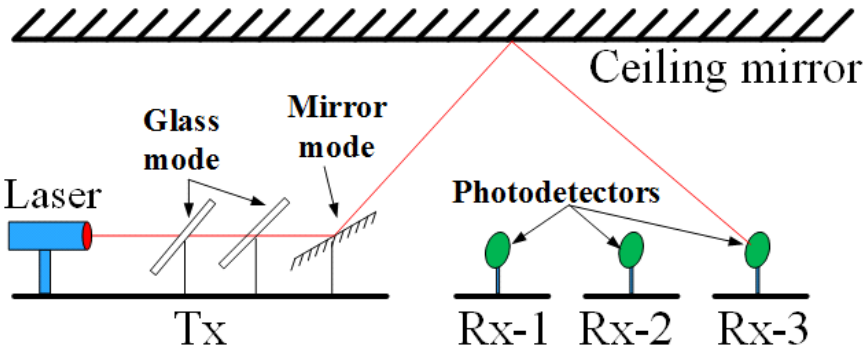

Figure 3.10: FireFly by Hamedazimi et al. [9]

Although power smart link should experience zero loss, the non-ideal behavior

of the ECVFL and laser beam Gaussian propagation lead to power loss. Moreover, it is not clear whether an attempt has been made to improve the performance of the non-smart link by testing for different specifications for the components used. Nonetheless, results show that the power smart link outperforms non-smart link. For example, at $L = 4$ m, the power loss of the power smart link is less than 7%, whereas non-smart link experiences loss of 59.07%. As the length of the link increases, so does the difficulty of obtaining the required focal length for zero loss propagation, and thus both links experience an increasing power loss. At $L = 15$ m, the power loss is 92.8% and 61.5% for the non-smart and smart links, respectively.

In [8], Riza and Marraccini discuss different applications in which power smart FSO links can be utilized. One of the applications is inter-rack communications in wireless DCNs. A transceiver is mounted to a pedestal platform that sits on top of each rack. The pedestal allows for vertical and rotational motion such that LOS links between different racks can be established [see Figure 3.9]. Power smart FSO link can adapt to the varying link length as a rack establishes the links with different racks in the DCN.

Riza and Marraccini focus their discussion on regular indoor, and containerized DCNs in which servers, storage, and networking equipments are placed in a standard shipping ($12.2\times2.4\times2.6$ m^3) containers. Containerized DCNs allow for mobility and modularity, and are easier and cheaper to build. Although highly flexible, mechanical components may significantly add to the complexity and latency of the system. This can increase the risk of failure and affect the availability and durability of DCN components. Moreover, it is easy to keep the length of the FSO links below 15 m in containerized DCNs. However, at the scale of mega DCNs, the effectiveness of power smart links will become less significant.

Electronically Configurable Links

Hamedazimi et al. propose *FireFly*, a hybrid FSO DCN [9,50]. Similar to the 60 GHz RF *Flyways* [44], all inter-rack communications in FireFly are performed using links that are reflected off a reflector (mirror) mounted to the ceil.

In FileFly, FSO transceivers are placed on ToRs. In order to perform link steering, the authors propose the use of switchable mirrors (SMs) or Galvo Mirrors (GMs). In the case of SMs, every FSO transceiver is equipped with several SMs (see Figure 3.10). SMs are pre-configured and aligned to a receiving FSO on a different rack. According to the states of SMs (i.e., glass/mirror), a link is directed to devices on other racks through the reflection off a mirror mounted to the ceiling. Links are established by switching relevant SMs to mirror/transparent states. On the other hand, a GM is a small mirror mounted on an axis that has limited rotation capability. A link is established by proper rotation of the mirror that deflects the incident beam.

Due to the limited number of FSO modules that can be mounted atop a ToR, a limited number of steering mechanisms (i.e., switchable and Galvo mirrors) must be provisioned and preconfigured so that the network robustness to future and unforeseen traffic patterns is guaranteed. To this end, the problem of designing a FireFly using each of the steering techniques are formulated as a constrained optimization problems. Moreover, the authors discuss different types of real-time reconfigurations required in FireFly, periodic and triggered reconfigurations. The communication and network reconfigurability is controlled using a centralized topology and routing managers. The authors propose a new goodness metric, dynamic bisection bandwidth (DBW), to evaluate the performance of the new flexible network design.

In [16,53,165], we propose a new class of non-blocking multicast FSO switch using non-moveable tri-state switching elements (T-SEs). A T-SE is a switching element that can be reconfigured in one of three states (Fig. 3.11): *Reflective*, Transmissive,

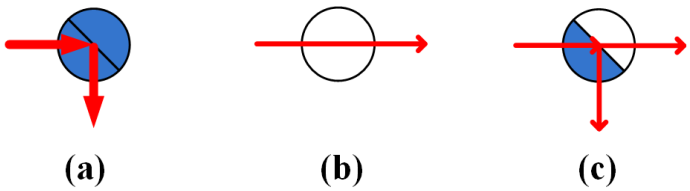

Figure 3.11: T-SE (a) R-State. (b) T-State. (c) S-State.

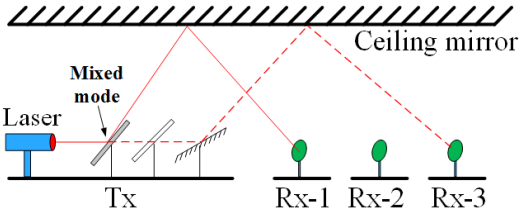

Figure 3.12: FlyCast by Bao et al. [10]

or *Splitting* state (half reflective/half transmissive). Any material similar to the one used in SMs can be used to realize T-SEs. Using the splitting state, a beam can split into any number of copies enabling multicast. We discuss the T-SEs further in Chapters 6 and 7.

It might be noted that in [9, 50], Hamedazimi et al. use the SMs only in the reflective and transmissive states, and thus links are limited to unicast. Using the design of FireFly and the concept of T-SEs used in our switch to provide multicast, Bao et al. propose FlyCast FSO DCN [10]. In FlyCast, the authors utilize the splitting (referred to as mixed) state of the SMs to enable multicast without the need for a switch. Figure 3.12 depicts the design of FlyCast. A transmitting rack is preconfigured to communication with three receivers. Reconfiguring the states of the SMs leads to different communication pattern. For example, configuring the first, second, SMs in the glass mode, and third mirror in mirror state will lead to the same link setup in Figure 3.10. On the other hand, by configuring the first, second, and third mirrors in mixed, glass, and mirror states, respectively, multicast is achieved

and the transmitted signal is sent to the first and third receivers.

Bao et al. use a ring topology to demonstrate the effectiveness of the FlyCast. A signal transmitted by a rack will require multiple hops to reach the destinations. Using FlyCast, a signal can be transmitted simultaneously and in a single hop to the destinations. Similar to FireFly, FlyCast is an SDN. The network controller computes the network topology which reduces to building a directed Steiner tree with constraints. Therefore, computing the topology problem is NP-hard, and thus heuristics are used to implement the control algorithm in the network controller.

In splitting state, light beam is split into two perpendicular beams: transmitted beam (along the path of the original incident beam), and reflected beam. Based on the design, transmitted and reflected beams may or may not have the same power. Bao et al. change the splitting ratio and compute the maximum number of possible signal splitting operations such that the signal remain detectable. The transmittance of the splitter is changed from 10% to 90%. Certainly the maximum number of splitting operations corresponds to the transmittance power of 90%. This is because higher transmitted power can endure larger number of splitting operations. This also matches our results in [52] as we will discuss later. A simple lab experiment is performed to calculate the splitting loss at transmittance of 50%. However, instead of using a SM, the authors use a regular beam splitter with transmittance of 50%.

Similar to the RF *Flyways* [44], the work by Hamedazimi et al. and Bao et al. [9,10,50] can provide full flexibility, nevertheless, implementation can be challenging. For example, any imperfection in the ceil mirror can impact the signal reflection leading to signal misalignment. Moreover, obstacles in the server floor (e.g., building columns and ducts) must be avoided, which may add to the design complexity of the DC. Finally, even though preconfiguration of FSO links are expected to be infrequent, it can be time consuming, require specialized manpower, and it will impact

the availability of the DCN.

3.4.2 Pure FSO DCNs

In [416], Davidson et al. present an extensive theoretical discussion of a pure FSO DCNs. The inventors conceptually discuss connecting DCN components such as: servers, racks, or a set of racks using FSO links, switches, ceiling mirror, mechanically or electrically controllable mirrors and/or beam splitters. However, since the goal of the patent is to cover as much design concepts as possible, the challenges and the details of connecting multiple DCN components using FSO links are not discussed.

Designs of intra and inter-rack FSO links in pure FSO DCNs are independent, and thus it is possible that a designer use preconfigured links for intra-rack, whereas inter-rack links can be mechanically or electronically configurable. Therefore, there is no clear-cut grouping of pure FSO DCNs designs as compared to hybrid DCNs. To improve the readability, however, we divide pure FSO DCN designs into two groups, preconfigured links, and mixed (preconfigured + mechanical steering).

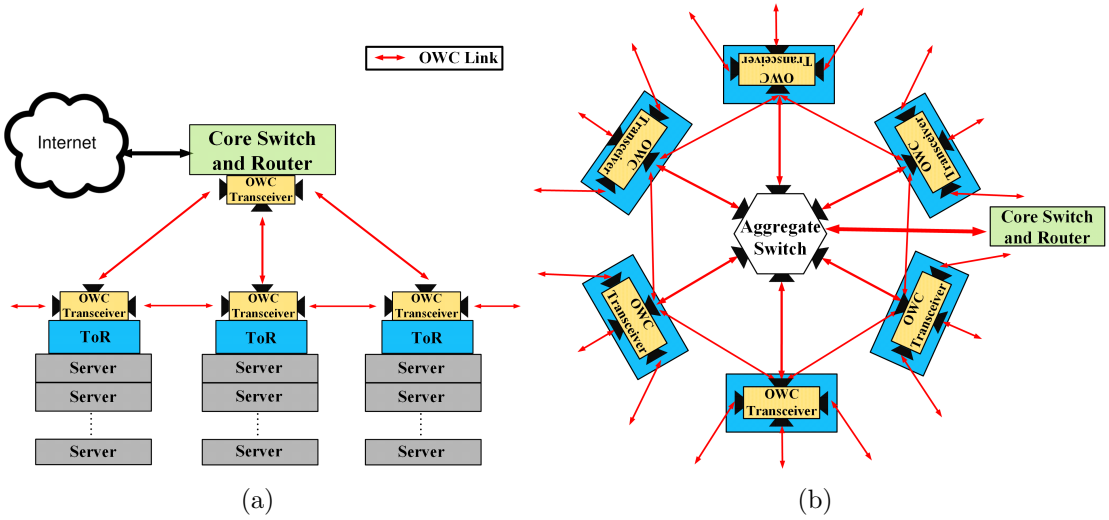

Figure 3.13: Design proposed by Arnon [11] (a) Side view. (b) Top view.

Preconfigured Links

In [11], Arnon discusses both, intra-rack and inter-rack communications using FSO. For intra-rack communication, server should be able to communicate with each other and with the ToR using inter-server OWC transceivers. However, the structure the inter-server OWC transceiver and the means of establishing FSO links between servers are not discussed.

In the case of inter-rack communication, racks are arranged in circular cells such that neighboring racks can communicate using LOS OWC links. Moreover, ToRs within a cell can communicate with Aggregate (or core) switches located at a higher layer as shown in Figure 3.13. Aggregate (or core) switches can communicate with each other at a higher layer on top of the layer of ToRs. However, a complete topology of a DC using the proposed design has not been addressed, and thus, it is not clear how racks, aggregate, and core switches, are connected on a large scale. Similar to the work by Vardhan et al. [5], cellular DCNs can lead to DC space underutilization.

Mixed (Preconfigured + Mechanical Steering)

A bi-directional point-to-point FSO link design utilizing high power, high speed vertical-cavity surface-emitting laser (VCSEL) arrays is presented by Joseph et al. [12]. The inventors discuss communication inside DCNs (i.e., inter/intra-rack) as one of the applications of their invention. They envision intra-rack communication to be performed using a ToR optical switch employing a multiple lens array. Servers in the rack send information to the ToR Switch as shown in Figure 3.14-(a). The optical switch then directs the information back to the servers using data shower beams. The switch can be placed at the top, bottom, or middle of the rack cabinet.

In the design proposed by Joseph et. al. [12], the optical switch must be equipped with number of transceivers equal to the number of servers. For large number of

servers, this design may become intractable or expensive. Moreover, an intensive alignment effort is needed to adjust each beam to hit the corresponding lens in the multiple lens array mounted to the lower surface of the switch.

For the inter-rack communications, optical switches or transceivers are mounted to a polygonal structure. For example, Figure 3.14-(b) depicts six switches (transceivers) mounted to a hexagonal structure. Similar to the work by Marraccini and Riza [8,417], the structure is mounted to a pedestal system that allows rotational and vertical height adjustments. This arrangement can be very useful for cellular FSO DCNs.

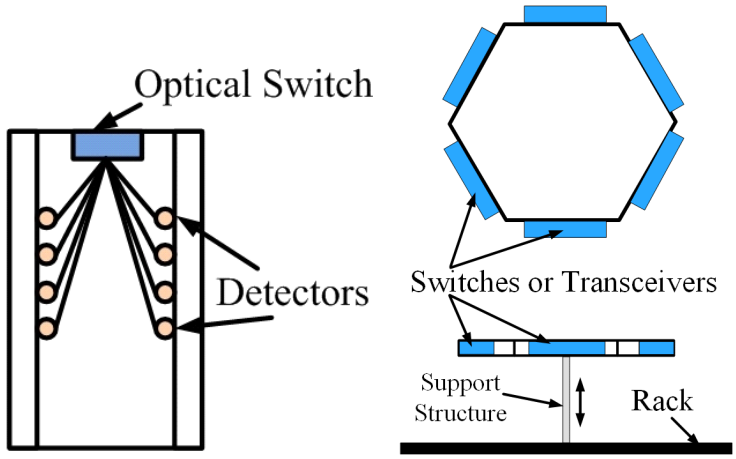

Figure 3.14: Design proposed by Joseph et al. [12] (a) Intra-rack. (b) Inter-rack top (top) and side (bottom) views.

3.5 Wireless DCNs: Challenges and Lessons

Applications hosted by DCNs (e.g., Hadoop and Spark) generate large demands for intra and inter-rack communication bandwidth. To meet such demands, new communication technologies must be capable of achieving high link and network capacities. However, realizing high-bandwidth links can be challenging, and these challenges vary

depending on the technology used for communication. In this section, we discuss the challenges facing the deployment of wireless technologies in DCNs and the lessons learned from the literature. We start by discussing the challenges that may face any wireless technology to be deployed in DCNs, then we focus our discussion on technology-specific challenges:

Security

In a DCN, often data is exchanged between nodes in different racks to complete tasks. Therefore, isolation of data from unintended nodes and services is a must to avoid security and privacy problems.

The limited transmission range of 60 GHz and the inability to penetrate obstacles prevent 60 GHz signals from traveling further than their intended target. Moreover, the use of narrow beam width makes it easier to target only the intended receiver. This makes 60 GHz technology immune to eavesdropping. On the other hand, one of the distinct advantages of FSO technology is its inherent PHY layer immunity to eavesdropping as compared to most RF technologies. Wireless DCN designers must take advantage of this feature and develop efficient low-overhead security protocols at higher networking layers. This means that less overhead, and more useful data can be transmitted leading to higher throughput and improved overall performance.

Small form factor of networking components

A typical rack is 0.078″ high, 23-25″ wide and 26-30″ deep. Servers and switches are inserted horizontally into the racks. The thickness of a module in a rack is measured in *Rack Unit (U)*, which is 1.8″. Most servers fit the 1U size, other servers may require 2U or larger sizes [412]. The designers are required to develop components and network interfaces of small form factor taking into consideration the dimension

constraints imposed by DCN commodity technologies.

Heat and air flow

DCN designers may change the rack arrangement in DCN floor (i.e., physical topology) instead of using the conventional row-based arrangement to fully utilize the flexibility provided by wireless links (e.g., cellular DCN design). Any change in the DCN floor, however, can cause changes in the air flow and heat distribution properties. This may in turn lead to inefficient cooling, and thus network component failure or higher power consumption. Moreover, it can also cause turbulence and may impact the performance of FSO links. Therefore, computational fluid dynamic (CFD) analysis must be performed for new DCN arrangements to understand the behavior of the air and heat flows and ensure functional and efficient DCN.

Agile Links

To address the hotspot problem encountered by wired DCNs, inter-rack wireless links must have a degree of reconfigurability. One of the main challenges faced by wireless DCN designers is establishing and maintaining wireless links between different servers or racks. There are several methods that can be used to realize agile links. Some of them work for both, RF and FSO, technologies, whereas other methods could be technology-specific.

- Mechanical steering. The main idea is to steer RF horn antenna or FSO transceiver. mounted to pedestals that sit on top of rack cabinets. Both rotation and height of the transceiver can be controlled allowing for establishing flexible wireless links [8, 12, 417].

As discussed earlier, mechanical components can add to the complexity and latency

of the system, and can increase the risk of failure. These limitations can be addressed using the following technology-specific solutions:

- RF Beamforming using phased array antennas can provide very fast steering, however experiences signal leakage, and thus weaker signals.
- FSO Preconfigurable-Electronically Reconfigurable Links. In this type of links, a link is electronically reconfigured to choose from preconfigured link configuration [9, 10, 50]. There is no guarantee, however, that the preconfigured links are efficient. Moreover, manual change of the preconfiguration is needed.

There is a need for new means for realizing agile wireless links in RF and FSO DCNs.

Obstruction-free wireless links

At the scale of mega DCNs, hundreds of racks must be interconnected, and thus wireless DCN should scale to meet this large link connectivity requirements. Network resources must be efficiently provisioned to meet the requirements of hosted DC services and applications, and to maintain a minimum level of availability. However, a critical impediment to the design of wireless DCN is the difficulty establishing *obstruction-free* wireless links to connect multiple adjacent network components. This is because LOS links can not be easily maintained as other components get in between the source and destination need to be connected leading to risk of link blocking [52]. Several solutions appear in the literature to overcome this problem. Different solutions present different tradeoffs with respect to simplicity and configurability. In the following, we discuss these solutions:

- Configurable Link + Ceil Reflector: this solution is proposed in both 60 GHz, and FSO DCN literature. In this design a configurable link is used to transmit

the signal towards a reflector (e.g., mirror in case of FSO). The signal reflects off of the reflector towards the destination node. The configurable link can be obtained using any of the techniques discussed in "Agile Links". This solution can provide obstruction-free links covering most of the DCN. However, alignment and configuration of the link can be complex. Moreover, it depends on the degree of reconfigurability of the transmitter.

- Cellular (circular, polygonal, or spherical) Design: although can provide limited configurability, cellular design guarantees simple LOS wireless links. In case of cellular design, wireless transceivers can be placed on ToRs at a height that is above the average human height, so human movements do not obstruct the link [85,86]. Cellular designs, however, usually involve unutilized space enclosed by the cells.

Containerized DCNs

Many existing and under development DCs utilize large open DCN floor design. However, as discussed in Section 3.4.1, containerized DCNs can present a cheaper and an efficient alternative design. A few papers discuss the deployment of 60 GHz RF and FSO technologies in the containerized DCN scenario [8, 44]. As a container becomes the building block of a DCN, intra and inter-container communication links must be designed.

At the scale of a container, problems related to cabling complexity may not be significant. Moreover, using wireless communication to replace the wiring infrastructure in a DCN container may help increase the number of servers by only a few. Therefore, studies are needed to ensure the viability of wireless technologies deployment in DCN containers.

Once proven viable, other technical issues must be taken into consideration during

the deployment of wireless communication in DCN containers. Confined space and metal walls make the container a challenging environment for 60 GHz links as signals may reflect off the walls leading to multipath fading. A possible solution to alleviate the multipath fading in containers is to cover the inner of the container with adsorbent materials, or by employing very narrow beam antennas [44]. On the other hand, environmentally controlled containers are very suitable for FSO communication.

Inter-container links carry the traffic of the container, and thus must provide higher bandwidth. However, 60 GHz can be of limited capacity with respect to the container traffic. On the other hand, FSO can provide the required capacity, however, it becomes prone to the environment impairments and techniques used for outdoor FSO links must be applied to mitigate such impairments. It is possible that multiple links and MIMO techniques can be used to provide the required inter-container traffic. In addition to the challenges and requirements discussed above, each technology can experience unique technology-specific challenges and requirements. In the following we discuss the challenges specific to 60 GHz RF, and FSO technologies.

3.5.1 Challenges for 60 GHz in DCNs

60 GHz Behavior Modeling and Analysis

In [406], Zaaimia et al. present initial measurements of 60 GHz RF channels in a real campus DCN. Authors perform experiments on two inter-rack measurement sets, cross aisle (racks from parallel rows) scenario set, and neighbor (on the same row) racks scenario set. Channel transfer function is measured using a channel sounder that is based on vector network analyzer. In order to verify the accuracy of measurements, the authors conduct ray tracing simulations as well. Needless to say, neighbor racks scenario show a 3 dB improvement in the link budget over cross aisle scenario.

The research on wireless DCNs is relatively novice. Therefore, large number of new unprecedented design concepts and topologies are emerging. All designs aim to fully utilize the flexibility presented by 60 GHz technology. A major conclusion from the study by Zaaimia et al. is that path loss of 60 GHz link is environment-dependent. Therefore, there is a current need for an accurate modeling scheme of wireless DCN environment. This can be a challenging task due to the high density of metal structure in DC. Moreover, having a design or simulation tool can be of great interest to DCN designers to test the physical topology of their DCNs.

RF Channel Allocation and Frequency Reuse

Channel allocation can be classified as fixed (FCA), dynamic (DCA), and hybrid (HCA). In FCA schemes, a channel or set of channels is permanently allocated to each RTU. In DCA, all channels are kept in a central pool and are assigned dynamically to new links. This assignment can be done by a central controller or the allocation scheme can be distributed. HCA is a combination combination of both FCA and DCA techniques. in HCA, the total number of channels available for service is divided into fixed and dynamic sets. Fixed set is assigned to RTUs, whereas the dynamic set is shared by all DCA.

In DCs, the decision of which channel allocation scheme to use mainly depends on the type of DCN. For example, in case of hybrid DCNs, wireless links are used to provide on-demand links to enhance the performance. Therefore, FCA is not a good choice as it will lead to channel underutilization due to the unused assigned channels, and DCA in this case is more suitable.

On the other hand, in case of pure DCN, performing scheduling every time a server sends a signal is not practical. Moreover, the traffic patterns can lead to unfairness as few servers can dominate the links. Therefore, using DCA in a pure DCN can be

inefficient. However, given the scale of DCNs and the large number of nodes and the limited number of channels, FCA in pure RF DCNs requires careful assignment and scheduling to reduce the impact of interference.

60 GHz technology has lower link range and very limited ability to penetrate obstacles. This in turn promotes frequency reuse. However, the frequency reuse in DCNs is not yet explored. We envision that wireless DCNs can benefit from the mature mobile network systems. For example, a DCN plane can be divided into logical cells. Each cell can be assigned a set of frequencies, such that the frequencies are used across the DCN. This way the channel allocation problem becomes at the scale of a cell, and thus simpler than the channel allocation and scheduling at the DCN scale. This will also lead to a faster allocation using developed heuristics or using any of the well-known evolutionary algorithms, such as Genetic Algorithm (GA) [418], Particle Swarm Optimization (PSO) [60], or Binary Harmony Search Algorithm (BHSA) [419].

3.5.2 Challenges for FSO in DCNs

Visible vs. infrared sources

The experiment by Chowdhury et al. [85, 86] has shed some light on the potentials, as well as limitations, of FSO links for DCNs. Although FSO links are capable of providing lossless high data rate transmission, point-to-point FSO links require careful installation and alignment [85, 86]. Using visible light sources can ease the alignment of FSO links in FSO DCNs. However, most off-the-shelf components such as LDs and optical modulators are manufactured for fiber optics, and thus operate in the infrared spectrum. This is because the attenuation of the glass in fiber optics is the lowest at the infrared region of the spectrum. Therefore, there is a current need for the development of communication components (e.g., high speed optical modulators)

required for establishing high data rate point-to-point FSO links using LDs operating in the visible region of the spectrum.

Artificial light sources

In the absence of the background radiation, ambient artificial light becomes the dominant source of noise for indoor FSO systems [52]. Conventionally, two types of ambient artificial light sources are used for indoor illumination, incandescent and fluorescent lights. Using high pass filters (HPF), fluorescent lights driven by a conventional ballast can be mitigated, whereas, fluorescent lights driven by electronic ballast are harder to mitigate.

Due to the good attributes of LEDs, such as, better light quality, low energy consumption, small size, and long lifetime, there is a trend towards using LEDs to replace traditional incandescent and fluorescent light sources for indoor illumination [75, 267]. Since LEDs have narrower power spectral densities (PSDs) as compared to that of incandescent and fluorescent lights, a possible solution to mitigate the effect of the artificial ambient light in DCNs is to illuminate the DC using LED sources that are out of band with respect to the LDs used for communication [52].

Vibration

In order to achieve high data rate links, point-to-point FSO links are used. However, point-to-point links require careful alignment so that sufficient optical power can be received. Vibrations due to server fans, discs, HVAC and UPS units can lead to link misalignment [420], and thus add to the complexity of the FSO link design. There are three possible solutions for the vibration problem:

- Use active vibration isolation (AVI) system [376]. Although this is suitable for lab experiments, in case of large number of links such as in DCNs, this solution

can be expensive.

- Increase the width of the beam such that it overfills the detector at the receiver side allowing for vibration tolerance. In case of minor misalignment due to vibration, the receiver will still be able to receive sufficient power to maintain the link. According to Hamedazimi et al. [50], 6 mm vibration tolerance is sufficient to handle minor misalignment due to vibration. This solution, however, requires the use of detectors with higher sensitivity, and thus more expensive transceivers must be used.

- Mount optical transceivers on a metal frame that is separate from the rack structure. This way, the impact of rack vibration is reduced. Links between the rack and the optical modules mounted on the frame can be established using short flexible optical fibre cables. This solution can't completely alleviate the impact of vibrations. Moreover, the metal frames can lead to underutilization of the DC space.

3.6 Chapter Summary

In this chapter, we compare the two potential candidate technologies for wireless communication in DCs, namely; 60 GHz and FSO. Comparison shows that both technologies are unlicensed and have link length suitable for the confined environment of DCs. Moreover, 60 GHz and FSO technologies depend on LOS links, but 60 GHz technology has lower practical bandwidth and can be affected by interference. On the other hand, FSO links require careful alignment to maintain the LOS.

We propose a classification that can be used to classify any DC, including existing wired and emerging wireless DCs. Our classification is based on the communication technologies used to realize the DCN. According to the proposed classification, wired

DCs can be classified as pure electrical/optical wired DC, or hybrid wired DC. On the other hand, wireless technology can be used either to augment wired DCs resulting in hybrid DCs, or to realize pure RF/FSO DC. We discuss different wireless-based DC designs and collate the major work in the field to jump-start researchers to tap into the growing research on wireless DCs.

Several research questions and design challenges must be investigated before wireless DCs can be realized. Based on the classification and the review of existing literature, we believe that the following two questions are the key research questions;

- Can a wireless technology alone satisfy the requirements of future DCs in a pure wireless DC fashion, or do we need hybrid DCs?
- Given a wireless technology, what is the best network architecture and topology?

Using the proposed classification, we now have a nearly complete picture for the design space of DCNs. By surveying the literature and mapping existing solutions to different possible designs in the proposed classification, it is now possible to easily identify new research areas. For example, in this chapter, we were able to identify that the area of hybrid wireless DCNs has not yet been explored.

Chapter 4

OWC-Bus

In this chapter, we propose a design of a data center network (DCN) using Optical Wireless Communications (OWC) technology. The proposed OWC-DC design is based on fixed, non-mechanical, OWC links facilitating the realization of fully connected OWC racks and rows/columns of racks. Each rack becomes a point of intersection of three fully connected sub-networks. We investigate requirements, advantages and challenges of the proposed design.

4.1 Towards the Design of a Pure OWC DCNs

It may be noted that a common impediment for all wireless DCN designs is the difficulty of connecting multiple adjacent network components, such as racks in a row or servers in a rack, using point-to-point LOS links.

Figure 4.1-(a) shows a DC in which racks are deployed in a row-based arrangement with J rows. Each row contains k racks. A rack can be identified using its row and column numbers (j, k), where, $(1 \leq j \leq J \; and \; 1 \leq k \leq K)$. For the ease of demonstration, each rack is represented by a rectangle labeled with the rack's coordinates $Rack(j, k)$.

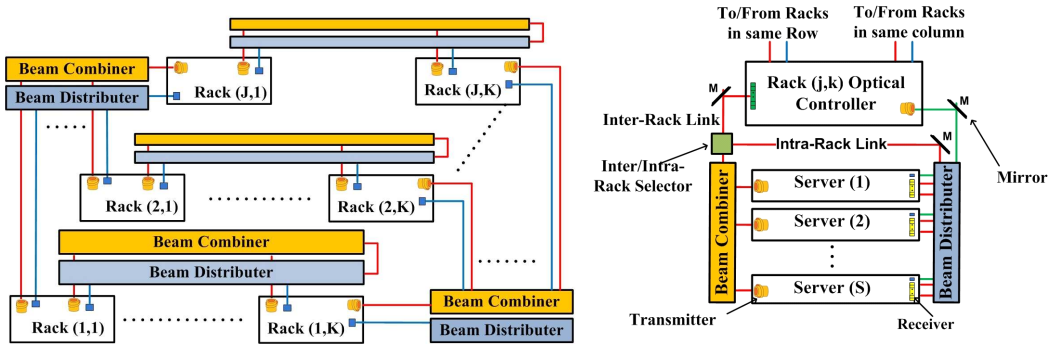

Figure 4.1: (a) Proposed Design of an OWC-DC. (b) Proposed Fully Connected, Switch-Free OWC Rack of Servers.

We start with the design of an OWC rack, in order to understand the design of the proposed OWC-DC.

4.1.1 Switch-Free OWC Rack

Figure 4.1-(b) shows a *switch-free* OWC rack comprising S servers. The servers are numbered from 1 to S from top to bottom of the rack. Therefore, a server in the $Rack(j,k)$ can be identified by its coordinates $Server(j,k,s)$, where, $(1 \leq s \leq S)$, is the number of the server. In order to achieve high data rate communication between servers within the same rack, servers must be connected using point-to-point OWC links.

In our design, each server is equipped with an optical transmitter on one side of the server, and an optical receiver comprising a photodetector (or an array of photodetectors) on the opposite side. Servers are mounted on the OWC rack such that all transmitters (receivers) of the servers are on the same side of the rack. The main idea is to direct the transmitted beams either for intra-rack, inter-rack, or both communications, using the intra/inter-rack selector. For intra-rack communication, the beams are directed to the other side of the rack where receivers are placed. Using a

beam distributer, beams are distributed to all servers allowing *switch-free* intra-rack communication. On the other hand, for inter-rack communication, the combined beam is directed to the *Rack Optical Controller (ROC)*.

Directing the beams around the rack can be done using a set of mirrors mounted to the structure of the rack. Any server can receive a copy of the S beams using beam splitters placed in front of the server to be able to intercept the beams.

Figure 4.1-(a) shows three rows (i.e., rows 1, 2, and J), and the first and last columns (i.e., columns 1 and K). ROCs within the same row (and similarly, ROCs within the same column) can be connected together using a method similar to the method used to connect servers within the same rack.

In case of intra-rack communication, S light beams from the S servers can be transmitted and received by all servers, simultaneously. Each transmitter has a separate optical path connecting it to all other servers. Therefore, there are no collision domains, instead, each server has its broadcast domain which must be managed efficiently so that, data are delivered to the intended destination(s) only. Many networking and addressing schemes can be used. A network topology of the rack can be changed according to the scheme selected. In the following, we briefly discuss three of such schemes:

- Time Division Multiple Access (TDMA), where, the frame of any source server s is divided into $S-1$ time slots (TSs). The server s transmits data to the server i using the TS i, where, $1 \leq i \leq S$ *and* $i \neq s$. The intra-rack network can be considered as S subnetworks, each subnetwork is a *bus network* with a single transmitter.

- Using a technique similar to optical burst switching (OBS), source server s sends a short optical packet prior to the data transmission. The short packet contains

addresses of the destination(s) and any other necessary information. The $S-1$ servers receive the short packet, intended destinations receive incoming data, and other servers ignore it. The topology of the network is similar to that of in TDMA case.

- Wavelength Division Multiplexing (WDM). Can help boosting the capacity of intra-rack links. Each receiver is assigned a wavelength, or multiple wavelengths. Using tunable transmitters and receivers, signals transmitted to other servers are delivered using the same beam at different wavelengths. In this case, the rack topology is a fully connected (complete mesh) network.

4.1.2 Rack Optical Controller (ROC)

For inter-rack communication, an ROC receives data from other racks to deliver to the servers in its rack, communicate with other racks in the same row/column, and relay the data received from any of the ROCs in the same row/column to any of the ROCs in the same column/row.

Racks are arranged in rows and columns, and it is possible to connect ROCs using the same method as for servers within the same rack. Moreover, communications between ROCs can follow same schemes discussed in the intra-rack communication. The functions performed by ROCs are very similar to a regular switch, however, it might be noted that unlike TOR switches, intra-rack communication is not dependent on the ROC. Moreover, each ROC is the intersection of three fully connected networks. This can be efficiently utilized in routing and DC network management. An ROC is expected to handle large amount of traffic compared to servers, therefore, we envision the use of WDM/DWDM to increase inter-rack link capacities. Two cases in inter-rack communication:

1. The source ROC is located on the same row/column of the destination ROC, and two-hops link is needed to perform the communication. The source server sends data to the source ROC, which forwards the data to the destination ROC, and finally, to the destination server.

2. The source and destination ROCs are neither located on the same row nor same column. In this case, a link with a minimum of three hops is needed. Source server sends data to source ROC, which in turn forwards the data to the ROCs on the same row or column. The ROC located at the row/column intersection of the source and destination ROCs will forward the data to the destination ROC then to the destination server. However, due to the full connectivity, other paths can be used for routing. The decision of transmitting the data to the row or the column ROCs depends on the used routing algorithm.

In order to realize rack topology equivalent to S bus subnetworks using current technology, S^2 wires are needed (i.e., 1600 wires/rack for $S = 40$). Similarly, a fully connected rack using the current technology requires a total of $(S^2 - S)/2$ full-duplex wire segments (i.e., 780 wires/rack for $S = 40$) where each server is equipped with, at least, S ports. This is almost impossible to manage and basically one of the main reasons why the star topology was adopted in the first place.

The small size of OWC components, and the ability to split a beam among S servers using a set of passive optical elements, help realize a fully connected rack using only S beams.

4.1.3 Indoor Point-to-Point LOS OWC Link

In this section, we provide a brief description of an indoor point-to-point, LOS OWC link.

The proposed design uses Laser Diodes (LDs) because they have high optical power outputs and can support transmission at high bit rates. We adopt Avalanche photodetectors (APDs) since they are preferred in systems that require high data rates and where the noise induced by ambient light is negligible because APDs have high cost and require high bias [51].

4.1.4 Optical Noise Sources

OWC links are deployed in a wide range of environments (e.g., indoor and outer space). Different noise sources affect the performance of the OWC link with varying degrees of severity depending on the environment. We first discuss the noise from different sources affecting indoor OWC links that can be mitigated in our design.

The absence of the noise due to background radiation (e.g., the sun) makes the ambient artificial light the dominant source of noise in DCs [51].

Point-to-point LOS links utilize transmitter and receivers with narrow field of view (FOV), therefore, these links are capable of rejecting majority of the ambient artificial light [51]. Moreover, using high pass filters (HPF), fluorescent lights driven by a conventional ballast can be mitigated, whereas, fluorescent lights driven by electronic ballast are harder to mitigate [51]. Since LEDs have narrower PSDs as compared to that of other light sources, a more efficient solution for the artificial ambient light would be to illuminate the DC using LED sources that are out of band of the LDs used in the DC. This way, the ambient artificial light can be easily mitigated.

On the other hand, there are three inevitable noise sources, namely; quantum (shot) noise, dark noise and thermal (Johnson) noise. The shot noise is due to the random arrival rate of photons from the transmitter and has a variance σ_q^2. On the other hand, dark noise is due to a very small current from the PD which is a combination of two currents: bulk (I_D) and surface leakage (I_L) currents with

variances (σ_{db}^2) and (σ_{dl}^2), respectively. Finally, the thermal noise exists in any circuit of equivalent resistance R_L and temperature T_e and modeled as a white Gaussian noise with zero mean and variance σ_{th}^2. The total noise variance σ_N^2 is given by:

$$N_T = \sigma_q^2 + \sigma_{db}^2 + \sigma_{dl}^2 + \sigma_{th}^2 \tag{4.1}$$

$$N_T = 2qRP_RBFM^2 + 2qI_DBFM^2 + 2qI_LB + \frac{4\kappa T_e B}{R_L} \tag{4.2}$$

where q is the electric charge, R is the PD's responsivity, P_R is the power received, B is the electronic bandwidth, M is the PD's gain factor, and F is the excess noise factor.

4.1.5 Link Budget

Using LDs, we can get very narrow beam with concentrated power, however, any beam propagating in the free space experiences a slight divergence. Short links might not be affected by this problem since it is possible to use PDs with light collecting areas that matches the spot size of the light beam. For long OWC links, collimators can be placed at certain points along the path to re-collimate the beams.

The diameter of the spot size of a beam that has a very small beam width angle θ and travels a distance D is approximately equal to $(\theta \cdot D)$ [106],

Assume a point-to-point, LOS link with a transmitted power P_t, transmitter and receiver optics efficiencies, η_T and η_R, respectively. The received unfaded power P_R is given by,

$$P_R = \eta_T \eta_R \mathcal{L}_{GL} P_T \tag{4.3}$$

where, $\mathcal{L}_{GL}$, denotes the geometrical loss which is the ratio between aperture area of the receiver (A_R) and the spot size area of the beam at the receiver (A_{im}), and is given by,

$$\mathcal{L}_{GL} = \frac{A_R}{A_{im}} = \left(\frac{D_R}{\theta D}\right)^2 \tag{4.4}$$

where, $D_R \leq \theta D$, and hence, Equation 4.3 becomes,

$$P_R = \eta_T \eta_R \left(\frac{D_R}{\theta D}\right)^2 P_T \tag{4.5}$$

4.2 Design and Analysis of an OWC Rack

In our design, servers are connected using point-to-point, non-LOS (NLOS) links formed using specular reflections (i.e., a set of mirrors and BSs). The difference between the link budget of a point-to-point, LOS link and that of NLOS with specular reflection is that, mirrors and BSs absorb light, and hence, might have efficiencies less than 100%. Moreover, a BS is used to split the light beam into two perpendicular beams: transmitted beam (along the path of the original incident beam), and reflected beam. Based on the design, transmitted and reflected beams may or may not have the same power. Therefore, in case of point-to-point, NLOS link, Eq. 4.5 must be extended to include the efficiencies and power reductions caused by mirrors and BSs. The losses and factors depend on the number and arrangement of mirrors and BSs in the design.

Figure 4.2 depicts the proposed design of a fully connected OWC rack. A typical OWC rack consists of S servers. Each server, s (for $1 \leq s \leq S$), is equipped with an optical transmitter T_s operating at wavelength λ_s. The power transmitted by a transmitting server s is denoted as P_{T_s} and the power efficiency of the transmitter's

lens is η_s.

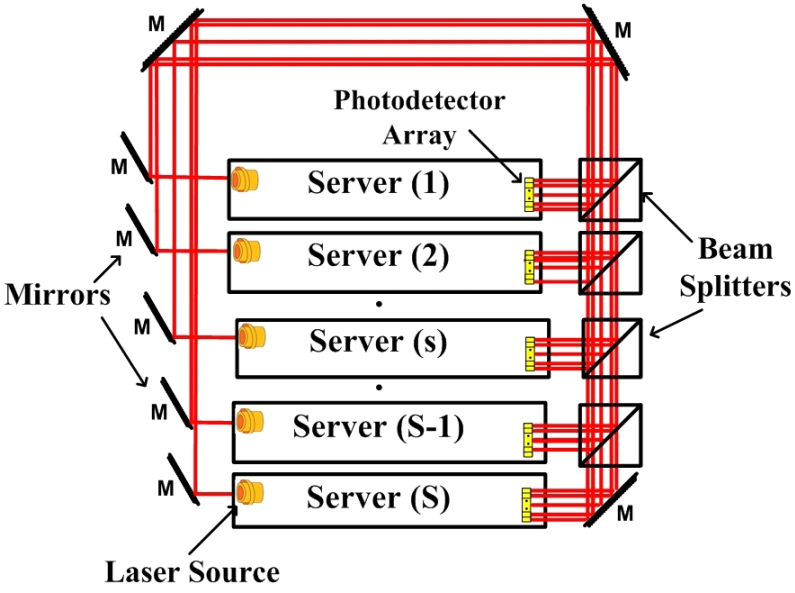

Figure 4.2: A Fully Connected OWC Rack of Servers.

An optical receiver is placed on the other side of the server with a PD array R_s to receive signals transmitted by the S servers. Each array contains S PDs, numbered from 1 to S. A PD s within the PD array R_s has a diameter D_{R_s}, power efficiency of the optical lens η_{R_s} and operates at the corresponding wavelength λ_s. It is assumed that the receiver is capable of handling the S input signals, using multiple receivers, a control plane, or a scheduler.

A mirror M_s is associated with each server s on the transmitter's side. On the other side of the server, a beam splitter BS_s is placed except for the server number S where the BS is replaced by the mirror M_S. Each mirror M_s has an efficiency of η_{M_s}, whereas, each BS has an efficiency of η_{BS_s}. A beam splitter BS_s splits the incident beam into two beams: reflected and transmitted with powers α_s and $(1-\alpha_s)$, respectively. As shown in Figure 4.2, two mirrors are used to direct the beams from transmission side to receiver side.

We consider the case where a single wavelength is used i.e., $\lambda_s = \lambda$, $1 \leq s \leq S$. In order to distinguish between transmitter and receiving servers, we use notation s for the transmitting server and s' for the receiving server, $1 \leq s, s' \leq S$. The received power by a server s' from transmitter server s is,

$$P_R(s, s') = P_{T_s} \cdot \eta_{T_s} \cdot \eta_{R_{s'}} \cdot \left(\frac{D_{R_{s'}}}{\theta_{s,s'} \cdot D_{s,s'}} \right)^2 \cdot \eta_M(s') \cdot \eta_{BS}(s') \cdot \Delta_{BS}(s') \tag{4.6}$$

where, $\theta_{s,s'}$, and $D_{s,s'}$ are the angle width, and the distance of the link between transmitter s and receiver s'. $\eta_M(s')$ and $\eta_{BS}(s')$ are the mirrors and BSs aggregated power efficiency functions, respectively. $\Delta_{BS}(s')$ is the aggregate power splitting function of BSs.

In a rack of 40 servers the maximum distance between a transmitter and a receiver does not exceed 5 meters. Therefore, it is possible to use PDs with light collecting area equal to the area of the beam at the PD. It is assumed that $D_R = \theta D$ for all transmitter-receiver combinations. This is a reasonable assumption since the beam diameter at the receiver is 2.5 mm, assuming a beam width angle of 0.5 $mrad$.

It is assumed that all transmitters and receivers are identical with the same power transmitted and optical efficiencies. It is also assumed that all mirrors have the same efficiency η_M and all BSs has the same efficiency η_{BS}. Then $P_R(s, s')$ becomes,

$$P_R(s, s') = P_T \cdot \eta_T \cdot \eta_R \cdot \eta_M(s') \cdot \eta_{BS}(s') \cdot \Delta_{BS}(s') \tag{4.7}$$

Figure 4.2 depicts that a link between two servers is reflected from three mirrors, except for server S, the number of mirrors is four. So, mirrors aggregated power efficiency function is,

$$\eta_M(s') = \begin{cases} \eta_M^3, & \text{for } 1 \leq s' \leq S-1 \\ \eta_M^4, & \text{for } s' = S \end{cases} \tag{4.8}$$

A link to a destination server s' traverses s' BSs except for server S, where the beam traverses $(S-1)$ BSs. Accordingly, BSs aggregated power efficiency function is given by,

$$\eta_{BS}(s') = \begin{cases} \eta_{BS}^{s'}, & \text{for } 1 \leq s' \leq S-1 \\ \eta_{BS}^{S-1}, & \text{for } s' = S \end{cases} \tag{4.9}$$

The number of BSs and the power ratio of the transmitted/reflected beams at each of the BSs affect the received power at each server. We assume that a BS s' reflects $\alpha_{s'}\%$ of the incident beam's power, and transmits $(1-\alpha_{s'})\%$. Hence, the power splitting function of BSs is,

$$\Delta_{BS}(s') = \begin{cases} \alpha_{s'} \prod_{j=1}^{s'-1} (1-\alpha_j), & \text{for } 1 \leq s' \leq S-1 \\ \prod_{j=1}^{S-1} (1-\alpha_j), & \text{for } s' = S \end{cases} \tag{4.10}$$

The signal-to-noise ratio (SNR) is given by [51],

$$SNR_{IM\text{-}DD} = \frac{I_p^2}{N_T} = \frac{(RMP_T)^2}{\sigma_q^2 + \sigma_{dl}^2 + \sigma_{db}^2 + \sigma_{th}^2} \tag{4.11}$$

4.3 Simulation and Results

In this section we present the analysis of the proposed OWC Rack and a cost estimate of the proposed OWC-DCN.

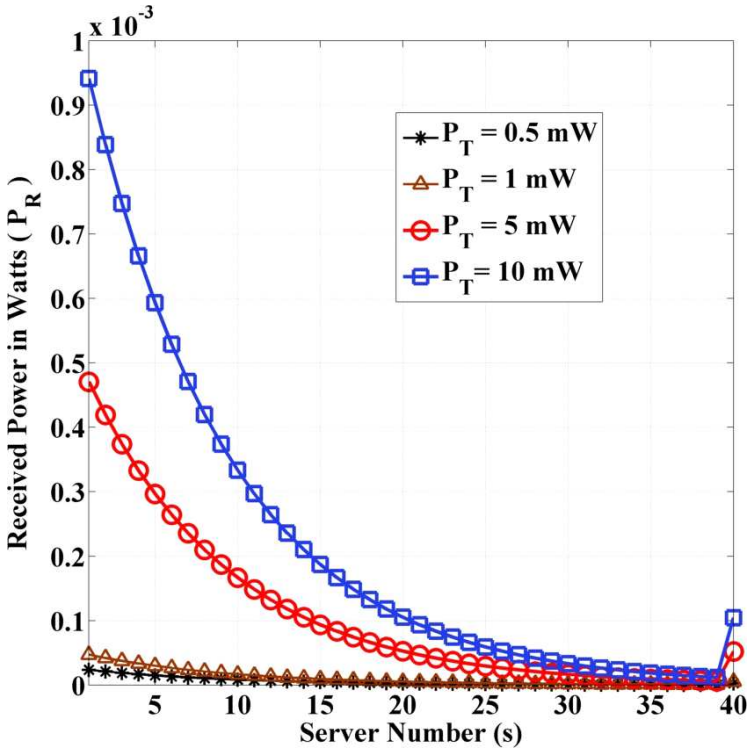

Figure 4.3: Received power by Servers.

4.3.1 Performance Analysis of OWC Rack

The electronic charge q is equal to 1.602×10^{-19}. PD responsivity (R) and gain factor (M) are assumed to be 0.9 and 3, respectively. Both, dark current and leakage currents are assumed to be $15nA$. The temperature and equivalent resistance of the receiver are assumed to be $290K$ and 1 $K\Omega$. We assume that the number of servers $S = 40$. Optical efficiency of all transmitters/receivers optics, mirrors and BSs are assumed to be 99%. For a BS s', the power of the reflected light beam $\alpha_{s'}$ is 10%, and hence, the power of the transmitted light beam is 90%. The wavelength is assumed to be 1500 nm.

The power received as a function of the position of the server in the rack is shown in Figure 4.3. The power reception falls as we move towards the bottom of the rack. Power levels are of the order of 10^{-3} W for transmitted power in the range of 0.5

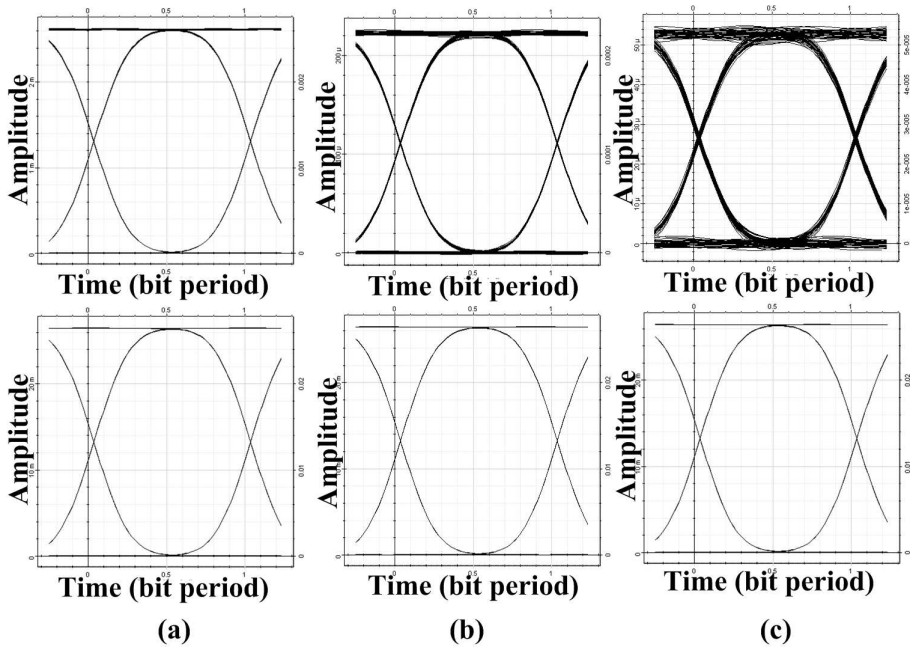

Figure 4.4: Eye Diagrams of OWC (top) and Fiber Optics (bottom) at 2.5 Gbps and $P_T = 10\ mW$ (a) s=1. (b) s=25. (c) s=39.

mW to 10 mW. There is a sudden improvement in the received power by the server S compared to the server $S-1$. This is due to the ratios of the BSs used where the last server receives 0.99×0.9 of the power incident to the BS number $S-1$ while the server $S-1$ receives 10% of that power.

In order to evaluate the performance of an OWC link within the rack, OptiSystem software was used. An OWC link was implemented with an OWC channel of five meters. We created a link with the same characteristics, however, it deploys a fiber optic instead of OWC. Both transmitters use OOK NRZ modulation scheme for simplicity, however, for higher data rates, other modulation schemes such as pulse position modulation (PPM) are preferred [51]

Figure 4.4 depicts the eye diagrams of the OWC and fiber optical links at 2.5 Gbps. Three servers are selected (i.e., server 1, 25 and 39). It is clear that as we move towards the bottom of the rack, the power received decreases, degrading

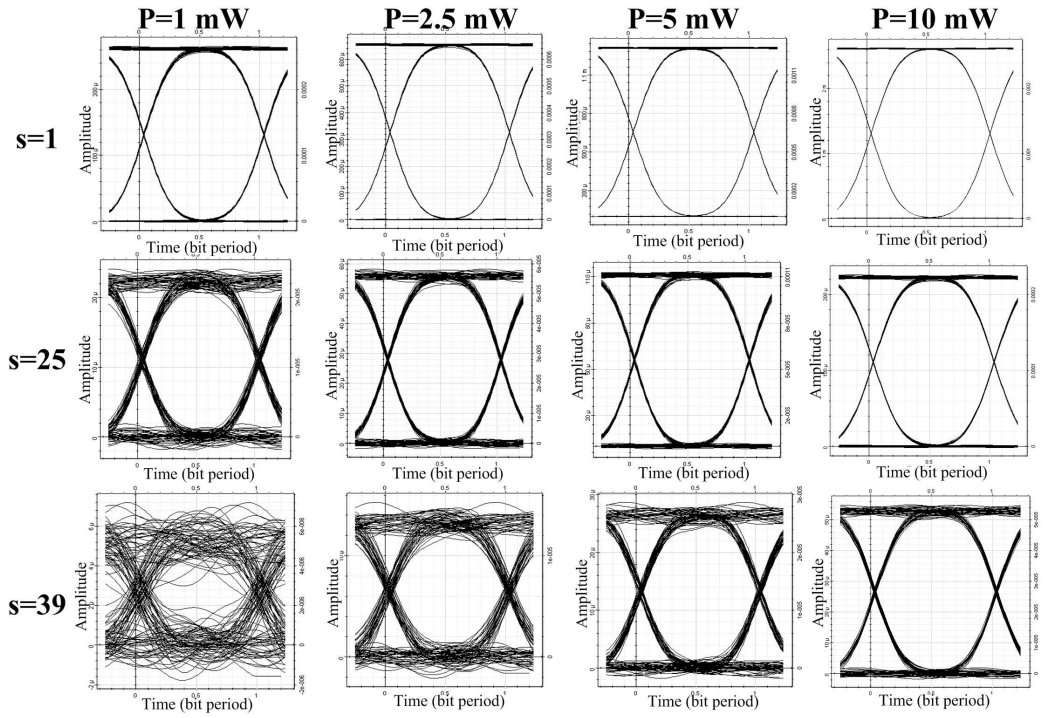

Figure 4.5: Eye Diagrams at different servers ($S = 1$, 25, and 39) using 2.5 Gbps and varying transmitted power (P_T).

the performance of the OWC link. On the other hand, it is difficult to notice any variation in the fiber optical link since the link is too short, and the received power is not affected by BSs or mirrors as in the OWC link.

Table 4.1 summarizes the performance of OWC and fiber optical links at different servers and different transmitting powers. As we move towards servers at the bottom of the rack, when transmitted power is low, Q-factor, eye height, and threshold all degrade and minimum BER increases. On the other hand, increasing the transmitted power improves the performance of the link allowing error-free communication.

Results in Table 4.1 suggest that for higher bit rates, using low power (near 1mW) is sufficient to realize low BER for servers near the top of the rack. On the other hand, it might be difficult to establish a link with servers near the bottom of the rack at this low transmitted power. Therefore, system optimization can be realized

Table 4.1: Summary of the OWC Link Performance Compared to the Optical Fiber Link.

		$P_T = 1\ mW$		$P_T = 5\ mW$		$P_T = 10\ mW$	
	s	OWC	Fiber	OWC	Fiber	OWC	Fiber
Max. Q Factor	1	110.4	253.8	227.0	276.9	274.8	284.4
	25	15.8	248.3	61.9	269.5	105.5	293.0
	39	3.84	257.0	18.8	286.7	33.1	276.0
Min BER	1	0	0	0	0	0	0
	25	1.5E-6	0	0	0	0	0
	39	6.1E-5	0	0	0	0	0
Eye Height	1	250E-6	2.6E-3	1.3E-3	13.0E-3	2.6E-3	26.0E-3
	25	1.8E-5	2.6E-3	100E-6	13.0E-3	210E-6	26.0E-3
	39	1.1E-6	2.6E-3	2.2E-5	13.0E-3	4.8E-5	26.0E-3
Thresh-old	1	3.0E-5	190E-6	100E-6	940E-6	180E-6	1.9E-3
	25	9.7E-6	180E-6	2.5E-5	960E-6	2.8E-5	1.9E-3
	39	2.4E-6	190E-6	1.1E-5	930E-6	2.3E-5	1.9E-3

by setting the power transmitted by each server based on the intended destination. This way, the power consumption can be minimized.

We perform further simulations to understand the performance of the OWC Rack at different servers and using different transmission powers. Figure 4.5 shows the eye diagrams at different servers (S) using 2.5 Gbps and different transmitted power (P_T). We chose $S = 1$ (top of the rack), $S = 25$ (middle of the rack), and $S = 39$ (bottom). Moreover, we vary the transmitted power using 1, 2.5, 5, and 10 mW. As expected, reducing the transmitted power does not significantly impact the received signal at $S = 1$. On the other hand, at $S = 25$ we notice degradation in the quality of the received signal at 1 and 2.5 mW. At $S = 39$, the quality of the received signal degrades as we reduce the power. At P_T = 1mW we notice a highly distorted eye indicating high noise, jitter, and inter-symbol interference (ISI).

4.3.2 Cost Estimate

Comparing OWC-DC to CDC is challenging. CDCs have been the main interest of the academic and industrial communities for long time. This implies that the cost-performance tradeoff of the wired technology has been improving over the last decades. On the other hand, OWC components for DCs may not exist yet. Therefore, we only aim to have an approximate sense of the OWC-DC cost. We consider the price of the TOR, aggregate and core switches following [6], however, we also include the cost of the network interface cards (NICs). Tables 4.2 and 4.3 depict the prices used in our calculations and the costs of three reference CDC configurations used to connect 10K servers for comparison, respectively [6].

Table 4.2: Cost of Different Components used in CDC

Component	**Price ($)**	**Minimum Unit**
NIC	80	1
TOR	8,000	1
Aggregate Switch (AS)	9,000	1
Core Switch (CS) Subunit	60,000	1
Core Switch (CS) Chassis	12,000	1
Core Switch (CS) Power Supply	3,500	3

Table 4.3: Total Cost of Different CDC Configurations

Configuration	**# TOR**	**# AS**	**# CS Subunit**	**# CS Chassis**	**Total Cost ($)**
CDC1	250	52	16	2	4,162,500
CDC2	250	48	12	2	3,886,500
CDC3	250	26	8	1	3,436,500

In case of the OWC-DC, we consider cost of OWC transceivers and ROCs. Since there is no reference for these prices, we estimate cost by refereing to the prices of

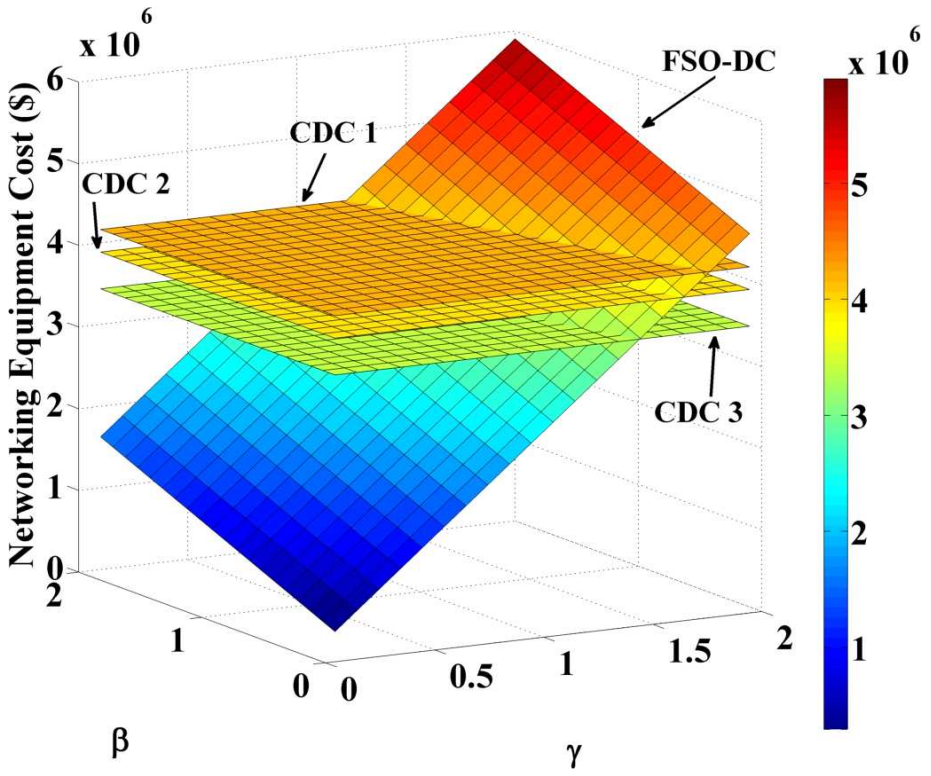

Figure 4.6: OWC-DC Cost Function Compared to CDCs.

CDC devices, e.g., we assume that the price of OWC transceiver is γ times the price of an NIC (C_{NIC}), and the price of an ROC is β times the price of an aggregate switch (C_{agg}), where $0.1 \leq \gamma,\ \beta \leq 2$. Therefore, the total cost of an OWC-DC is:

$$C_{OWC-DC} = J \cdot K \cdot [\gamma \cdot S \cdot C_{NIC} + \beta \cdot C_{agg}] \tag{4.12}$$

Figure 4.6-(b) depicts the cost function of the OWC-DC. It might be noted that, at $\gamma = \beta = 2$, the cost of OWC-DC is approximately 1.7 times the CDC3, and around 1.4 times the price of CDC1. However, there is still a range where, γ and β are greater than one, and yet, the price of the OWC-DC is cheaper or comparable to that of the CDC. We expect that, the cost of OWC technology will decrease as it is commercialized, leading to further reduction in the cost OWC-DC.

OWC-DC has another advantage over CDC is that an upgrade in a DC (e.g. from 10 Gbps to 40/100/400 Gbps or higher) will require huge investment and changes in the CDC as cables and switches must be replaced. OWC-DC presents a more modular architecture that is highly scalable with little upgrade required.

4.4 Chapter Summary

An OWC-DC design and associated link budget analysis for a fully-connected rack of servers is presented. Simulation shows that the proposed design realizes high data rates within a rack. Our cost analysis shows that the cost of the proposed OWC-DC design is comparable to that of conventional wired DCs. It is expected that the cost of the proposed design will decrease as OWC technology is commercialized. The proposed design is highly suitable for scaling and upgrading DCs. The proposed design addresses many problems and limitations of the current art, but several issues remain to be investigated.

Chapter 5

OWCell: Optical Wireless Cellular Data Center Design

In this chapter, we propose OWCells, a class of optical wireless cellular data center network architectures in which fixed line of sight (LOS) optical wireless communication (OWC) links are used to connect racks of servers arranged in regular polygonal topologies. We present the OWCell DCN architecture, develop its theoretical underpinnings, and investigate routing protocol and OWC transceiver design.

The chapter is organized as follows. In Section 5.1, we discuss the proposed cellular OWCell architectures. Results and analysis are discussed in Section 5.2 followed by future directions in Section 5.3. Conclusions are presented in Section 5.4.

5.1 Design of OWCell DCNs

In this section, we present our design philosophy for the proposed OWCell DCN architecture and develop its theoretical underpinnings.

From the discussion in previous chapters, it is clear that conventional row-based

rack arrangement in DCNs substantially hinders establishing inter-rack LOS wireless links. Therefore, recent research on RF DCNs propagates the use of polygonal arrangement of racks instead of rows [5,6]. Similarly, in [11], the authors present a very high-level description on intra- and inter-rack communications using OWC.

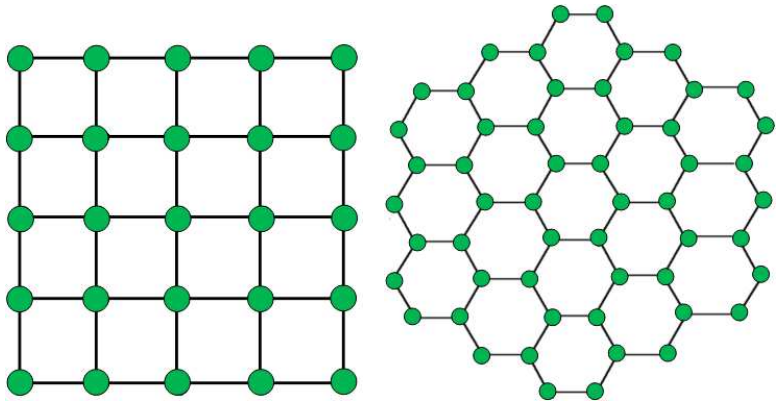

(a) (b)

Figure 5.1: Examples of multiprocessor and NoC network topologies using polygons (a) Square. (b) Hexagonal.

In large multiprocessor and networks on chip (NoC) systems, several studies considered arranging processors in a mesh of polygonal cells [421]. Figure 5.1 shows the commonly used square and hexagonal multiprocessor and NoC network topologies, where nodes represent the processors and edges represent connection links. Since the inter-processor links are established using wires, it is difficult to connect processors across the polygonal cells, and thus processor connections are limited to neighbor processors.

To achieve high data rate transmission using OWC links, line-of-sight (LOS) links are required. Conventional row-based arrangement of racks in DCNs is not an effective choice as it makes establishing LOS inter-rack FSO links a challenging task. To overcome this challenge, racks can be placed in regular polygonal arrangements, which we refer to as a *cell of racks (CoR)*. In this chapter, we propose OWCell DCNs

(OWCells for brevity), a class of OWC DCNs built using Interconnected CoRs where racks in a CoR can communicate using LOS OWC links. We analyze and establish the graph-theoretic properties related to the proposed OWCell DCN architectures. We also perform simulations to analyze the proposed OWCells and compare it to existing DCNs.

5.1.1 Design Philosophy

In our design, we use a *cell of racks (CoR)* as a building block for OWCells. To facilitate LOS communication, racks in a CoR are arranged in a regular polygonal topology by placing racks at its vertices. Figure 5.2-(a) depicts three possible designs of CoR using three basic polygons; square, hexagon, and octagon. We assume that racks in a CoR are fully connected, and thus each ToR is equipped with an OWC transceiver that allows the rack to simultaneously communicate with all other racks in the same CoR using LOS OWC links, as shown in Figure 5.2-(a) for one of the racks. A CoR, therefore, can be represented by a complete graph where nodes represent ToRs, and edges represent intra-CoR inter-rack OWC links. Figure 5.2-(b) shows the corresponding graphs of the CoRs proposed in Figure 5.2-(a). CoRs of the same type are then interconnected in a mesh arrangement to realize a DCN.

As stated above, a CoR can be represented by a complete graph, K_n, where $n \in \mathbb{Z}^+$. After investigating different values, we find that $n = 4,\ 6$, and 8 are very promising for designing OWCells. Using one of these three polygons as a building block, any rectangular mesh DCN can be realized.

By interconnecting CoRs we obtain a *complete graph mesh (CGM)*, that represents the OWCell, denoted as $\mathcal{C}(n, t, S)$, where n is the number of ToRs in a CoR, t represents the order of the CGM, and S represents the number of servers per rack. A CoR is a CGM of order 1, denoted by $\mathcal{C}(n, 1, S)$, and thus represents the building

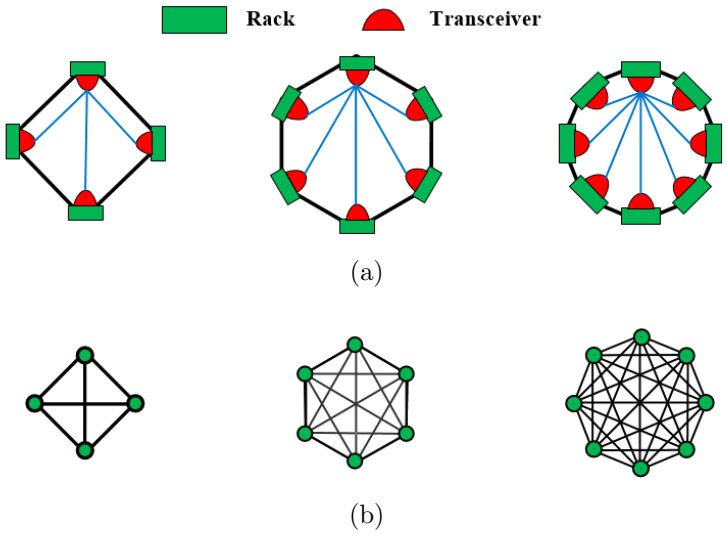

Figure 5.2: Examples of the proposed polygonal OWCell DCN (a) Topology (b) $\mathcal{C}(n, 1, S)$, for $n = 4$, 6, and 8.

block for an OWCell. Figure 5.2-(b) depicts $\mathcal{C}(4, 1, S)$, $\mathcal{C}(6, 1, S)$, and $\mathcal{C}(8, 1, S)$.

We use the notation $\mathcal{C}(4d, t, S)$ to refer to the special class of graphs with number of nodes, $n = 4d$ for $d \in \mathbb{Z}^+$. We construct square CGMs for all graphs in this class. A second order (i.e., $t = 2$) CGM, $\mathcal{C}(4d, 2, S)$, is obtained by arranging four CoRs in a 2×2 square grid such that adjacent CoRs share a node [see Figure 5.3-(a)]. In general, CGM mesh of order t, $\mathcal{C}(4d, t, S)$, is obtained by arranging t^2 CoRs in a $t \times t$ square grid with adjacent CoRs sharing a single node.

On the other hand, in case of hexagonal CoRs, we build hexagonal meshes instead of square meshes [422]. The $\mathcal{C}(6, 2, S)$ is obtained by adding six CoRs around $\mathcal{C}(6, 1, S)$, where each of the added CoRs shares a node with $\mathcal{C}(6, 1, S)$ as shown in Figure 5.3-(b). Inductively, a $\mathcal{C}(6, t, S)$ is obtained from $\mathcal{C}(6, t - 1, S)$ by adding a layer of CoRs around the boundary of $\mathcal{C}(6, t - 1, S)$.

Table 5.1 summarizes the total number of CoRs, ToRs (N), servers, inter-rack links, bisection width, diameter, and minimum and maximum degrees for $\mathcal{C}(4d, t, S)$ and $\mathcal{C}(6, t, S)$.

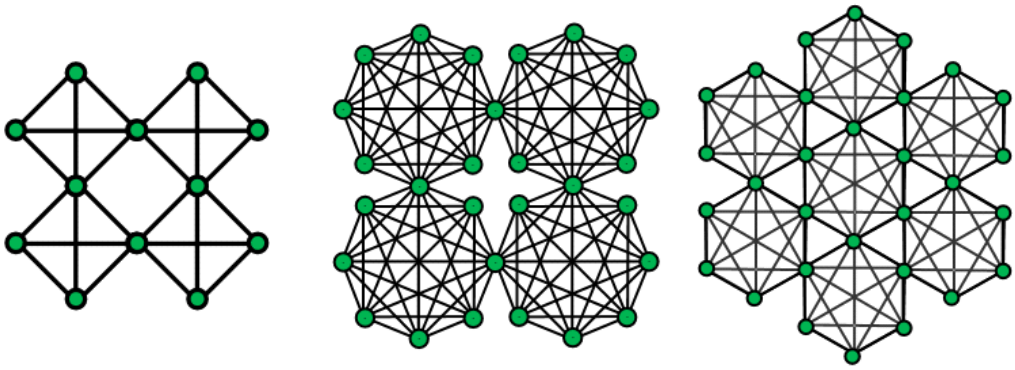

(a) (b)

Figure 5.3: Examples of the proposed OWCell DCN topologies, $\mathcal{C}(n, 2, S)$: (a) $n = 4$, and 8 (b) $n = 6$.

Table 5.1: Properties of Complete Graph Meshes, $\mathcal{C}(n, t, S)$.

Property	$\boldsymbol{n = 4d}$, $\forall \boldsymbol{d} \in \mathbb{Z}^+$	$\boldsymbol{n = 6}$
Number of CoRs	t^2	$3t^2 - 3t + 1$
Number of ToRs (N)	$(n-2)t^2 + 2t$	$9t^2 - 3t$
Number of Servers	$((n-2)t^2 + 2t) \times S$	$(9t^2 - 3t) \times S$
Number of Links	$\frac{n(n-1)}{2}t^2$	$45t^2 - 45t + 15$
Bisection Width	t even: $(n-1)t$ t odd: $(n-1)(t-1) + (\frac{n}{2})^2$	$16t - 13 \; \forall \; t > 1$
Diameter	$2t - 1$	
Maximum Degree ($\boldsymbol{\Delta}$)	$2(n-1)$	
Minimum Degree ($\boldsymbol{\delta}$)	$(n-1)$	

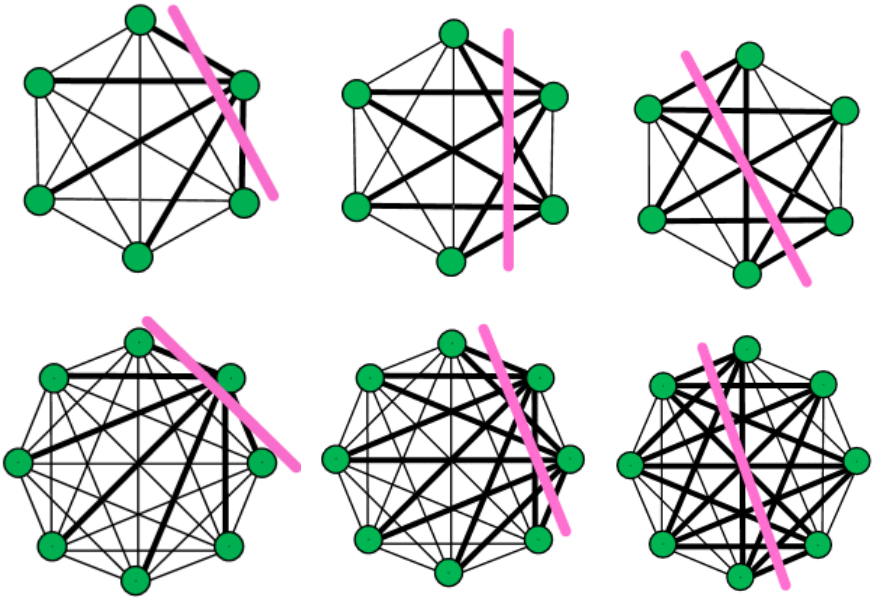

(a) (b) (c)

Figure 5.4: Different partitioning in CGM_1^6 (top) and CGM_1^8 (bottom). Bold edges form the corresponding cut-set. (a) $n-1$ (b) $2(n-2)$ (c) $(\frac{n}{2})^2$

We find that the class of mesh networks with number of nodes, $n = 4d$ for $d \in \mathbb{Z}^+$ admit elegant theoretical analysis. Therefore, in the following, we analyze $\mathcal{C}(4d, t, S)$ in detail and develop its theoretical properties. As mentioned earlier, graphs with $n = 4d$ have similar properties and analysis, and thus the following analysis can be easily extended to any $\mathcal{C}(4d, t, S)$ OWCell. Moreover, similar analysis can be directly obtained for $\mathcal{C}(6, t, S)$.

Theorem 1. *The total number of ToRs (N), servers and links in a $\mathcal{C}(4d, t, S)$ OWCell are $(n-2)t^2 + 2t$, $((n-2)t^2 + 2t) \times S$, and $(n(n-1)/2)t^2$, respectively.*

Proof. A $\mathcal{C}(4d, t, S)$ has t^2 CoRs. Each CoR shares one rack with adjacent CoRs along the width and height of the network. Every row and column has $(t-1)$ shared racks. The total number of racks is $N = nt^2 - (t-1)t - (t-1)t = (n-2)t^2 + 2t$. Each rack has S servers. It follows that, the total number of servers is $S \times N = S \times ((n-2)t^2 + 2t)$.

Every CoR is a complete graph K_n and has $n(n-1)/2$ links, hence total number of links is $(t^2)(n(n-1)/2)$. Figure 5.3-(a) shows a network with $t = 2$ and $n = 4$ with 12 ToRs and 24 links. □

Bisection width is the minimum bandwidth available between two network parts with equal number of nodes in each partition. If all links have the same capacity, finding the bisection width reduces to finding a minimum cut-set such that the network is partitioned into two halves.

To find the cut leading to the bisection width in the proposed OWCell, we have to cut some building blocks, $\mathcal{C}(n, 1, S)$, of the DCN. We are interested in two possible cuts of a $\mathcal{C}(n, 1, S)$ in which we separate a single node (one-node cut) and bisect $\mathcal{C}(n, 1, S)$. In general, for a $\mathcal{C}(n, 1, S)$, separating a one-node cut results in a cut-set of $n-1$ edges, whereas bisecting a $\mathcal{C}(n, 1, S)$ leads to a cut-set of $(n/2)^2$ edges. Figures 5.4-(a) and (b) depict the two cuts, respectively, for $\mathcal{C}(8, 1, S)$, where bold edges form the corresponding cut-set.

Theorem 2. *The bisection width of OWCell DCNs, $\mathcal{C}(n, t, S)\ \forall\ n = 4d$, is $(n-1)t$ if t is even (see Figure 5.5).*

Proof. Figure 5.5 depicts the general case of $\mathcal{C}(8, t, S) : t$ is even. It may be noted that, the two middle columns (or rows) of CoRs share t ToRs. We stretch the graph around the shared ToRs as shown in Figure 5.5 to facilitate the calculation of the bisection width. Except for these t shared ToRs, we can divide the $\mathcal{C}(8, t, S)$ into two equal and symmetric parts. However, to bisect $\mathcal{C}(8, t, S)$, we have to divide the t shared ToRs equally between the two parts. To do so, we perform t one-node cuts such that the upper $\frac{t}{2}$ ToRs become part of the left (shaded) half and the lower $\frac{t}{2}$ ToRs join the right (unshaded) half. The vertical solid line in Figure 5.5 shows the corresponding cut. Since we perform t one-node cuts; each resulting in a cut set of

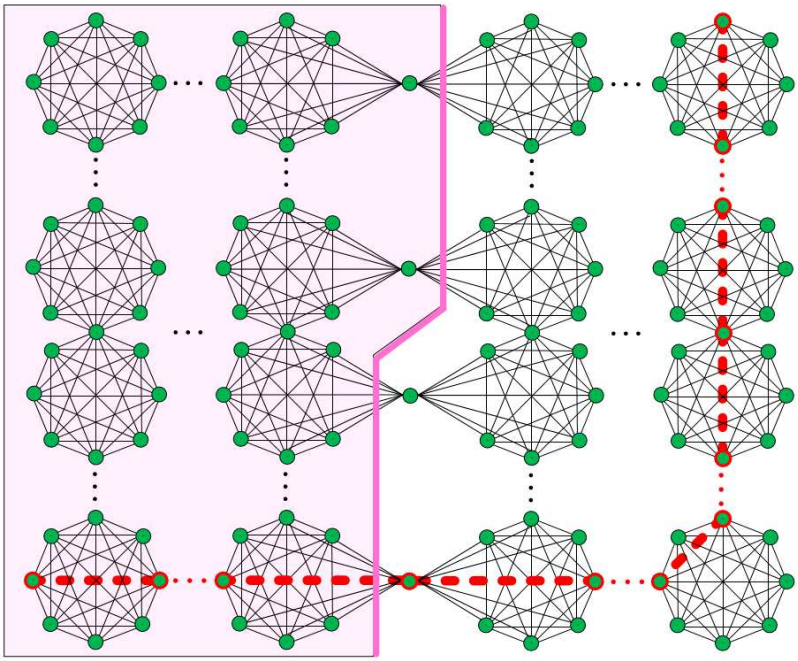

Figure 5.5: Bisection width (solid) and diameter (dashed) in $\mathcal{C}(8, t, S)$ for even t. The graph is stretched around the column of shared ToRs to illustrate the bisection width.

$n - 1 = 7$ edges, the bisection width becomes 7t.

In general, for $\mathcal{C}(4d, t, S),\ \forall\ d,\ t \in \mathbb{Z}^+ : t$ is even, there are t shared ToRs, and we need t one-node cuts to halve the t shared ToRs. Each one-node cut leads to a cut-set of $n - 1$ edges, and thus the bisection width is $(n - 1)t$. □

Theorem 3. *Bisection width of OWCell DCNs,* $\mathcal{C}(n, t, S)\ \forall\ n = 4d$ *and odd* t*, is* $(n - 1)(t - 1) + (n/2)^2$.

Proof. In case of, $\mathcal{C}(8, t, S) : t$ is odd, the network can be divided into two parts each containing $\frac{t-1}{2}$ columns (or rows) of CoRs with a column (row) of CoRs shared by the two network parts (see Figure 5.6). To bisect the network, we need to equally split the middle column of CoRs between the left and right parts of the network. The middle column contains an odd number, t, of CoRs. Therefore, each network half can take $\frac{t-1}{2}$ CoRs leaving a single (centered) CoR to be split between the two

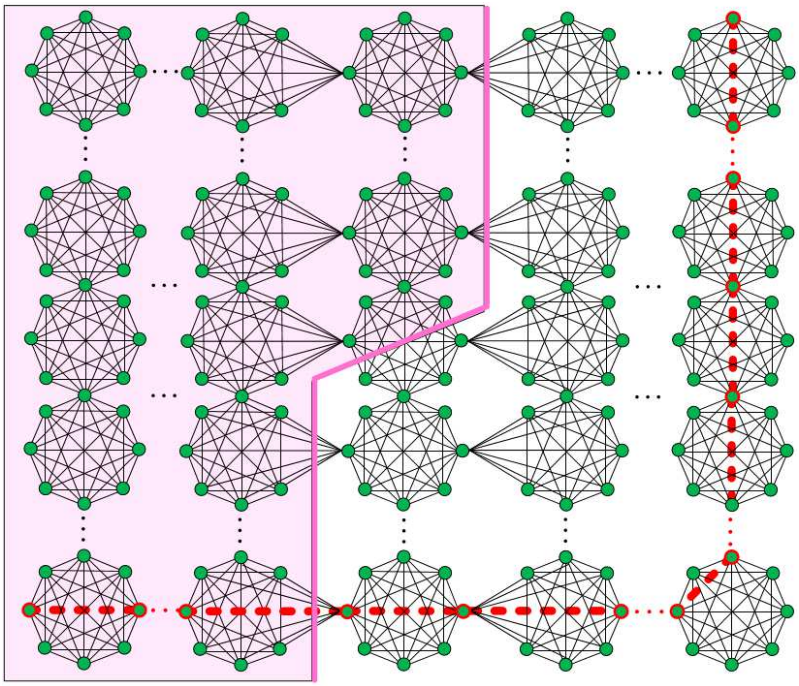

Figure 5.6: Bisection width (solid) and diameter (dashed) in $\mathcal{C}(8, t, S)$ for odd t. The graph is stretched around the shared column of CoRs to illustrate the bisection width.

halves. The vertical solid line in Figure 5.6 illustrates the corresponding cut where $\frac{t-1}{2}$ one-node cuts are performed followed by a bisection of the center CoR and then another $\frac{t-1}{2}$ one-node cuts. The bisection width therefore becomes $7(t-1) + \left(\frac{n}{2}\right)^2$.

A $\mathcal{C}(4d, t, S) : t$ is odd, requires $t-1$ one-node cuts each with a cut-set of $n-1$ edges, and bisecting one $\mathcal{C}(4d, 1, S)$ with a cut-set of $(\frac{n}{2})^2$, and thus the bisection width is $(n-1)(t-1) + (\frac{n}{2})^2$.

□

Theorem 4. *Bisection width of OWCell DCNs,* $\mathcal{C}(6, t, S)$ *is* $16t - 13 \; \forall \; t > 1$.

Proof. Figure 5.7-(a) depicts the case of $\mathcal{C}(6, 2, S)$. We can think of a $\mathcal{C}(6, t, S)$ as an inner hexagonal CoR $\mathcal{C}(6, 1, S)$ surrounded by a tier that is formed of six CoRs. In that case, the bisection width can be obtained by using a one-node cut for each

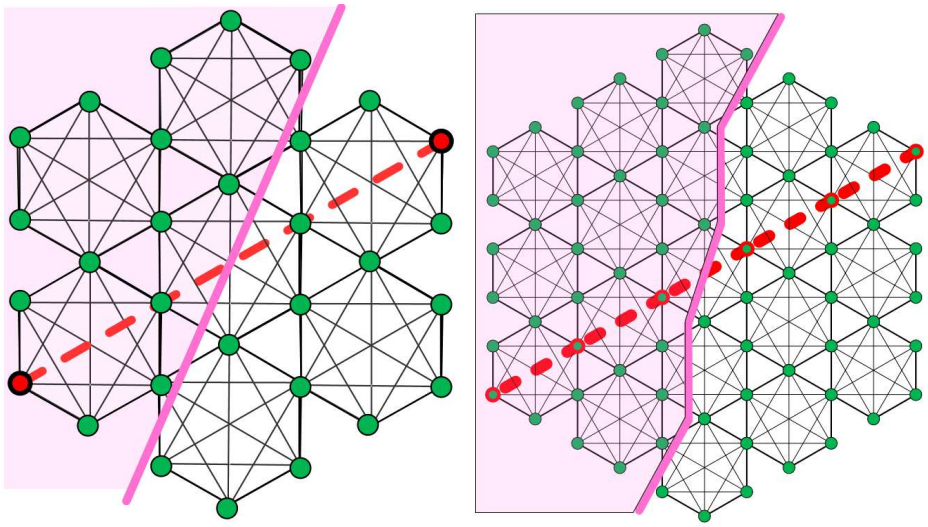

(a) (b)

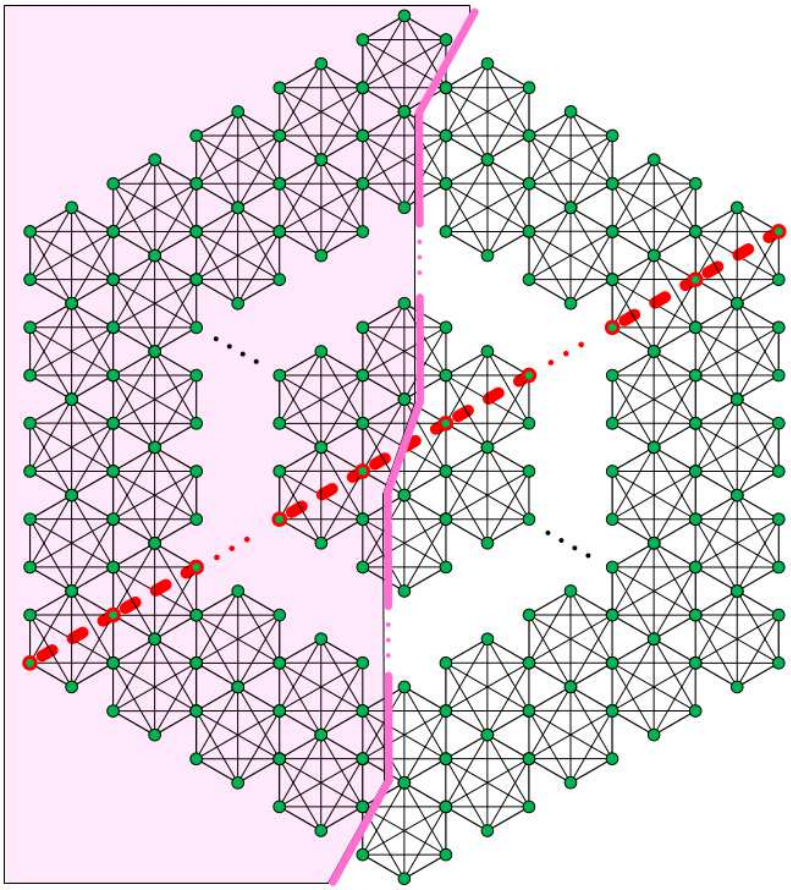

(c)

Figure 5.7: Bisection width (solid) and diameter (dashed) in $\mathcal{C}(6, t, S)$. (a) $t = 2$ (b) $t = 3$ (c) General case.

of the two cells in the surrounding tier (i.e., $2 \times (n-1)$), leaving the center CoR to be split between the two halves $(\frac{n}{2})^2$) for a total bisection width of $2(n-1) + \frac{n}{2})^2$. Increasing t by one means adding another tier of CoRs between the inner CoR and the outer tier of CoRs [see Figure 5.7-(b)]. This increases the bisection width by a number of links equivalent to two two-node cuts (i.e., $2(n-2)$). Figure 5.7 shows the general case of $\mathcal{C}(6,t,S)$. The order of the graph t can be divided into; one inner CoR $(\frac{n}{2})^2$), two outer CoRs with one-node cuts $(2 \times (n-1))$, and $2t-4$ intermediate CoRs with two-node cuts $((2t-4) \times (2n-4))$. This leads to a total bisection width of $\frac{n}{2})^2 + 2 \times (n-1) + \times (2t-4) \times (2n-4)$. For $n = 6$, this can be reduced to $16t-13$. □

Theorem 5. *The network diameter of* $\mathcal{C}(4d,t,S)$ *and* $\mathcal{C}(6,t,S)$ *is* $(2t-1)$.

Proof. The distance between two racks is maximum when the racks are at the extreme ends of the diagonal of the network. Dashed lines in Figures 5.5, 5.6, and 5.7 show the diameter of $\mathcal{C}(8,t,S)$ and $\mathcal{C}(6,t,S)$, respectively. Moving from one CoR to an adjacent CoR takes exactly one hop, and moving within a CoR is at most one hop. In case of $\mathcal{C}(4d,t,S)$, each side can be traversed in $t-1$ hops plus the one hop within the bottom right CoR, hence the diameter is $2(t-1)+1 = 2t-1$. It may be noted that, there are several paths between the ToRs selected. However, all such paths follow the *Taxicab geometry* leading to the same path length of $2t-1$. The same argument applies to the $\mathcal{C}(6,t,S)$. □

5.1.2 Multipoint OWC System Design for OWCell DCNs

Most existing commercial OWC transceivers are designed for outdoor point-to-point links. To operate under the varying and/or severe weather conditions, high powered lasers and relatively expensive components are used. On the other hand, the simple design requirements by indoor OWC systems, such as short range links, in addition

to the absence of the outdoor environmental impairments, makes it possible to design cheap OWC transceivers by coupling optical fiber ends directly with collimators to realize OWC links. In [86], Chowdhury et al. demonstrate transmission of a 10 Gbps cable television RF signals over an almost lossless 15 m point-to-point indoor OWC link in an environment similar to that of DCNs.

To avoid mechanically steerable transceivers, a number of fixed transceivers equal to the number of racks in the CoR (i.e., n) must be used. Since the space of the ToR is limited, multipoint OWC system with dense packaging of transceiver elements may help utilize the space of the ToR. In [423], Heng et al. propose a multipoint OWC system that is designed for long-range mobile flight terminals such as satellites or unmanned aerial vehicles flying within a cluster. Due to the long range and mobility requirements of the application, a sophisticated transceiver design is used that includes micro-electro-mechanical-system (MEMS) switches, controller, and mechanically mounted transmitters. OWC links in OWCell DCNs, however, are shorter and fixed, and thus we can use a simplified multipoint OWC system (see Figure 5.8) that is based on that of Heng et al. [423].

Transmitters and the receiver are separated. A ball lens is used to capture the incoming beams from all n racks in the CoR. Captured beams are coupled into optical fibers placed at the focal point of the ball lens. The beams will be subsequently exited into free space and detected by the corresponding optical communication detector [423]. Beam divergence in OWCell DCNs is expected to be limited compared to that of outdoor links due to the short range of OWC links in DCNs. Therefore, the use of a big ball lens at the receiver is not required leading to smaller form factor and better utilization of the limited ToR space. The number of transmitters must be equal to the number of n racks in the CoR and cannot be reduced. Each transmitter, however, is simply a single-mode fiber connected to the beam collimator

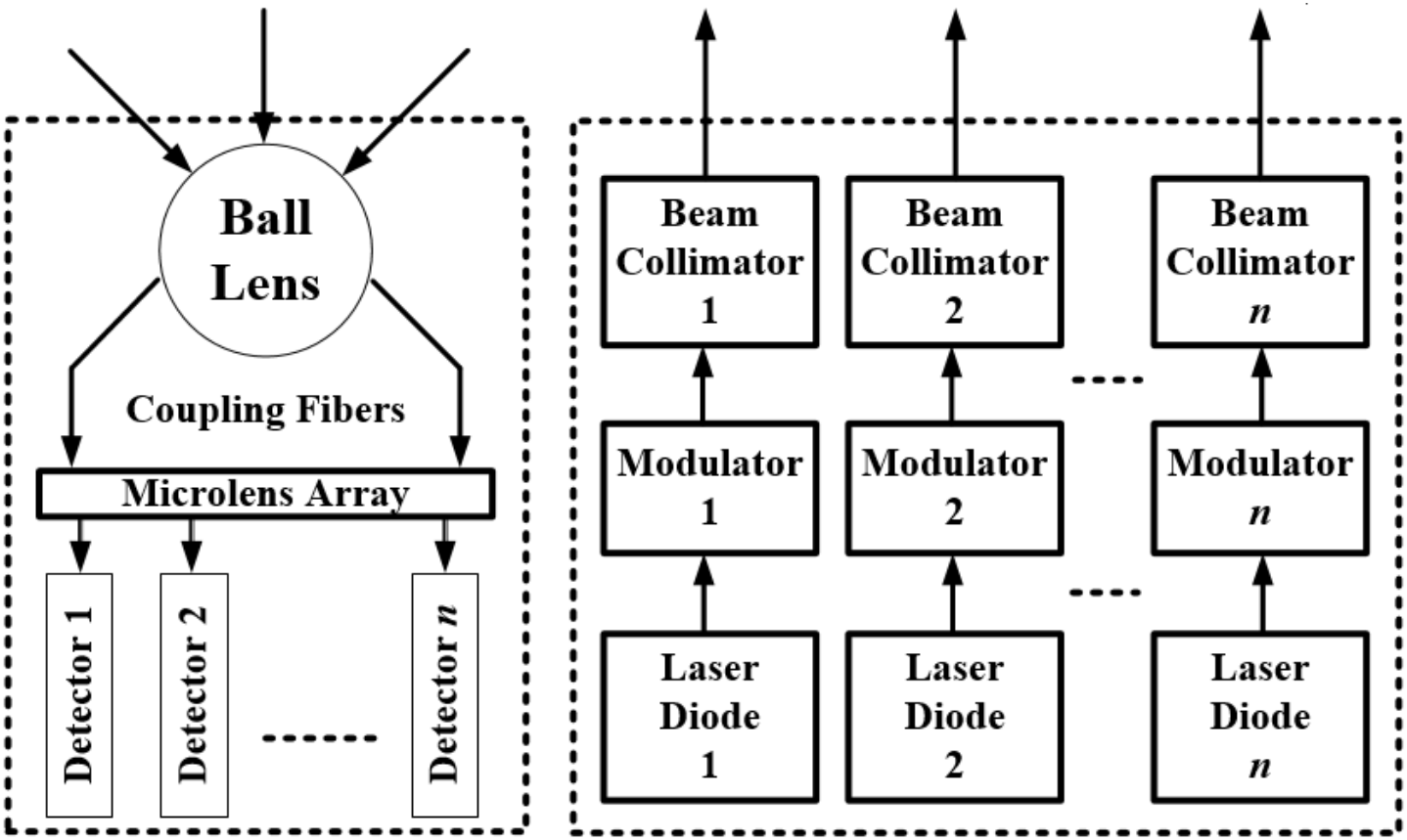

Figure 5.8: ToR OWC transceiver design.

to transmit the modulated optical beam from the laser source. Therefore, transmitters are expected to be smaller and cheaper as compared to conventional OWC transceiver. This way a single OWC receiver and multiple smaller transmitters replace multiple large expensive transceivers.

5.1.3 Switching and Routing Protocol

The traffic in a data center is comprised of large (elephant) and small (mice) flows. Although the small flows are greater in number (around 80%), large flows carry about 95% of data [384]. The type of optical switching technique used in a network has a significant impact on the performance of the network.

In optical communication, there are three switching techniques, namely; optical circuit switching (OCS), optical packet switching (OPS), and optical burst switching (OBS). Due to the immaturity of OPS, we consider only OCS and OBS switching technologies. However, the long setup time of OCS may lead to high latency especially for mice flows because the duration of the flow is short relative to the set up time. On the other hand, OBS is suitable for mice flows but not the elephant flows. Hybrid switching, in which OCS and OBS switching technologies are integrated, can provision high speed, on-demand, and high bandwidth communications for both long duration and bursty flows in DCs. We assume that each ToR in OWCell DCN employs hybrid switching.

The uniform structure of OWCell DCNs facilitate the use of low computational and storage cost geographical routing protocols. In this chapter, we consider OWCells with square CoRs ($n = 4$). In a $C(4, t, S)$ network (see Figure 5.9), there are $2t^2 + 2t$ racks arranged in $2t + 1$ rows and $2t + 1$ columns, numbered bottom ($y = 0$) to top ($y = t + 1$) and left ($x = 0$) to right ($x = t + 1$), respectively. A server s where $1 \leq s \leq S$ is geographically identified using the tuple (x, y, z), where x and y are

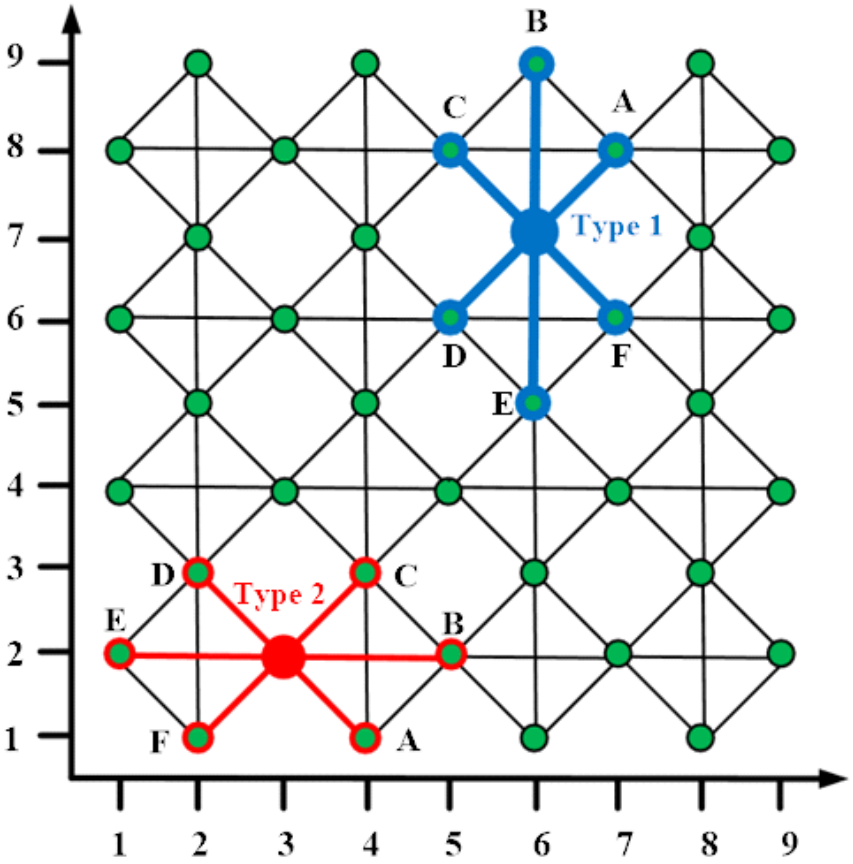

Figure 5.9: Types of nodes in $\mathcal{C}(4, t, S)$ OWCell DCN. Type 1 nodes (even-column/odd-row indices) and Type 2 nodes (odd-column/even-row).

coordinates of the rack, and z corresponds to the ordinal number for the server within a rack.

Algorithm 1: Basic Routing in $\mathcal{C}(4, t, S)$ OWCell DCN.

Input: A source rack Src and a destination rack $Dest$.
Output: A path P from Src to $Dest$

```
1  Current ← Src
2  Path ← Src
3  while Current ≠ Dest do
4      △x = Dest.x − Current.x
5      △y = Dest.y − Current.y
6      if Current.y is even then
7          Next ← route_type1(Current, △x, △y)
8      else
9          Next ← route_type2(Current, △x, △y)
10     Path ← Append(Path, Next)
11     Current ← Next
12 Return Path;
```

Algorithm 1 shows the routing in $C(4, t, s)$. There are two types of nodes in the proposed OWCell (see Figure 5.9). Nodes with even-column/odd-row (Type 1 nodes), and nodes with odd-column/even-row (Type 2 nodes). To determine the output port at each node, the coordinates of the current and destination racks are compared and the difference is calculated as $\triangle x = x_{destination} - x_{current}$ and $\triangle y = y_{destination} - y_{current}$. Depending on the type of the node and the values of $\triangle x$ and $\triangle y$, the output port is determined (Lines 7 and 9) according to Table 5.2.

Table 5.2: Selection of routing output port in $\mathcal{C}(4, t, S)$.

	$route_type1$		$route_type2$	
	$\triangle x \geq 0$	$\triangle x < 0$	$\triangle x \geq 0$	$\triangle x < 0$
$\triangle y \geq 0$	A or B	B or C	B or C	D or E
$\triangle y < 0$	E or F	D or E	A or B	E or F

5.1.4 Putting It All Together

In Section 5.1.2, we discuss the design of a multipoint transceiver for inter-rack communications in the proposed OWCell design. In Section 5.1.3, we discuss the routing and switching schemes for inter-rack communications. In this section, we put everything together to design a ToR switch that can perform the required intra- and intra-rack communications.

Figure 5.10 depicts the proposed design of the ToR in the proposed OWCell DCNs. Received light beams are directed to a stage of 1×2 splitters. The splitters are responsible of directing the received beams depending on the destination of the traffic. There are three possible scenarios.

1. The corresponding rack is the destination rack. In this case, the splitters should direct the beams to the $(S + n) \times (S + n)$ Electronic Switch Fabric.

2. Current rack is a relay node in the path of the traffic. Splitting stage must direct the beams to the transmitters through the $n \times n$ FSO switch.

3. Current rack is one of the multicast destinations of the received traffic. In this case, the splitters must direct a copy of the received signal to the $(S+n)\times(S+n)$ Electronic Switch Fabric and another copy to the $n \times n$ FSO switch.

Different technologies can be used to implement the splitting stage. For example, fixed 1×2 splitters. In this case, the splitting stage will always split the beams. Although simple, it is inefficient to generate undesired copies of the received signals in Cases 1 and 2.

To overcome this problem, a configurable splitting stage can be obtained using technologies such as Micro-Electro-Mechanical-Systems (MEMS). In this case, MEMS splitters can be used such that when the MEMS element is in the lay position, the

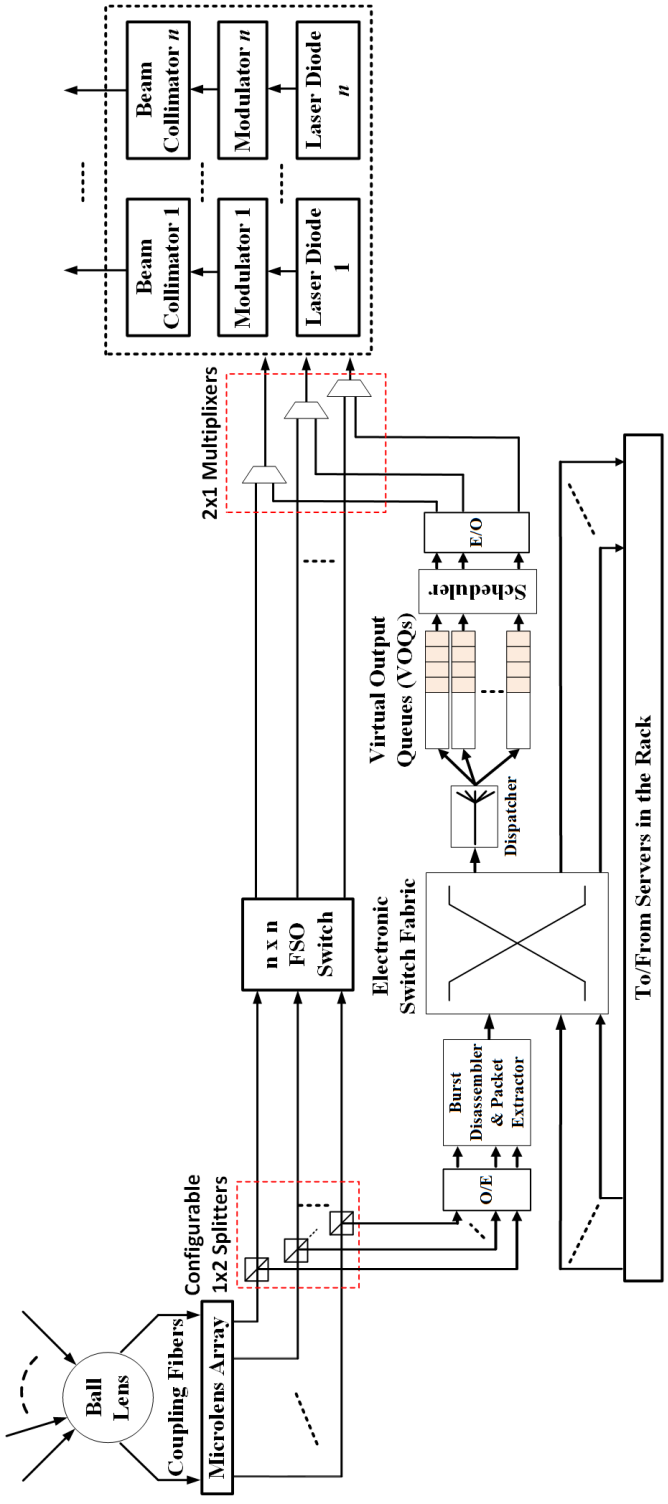

Figure 5.10: ToR OWC complete transceiver design.

beam will be directed to the $n \times n$ FSO switch. When the MEMS element is in the up position, the beam will be split into two copies. This resolves the problem of the undesired split in Case 1. However, the splitting is still inevitable in Case 2. In fact, the discussed design of the 1×2 splitting stage in the ToR is a good introduction for the problem encountered in existing FSO switches. We discuss these issue in details and propose an efficient solution for the problem in Chapters 6 and 7).

The local copy generated in the splitting stage is then directed to the Electronic Switch Fabric after being converted from optical to electrical domain using O/E converters. The Electronic Switch Fabric receives traffic from S servers and n OWC receivers. It perform the required switching by directing the traffic to one (or many) of the S servers and n transmitters connected to its output ports.

The n transmitters receive traffic either from the Electronic Switch Fabric (traffic from servers intended for inter-rack communication) or from the FSO switch (inter-rack traffic using the corresponding traffic as an intermediate node). In the former case, the traffic is first converted from the electrical to the optical domain using E/O converters. In the latter, the traffic is already in the optical domain and no need for conversions. Multiplexers are used to select the one of the two traffic links to be connected to the transmitters.

Splitters and multiplexers are controlled using control signals from the ToR controller. Controller and controlling signals are now shown for simplicity. Moreover, if OBS is used, the traffic directed from the Electronic Switch Fabric to the transmitters must go through an OBS assembly and queuing stage before being directed to the transmitters.

5.2 Simulation and Results

In this section, we describe the experiments and analyze the results obtained.

5.2.1 Simulation Setup

We develop a flow-level simulator to study the performance of the proposed OWCell architecture for different network sizes (i.e., total number of servers). Flows greater than 25 MB are considered large flows, whereas small flows are assumed to be less than 8 MB in size [384]. The source and destination servers are chosen randomly which are mapped to the corresponding ToRs. We consider only inter-rack traffic because intra-rack traffic do not traverse the links in the topology and inter-rack traffic are the most likely candidates for over-subscription. We assume links with uniform transmission capacity of 1 Gbps. OCS connection setup time is assumed to be 1 ms, while the processing time at each node for the OBS path setup is considered to be 20 μs [384] We use the buffer-triggered OBS. If a burst is blocked due to contention, then all the packets in the bursts are dropped. In the following, we perform different studies to validate and compare the proposed OWCell DCN.

5.2.2 Impact of OWCell Design Space on its Performance

OWCell has a parametric design space. For a fixed total number of servers, the selection of t and S can make OWCell expand either vertically or horizontally. Increasing the number of servers per rack, S, leads to vertical expansion and a reduction in the order, t, of OWCell architecture as a smaller number of racks is required. On the other hand, reducing the number of servers per rack means that larger number of racks are required (horizontal expansion) to achieve the desired DCN size. In this study, we investigate the impact of the vertical and horizontal expansion of OWCell

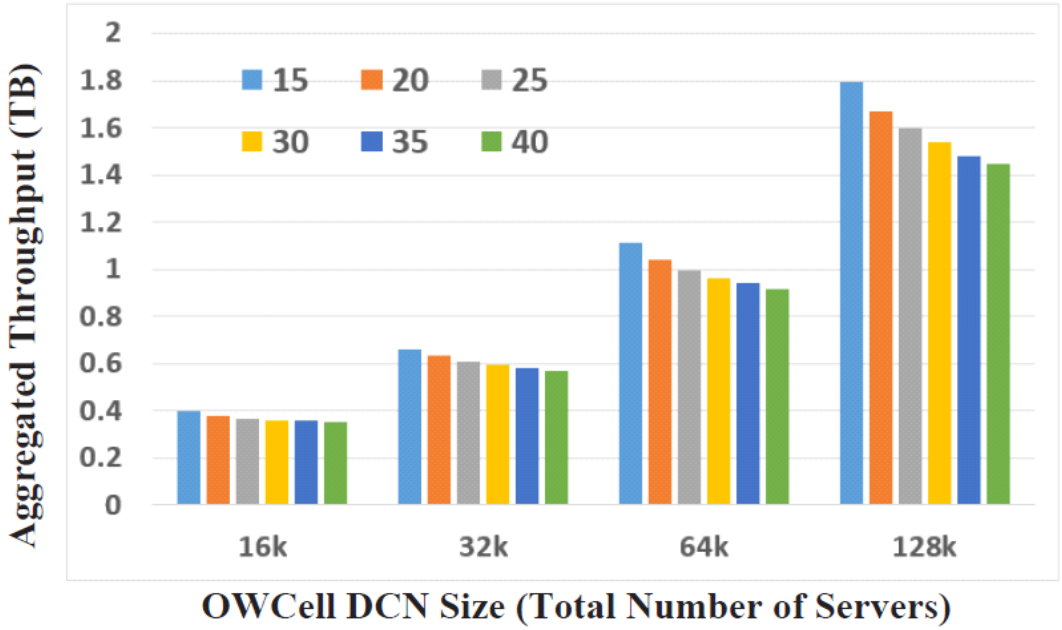

Figure 5.11: Aggregated throughput of $\mathcal{C}(4, t, S)$ for different OWCell DCN sizes and different servers per rack $S = 15$ (most left), 20, 25, 30, 35, and 40 (most right).

on its performance.

We vary the number of server per rack (for a fixed OWCell DCN size) from 10 to 40 with a step of 5. Figure 5.11 depicts the performance, in terms of aggregate throughput, of four OWCell DCN networks with 16k, 32k, 64k, and 128k total number of servers at different values of servers per rack. At fixed DCN size, e.g., 16K, as the number of servers per rack increases, the number of links and ToRs decreases from 1066 ($S = 15$) to 400 ($S = 40$) and we notice a degradation in the performance of OWCell. This is consistent for the four different sizes of the OWCell DCNs. We notice that the overall DCN traffic increases as the size of the DCN increases and so does the accepted and rejected traffic (see Figure 5.11).

Figure 5.12 shows the impact of increasing the DCN size while maintaining the same network order t. This can be achieved by increasing the number of servers per rack. The combination graph in Figure 5.12 shows the throughput in TBs and as a percentage of the total traffic injected in the network. Even though the total number

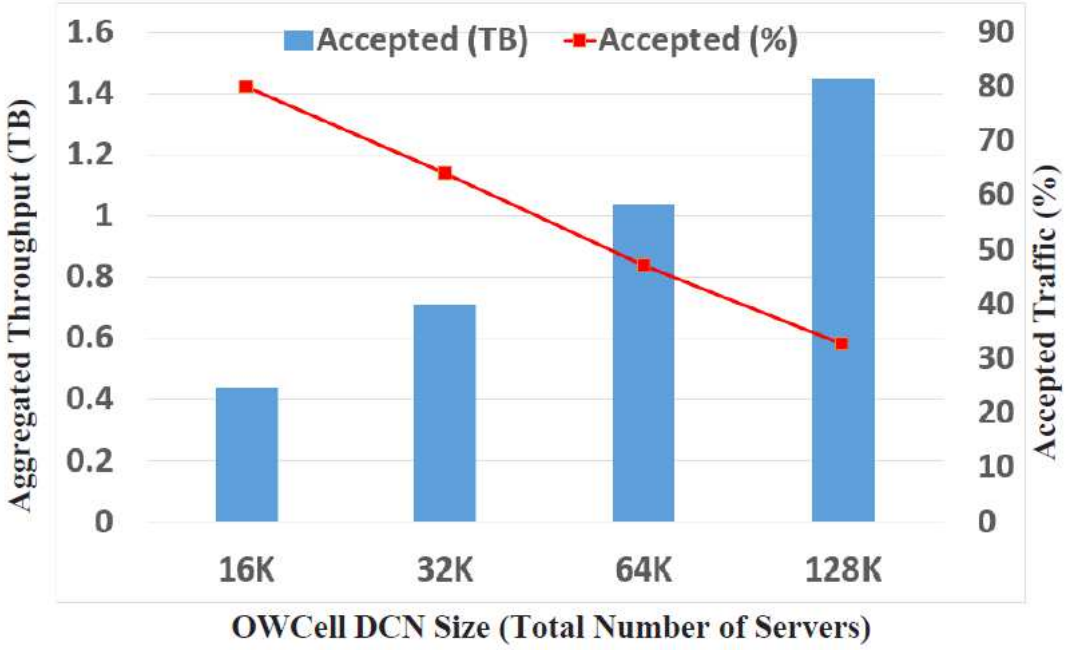

Figure 5.12: Performance of $\mathcal{C}(4, 40, S)$ for different DCN Sizes.

of Bytes delivered by the network increases, we can see that the percentage of accepted traffic is still decreasing. This is because the network has to handle increasing traffic while maintaining the same network order t, and thus number of inter-rack OWC links.

5.2.3 Hybrid vs. OCS Switching in OWCell

As mentioned earlier, the switching technique used has an impact on the performance of the network. Figure 5.13 depicts a comparison of the performance of a 16k servers OWCell DCN using OCS and hybrid (OCS+OBS) switching. On average, hybrid switching outperforms OCS.

The graph in Figure 5.13 can be divided into three regions. In region 1, OCS outperforms hybrid switching. This is because, in case of OCS, all the links are initially empty and most of the flows are routed successfully. On the other hand,

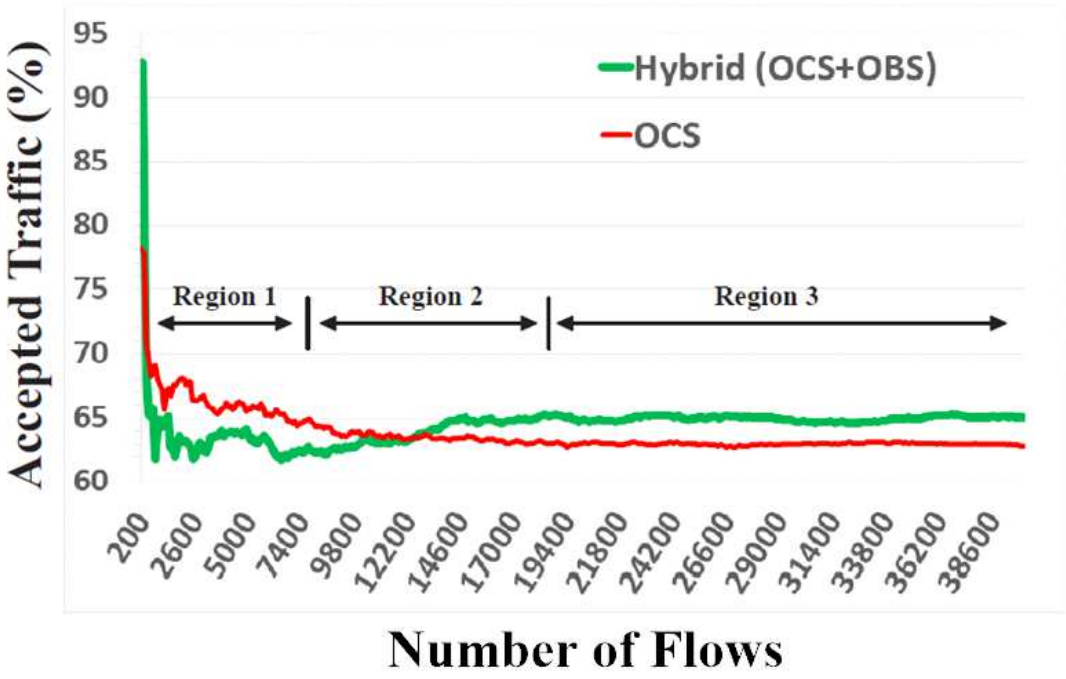

Figure 5.13: Performance of Hybrid Switching vs. OCS in a 16k server OWCell DCN $\mathcal{C}(4, 14, 40)$.

the buffers of the OBS in the hybrid switching are empty and the mice flows, which represent 80% of the flows and routed by OBS, are still being stored in the buffers. Therefore, the performance of hybrid switching is reflective of only the long flows which are routed using OCS.

In region 2, performance of the hybrid switching improves and outperforms OCS. This is because the OBS buffers start getting full and the combined flows are generated leading to a better utilization of link bandwidth as compared to OCS which still reserves bandwidth for all flows, including the mice flows.

As the number of flows in the network increases, accumulation and discharge of flows in the buffers of OBS is constant and the network saturates (see region 3). As expected, for mixed traffic with large number of mice flows, hybrid switching improves the utilization of links and presents a better performance as compared to that of OCS.

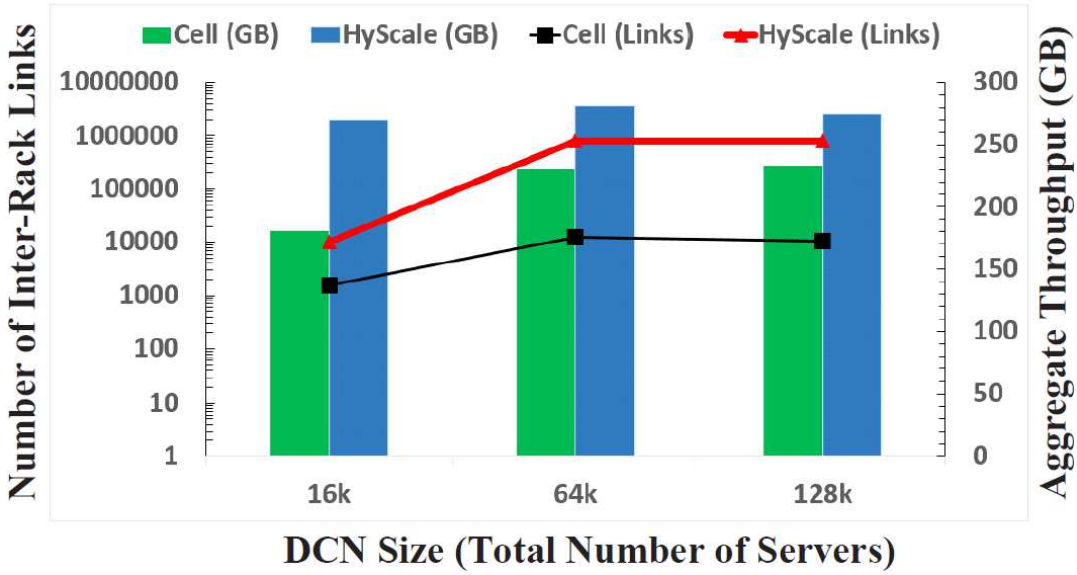

Figure 5.14: Comparison of throughput and number of inter-rack links (log scale) of OWCell vs. HyScale DCN.

5.2.4 Performance Comparison of OWCell and HyScale

In this study, we compare OWCell and HyScale [384] DCNs of different sizes (16k, 64k, and 128k servers) which is proven to outperform the conventional Fat Tree DCN (see [384]). Figure 5.14 depicts a combination graph of the aggregate throughput in GBs and number of inter-rack links. As we can see, OWCell DCN can achieve a performance that is within 15-25% that of HyScale using significantly lower number of links that is in the order of 95-98% compared to that of HyScale.

It is worth pointing that, the colossal difference in the number of links between HyScale and OWCell is the main reason why HyScale outperforms OWCell. HyScale has lower diameter as compared to OWCell. Moreover, the large number of links facilitate lower average hop count (see Table 5.3). However, the substantial reduction in the number of links (i.e., 95-98%), and hence cost, shows that the proposed OWCell can help overcome the wiring problem of conventional wired DCNs while maintaining a comparable performance. As we shall discuss in the next section, increasing the

order of the CoRs and the use of a coexisting OWC network are expected to improve the performance of the OWCell design.

5.3 Discussions

The incorporation of wireless technologies into DCNs is still in its infancy, and thus further research and development is needed to make wireless DCNs an efficient and practical reality. In this section, we discuss future research directions related to the proposed OWCell DCN architecture. Some interesting design considerations and open questions involve:

- **Hybrid versus Pure DCNs.** As we mentioned before, wireless links can be used to augment existing wired DCNs or to realize a pure wireless DCN. However, it is not yet clear which type of DCNs can provide a more efficient solution. Pure wireless DCNs are envisioned to solve cabling complexity and hot spot problems. However, it is possible that some degree of wired connectivity for intra/inter-rack communication can benefit the performance [6]. In order to answer this question, all possible solutions on the DCN design space including pure wired DCNs, hybrid DCNs, and pure wireless DCNs must be explored. Large number of possible DCN realizations fall under the umbrella of hybrid DCNs. Thus, it is important to find the optimum combination of wired and wireless networks to realize an efficient DCN.

- **Goodness Metrics.** The bisection bandwidth and diameter metrics used commonly to model the static prospective of the topology which is suitable for wired DCNs [9, 50]. To characterize the flexible and dynamic network topology a flexible wireless DCN can provide, a notion of dynamic bisection bandwidth or at least a lower (upper) bounds is needed [9, 50].

- **Network Architecture.** While it is intuitive to replace wired links by wireless links using the same DCN arrangement, we believe that the flexibility provided by wireless links can not be fully exploited unless new topologies and DCN arrangements are used. A network architecture must address the requirements of future DCNs, including scalability, high capacity, and fault tolerance. Characteristics of 60 GHz and FSO technologies, such as, the short transmission range, necessity of LOS, and the interference among 60 GHz wireless links must be taken into consideration [405, 424].

- **Cost Tradeoffs.** In pure wireless DCN, switching and communication functionalities are shifted from few powerful, high-power, and high-cost nodes (switches, and routers) to a large number of low-power and low-cost end points (i.e., servers). It is crucial to understand the cost structure of individual nodes to decide whether one or a combination of these design possibilities will lead to an efficient cost-effective DCN [6].

- **Visible Light Communication (VLC).** VLC is another rapidly emerging technology in which light emitting diodes (LEDs) are used to provide VLC data links as well as illumination. We envision that, not only LEDs can be used for illumination in DCNs, but also it can be utilized for communication and networking (e.g., unicast/broadcast of control signals).

Unlike most existing research on OWC DCNs, we believe that row-based arrangement of racks is a limiting factor in the development of OWC DCNs. Therefore, new DCN architectures are needed to adapt to the LOS requirements by OWC links and to fully exploit its advantages. In this chapter, we propose OWCell DCN architecture that is developed using CoRs. It may be noted, however, that the OWCell design presented and analyzed in this chapter uses square cells ($n = 4$). We believe that,

using higher order cells, i.e., hexagons ($n = 6$) or octagons ($n = 8$), will improve the performance of the proposed OWCell DCN as it will result in larger number of OWC links, and thus more paths between any two servers in the DCN.

The uniform structure of OWCell DCN architectures facilitates the use of low computational and storage cost geographical routing protocol. We present a simple deterministic routing protocol that depends on the geographical coordinates of the source (current) and destination racks. However, it is possible to fine-tune the routing protocol for more flexible routing and enhancing the fault tolerance of the OWCell.

Table 5.3: Number of Inter-Rack Links and Average Hop Count in OWCell and HyScale.

DCN Size	**OWCell**		**HyScale**	
	Links	**Average Hop Count**	**Links**	**Average Hop Count**
16k	1536	12.5483	10240	6.16
64k	12696	32.691	802816	8.09
128k	10584	29.8768	802816	8.12

From the analysis in Section 5.2, we have seen that vertical expansion (i.e., larger number of servers per rack and less number of racks) can lead to a degradation in the performance of OWCell. Therefore, horizontal expansion is preferable. However, this can pose a challenge to the OWCell design as horizontal expansion leads to larger network diameter, and thus higher average hop count which in turn can lead to longer latency. To overcome this problem, we plan to investigate the design of OWCell DCNs with a coexisting OWC network [11]. The coexisting network can provide shorter paths and less hops for long distance connections, and thus counteract the impact of the horizontal expansion.

5.4 Chapter Summary

We propose OWCells, cellular optical wireless DCN architectures. We present an OWCell with square cells and develop its theoretical properties. Flow-level simulations are conducted to validate and compare the performance of OWCell. The impacts of OWCell design parameters on its performance are investigated. We compare the performance of OWCell using OCS and hybrid (OCS+OBS) switching schemes. We also compare the performance of OWCell and HyScale DCN, a switch-centric hybrid optical DCN. Finally, we discuss future research directions and approaches to improve the performance of the proposed OWCell DCN.

Chapter 6

New Class of Multicast Free Space Optical Switches

Enabling multicast in optical networks requires the use of multicast-capable optical switches. In this chapter, we propose a new class of strictly nonblocking (SNB) *multicast-capable* FSO switches. Our design exploits non-movable tri-state switching elements (T-SEs) that support signal splitting and switching simultaneously and seamlessly, and thus, separate splitting stages used in the conventional multicast switches are not needed.

6.1 Introduction

Applications hosted by DCs generate large demands for bandwidth with different communication patterns involving a combination of unicast, multicast, in-cast, and all-to-all-cast traffics [24, 54]. For example, Hadoop and Spark require in-cast traffic delivery during the shuffle stage of MapReduce, and require multicast for data replication, parallel database join operation, as well as data dissemination in virtual

machine (VM) provisioning [54].

Optical technologies have been long seen as a viable solution; not only for providing high-bandwidth [14, 425, 426], but also for implementing multicasting more efficiently compared to higher layers implementations (e.g., application layer). Realizing multicast in the optical layer requires the development of efficient *multicast-capable optical switches*.

As pointed earlier, real world DC traffic traces show that more than 95% of the data are being transferred by the top 10% largest elephant flows (i.e., flows with large amount of data) [29]. Researchers are currently investigating DC optical interconnects using hybrid optical switching schemes in which fast and slow optical switches are used simultaneously [427–430]. Fast optical switches are used for packet and small bursts of data, whereas, slow optical switches are used for long lived (circuit and long burst) traffic. Therefore, there is a current practical need for slow, yet, efficient and cheap multicast optical switches.

Most existing FSO designs are for unicast [426], and hence, incorporating multicast into these switches require additional hardware (e.g., splitters). This results in a higher complexity; and thus, cost. Moreover, the existence of a splitting stage adds to the overall basic switching structure, and thus, can potentially add to the overall loss experienced by the signal due to Gaussian beam divergence. Accordingly, the design of multicast FSO switches with reduced complexity and path lengths is an interesting yet challenging problem. To this end, we propose a new $N \times N$ *strictly nonblocking (SNB) multicast FSO* switch using *non-movable* tri-state SEs (T-SEs). Compared to existing multicast optical switches, the new switches are shown to exhibit a substantial reduction in hardware complexity, path lengths, and have reduced costs.

The remainder of the chapter is organized as follows. In Section 6.2, we discuss preliminaries and review existing FSO multicast switches. We dedicate Sections 6.3

and 6.4 to present and discuss the properties of the new class of FSO SNB multicast switches. Performance evaluation is presented in Section 6.5. We summarize the chapter in Section 6.6.

6.2 Preliminaries and Related Work

In this section, we introduce notations and definitions and review existing FSO switches.

6.2.1 Notation and Basic Concepts

An $N \times M$ switch has N input ports; $\mathcal{I} = \{I_0, \cdots, I_{N-1}\}$, and M output ports; $\Omega = \{O_0, \cdots, O_{M-1}\}$. A connection request between an input port I_p, $1 \leq p \leq N$, and an ordered set of output port(s) Ω_p, $\Omega_p \subseteq \Omega$, is denoted by $\mathcal{R}_p = \langle I_p, \Omega_p \rangle$. A request $\mathcal{R}_p$ is said to be a multicast if $1 < |\Omega_p| < N$, a unicast if $|\Omega_p| = 1$, or a broadcast if $|\Omega_p| = M$ (i.e., $\Omega_p = \Omega$). A set of all requests in an $N \times M$ switch, $\mathcal{R}^{N \times M}$, can be any combination of unicast requests Γ, $1 \leq |\Gamma| \leq \min(N, M)$, and multicast requests Ψ, $1 \leq |\Psi| \leq \min(N, \lfloor M/2 \rfloor)$. In the following, we summarize the basic concepts of optical switching networks used in this dissertation.

- *Input/Output Port Symmetry.* In general, an optical switch consists of an arbitrary number of input and output ports. If the number of the input and output ports is the same, the switch is said to be *homogeneous*, otherwise, it is called *heterogeneous*. In this dissertation, we focus only on homogenous optical switches (i.e., $M = N$). The analysis and results, however, can be easily extended to the case of $M \neq N$.

- *Blocking Characteristics.* A switch is said to be *nonblocking* if it can realize any possible interconnection pattern among inputs and outputs, otherwise, it

is called *blocking*. A nonblocking switching network can be *rearrangeable nonblocking* (RNB), *Wide-sense Nonblocking* (WNB), or *Strict-sense Nonblocking* (SNB). A network is said to be RNB if establishing a new connection may require some existing connections to be reconfigured, whereas in SNB and WNB, no reconfiguration is needed. A switching network is WNB if there exists a routing strategy to establish all connections, one at a time, without reconfiguring any existing connection. SNB networks, on the other hand, require no reconfiguration under any routing strategy. In this dissertation, we consider both SNB and RNB classes of switches.

6.2.2 MEMS-Based FSO Multicast Switches

Several multicast optical switch architectures have been investigated in the literature (e.g., [13,425,431]). Optical *splitter-and-delivery (SaD)* is a well-known SNB multicast switch [13]. Figure 6.1 shows an $N \times N$ SaD switch where each input beam is initially split to N identical branches using $1 \times N$ splitter. Corresponding branches from all N splitters are connected to one output port. Thus, any input can be connected to any number of output ports. It is worth noting that the SaD switch does not distinguish between unicast and multicast requests, which results in unnecessary splitting and signal losses. To overcome unnecessary splitting, configurable splitters may be used which adds to the complexity of the design and control of the switch [431].

A MEMS-based multicast FSO switch can be implemented using the SaD architecture [13] by replacing the 1×2 switches with MEMS mirrors, and we refer to this switch as *SaD-I*. In Figure 6.2-(a) we propose a possible realization of a 1×4 FSO splitter. The total number of components used in a $1 \times N$ splitter is $\Phi = 2^{\lceil log_2(N) \rceil + 1} - 2$.

SaD-I can be further improved by employing configurable splitters (we refer to it as *SaD-II*) [431]. Figure 6.2-(b) shows a possible realization of a configurable 1×4

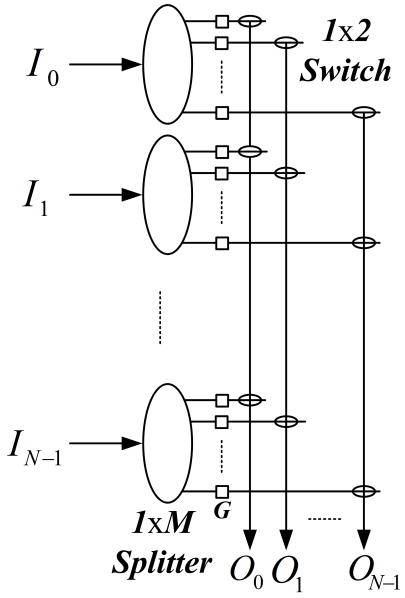

Figure 6.1: $N \times N$ SaD switch [13].

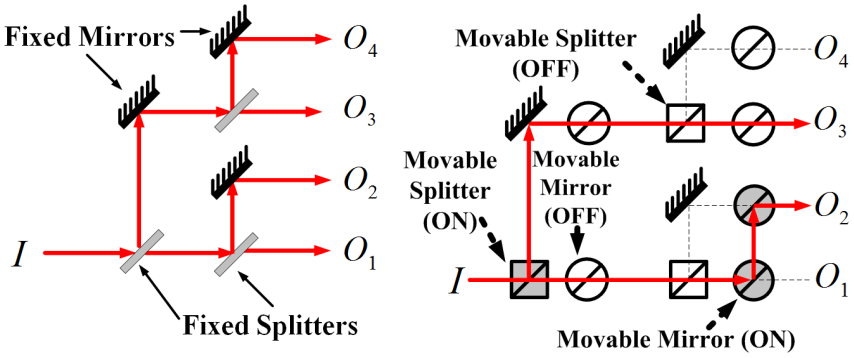

(a) (b)

Figure 6.2: Possible realization of 1×4 FSO splitter (a) Conventional. (b) Configurable.

splitter. The total number of components used in a $1 \times N$ configurable splitter is 2Φ. In SaD-II switches, each input beam is divided into a number of beams equal to the cardinality of the output set ($|\Omega_p|$), eliminating unnecessary splitting [431]. It can be seen that SaD-II behaves like 2D MEMS and SaD-I in the case of unicast and broadcast, respectively.

A switch that treats unicast and multicast requests separately is proposed in [14, 425]. The architecture combines a $d \times N$ SaD switch and an $N \times (N + d)$ three-plane switch [see Figure 6.4] to realize an SNB switch (SUM-SaD). Unicast requests are switched by the three-plane switch, and only multicast requests are delivered by the SaD. Thus, splitting loss for unicast and multicast is similar to that of SaD-II and SaD-I, respectively.

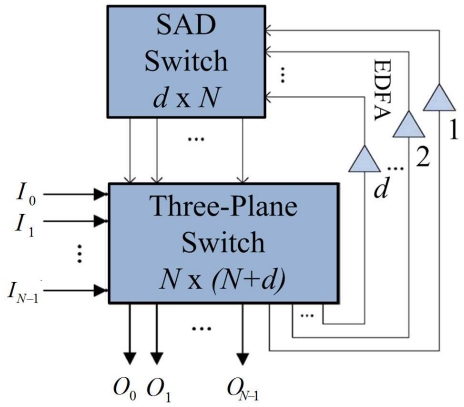

Figure 6.3: $N \times N$ SUM-SaD switch [14].

In [15], Lin et al. propose an FSO 2D MEMS switch that performs bridging to restore failed links. Bridging can thought of as a special case of multicast where an input signal is forwarded to exactly two outputs.

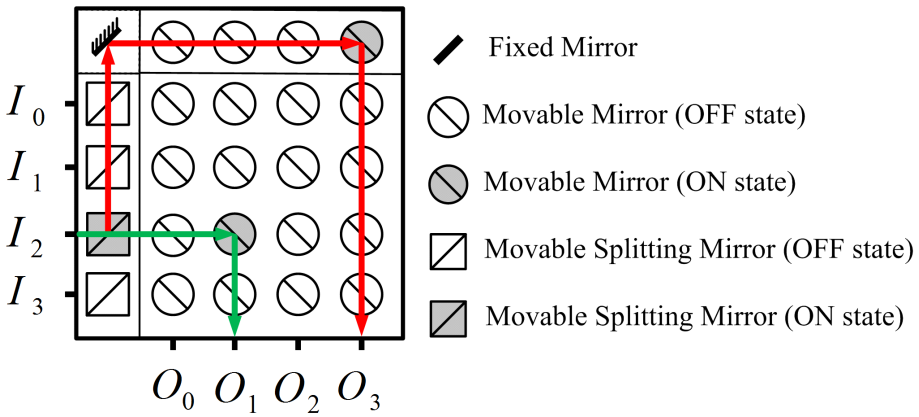

Figure 6.4: $N \times N$ MEMS switch with one-port bridging capability [15].

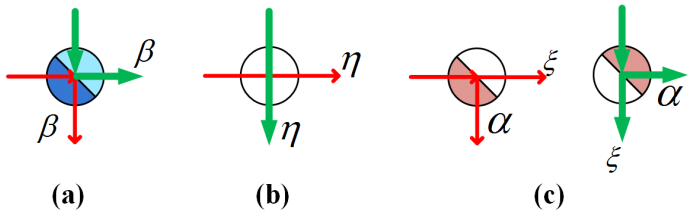

Figure 6.5: T-SE (a) R-State. (b) T-State. (c) S-State.

6.3 Proposed Strictly Non-Blocking (SNB) Multicast FSO Switch Design

We propose a new class of SNB multicast FSO crossbar switches using tri-state switching elements (T-SEs). A T-SE is placed at every node i.e., row-column intersection. $SE(p, q)$ denotes a T-SE at the intersection of input port p, and output port q, $(1 \leq p \leq N$, and $1 \leq q \leq M)$.

A T-SE can be configured (see Figure 6.5) in one of three states; *Reflective* (R), Transmissive (T), or *Splitting* state (S), half reflective/half transmissive [16, 165]. SE(p, q) denotes a T-SE at the intersection of input port p, and output port q. The configuration of SE(p, q) is denoted by $\tau(p, q, \chi)$, where $\chi \in \{R, T, S\}$, represents the state of the T-SE.

Figure 6.6 shows the four possible configurations of the basic 2×2 proposed switch

where the S-state is used to perform the required multicasting.

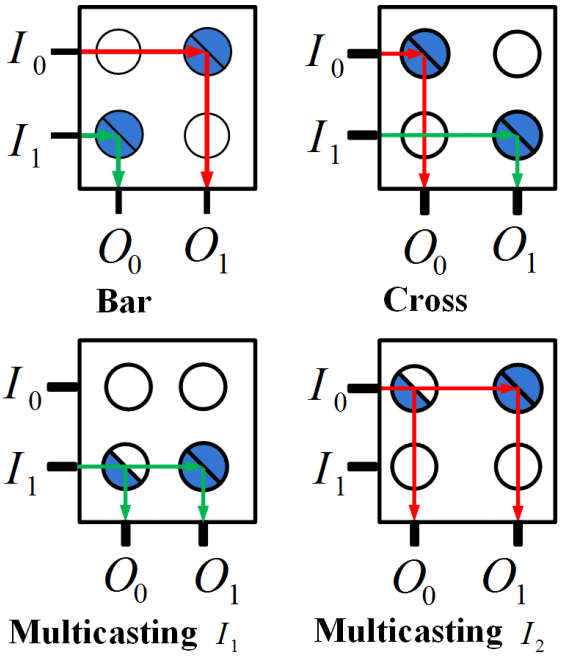

Figure 6.6: Switching modes in a proposed 2×2 switch.

Fig. 6.7 shows a 6×6 crossbar employing T-SEs with one unicast: $\langle 6, 4\rangle$, and two multicast requests: $\langle 3, \{1, 3, 6\}\rangle$ and $\langle 4, \{2, 5\}\rangle$. Request $\langle 3, \{1, 3, 6\}\rangle$ is realized by configuring T-SEs as follows: $\tau(3, 1, S)$, $\tau(3, 3, S)$, and $\tau(3, 6, R)$.

6.3.1 Switch Configuration

The configuration (routing) of unicast connections on the proposed switch follows the conventional crossbar switch. For multicast connection, we propose Algorithm 2 to systematically configure T-SEs. Algorithm 2 in each iteration processes a request $\mathcal{R}_p \in \mathcal{R}$, and configures the corresponding T-SEs. It is assumed that all T-SEs are initially in the T-state.

Let $\Omega_p = \{O^p_{q,k} \mid 1 \leq q \leq M, 1 < k \leq |\Omega_p| \text{ and } \forall v, w \in k;\ O^p_{q,v} < O^p_{q,w} \text{ if } v < w\}$. In Algorithm 2, a request $\langle I_p, \Omega_p\rangle$ can be processed by configuring $\tau(p, j, \chi),\ \forall\ O^p_{j,k} \in \Omega_p$, as follows:

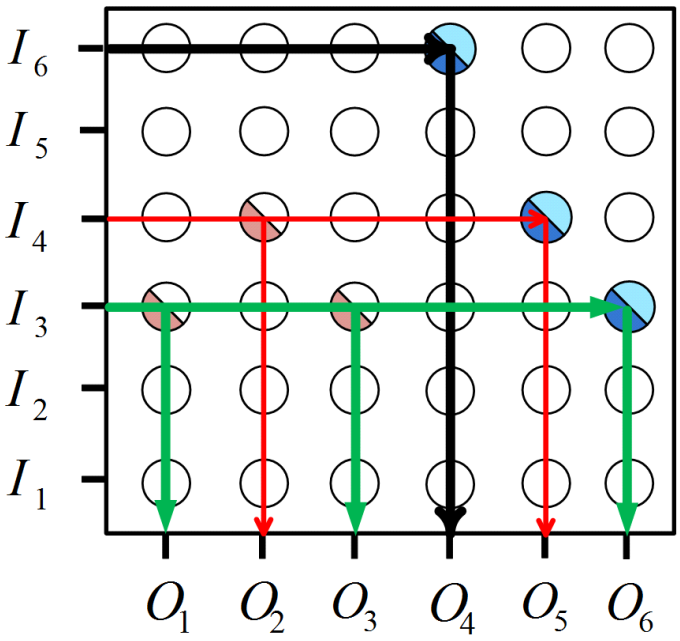

Figure 6.7: Multicast in 6×6 crossbar using T-SEs.

$$\tau(p, j, \chi) = \begin{cases} \tau(p, j, S), & \text{if } 1 \leq k \leq |\Omega_p| - 1 \\ \tau(p, j, R), & \text{if } k = |\Omega_p| \end{cases} \tag{6.1}$$

6.4 Switch Properties

In the following, we analyze the proposed switch with respect to, hardware complexity, signal path length, and number of T-SEs in the S-state.

6.4.1 Switch Blocking Characteristics

In the following, we prove Theorem to establish that the proposed switch employing T-SEs is an SNB multicast switch.

Theorem 6. *Theorem1 An $N \times N$ crossbar switch employing T-SEs is strictly non-blocking multicast switch.*

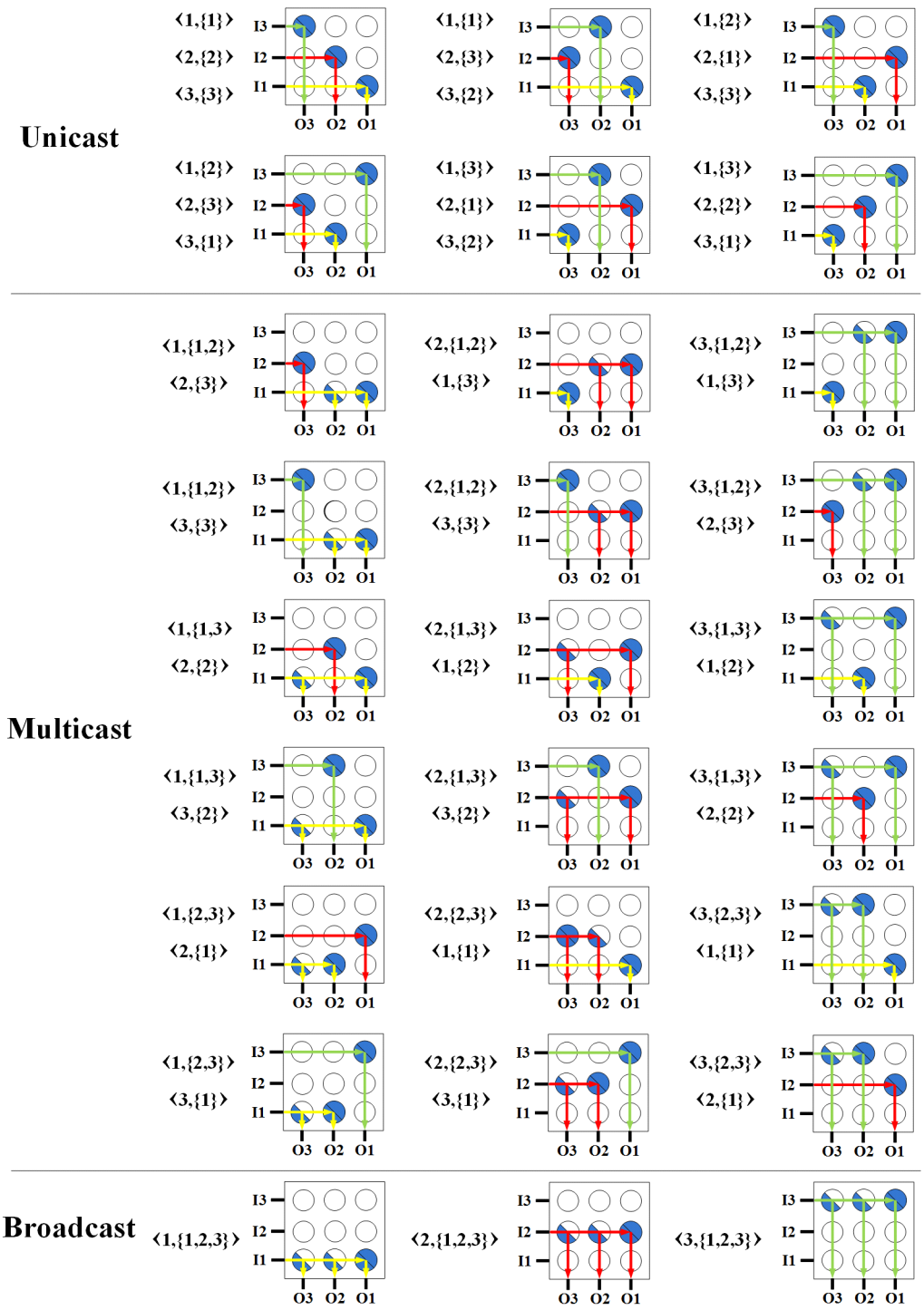

Figure 6.8: Possible permutations using the proposed 3×3 switch.

Algorithm 2: Multicast Connection Routing

Input: Set of requests $\mathcal{R}$.
Output: States of the NM T-SEs.

```
1  for p = 1 → |R| do
2      Counter ← |Ω_p|
3      j ← 0
4      while Counter ≥ 1 AND j ≤ N − 1 do
5          if j ∈ Ω_p then
6              if Counter > 0 then
7                  Configure τ(p, j, S)
8              else
9                  Configure τ(p, j, R)
10             j ← j + 1
11             Counter ← Counter − 1
12         else
13             j ← j + 1
14 Route light beam from input to output ports
```

Proof. We will use induction to prove the theorem. It is clear that all permutations, multicast assignments, and broadcast connections can be realized for the 3×3 switch (i.e., $N = 3$) as shown in Figure 6.8. For simplicity, we change the indexing of ports. This change does not affect the functionality or the performance of the switch in any way.

Assume that an $(N-1) \times (N-1)$ switch is strictly nonblocking. Hence, it is always possible to connect any idle input terminal to an arbitrary set of idle output terminals independent of its current state. By induction, we wish to prove that an $N \times N$ switch is also strictly nonblocking.

For induction step, an $N \times N$ switch can be obtained by adding a row and a column to the $(N-1) \times (N-1)$ switch as shown in Figure 6.9. The set of requests, $\mathcal{R}^{N \times N}$, for $N \times N$ switch can be defined as $\mathcal{R}^{N \times N} = \mathcal{R}^{(N-1) \times (N-1)} \cup \mathcal{R}_N$, where $\mathcal{R}_N = \langle I_N, \Omega_N \rangle$. The added $2N-1$ T-SEs are configured in the T-state. This way, none of the $N-1$ inputs is affected, and therefore, the functionality and the state of

the $(N-1) \times (N-1)$ sub-switch is not affected. For the $N \times N$ switch to be strictly nonblocking, it is sufficient to show that:

1. The input I_N can request any arbitrary set, Ω_N, of idle output terminals including the new N^{th} output port, O_N, without changing the states of any of the T-SEs of the $(N-1) \times (N-1)$ sub-switch, and

2. The output O_N can be requested by any of the input ports including the new N^{th} input port, I_N, without changing the states of any of the T-SEs of the $(N-1) \times (N-1)$ sub-switch.

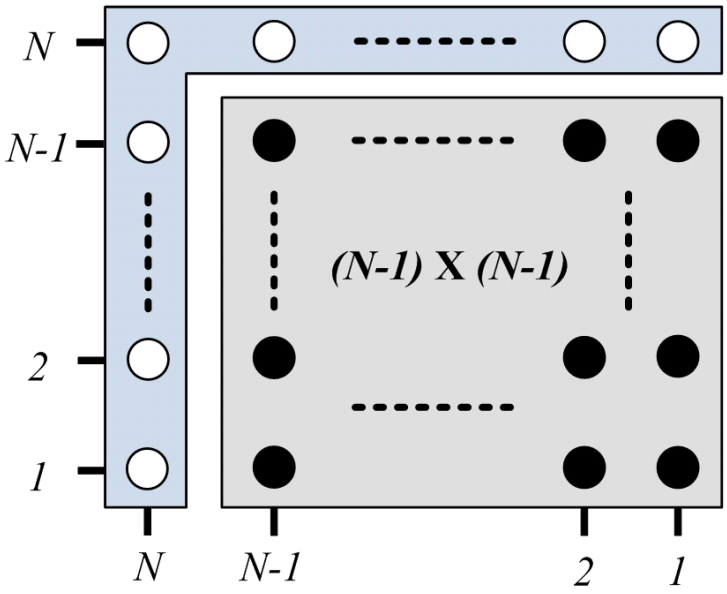

Figure 6.9: An $N \times N$ switch with an $(N-1) \times (N-1)$ subswitch used in the induction step.

In general, for a request $\langle I_p, \Omega_p \rangle$, the switch is configured based on *descending order* of ports in Ω_p. All possible scenarios can be summarized in the following four cases based on the status of $\mathcal{R}_N$, and O_N.

Case 1. $\Omega_N = \emptyset$, *and* $O_N \notin \Omega_i$, *where* $1 \leq i \leq |\mathcal{R}^{N \times N}|$.

The added row and column of T-SEs have no impact on the $(N-1) \times (N-1)$ sub-switch because $\Omega_N = \emptyset$ has not changed. Hence, the $N \times N$ switch is SNB.

Case 2. *$\Omega_N \neq \emptyset$, and $O_N \notin \Omega_i$, where $1 \leq i \leq |\mathcal{R}^{N \times N}|$.*

Let $\Omega_p = \{O^p_{q,k} \mid 1 \leq q \leq N, 1 < k \leq |\Omega_p| \text{ and } \forall\ v, w \in k; O^p_{q,v} < O^p_{q,w} \text{ if } v < w\}$. The request $\mathcal{R}_p$ can be processed by configuring $\tau(p, j, \chi),\ \forall\ O^p_{j,k} \in \Omega_p$, as follows:

$$\tau(p, j, \chi) = \begin{cases} \tau(p, j, S), & \text{if } 1 \leq k \leq |\Omega_p| - 1 \\ \tau(p, j, R), & \text{if } k = |\Omega_p| \end{cases} \tag{6.2}$$

In this case, the request $\mathcal{R}_N$ can be processed by configuring $\tau(N, j, \chi),\ \forall\ O^N_{j,k} \in \Omega_N$, as follows:

$$\tau(N, j, \chi) = \begin{cases} \tau(N, j, S), & \text{if } 1 \leq k \leq |\Omega_N| - 1 \\ \tau(N, j, R), & \text{if } k = |\Omega_N| \end{cases} \tag{6.3}$$

It is easy to see that an idle output in the $(N-1) \times (N-1)$ sub-switch indicates that all the T-SEs in its column are in the T-state. Therefore, no states need to be changed in the $(N-1) \times (N-1)$ sub-switch. It follows that the $N \times N$ switch is SNB.

Case 3. *$O_N \in \Omega_N$.*

This case follows the analysis in Case 2 except that Ω_N has at least one output (i.e., O_N). From Equation (6.3), if the request is unicast, then $SE(N, N)$ is configured in the R-state (i.e., $\tau(N, N, R)$). If there are other output ports in Ω_N, then we will have $\tau(N, N, S)$, $\tau(N, j, S)$ for $2 \leq k \leq |\Omega_p| - 1$, and $\tau(N, j, R)$ for $k = |\Omega_p|$.

Case 4. *$O_N \in \Omega_x$, where $x \neq N$ and $\mathcal{R}_x \in \mathcal{R}^{(N-1)\times(N-1)}$.*

The request $\mathcal{R}_N$ can be realized using the same argument as in Case 2. If $\mathcal{R}_x \in \Gamma$, then this can be easily realized by configuring $\tau(x, N, R)$, making the $N \times N$ switch SNB. On the other hand, if $\mathcal{R}_x \in \Psi$, the request can be realized by configuring $\tau(x, N, S)$, where the input signal I_x is split at $\tau(x, N, S)$. Accordingly, one part of the signal goes to the output port O_N, whereas the other part goes to the $(N-1)\times(N-1)$ sub-switch. The $(N-1) \times (N-1)$ sub-switch is assumed to be SNB, and therefore, the $N \times N$ switch is SNB. □

6.4.2 Hardware complexity

In the proposed switch, signal splitting and switching are performed simultaneously and seamlessly. Therefore, the proposed design supports multicast without separate splitting stage, and thus has lower complexity. The hardware complexity is directly proportional to the total number of T-SEs required. An $N \times N$ proposed SNB multicast switch requires a total of N^2 T-SEs.

Theorem 7. *The proposed SNB multicast FSO switch is optimal w.r.t hardware complexity as compared to all existing SNB multicast switches.*

Signal path length

The performance of the proposed switch depends on the number of T-SEs traversed by the light beam, and the number of splitting operations. For an $N \times N$ switch the number of T-SEs in the shortest and longest signal paths is 1 and $(2N-1)$, respectively.

Lemma 1. *The minimum and maximum number of T-SEs configured in S-state is 1 and $N-1$, respectively.*

Proof. This directly follows from the minimum and maximum cardinalities of multicast connections which is 2 and N including broadcast case, respectively. □

Lemma 2. *For all requests at a given time, the total number of T-SEs configured in the S-state is given by* $N_\Psi - |\Psi|$*, where* $2 \leq N_\Psi \leq N$ *is the number of output ports in all multicast requests at that time* $N_\Psi = \sum_{w=1}^{|\Psi|} \Omega_w, \ \forall \ \mathcal{R}_p \in \Psi$.

Proof. For each multicast request $\langle I_p, \Omega_p \rangle$, all T-SEs in the row corresponding to the input port and columns corresponding to output ports in Ω_p are configured in the S-state except for last output port in Ω_p which is configured in the R-state. Therefore, the total number of T-SEs in the R-state out of N_Ψ is equal to the total number of multicast requests $|\Psi|$. □

6.4.3 Signal Power Loss

An optical signal undergoes losses as it propagates from input to output ports in an FSO switch. There are two types of losses: insertion/coupling, and splitting losses.

Insertion and Coupling Losses. This is mainly due to the Gaussian beam divergence experienced by any beam propagating in free space [432]. Extensive analysis and studies has been performed to characterize the performance of 2D MEMS with respect to the insertion and coupling losses. Insertion and coupling losses in our design follow the analysis used for MEMS switches [432] but with the following two differences:

1. In MEMS-based multicast switches, an optical beam must propagate through a splitting stage before being switched by a crossbar. However, in the proposed switch, an optical beam propagates only through a crossbar in which, splitting and switching are performed simultaneously and seamlessly. This can reduce the insertion loss due to Gaussian beam divergence.

2. In MEMS, mechanical motion of the mirrors result in angular misalignment leading to inefficient coupling. The proposed design, however, employs only non-movable parts and is free of such losses.

Splitting Losses. Splitting losses are the losses encountered by the light beam due to the splitting required for multicasting. In SaD-based switches, an input beam is split using a $1 \times N$ splitter into N and $|\Omega_p|$ equal signals in case of conventional and configurable splitters, respectively. Following the splitting stage, a beam travels in free space from the input to output ports in a crossbar reflecting off of a *single* mirror.

In the proposed design, the beam may incur losses due to the *cascaded* splitting nature of the crossbar as it propagates through a chain of non-movable T-SEs along its path to the output. Let β and η be the reflection and transmission efficiencies of T-SE in the $R-$ and $T-$states, respectively. We refer to the percentage of the power reflected by a T-SE in the S-state as α, and the transmitted power of the beam is ζ (Figure 6.5). In our proposed switch, splitting losses depend on the cardinality of the output set $|\Omega_p|$, and thus, we have two cases.

Case 1: Unicast ($|\Omega_p| = 1$). Power loss is due to the reflection from $SE\left(p, O_{q,1}^{p}\right)$, transmission losses of the $(N-1-p)$ T-SEs before the reflection, and transmission losses of the q T-SEs after the reflection. The loss in the unicast case $[\mathrm{L}_{UC}\left(I_p, O_{q,1}^{p}\right)]$ is given by:

$$\mathrm{L}_{UC}\left(I_p, O_{q,1}^{p}\right) = 10\log_{10}\left(\beta \cdot \eta^{N-1-p+q}\right) \tag{6.4}$$

The lower (upper) bounds for L_{UC} are related to the shortest (longest) path traversed by the light beam:

$$10\log_{10}\left(\beta\right) \leq \mathrm{L}_{UC} \leq 10\log_{10}\left(\eta^{2(N-1)} \cdot \beta\right) \tag{6.5}$$

Case 2: Multicast ($1 < |\Omega_p| < N$). The optical losses of an output $O^p_{q,k} \in \Omega_p$ is due to the transmission losses of $(N - p + q - k)$ T-SEs in the T-state, transmission losses of $k - 1$ T-SEs in the S-state, and the reflection loss of a T-SE in the S or R-state. The losses in the multicast case $\mathrm{L}_{MC}\left(I_p, O^p_{q,k}\right)$ is given by

$$\mathrm{L}_{MC}\left(I_p, O^p_{q,k}\right) = 10\log_{10}\left((\sigma \cdot \alpha + (1-\sigma)\cdot\beta)\cdot\eta^{N-p+q-k}\cdot\zeta^{k-1}\right) \tag{6.6}$$

where $\sigma = 1$ for $1 \leq k < |\Omega_p|$ and $\sigma = 0$ for $k = |\Omega_p|$. Using Lemmas 1 and 2, the lower (upper) bounds for losses in multicast requests are given by,

$$10\log_{10}(\alpha) \leq \mathrm{L}_{MC} \leq 10\log_{10}\left(\beta\cdot(\eta\cdot\zeta)^{N-1}\right) \tag{6.7}$$

The equations for the broadcast case (*i.e.*, $|\Omega_p| = N$) can be easily deduced from Equation (7.5) and inequality (6.7) by setting $|\Psi| = 1$ and $M_\Psi = N$.

6.4.4 Switching Delay

The switching latency of the T-SEs depends on the properties of its material. In the case of the e-TransFlector material, the switching delay ranges from 10 ms to 100 ms at 20°C [433]. In [50], the switching latency of a $12" \times 15"$ switchable mirror (SM) based e-TransFlector and tuned for IR spectrum is about 250 ms. The authors expect that, for a $1" \times 1"$ SM, the switching latency will be around 20 ms since the switching latency is proportional to the surface area of the SM [50]. We envision that the dimensions of the T-SEs in the proposed switch are much smaller than $1" \times 1"$, thus, the switching delay can be reduced.

6.5 Performance Evaluation

2D FSO crossbars are generally of low scalability due to the Gaussian beam propagation loss which becomes the dominant source of losses at high-port count [434]. Therefore, in this section, we present a comparative analysis of the proposed switch with respect to hardware complexity, power splitting, and cost for $N = 8$ (i.e., 8×8 switches).

6.5.1 Hardware Complexity

We decompose all switches into five basic elements, namely; fixed/movable mirrors, fixed/movable splitting mirrors, and T-SEs. Table 7.1 summarizes the hardware complexity of architectures under consideration. Figure 7.6 depicts the hardware complexity for an $N = 8$.

Table 6.1: Summary of Hardware Complexity of Different Architectures $\Phi = \left(2^{(\lceil log_2(N) \rceil + 1)} - 2\right)$.

	Movable Mirror	**Fixed Mirror**	**Movable Splitter**	**Fixed Splitter**	**T-SE**
SaD-I	N^2	$N\Phi/2$	-	$N\Phi/2$	-
SaD-II	$N^2 + N\Phi$	$N\Phi/2$	$N\Phi/2$	-	-
SUM-SaD	$2N^2$	$N\Phi/4$	-	$N\Phi/4$	-
Proposed	-	-	-	-	N^2

In SaD-I, all requests including unicast undergo $1 \times N$ splitting. Therefore, no extra hardware is needed to separate unicast connections leading to a lower hardware complexity for SaD-I. SaD-II is similar to SaD-I except that configurable splitters are used to separate unicast and multicast connections. Even for multicast connections, SaD-II is capable of splitting the input beam to the exact size of the output set. However, this comes at the expense of additional hardware and control complexity. SUM-SaD separates unicast and multicast connections and has lower hardware

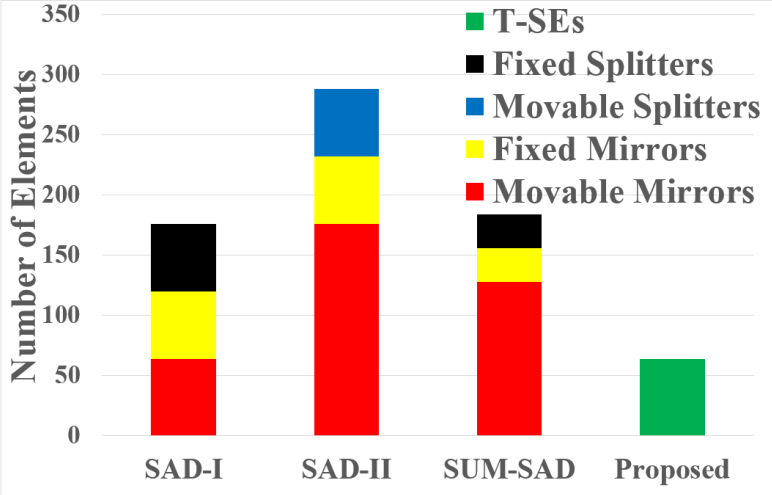

Figure 6.10: Hardware complexity for an 8×8 switch.

complexity as compared to that of SaD-II. Hardware complexity of SUM-SaD is comparable to that of SaD-I, however, it uses more movable components. On the other hand, the proposed crossbar switch using T-SEs is capable of separating the unicast and multicast connections using smaller number of hardware components (i.e., N^2) as compared to SaD-based switches.

6.5.2 Power Splitting Properties

To evaluate the performance of the proposed switch, we calculate the power penalties of the four architectures of size 8×8. We calculate the losses at the eight output ports for all 255 possible combinations of different output set sizes. Since the splitting loss in the proposed switch depend on the input port, we calculate the signal loss for the 1^{st} and 8^{th} input ports to represent the lower and upper bounds of the splitting loss, respectively.

We use the commercial specifications reported by KentOptronics [433] for the tri-state material e-TransFlector which can be tuned to operate in the IR spectrum range used by existing optical communication networks. For example, in [50], Hamedaz-

imi et al. demonstrated a proof-of-concept of an FSO communication link for DC communication using the e-TransFlector material tuned for IR spectrum. Accordingly, we set both reflectance in R-state (β) and transmittance in T-state (η) to 87%, whereas for the S-state, both transmittance (ζ) and reflectance (α) are set to 43%. We assume that the optical efficiency of all fixed/movable mirrors, and splitters are 99%, and 49%, respectively [435].

In case of SaD-I, the power loss is independent of the output set size, and is given by,

$$\mathrm{L}_{SaDI} = 10\log_{10}(0.99) + 10\log_{10}(1/N) \tag{6.8}$$

For SaD-II, the unnecessary splitting is avoided, and thus splitting loss depends on $|\Omega_p|$, and is given by:

$$\mathrm{L}_{SaDII} = 10\log_{10}(0.99) + 10\log_{10}(1/|\Omega_p|) \tag{6.9}$$

Figures 7.7-(a), (b), and (c) depict the average minimum, average, and average maximum splitting power loss of the four switch architectures under consideration at different sizes of output sets.

In case of unicast, SaD-II and SUM-SaD have the same performance that is better than other architectures (see Figure 7.7). This is because the unicast connections are switched separately without incurring any additional losses. On the other hand, SaD-I has the highest power penalty ($\approx$ 9.3 dB) due to the fact that unicast connections undergo unnecessary forced power splitting. Although the proposed architecture does not enforce splitting for unicast connections, there are additional losses of 4.53 dB and 7 dB for input ports 1 and 8, respectively. This is due to the propagation of the beam through the non-moveable T-SEs configured in the T-state along its path.

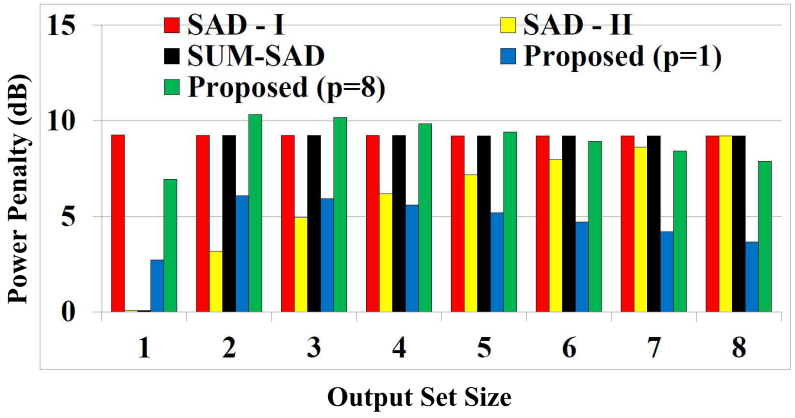

(a)

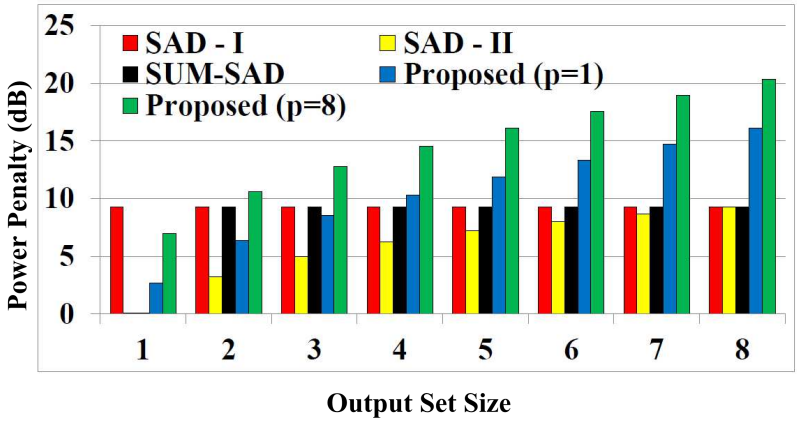

(b)

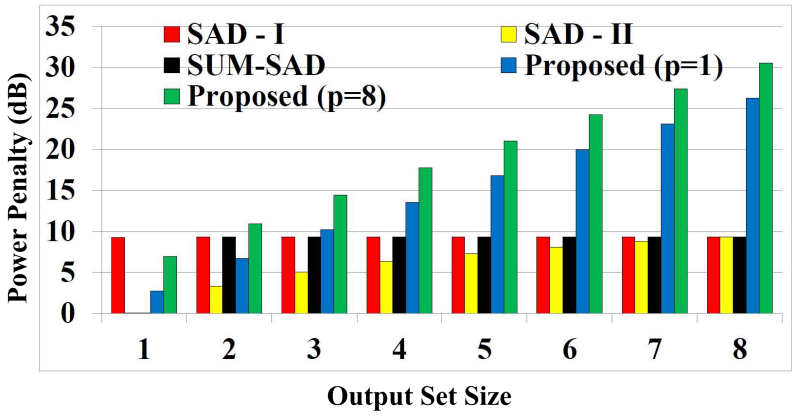

(c)

Figure 6.11: Splitting power penalty in an 8×8 switch (a) Minimum. (b) Average. (c) Maximum.

Even though this does not split the beam; however it adds additional losses due to the imperfection of the material.

In case of multicast (i.e., starting from output set size of two), it can be observed that as the size of the output set increases, so does the average and average maximum power penalties in all architectures except for the SaD-I and SUM-SaD, they have a fixed power loss ($\approx$ 9.3 dB). This is because SaD-I and SUM-SaD perform fixed full splitting for all input signals regardless of the size of output set.

The average minimum power loss in case of SaD-II also increases as the size of the output set increases, whereas, the average minimum loss is fixed for SaD-I and SUM-SaD due to the full splitting property. The average minimum losses in the proposed switch are monotonically decreasing starting with output size of two. However, we observe an increase in the average minimum losses from output size of one to output size of two.

Average minimum (maximum) losses depend on the number of combinations at different sizes of output sets. This number increases starting from output set size of one (i.e., eight possible combinations of unicast) to four (i.e., 70 possible combinations) and then decreases.

Regardless of the decrease in the number of combinations starting from output set size of four, average maximum loss experiences a monotonic increase as the aggregated maximum loss becomes dominant, whereas the average minimum loss decreases as the size of the output set increases.

The proposed switch outperforms both SaD-I and SUM-SaD up to an output size of two, whereas, its performance is comparable to the other architectures up to output set size of four, after which the power loss increases.

It is worth pointing that we only consider the splitting losses in our analysis. Although MEMS-based switches show relatively lower splitting power losses, MEMS-

based switches incur additional losses due to the Gaussian beam losses due to the propagation of the beam in the separate splitting stage, and the angular misalignment of the micro-mirrors [15, 432]. Losses due to angular misalignment can become more significant if the light beam experiences multiple reflections such as in $1 \times N$ beam splitters [436, 437].

High power losses can cause the signal power to fall below the sensitivity of the optical receiver, and thus amplification at the input ports may be needed. It might also be noted that the proposed switch experiences variation in the splitting power losses at output ports. For example, in case of output set size of eight, the variation between the minimum and maximum splitting loss is 25 dB (see Figure 7.7). In order to alleviate the impact of the varying power loss at the outputs, variable optical attenuators (VOAs) must be used at the output ports to equalize the impact of the insertion loss such that the power of the received signal falls within the dynamic range of the optical receiver [438].

Even though MEMS-based switches do not demonstrate differences between minimum and maximum splitting power losses at the output ports as compared to the proposed switch, MEMS-based switches still need pre-amplifiers, e.g., SUM-SaD [see Figure 6.4], and variable optical attenuators due to the losses encountered by the signal in the splitting stage.

Table 7.2 summarizes the number of amplifiers and VOAs required by the switches investigated. The proposed switch, SaD-I and SaD-II need N amplifiers, and N VOAs. However, SUM-SaD switches require N VOAs and $N/2$ amplifiers. This is because only $N/2$ of the inputs are propagating through the splitting stage as shown in Figure 6.4.

Table 6.2: Number of Amplifiers and VOAs.

	Amplifiers	**VOAs**
SaD-I	N	N
SaD-II	N	N
SUM-SaD	$N/2$	N
Proposed	N	N

6.5.3 Switch Cost Analysis

From the discussion above, the total cost (C_{tot}^{arch}) of a switch architecture $arch$ depends on the costs of VOAs (C_{VOA}^{arch}), amplifiers (C_{amp}^{arch}), and switching elements (C_{sw}^{arch}) used, and is given by,

$$C_{tot}^{arch} = C_{VOA}^{arch} + C_{amp}^{arch} + C_{sw}^{arch} \tag{6.10}$$

where $arch$ can be SaD-I, SaD-II, SUM-SaD, or the proposed switch. C_{VOA}^{arch} and C_{amp}^{arch} depend on the number of VOAs (N_{VOA}^{arch}) and amplifiers (N_{amp}^{arch}) used, respectively.

From Table 7.2, SaD-I, SaD-II, and the proposed switch architectures employ N VOAs at the output ports and N amplifiers at the input ports. However, SUM-SaD switch architecture requires N VOAs and only $N/2$ amplifiers. Therefore, SUM-SaD architecture has a cost advantage over SaD-I, SaD-II, and the proposed architecture with respect to C_{amp}.

We can expand C_{sw}^{arch} further and express it as a function in the cost of a fixed (mirrors/splitters) component C_f, a movable (mirror/splitter) component C_m, and a T-SE C_{tse}. Given the cost of each component, we can use Table 7.1 to calculate C_{sw}^{arch} as follows:

$$C_{sw}^{arch} = N_f^{arch} \cdot C_f + N_m^{arch} \cdot C_m + N_{tse}^{arch} \cdot C_{tse} \tag{6.11}$$

where N_f^{arch}, N_m^{arch}, and N_{tse}^{arch} are the numbers of fixed, moveable, and T-SE switching

elements used in the switch *arch*, respectively.

We use a relative cost model to quantify and compare the cost of the proposed switch. We use the cost of the fixed elements, C_f, as reference since the cost of these components is relatively stable compared to the other two types.

Let ρ be the ratio of the cost of a movable versus fixed components, i.e., $\rho = C_m/C_f$. Similarly, let μ be the ratio of the cost of a T-SE versus a fixed component, i.e., $\mu = C_{tse}/C_f$. To evaluate the cost effectiveness of the proposed switch as compared to SaD-I switch, we use the total number of fixed and movable components in Table 7.1 to setup the following inequality:

$$N^2 C_m + N\Phi C_f \geq N^2 C_{tse} \tag{6.12}$$

By simplifying the inequality (6.12), it is straightforward to show that the proposed switch has a smaller overall cost as compared to that of SaD-I if and only if the value of σ satisfies the following inequality:

$$\rho_{SaD-I} \geq \mu - \frac{\left(2^{(\lceil log_2(N) \rceil + 1)} - 2\right)}{N} \tag{6.13}$$

Similarly, we can compute a lower bound on the value of ρ for the SaD-II and SUM-SaD as follows:

$$\rho_{SaD-II} \geq \frac{\mu N - 2^{\lceil log_2(N) \rceil} - 1}{N + 3 \times 2^{\lceil log_2(N) \rceil} - 3} \tag{6.14}$$

$$\rho_{SUM-SaD} \geq \frac{\mu N - 2^{\lceil log_2(N) \rceil} - 1}{2N} \tag{6.15}$$

Figure 7.9 plots the ratio ρ/μ to provide an insight on the relationship between the cost of a T-SE and that of a movable component. Moreover, we plot the function

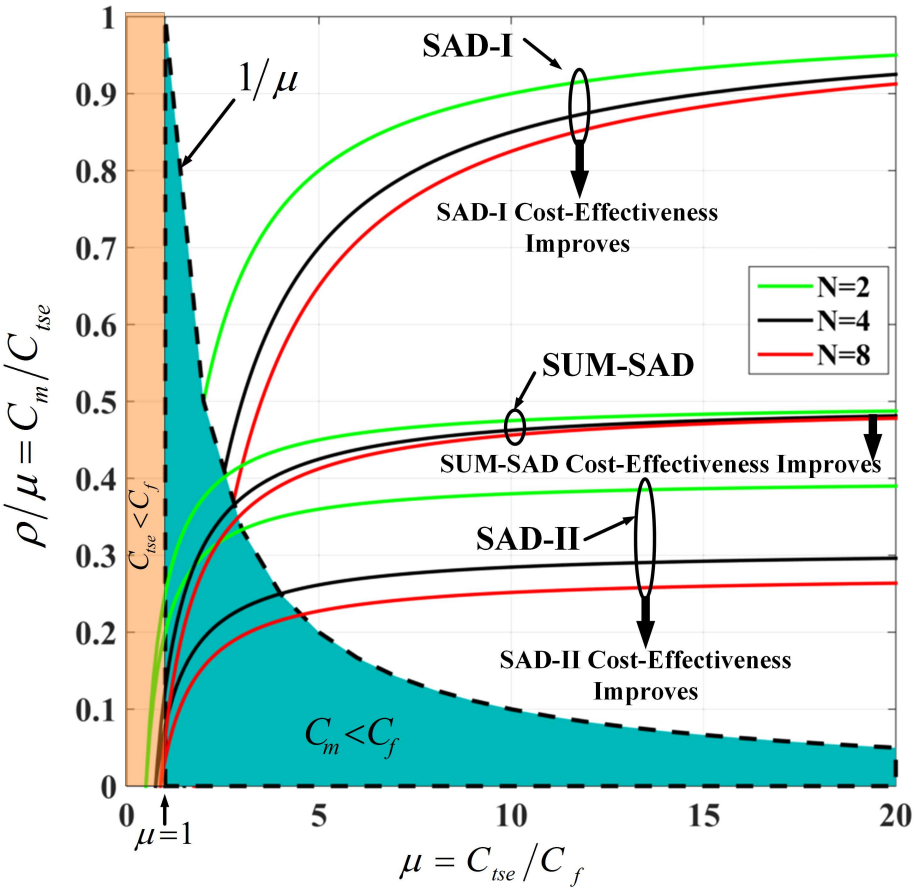

Figure 6.12: Comparative cost analysis for the proposed switch. The curves represent the relative cost effectiveness of the proposed switch as compared to the existing SaD switches with respect to SEs. Shaded regions are invalid design regions. White region above (below) a curve indicates that the proposed switch is more (less) cost effective compared to the corresponding SaD switch for specific number of ports N.

$1/\mu$ (i.e., $\rho = 1$) which corresponds to the case $C_m = C_f$. Obviously, the cost of a MEMS mirror $C_m > C_f$. Therefore, we consider the shaded area below the curve $1/\mu$ as an *invalid design region*. It is not expected that the cost C_{tse} will be less than C_f. Therefore, we have also excluded the area corresponding to $\mu < 1$.

Given the cost of various hardware components, one can use Figure 7.9 to compare the cost effectiveness of the proposed design with respect to SaD-based switches at different port sizes ($N = 4,\ 8,\ 16,$ and 32). For $N = 4$, even if the cost of a T-SE is ten times the cost of fixed components (i.e., $C_{tse} = 10 \times C_f$), the proposed switch will

be more cost effective as compared to the SaD-I, SaD-II and SUM-SaD, when C_{tse} is at most 1.18, 3.5 and 2.16 times C_m, respectively.

6.6 Chapter Summary

We propose a new class of SNB FSO multicast switches using tri-state switching elements (T-SEs). In the proposed switch, TSEs simultaneously support signal splitting and switching without the need for separate splitting stages used in the conventional multicast switches. Thus, a beam propagating in the proposed switch avoids the propagation loss that may be encountered by an optical beam passing through a splitting stage followed by a crossbar as in SaD-based switches. This leads to lower insertion loss that is due to the Gaussian beam divergence. An $N \times M$ SNB multicast switch requires *only* NM *non-movable* T-SEs. Comparison with existing optical multicast switches shows that the proposed switch provides multicast capability with lower hardware complexity and a comparable performance. Cost analysis for the proposed switch shows that its cost is lower than SaD-based switches, even if the cost of the T-SE is is 1.2 to 3.5 times that of MEMS mirror.

Chapter 7

Proposed Rearrangeably Non-Blocking Multicast FSO Switch

In this chapter, we propose an $N \times N$ RNB multicast FSO switch. Our design exploits *non-movable* tri-state switching elements (T-SEs). The proposed switch exhibits an optimal hardware complexity as it requires only $N(N+1)/2$ T-SEs. In addition, we present a simple routing algorithm that systematically establishes connections over the new switch.

7.1 Introduction

Another important switch design aspect is its blocking characteristics. A strictly nonblocking (SNB) switch allows an input signal to be directed to any available output, or a set of outputs (if multicast-capable), irrespective of the current state of the switch. A rearrangeably nonblocking (RNB) switch allows an input signal to

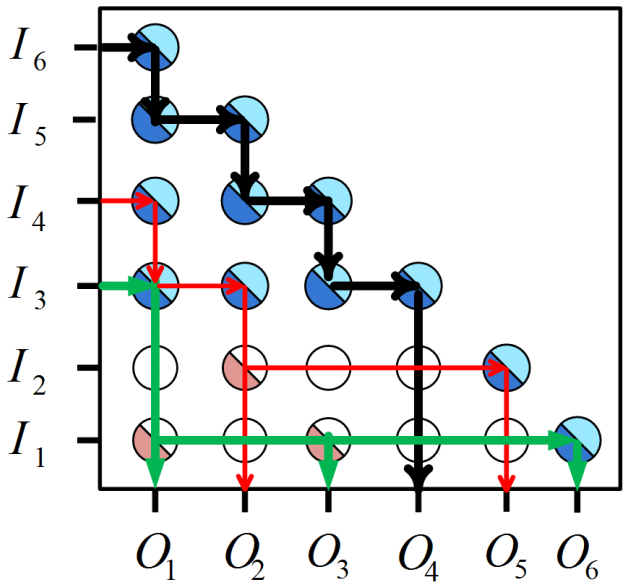

Figure 7.1: Multicast in 6×6 proposed switch using T-SEs.

be directed to one or more available outputs, however, rearranging already existing connections may be required. SNB switches have better blocking attributes compared to RNB switches at the cost of increased hardware complexity. In some realistic cases; however, RNB design is sufficient if the requests are known a priori [436]. For example, in wavelength division multiplexing (WDM) or dense WDM (DWDM) backbone networks, setup of connections is based on demands of multiple Gbps links, and thus connections can tolerate relatively long setup time involving rearranging existing connections to host a new one [434]. Therefore, designing RNB switches is of a practical interest.

The remainder of this chapter is organized as follows. We dedicate Sections 7.2 and 7.3 to present and analyze the new RNB multicast switch. Comparative analysis is presented in Section 7.4, followed by chapter summary in Section 7.5.

7.2 Proposed RNB Multicast FSO Switch

In this section, we propose a new RNB multicast switch and present a routing algorithm to systematically establish connections over the proposed switch. In the next section, we present and analyze the properties of the proposed switch.

In our design, we aim to use the minimum number of T-SEs to perform RNB multicast switching without impacting the performance of the switch. Therefore, in the proposed switch, a T-SE is placed at the intersection of input port p and output port q only if $p \leq q$. This leads to a triangular switch in which a row corresponding to input port p contains $N + 1 - p$ T-SEs as shown in Figure 7.1.

Figure 7.1 depicts a 6×6 proposed triangular switch with one unicast: $\langle 6, 4 \rangle$, and two multicast requests: $\langle 3, \{1, 3, 6\} \rangle$ and $\langle 4, \{2, 5\} \rangle$. Both T-SE sides reflect light in the R-state. Light beam incident to any of the T-SE sides can propagate through or split in the T and S-states, respectively. The proposed switch requires only $N(N + 1)/2$ T-SEs.

7.2.1 Proposed Request Routing Algorithm

Algorithm 3 is proposed for the configuration (routing) of connections on the proposed multicast switch. In this algorithm, let $\Omega_p = \{O^p_{q,k} \mid 1 \leq q \leq N, 1 < k \leq |\Omega_p|$ and $\forall v, w \in k;\ O^p_{q,v} < O^p_{q,w}$ if $v < w\}$.

The proposed iterative algorithm involves elimination process, where $\hat{N}$ denotes the virtual switch size, $\hat{p}$ and $\hat{O}^p_{q,k}$ denote the input and output port index, respectively.

7.2.2 Example

To illustrate the proposed algorithm, we discuss an example that covers different switching scenarios. Figure 7.2 depicts an 8×8 switch with three unicast and two mul-

Algorithm 3: Request Routing

Input: Set of Requests $\mathcal{R}$.
Output: States of the $N(N+1)/2$ T-SEs.

$\hat{N} \leftarrow N$
for $Counter = 1 \rightarrow |\mathcal{R}|$ **do**
  Update list of virtual input and output ports
  if $(\mathcal{R}_p \in \Gamma \;||\; (\mathcal{R}_p \in \Psi \;\&\&\; \hat{p} > 1))$ **then**
    if $\hat{O}^p_{q,1} \leq \hat{N} + 1 - \hat{p}$ **then**
      Configure $\tau(d, \hat{O}^p_{q,1}, R)$ for $d = \hat{p} \rightarrow \hat{N} + 1 - \hat{O}^p_{q,1}$
      Eliminate SE$(\hat{p}, d)$ for $d = 1 \rightarrow \hat{O}^p_{q,1}$
    else
      $i \leftarrow \hat{p}$
      $j \leftarrow \hat{N} + 1 - \hat{p}$
      while $j < \hat{O}^p_{q,1}$ **do**
        Configure $\tau(i, j, R)$ and $\tau(i-1, j, R)$
        $i \leftarrow i - 1$
        $j \leftarrow j + 1$
      Configure $\tau(i, j, R)$
      Eliminate SE$(\hat{p}, d)$ for $d = 1 \rightarrow \hat{N} + 1 - \hat{p}$
      Eliminate SE$(d, \hat{N} + 1 - d)$ for $d = i + 1 \rightarrow \hat{p} - 1$
  if $\mathcal{R}_p \in \Gamma$ **then**
    Eliminate SE$(d, \hat{O}^p_{q,1})$ for $d = 1 \rightarrow \hat{N} + 1 - \hat{O}^p_{q,1}$
    $\hat{N} \leftarrow \hat{N} - 1$
  else
    for $d = \hat{O}^p_{q,1} \rightarrow \hat{O}^p_{q,|\Omega_p|-1}$ **do**
      Configure $\tau(1, d, S)$
      Eliminate SE(w, d) for $w = 1 \rightarrow \hat{N} + 1 - d$
    for $d = 1 \rightarrow \hat{N} + 1 - \hat{O}^p_{q,|\Omega_p|}$ **do**
      Configure $\tau(d, \hat{O}^p_{q,|\Omega_p|}, R)$
      Eliminate SE$(d, \hat{O}^p_{q,|\Omega_p|})$
    Eliminate SE$(1, d)$ for $d = 1 \rightarrow \hat{O}^p_{q,|\Omega_p|}$
    $\hat{N} \leftarrow \hat{N} - |\Omega_p|$
Route light beams of all requests $\mathcal{R}$.

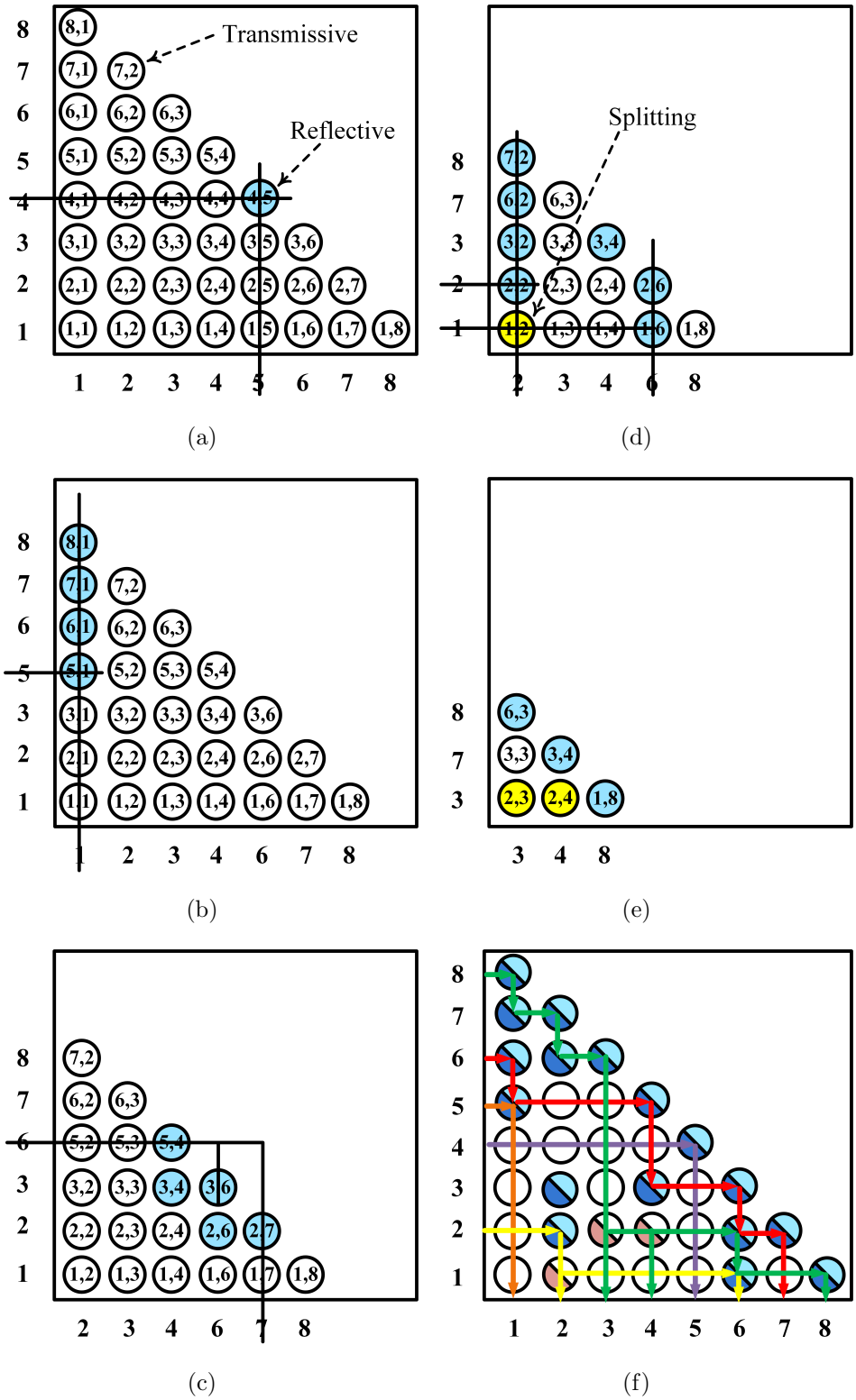

Figure 7.2: This figure illustrates the process of configuring an 8×8 proposed switch with three unicast and two multicast requests using Algorithm 1. Black lines indicates the T-SEs that will be eliminated at the end of current iteration. Each subfigure shows the accumulative result of a request being routed. (a) Unicast request $\langle 4, 5 \rangle$. (b) Unicast request $\langle 5, 1 \rangle$. (c) Unicast request $\langle 6, 7 \rangle$. (d) Multicast request $\langle 2, \{2, 6\} \rangle$. (e) Multicast request $\langle 8, \{3, 4, 8\} \rangle$. (f) Fully configured switch with all requests.

ticast requests configured using Algorithm 3; namely: $\langle 4, 5\rangle$, $\langle 5, 1\rangle$, $\langle 6, 7\rangle$, $\langle 2, \{2, 6\}\rangle$, and $\langle 8, \{3, 4, 8\}\rangle$. We use T-SEs with solid colors in Figures 7.2 (a)-(e). White, blue, and yellow-filled circles are used to refer to a T-SEs in T, R, and S-states, respectively. Then the final solution is presented using T-SE symbols discussed in Figure 6.5.

To configure the switch, we first process the, $|\Gamma| = 3$, unicast requests. Requests $\langle 4, 5\rangle$ and $\langle 5, 1\rangle$ [Figures 7.2-(a) and (b), respectively] have $q \leq N + 1 - p$, and hence, there is a T-SE that can directly reflect the light beam from I_p to O_q. When a T-SE is configured in the R-state, all T-SEs corresponding to the same column q and higher input ports are also configured in the R-state (line 6). This guarantees that the light routed from these input ports reach their destinations through multiple reflections [436]. After each iteration, the row (lines 19-20) and the column (line 7) of the configured T-SEs are crossed and remaining T-SEs are used to realize a smaller virtual switch.

Figure 7.2-(c) shows realization of the request $\langle 6, 7\rangle$, where $q > N + 1 - p$. Here, at least three reflections are needed in order to connect I_p to O_q (lines 9-15). After processing unicast requests, a virtual switch is defined by eliminating the input row (lines 19-20), output column, and any diagonal SEs used in routing path (lines 16-17).

After processing unicast requests, we process multicast requests in an ascending order of the input port indices. Fig 7.2-(d) depicts the realization of the multicast request $\langle 2, \{2, 6\}\rangle$. For a multicast request, first we configure routing as in unicast case from the input port to the lowest index output port in the request (i.e., I_2 to O_2 in this example). After the first output port, a series of split operations ending in a reflect operation are configured in the lowest row of the switch (i.e., $\hat{p} = 1$) to route the signal to other output ports (lines 22-29). Similarly, the multicast request $\langle 8, \{3, 4, 8\}\rangle$ is realized [see Figure 7.2-(e)]. The switch with all requests configured is

shown in Figure 7.2-(f).

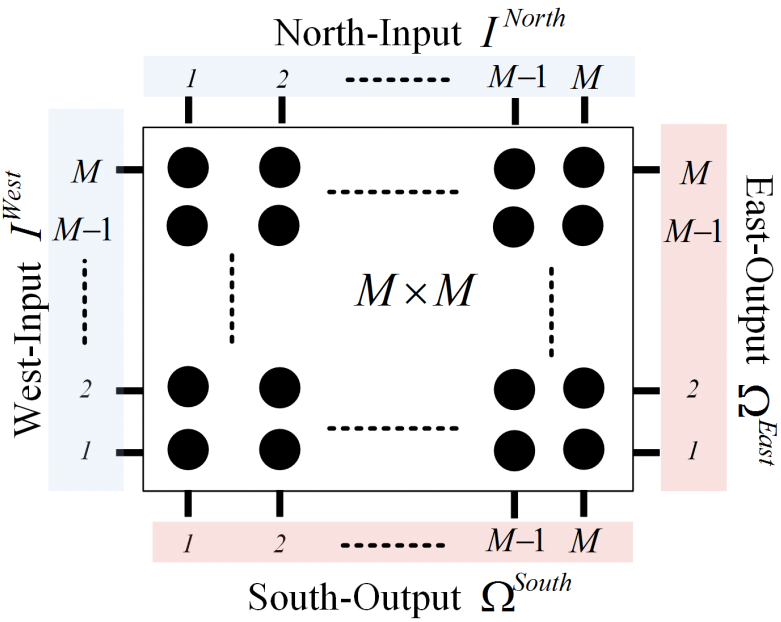

Figure 7.3: $M \times M$ rectangular sub-switch.

7.3 Properties of the Proposed Switch

In this section, we prove that the proposed switch is RNB and discuss it's properties including hardware complexity, signal path length, and switch reconfigurability.

7.3.1 Switch Blocking Characteristics

In the following, we prove Theorem 8 to establish that the proposed triangular switch employing T-SEs is an RNB multicast switch. We start by proving the following lemma that is used in the proof of the theorem. In this lemma, we consider a rectangular switch as shown in Figure 7.3. The North and West sides of the switch are used as inputs and are referred to as I_p^{North} and I_p^{West}, respectively, where $1 \leq p \leq M$. The South and East sides are used for outputs and the corresponding sets of output

ports are referred to as $\Omega^S = \{O_1^{South}, \cdots, O_M^{South}\}$ and $\Omega^E = \{O_1^{East}, \cdots, O_M^{East}\}$, respectively.

Lemma 3. *An $M \times M$ crossbar with $2M$ input and $2M$ output ports shown in Figure 7.3 is SNB under the following conditions:*

1. $1 \leq |\mathcal{R}^{M \times M}| \leq M$.
2. *a West-input I_p^{West}, $1 \leq p \leq M$ can be switched to an arbitrary unused subset of South-output ports Ω_p^{South}, and/or the corresponding East-output port O_p^{East}.*
3. *a North-input I_p^{North} where $1 \leq p \leq M$ can be switched to an arbitrary unused subset of South-output ports $\{O_y^{South} | p \leq y \leq M\}$ and/or anyone of the unused East-output ports $\{O_z^{East}\}$, where $1 \leq z \leq M$.*

Proof. Assume that all of the requests are from West-input ports $I_1^{West}, \ldots, I_M^{West}$. For each request $\mathcal{R}_p = \langle I_p^{West}, \Omega_p \rangle$, one of the following cases applies:

Case 1. $\boldsymbol{\Omega_p = O_p^{East}}$

All T-SEs are configured in the T-state and the light directly propagates towards the corresponding East-output port O_p^{East}.

Case 2. $\boldsymbol{\Omega_p \in \Omega^{South}}$

The T-SEs corresponding to the output ports are configured in the S-state except for the T-SE corresponding to the last output which is configured in the R-state.

Case 3. $\boldsymbol{\Omega_p \in \Omega^{South} \cup O_p^{East}}$

All T-SEs corresponding to the output ports in Ω^{South} are configured in the S-state and no T-SE in the row is configured in the R-state. This way, part of the signal propagates towards the corresponding East-output port O_p^{East}.

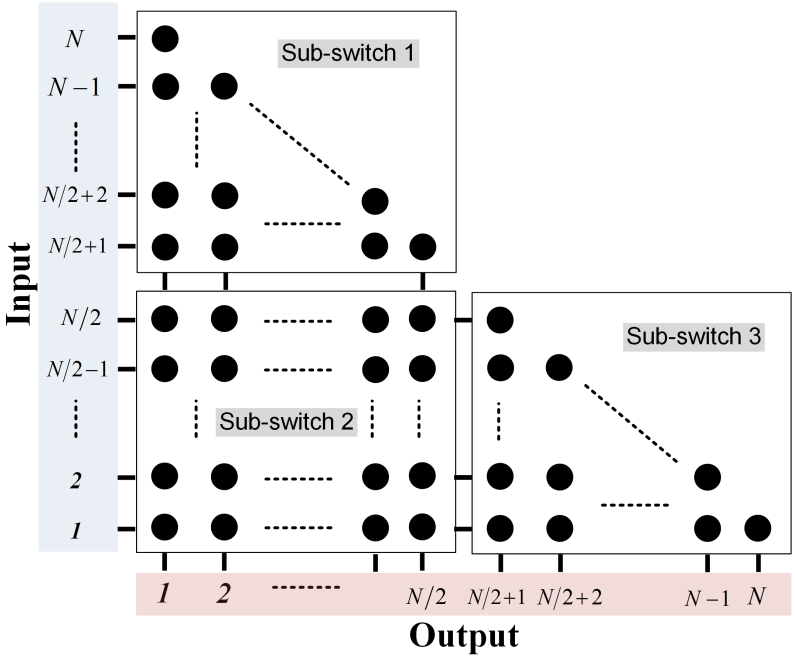

Figure 7.4: General structure of an $N \times N$ triangular switch.

For a canceled request by any of the West-input ports $I_1^{West}, \ldots, I_M^{West}$, there can be a request by one of the North-input ports $I_1^{North}, \ldots, I_M^{North}$. This also means that all T-SEs in the row corresponding to the canceled request are configured in T-state and can be used by any new request. Hence, light beam from the North-input port of the new request can be directed through its corresponding column until it gets to the row of the canceled request where splitting is performed.

Therefore, an $M \times M$ crossbar shown in Figure 7.3 is SNB under the three aforementioned conditions. □

Theorem 8. *The proposed triangular switch employing T-SEs is a rearrangeable nonblocking multicast switch.*

Proof. After processing the $|\Gamma|$ unicast requests, we get a triangular switch to process multicast requests. Assume an $N \times N$ triangular switch (see Figure 7.4). We want to prove that an $N \times N$ triangular switch used to process $|\Psi|$ multicast requests, where $1 \leq |\Psi| \leq N/2$, is RNB.

We will use induction to prove the theorem. We assume that $N = 2^k$, where $k \in \mathbb{N}^+$. For the basis case, it is clear that all permutations, multicast assignments, and broadcast requests can be realized for a 2×2 switch (i.e., $k = 1$).

Assume by induction that an $N \times N$ triangular switch, where $N = 2^{k-1}$ is RNB. By induction, we wish to prove that an $N \times N$ switch, where $N = 2^k$ is also RNB.

For induction step, an $N \times N$ triangular switch can be divided into three sub-switches (see Figure 7.4): an $N/2 \times N/2$ rectangular sub-switch, and two $N/2 \times N/2$ triangular sub-switches. The sub-switches are numbered from 1 to 3 in counter-clockwise order.

Both $N/2 \times N/2$ triangular sub-switches are triangular switches of dimension 2^{k-1}, and thus are RNB by induction hypothesis.

Therefore, for an $N \times N$ triangular switch shown in Figure 7.4 to be RNB, we only need to prove that the $N/2 \times N/2$ rectangular sub-switch is SNB for processing requests from input ports $I_1, \cdots, I_{N/2}$ and inputs from sub-switch 1 (i.e., outputs from sub-switch 1).

Using Lemma 1, one can see that the sub-switch 2 is equivalent to the switch in Figure 7.3. Input ports $I_1, \cdots, I_{N/2}$ are equivalent to the West-inputs, and inputs from sub-switch 1 are equivalent to the North-input ports. Moreover, the output ports $O_1, \cdots, O_{N/2}$ are equivalent to the South-output ports Ω^{South}, whereas output ports connecting sub-switches 2 and 3 are equivalent to the East-output ports. Therefore, the $N/2 \times N/2$ rectangular sub-switch (i.e., sub-switch 2) is SNB, and thus the $N \times N$ triangular switch is RNB. □

7.3.2 Hardware Complexity

This is directly proportional to the total number of T-SEs. An $N \times N$ proposed RNB multicast switch requires a total of $N(N+1)/2$ T-SEs. Since the T-SEs of the diagonal are either in the T- or R-state, the number of T-SEs can be reduced to $N(N-1)/2$ by replacing the N diagonal T-SEs with fixed mirrors.

Theorem 9. *The proposed RNB multicast FSO switch is optimal w.r.t hardware complexity as compared to all existing multicast switches.*

Proof. In [439], it is shown that the number of elementary 2×2 switches in an $N \times N$ planar optical RNB unicast switch is at least $N(N-1)/2$. Also, from [436], the lower bound for a 2D *unicast* RNB MEMS switch is $N(N+1)/2$. The proposed RNB multicast FSO switch needs only $N(N-1)/2$ T-SEs (elementary 2×2 switches) and N fixed mirrors. Since the hardware complexity of the proposed switch is equal to the lower bound of a unicast switch, it must be optimal. □

7.3.3 Signal Path Length

Several signal paths are possible between a fixed input-output pair (I_p, O_q), $1 \leq p,\ q \leq N$, the number of which can be computed using enumerative combinatorics [440]. It may be noted, however, that all paths follow the *Taxicab geometry* leading to the following lemma.

Lemma 4. *The length, $\Delta(p,q)$, of any of the possible paths between a fixed pair of input-output ports is expressed in terms of the number of T-SEs traversed by the beam and is given by, $\Delta(p,q) = p + q - 1$ [440].*

The path length is constant for a fixed input-output pair (I_p, O_q) and is known a priori, however, the numbers of T-SEs in the T- and R-states are dependant on co-existing connections.

Lemma 5. *It is possible to establish lower and upper bounds for the number of T-SEs in R-state from I_p to O_q, $\mathcal{E}_R(p,q)$, based on the relation between p and q.*

Proof. If $q \leq N+1-p$, this implies that there is a T-SE at the intersection of the row p and column q of the proposed switch. In this case, the input signal can be directed to the output port via a reflection off of that T-SE configured in R-state. Thus, $\mathcal{E}_R(p,q)$ is given by,:

$$\mathcal{E}_R(p,q) = 1 \tag{7.1}$$

On the other hand, if $q > N+1-p$, then there is not a T-SE at the intersection of the row p and column q. At least three reflections are, therefore, needed to direct the input signal to the output port. The lower (upper) bounds for $\mathcal{E}_R(p,q)$ are given by,

$$3 \leq \mathcal{E}_R(p,q) \leq 2min(p-1, q-1) + 1 \tag{7.2}$$

□

7.3.4 Total Number of Splitting Operations

The performance of the proposed switch depends on the number of splitting operations given by the following Lemmas.

Lemma 6. *In multicast, the minimum and maximum number of T-SEs configured in S-state are similar to that of the SNB switch [16] and are equal to 1 and $N-1$, respectively.*

Proof. This directly follows from the minimum (of 2) and maximum (of N) cardinalities of outputs. □

Lemma 7. *For all requests at a given time, the total number of T-SEs configured in the S-state is given by* $N_\Psi - |\Psi|$*, where* $2 \leq N_\Psi \leq N$ *is the number of output ports in all multicast requests at a certain point of time* $N_\Psi = \sum_{w=1}^{|\Psi|} \Omega_w,\ \forall\ \mathcal{R}_p \in \Psi$*, and* $|\Psi|$ *is the total number of multicast requests.*

Proof. For each multicast request $\langle I_p, \Omega_p \rangle$, using Algorithm 3, all T-SEs in the first row and columns corresponding to output ports in Ω_p are configured in the S-state except for last output port in Ω_p which is configured in the R-state. Therefore, the total number of T-SEs in the R-state out of N_Ψ is equal to the total number of multicast requests $|\Psi|$. □

7.3.5 Signal Power Loss

An optical signal in multicast switch undergoes insertion/coupling and splitting losses as it propagates from input to output ports. Insertion/coupling loss is mainly due to the Gaussian beam divergence experienced by any light beam propagating in free space [432], and thus depends on the architecture of the switch. Extensive analysis and studies has been performed to characterize the insertion/coupling loss in 2D MEMS crossbar. Insertion/coupling loss in the proposed design follows the analysis used for MEMS switches [432] but with the following two differences:

1. In MEMS-based multicast switches, a beam must propagate through a splitting stage before being switched by a crossbar. On the other hand, an optical beam propagates only through a single stage in the proposed triangular switch, which may lead to a shorter total propagation distance, and thus lower insertion loss.

2. Mechanical motion of the mirrors in MEMS switches results in angular misalignment leading to inefficient coupling. Our proposed design employs only *non-movable* parts, and hence, is free of such losses.

Splitting Losses are the losses encountered by the light beam due to the splitting required for multicasting. Let β and η be the reflection and transmission efficiencies of T-SE in the $R-$ and $T-$states, respectively. We denote the percentage of the power reflected by a T-SE in the S-state as α, and the transmitted power of the beam is ζ (Figure 6.5). In the proposed switch, splitting losses depend on the cardinality of the output set $|\Omega_p|$, and thus, we have two different cases.

Case 1: Unicast ($|\Omega_p| = 1$). The power loss is due to the reflection and transmission losses of the T-SEs configured; respectively, in the R- and T-states along the path, and thus depends on the number of T-SEs configured in R-state [i.e., $\mathcal{E}_R(p,q)$]. From Lemma 4, the length of a path $\Delta(p,q)$ is known. Given $\mathcal{E}_R(p,q)$, the number of T-SEs configured in the T-state is $\Delta(p,q) - \mathcal{E}_R(p,q)$. Since β and η are the reflection and transmission efficiencies of T-SE in the R and $T-$states, respectively, the power penalty in a unicast request, $\mathrm{L}_{UC}(p,q_1)$, can be expressed as follows,

$$\mathrm{L}_{UC}(p,q_1) = 10\log_{10}\left[\beta^{\mathcal{E}_R(p,q)} \cdot \eta^{\Delta(p,q)-\mathcal{E}_R(p,q)}\right] \tag{7.3}$$

For $q \leq N+1-p$, $\mathcal{E}_R(p,q) = 1$ (according to Lemma 5), and thus the power loss is given by,

$$\mathrm{L}_{UC}(p,q_1) = 10\log_{10}\left[\beta \cdot \eta^{\Delta(p,q)-1}\right] \tag{7.4}$$

Case 2: Multicast ($1 < |\Omega_p| < N$). Power loss at an output port O_q, that is part of a multicast output set, Ω_p, is due to reflection and transmission losses of the T-SEs in the path configured in R, T, and S-states.

Depending on the position, k, of the output port O_q in the output set Ω_p, we can define how many splitting processes the signal has to go through. For example, the input signal experience $k-1$ splits before it reaches the k^{th} output port in Ω_p.

Therefore, the power loss due to these splits can be calculated as $\log_{10}(\zeta^{k-1})$.

Moreover, all outputs in Ω_p are reached via a reflection off of a T-SE configured in the S-state, except for the last output port which is reached using a reflection off of a T-SE in the R-state. Therefore, for all signals we reduce the power by $\log_{10}(\alpha)$ except for the last output port, we reduce its power by $\log_{10}(\beta)$.

Since we know the path length, $\Delta(p,q)$, from Lemma 4, this means that the remaining $\Delta(p,q)-k$ T-SEs in the path can be either in the T or R-states depending on the route allocated using Algorithm 3. Given $\mathcal{E}_R(p,q)$, we can use the following equation to express splitting power loss in case of multicast $\mathrm{L}_{MC}\left(I_p, O^p_{q,k}\right)$,

$$\mathrm{L}_{MC}\left(I_p, O^p_{q,k}\right) = 10\log_{10}\left((\sigma\cdot\alpha+(1-\sigma)\cdot\beta)\cdot\beta^{\mathcal{E}_R(p,q)}\cdot\eta^{\Delta(p,q)-k-\mathcal{E}_R(p,q)}\cdot\zeta^{k-1}\right) \quad \text{dB} \tag{7.5}$$

where $\sigma = 1$ for $1 \leq k < |\Omega_p|$ and $\sigma = 0$ for $k = |\Omega_p|$ to choose from α and β depending on k.

Below, we prove Theorem 10 to show that the splitting loss analysis of the proposed $N \times N$ RNB switch when $\eta = \beta$ is similar to that of an $N \times N$ SNB switch presented in [16].

Theorem 10. *Splitting loss at output ports in the proposed RNB switch are similar to that of an SNB switch [16] if $\eta = \beta$.*

Proof. Path length of the connections from I_p to O_q (as a unicast request or part of a multicast request) is fixed. Similarly, the number of splitting operations for $\mathcal{R}_p$ is fixed, and thus, the remaining T-SEs are either in $T-$ or in $R-$state. Since both $T-$ and $R-$states have the same power losses, the overall loss is similar to that of in our SNB switch discussed in Chapter 6. □

Based on Theorem 10, we can use power loss equations in [16] to calculate splitting power loss in the proposed switch. Equation (7.3) for the power penalty in a unicast request becomes,

$$\mathrm{L}_{UC}(p, q_1) = 10\log_{10}\left(\eta^{\Delta(p,q)}\right) = 10\log_{10}\left(\beta^{\Delta(p,q)}\right) \tag{7.6}$$

Similarly, Equation (7.5) for the power penalty of multicast requests can be expressed as,

$$\mathrm{L}_{MC}\left(I_p, O_{q,k}^{p}\right) = 10\log_{10}\left((\sigma\cdot\alpha + (1-\sigma)\cdot\beta)\cdot\eta^{N-p+q-k}\cdot\zeta^{k-1}\right) \quad \mathrm{dB} \tag{7.7}$$

7.3.6 Switching Delay

The switching latency depends on the switching speed and the properties of the material used to realize T-SEs. The switching latency of a $1" \times 1"$ switchable mirror (SM) based e-TransFlector and tuned for IR spectrum is in the range of 1-10 ms at room temperature ($22°C$). The dimensions of the T-SEs in the proposed switch are expected to be much smaller than $1" \times 1"$. Since the switching latency is proportional to the surface area of the SM, the switching delay can be reduced. Moreover, as the technology of the materials used to realize T-SEs improves, more responsive T-SEs can be developed, and thus faster switches can be realized.

7.3.7 Switch Reconfigurability

For an $N \times N$ SNB crossbar [16, 441] discussed in Chapter 6, a square substrate with N^2 T-SEs is required. On the other hand, two of the proposed $N \times N$ RNB triangular switches would require a triangular substrate with $2 \times (N(N+1)/2) = N(N-1)$

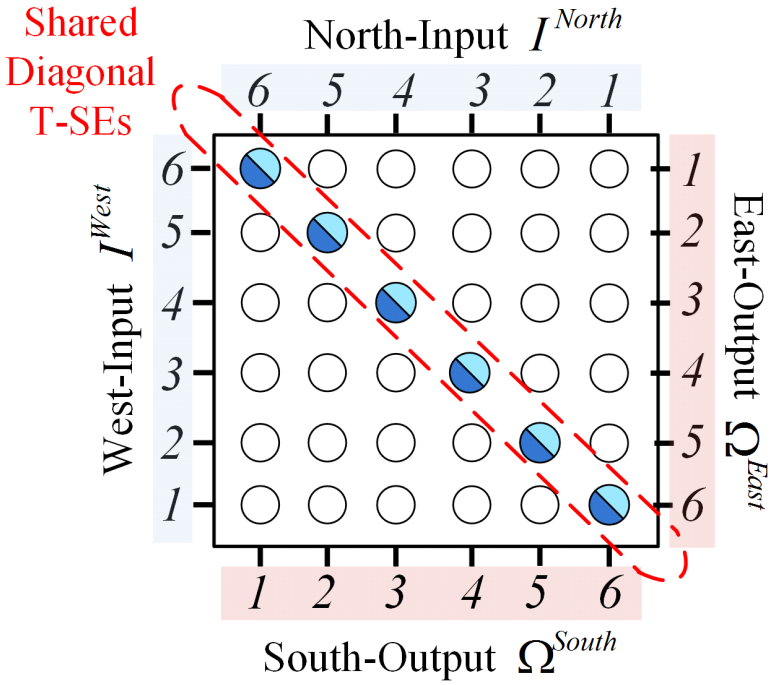

Figure 7.5: Two 6×6 RNB switches on a single square substrate.

T-SEs. However, as discussed earlier, the diagonal T-SEs in the proposed switch are either in the T or R-states, and thus diagonal T-SEs can be replaced with fixed mirrors, or can be configured permanently in the R-state. This way, two of the proposed $N \times N$ RNB triangular switches can share the diagonal T-SEs, and hence both switches can be accommodated on a single square substrate with N^2 T-SEs as shown in Figure 7.5.

It might be noted that we can obtain a very flexible switch using the setup in Figure 7.5. This switch can operate as two $N \times N$ RNB switches or a single $N \times N$ SNB switch for I^{West}-Ω^{South} or I^{North}-Ω^{East}. Moreover, the switch in Figure 7.5 can also operate as a $2N \times 2N$ switch (see Figure 7.3) under the constraints outlined in Lemma 3.

7.4 Comparative Analysis

2D FSO switches are generally of low scalability due to the Gaussian beam propagation loss which becomes the dominant source of losses at high-port count [438]. In this section, we present a comparative analysis of the proposed switch with respect to hardware complexity, power splitting, and cost for $N = 8$ (i.e., 8×8 switches).

7.4.1 Hardware Complexity Comparison

We decompose all switches into five basic SEs, namely; fixed/ movable mirrors, fixed/movable splitting mirrors, and T-SEs. Table 7.1 summarizes the hardware complexity of architectures under consideration. Figure 7.6 depicts the hardware complexity for $N = 8$.

Table 7.1: Summary of Switching Hardware Complexity of Different Architectures $\Phi = \left(2^{(\lceil \log_2(N) \rceil + 1)} - 2\right)$.

	Movable Mirror	**Fixed Mirror**	**Movable Splitter**	**Fixed Splitter**	**T-SE**
SaD-I	N^2	$N\Phi/2$	-	$N\Phi/2$	-
SaD-II	$N^2 + N\Phi$	$N\Phi/2$	$N\Phi/2$	-	-
SUM-SaD	$2N^2 + N$	$N\Phi/4$	-	$N\Phi/4$	-
Crossbar (T-SE)	-	-	-	-	N^2
Proposed	-	N	-	-	$\frac{N(N-1)}{2}$

In SaD-I, unicast request must undergo $1 \times N$ splitting. Therefore, no extra hardware is needed to separate unicast requests. SaD-II is similar to SaD-I except that configurable splitters are used to separate unicast and multicast requests, and to split the input beam to the exact size of the output set. However, this comes at the expense of additional hardware and control complexity. SUM-SaD separates unicast and multicast connections and has lower hardware complexity as compared to

that of SaD-II. Although comparable to SaD-I with respect to hardware complexity, SUM-SaD uses more movable SEs.

Similar to SaD-II, SNB crossbar using T-SEs and the proposed switch can separate unicast and multicast requests, and can also split a beam into a number of beams equal to the size of the output set. A crossbar required N^2 T-SEs, whereas, the proposed RNB switch requires only $N(N-1)/2$ T-SEs and N fixed mirrors. For $N = 8$, the proposed switch demonstrates 87.5% and 43.8% savings in total number of SEs as compared to SaD-II and the crossbar with T-SEs, respectively.

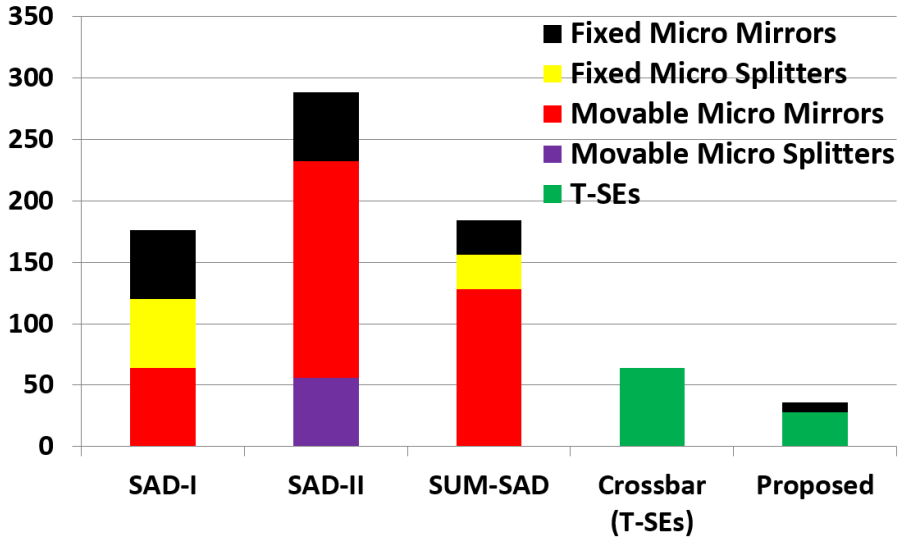

Figure 7.6: Hardware complexity for 8×8 switches.

7.4.2 Comparison of Splitting Losses

In the previous section, we have shown that the proposed switch can achieve up to 87% reduction in hardware complexity as compared to that of existing switches. In this section, we show that the hardware complexity improvement achieved does not sacrifice the power splitting and scalability properties of the switch. To this end, we discuss the power penalties for the five architectures of size 8×8 by computing the

losses at 8 output ports for all 255 combinations of output set sizes. Since the loss in the proposed switch depends on the input port, losses for the 1^{st} (best-case) and 8^{th} (worst-case) are presented.

In case of SaD-I, signal power loss is independent of output set size $|\Omega_p|$, as N-way splitting is enforced, and is given by,

$$\mathrm{L}_{SaDI} = 10\log_{10}(0.99) + 10\log_{10}(1/N) \quad \mathrm{dB} \tag{7.8}$$

For SaD-II, the unnecessary splitting of SaD-I is avoided, thus, splitting loss is dependent on $|\Omega_p|$ and is given by:

$$\mathrm{L}_{SaDII} = 10\log_{10}(0.99) + 10\log_{10}(1/|\Omega_p|) \quad \mathrm{dB} \tag{7.9}$$

We use the commercial specifications reported by KentOptronics [433] for the tri-state material e-TransFlector which can be tuned to operate in the IR spectrum range used by existing optical communication networks. For example, in [50], Hamedazimi et al. demonstrated a proof-of-concept for an FSO communication link for data center communication using the e-TransFlector material tuned for IR spectrum. Accordingly, we set both reflectance in R-state (β) and transmittance in T-state (η) to 87%, whereas for the S-state, both transmittance (ζ) and reflectance (α) are set to 43%. We assume that the optical efficiency of all fixed/movable mirrors, and splitters are 99%, and 49%, respectively [435].

In the power loss study, we use the term *proposed* to refer to both SNB and RNB T-SE based switches. Figures 7.7-(a), (b), and (c) depict the average minimum, average, and average maximum splitting power loss of the five switch architectures under consideration at different sizes of output sets.

SaD-II and SUM-SaD can switch unicast connections separately without incur-

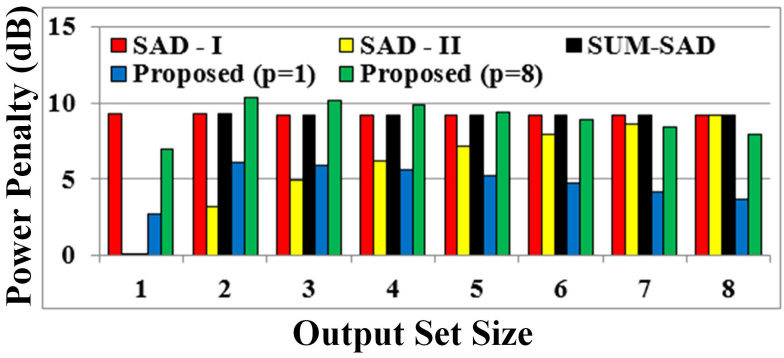

(a)

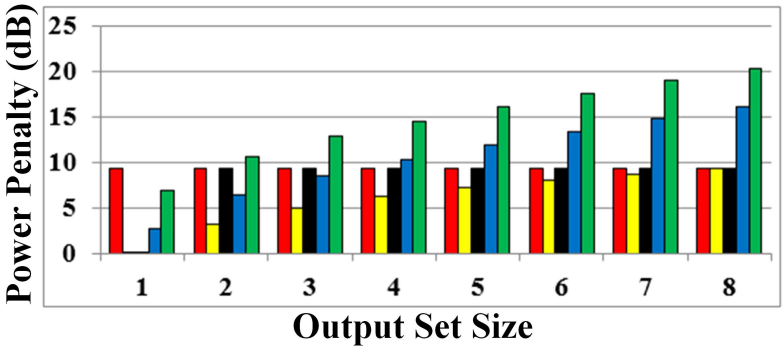

(b)

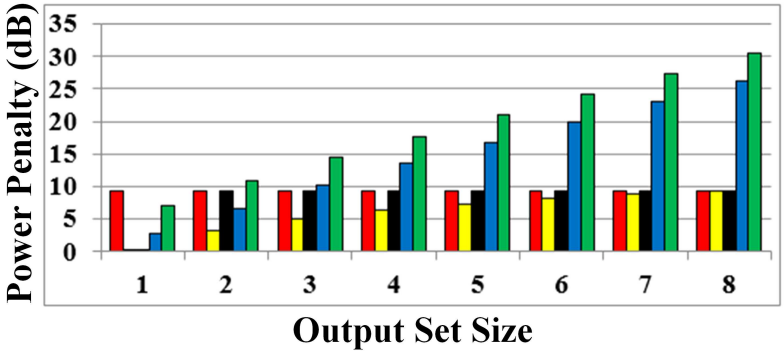

(c)

Figure 7.7: Splitting power penalty in an 8×8 switch [16] with $\alpha = \zeta = 43\%$, and $\eta = \beta = 87\%$ (a) Minimum. (b) Average. (c) Maximum.

ring any additional losses, and thus SaD-II and SUM-SaD have the same performance that outperforms other architectures in case of unicast. On the other hand, unicast requests switched using SaD-I are penalized $\approx$ 9.3 dB as SaD-I enforces full power splitting even for unicast connections. Proposed architecture does not enforce splitting for unicast connections, however there are additional losses of 4.53 dB and 7 dB for input ports 1 and 8, respectively. This is due to the propagation of the beam through the non-moveable T-SEs configured in the T-state along its path which adds additional loss due to the imperfection of the material.

In case of multicast (i.e., starting from output set size of two), it can be observed that as the size of the output set increases, so does the average and average maximum power penalties in all architectures except for the SaD-I and SUM-SaD, they have a fixed power loss ($\approx$ 9.3 dB). This is because SaD-I and SUM-SaD perform fixed full splitting for all input signals regardless of the size of output set. The proposed switch outperforms both SaD-I and SUM-SaD up to an output size of two, whereas, its performance is comparable to the other architectures up to output set size of four, after which the power loss increases.

Splitting power loss depends on the number of combinations at different sizes of output sets. This number increases starting from output set size of one (i.e., eight possible combinations of unicast) to four (i.e., 70 possible combinations) and then decreases to become one possible combination of broadcast. Regardless of the decrease in the number of combinations starting from output set size of four, average maximum loss experiences a monotonic increase as the aggregated maximum loss becomes dominant, whereas the average minimum loss decreases as the size of the output set increases.

High power losses can cause the signal power to fall below the sensitivity of the optical receiver, and thus amplification at the input ports may be needed. Moreover,

power loss at an output port can vary depending on the configuration of the switch. For example, in case of output set size of eight, the variation between the minimum and maximum splitting loss in the proposed switch is 25 dB (see Figure 7.7). Therefore, variable optical attenuators (VOAs) must be used at the output ports to equalize the impact of the insertion loss such that the power of the received signal falls within the dynamic range of the optical receiver [438].

It might be noted that MEMS-based switches show relatively lower splitting power losses and do not demonstrate differences between minimum and maximum splitting power loss at the output ports as compared to the proposed switch. This is because we only consider the splitting losses in our analysis. MEMS-based switches, however, incur additional Gaussian beam loss due to the propagation of the beam in the separate splitting stage, and loss due to the angular misalignment of the micro-mirrors [15,432] which can become significant if the light beam experiences multiple reflections such as in $1 \times N$ beam splitters [436, 437]. Therefore, MEMS-based switches still need pre-amplifiers, e.g., SUM-SaD [see Figure 6.4], and variable optical attenuators due to the non-splitting losses encountered by the signal.

Table 7.2 summarizes the number of amplifiers and VOAs required by the switches investigated. The proposed switch, SaD-I, SaD-II, and TSE-based crossbar need N amplifiers, and N VOAs, whereas SUM-SaD switch requires N VOAs and only $N/2$ amplifiers. This is because only $N/2$ of the inputs are propagating through the splitting stage as shown in Figure 6.4.

Gaussian beam propagation loss is considered the main limiting factor for realizing FSO switches with high scalability. However, other factors, such as material imperfection of T-SE and signal splitting properties, can also limit the scalability of the proposed switch.

The technology of the material used to realize T-SEs is still in its infancy. We use

Table 7.2: Number of Amplifiers and VOAs.

	Amplifiers	**VOAs**
SaD-I	N	N
SaD-II	N	N
SUM-SaD	$N/2$	N
Crossbar (T-SEs)	N	N
Proposed	N	N

modest values for the material transmittance and reflection efficiencies (i.e., $\eta = \beta =$ 87%, and $\alpha = \zeta = 43\%$ for a 50/50 reflection/ transmission splitting ratio). However, as the quality of the material continues to improve, so will the performance of the proposed switch.

To understand the impact of the quality of the material used on the performance of the proposed switch, we calculate splitting power loss for the proposed switch assuming improved T-SE efficiencies. We assume that $\eta = \beta = 99\%$ instead of 87%. For the splitting state, we set $\alpha = \zeta = 49\%$ instead of 43%. To measure the improvement in the performance of the proposed switch due to the improved material quality, we consider the worst request scenario, that is, a broadcast request from the 8^{th} input port. We notice an overall reduction in the splitting power penalty for the proposed switch based on the improved parameters. For example, a reduction in the power penalty of 8.5 dB (equivalent to an improvement of 28%) in the case of broadcast from the 8^{th} input port is achieved.

Another factor that limits the scalability of the proposed switch is the *cascaded* splitting nature of signal power along the way from the input to the outputs. This splitting behavior results in higher power loss and unequal signal power at output ports. For example, to multicast a signal to four outputs, using a SaD switch will result in 1/4 of the input power at each of the four outputs as compared to 1/2, 1/4, 1/8, and 1/8 of the input power in case of the proposed switch. One way to alleviate

this incremental power loss is to change the splitting ratio of the T-SE such that a small fraction of the input signal (e.g., 10%) is tapped at each output port and the remaining 90% of the power is forwarded to the subsequent output ports.

We evaluate the impact of changing the T-SE splitting ratio by calculating the splitting power penalty for the proposed switch assuming 10/90 splitting reflection/ transmission ratio while maintaining $\eta = \beta = 87\%$. Changing the splitting ratio led to an improvement in the performance of the proposed switch and a reduction of 13.5 dB in the power penalty in case of broadcast from the 8^{th} input port. This is equivalent to an improvement of 44.3%.

It is possible to further improve the overall performance of the proposed switch by improving the quality of the material used and also changing the T-SE splitting ratio. Figures 7.8-(a), (b), and (c) depict the average minimum, average, and average maximum splitting power loss at different sizes of output sets assuming improved T-SE quality (i.e., $\eta = \beta = 90\%$) while maintaining a splitting ratio of 10/90. Significant decrease in the power penalty can be observed. In case of broadcast from the 8^{th} input, the maximum splitting power penalty is 13 dB which is less than that of in Figure 7.7 by 17.44 dB indicating an improvement of 57.2%.

7.4.3 Cost Analysis

From the discussion above, the total cost (C_{tot}^{arch}) of a switch architecture $arch$ depends on the costs of VOAs (C_{VOA}^{arch}), amplifiers (C_{amp}^{arch}), and switching elements (C_{sw}^{arch}) used, and is given by,

$$C_{tot}^{arch} = C_{VOA}^{arch} + C_{amp}^{arch} + C_{sw}^{arch} \tag{7.10}$$

where $arch$ can be SaD-I, SaD-II, SUM-SaD, or the proposed switch. C_{VOA}^{arch} and C_{amp}^{arch}

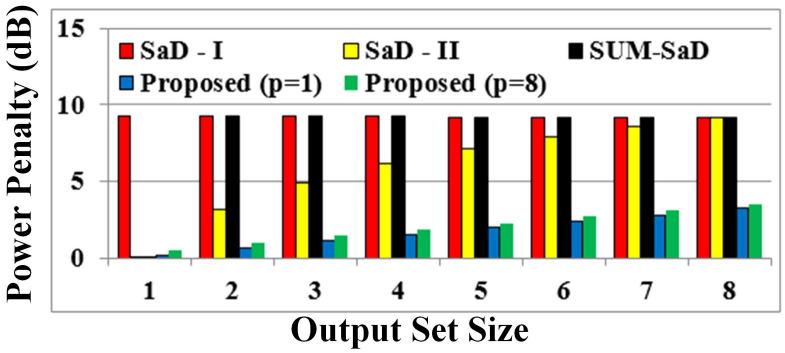

(a)

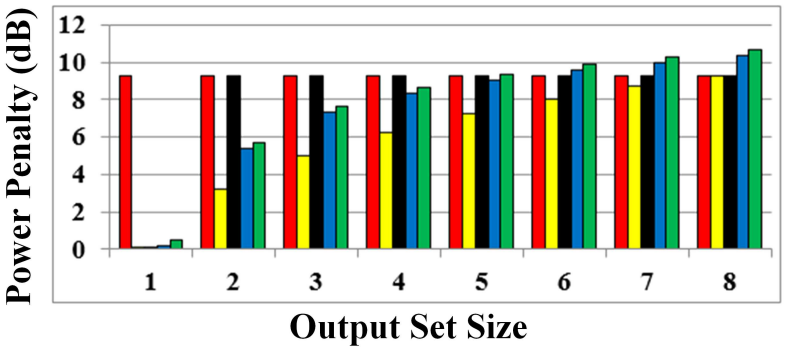

(b)

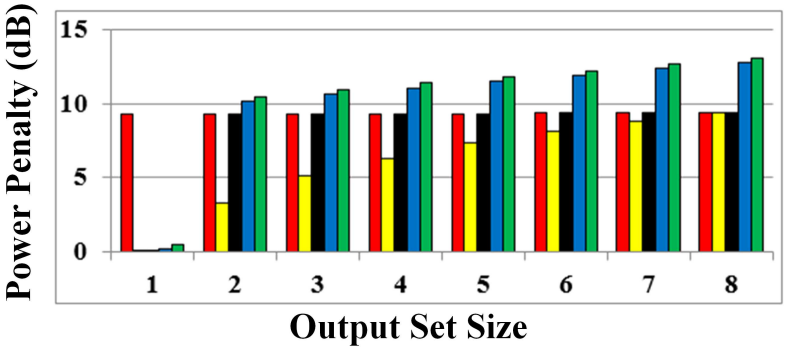

(c)

Figure 7.8: Splitting power penalty in an 8×8 switch with $\alpha = 10\%$, $\zeta = 90\%$, and $\eta = \beta = 99\%$ (a) Minimum. (b) Average. (c) Maximum.

depend on the number of VOAs (N_{VOA}^{arch}) and amplifiers (N_{amp}^{arch}) used, respectively.

From Table 7.2, SaD-I, SaD-II, and the proposed switch architectures employ N VOAs at the output ports and N amplifiers at the input ports. However, SUM-SaD switch architecture requires N VOAs and only $N/2$ amplifiers. Therefore, SUM-SaD architecture has a cost advantage over SaD-I, SaD-II, and the proposed architecture with respect to C_{amp}.

We can expand C_{sw}^{arch} further and express it as a function in the cost of a fixed (mirrors/splitters) component C_f, a movable (mirror/splitter) component C_m, and a T-SE C_{tse}. Given the cost of each component, we can calculate C_{sw}^{arch} as follows:

$$C_{sw}^{arch} = N_f^{arch} \cdot C_f + N_m^{arch} \cdot C_m + N_{tse}^{arch} \cdot C_{tse} \tag{7.11}$$

where N_f^{arch}, N_m^{arch}, and N_{tse}^{arch} are the numbers of fixed, moveable, and T-SE switching elements used in the switch $arch$, respectively, and can be obtained from Table 7.1.

We use a relative cost model to quantify and compare the cost of the proposed switch. We use the cost of the fixed elements, C_f, as reference since the cost of these components is relatively stable compared to the other two types.

Let $\rho = C_m/C_f$ and $\mu = C_{tse}/C_f$. To evaluate the cost effectiveness of the proposed switch as compared to SaD-I, we use the total number of fixed and movable components in Table 7.1 to setup the inequality:

$$N^2 C_m + N\Phi C_f > \frac{N(N-1)}{2} C_{tse} + NC_f \tag{7.12}$$

From Equation (7.12), it is easy to show that, the proposed switch has a smaller overall cost as compared to that of SaD-I iff:

$$\rho_{SaD-I} > \frac{(N-1)\mu + 2 - 2\Phi}{2N} \tag{7.13}$$

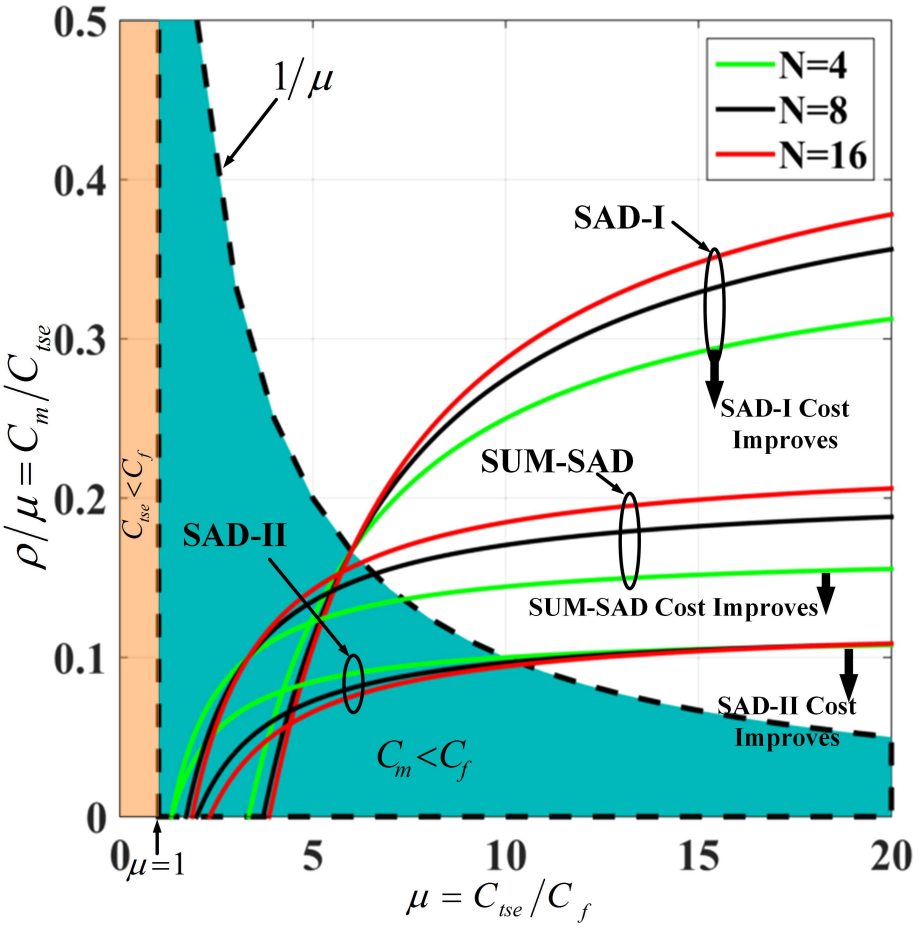

Figure 7.9: Comparative cost analysis for the proposed switch. The curves represent the relative cost effectiveness of the proposed switch as compared to the existing SaD switches with respect to SEs. Shaded regions are invalid design regions. White region above (below) a curve indicates that the proposed switch is more (less) cost effective compared to the corresponding SaD switch for specific number of ports N.

Similarly, we can compute a lower bound on the value of ρ for the SaD-II and SUM-SaD as follows:

$$\rho_{SaD-II} > \frac{(N-1)\mu + 2 - \Phi}{2N + 3\Phi} \tag{7.14}$$

$$\rho_{SUM-SaD} > \frac{(N-1)\mu + 2 - \Phi}{4N + 2} \tag{7.15}$$

Figure 7.9 plots the ratio ρ/μ to provide an insight on the relationship between the

cost of a T-SE and that of a movable component. Given the cost of various hardware components, one can use Figure 7.9 to determine the cost effectiveness of the proposed design with respect to switching elements as compared to SaD-based switches at different port sizes ($N = 4,\ 8,$ and 16). The function $1/\mu$ (i.e., $\rho = 1$) corresponds to the case in which $C_m = C_f$. Obviously, the cost of a moveable element $C_m > C_f$, and thus the shaded area below the curve $1/\mu$ is considered as an *invalid design region*. It is not expected that C_{tse} will be less than C_f. Therefore, we have also excluded the area corresponding to $\mu < 1$. White region above (below) a curve indicates that the proposed switch is more (less) cost effective compared to the corresponding SaD switch for specific number of ports N. For example, for $N = 4$, even if the cost of a T-SE is 15 times the cost of fixed components (i.e., $\mu = 15$), the proposed switch will be more cost effective as compared to the SaD-I, SUM-SaD, and SaD-II even when C_{tse} is 3.5, 6.7, or 10 times C_m, respectively, corresponding to ρ/μ ratios of 0.29, 0.15, and 0.1, respectively.

7.5 Chapter Summary

We propose a new FSO multicast rearrangeable non-blocking (RNB) switch architecture using tri-state switching elements (T-SEs). In our design, signal splitting and switching are simultaneously performed within the same stage, and thus separate splitting stages, used in the conventional multicast switches, are not needed. The advantages of the switch proposed are twofold: first, significant reduction in hardware complexity as an $N \times N$ switch with full multicast capability requires *only* $N(N+1)/2$ *non-movable* SEs; and secondly, a beam propagating in the switch proposed avoids the propagation loss that may be encountered by an optical beam passing through a splitting stage followed by a crossbar as in SaD-based switches. This leads to lower

insertion loss that is due to the Gaussian beam divergence. Comparison with existing optical multicast switches shows that the proposed switch provides multicast capability with lower hardware complexity and a comparable performance. Cost analysis shows that, for $N = 4$, the overall cost of the new design is lower than that of existing SNB switches even if the T-SE is 4 to 10 times the cost of typical MEMS mirrors.

Chapter 8

Conclusions and Future Research Directions

In this dissertation, we address the problem of cabling complexity in wired DCNs. To this end, we propose OWCells, a class of optical wireless cellular data center network architectures in which fixed line of sight (LOS) optical wireless communication (OWC) links are used to connect the racks arranged in regular polygonal topologies. We present the OWCell DCN architecture, develop its theoretical underpinnings, and investigate routing protocols and OWC transceiver design. To realize a fully wireless DCN, servers in racks must also be connected using OWC links. There is, however, a difficulty of connecting multiple adjacent network components, such as servers in a rack, using point-to-point LOS links. To overcome this problem, we propose and validate the feasibility of an FSO-Bus to connect multiple adjacent network components using NLOS point-to-point OWC links. As part of the design of the OWC transceiver, we develop a new class of strictly and rearrangeably non-blocking multicast optical switches in which multicast is performed efficiently at the physical optical (lower) layer rather than upper layers (e.g., application layer).

In Chapter 2, we present a simple, yet powerful classification scheme for FSO technology. In this scheme, an FSO link can be classified as a combination of four different criteria, namely: Environment (ε), Coverage Type (κ), LOS Availability (α), Mobility (μ), and link distance (δ). An FSO link can be deployed in an indoor, terrestrial, space, or UW scenario. The link can be either a point or cellular coverage which can be realized using a LOS or NLOS link. Furthermore, a link can be fixed or mobile. Using the discussed four criteria, we were able to develop a generic classification that can be used to categorize different FSO links including recently evolving schemes in which other classifications in the literature fall short. In particular, the proposed classification scheme describes any FSO link configuration as a tuple ($\varepsilon/\kappa/\alpha/\mu/\delta$). We discuss all possible FSO link configurations in the four different environments. We provide examples for each FSO link configuration by listing selected recent references and related research efforts. Moreover, we briefly discuss the impairments experienced by each link type and their possible solutions. We also use the proposed classification scheme to review existing FSO standards and recommendations. IrDA has produced a set of standards aiming for high data rate short FSO links. JEITA CP-1221, CP-1222, CP-1223, IEEE 802.15.7, and IEEE 802.15.7r1 standards are designed for short/medium range VLC supporting low data rate links. On the other hand, limited efforts are directed towards standardizing terrestrial, space, and underwater FSO links. For example, a single recommendation for terrestrial FSO links, ITU-R F.2106-1, was proposed by ITU.

In Chapter 3, we propose a classification that can be used to classify any DC, including existing wired and emerging wireless DCs. Our classification is based on the communication technologies used to realize the DCN. According to the proposed classification, wired DCs can be classified as pure electrical/optical wired DC, or hybrid wired DC. On the other hand, wireless technology can be used either to augment

wired DCs resulting in hybrid DCs, or to realize pure RF/FSO DC. We discuss different wireless-based DC designs and collate the major work in the field to jump-start researchers to tap into the growing research on wireless DCs. Using the proposed classification, we now have a nearly complete picture for the design space of DCNs. By surveying the literature and mapping existing solutions to different possible designs in the proposed classification, it is now possible to easily identify new research areas. For example, in this chapter, we were able to identify that the area of hybrid wireless DCNs has not yet been explored.

In Chapter 4, we present an OWC-DC design and discuss the associated link budget analysis for a fully-connected rack of servers. Simulation shows that the proposed design realizes high data rates within a rack. Our cost analysis shows that the cost of the proposed OWC-DC design is comparable to that of conventional wired DCs. It is expected that the cost of the proposed design will decrease as OWC technology is commercialized. The proposed design addresses many problems and limitations of the current art, but several issues remain to be investigated.

Although the design proposed in Chapter 4 present a useful design for OWC rack of servers, the conventional row-based DCN arrangement forms a great impairment for wireless connectivity in DCNs. We dedicate Chapter 5 to discuss the proposed cellular optical wireless DCN architectures, OWCells, that can overcome the problems encountered by conventional row-based DCNs. Different polygonal shapes can be used to design OWCell; square, hexagon, and octagon. We present an OWCell using the three different cells and develop their theoretical properties. Flow-level simulations are conducted to validate and compare the performance of OWCell using square cells. The impacts of OWCell design parameters on its performance are investigated. We compare the performance of OWCell using OCS and hybrid (OCS+OBS) switching schemes. We also compare the performance of OWCell and HyScale DCN,

a switch-centric hybrid optical DCN. Finally, we discuss future research directions and approaches to improve the performance of the proposed OWCell DCN.

An essential component in optical networks is the optical switch. In Chapter 6 we propose a new class of strictly non-blocking (SNB) FSO multicast switches using tri-state switching elements (T-SEs). In the proposed switch, TSEs simultaneously support signal splitting and switching without the need for separate splitting stages used in the conventional multicast switches. Thus, a beam propagating in the proposed switch avoids the propagation loss that may be encountered by an optical beam passing through a splitting stage followed by a crossbar as in SaD-based switches. This leads to lower insertion loss that is due to the Gaussian beam divergence. An $N \times M$ SNB multicast switch requires *only* NM *non-movable* T-SEs. Comparison with existing optical multicast switches shows that the proposed switch provides multicast capability with lower hardware complexity and a comparable performance. Cost analysis for the proposed switch shows that its cost is lower than SaD-based switches, even if the cost of the T-SE is is 1.2 to 3.5 times that of MEMS mirror.

We also propose a new FSO multicast rearrangeable non-blocking (RNB) switch architecture using tri-state switching elements (T-SEs) in Chapter 7. The advantages of the switch proposed are twofold: first, significant reduction in hardware complexity as an $N \times N$ switch with full multicast capability requires *only* $N(N+1)/2$ *non-movable* SEs; and secondly, a beam propagating in the switch proposed avoids the propagation loss that may be encountered by an optical beam passing through a splitting stage followed by a crossbar as in SaD-based switches. This leads to lower insertion loss that is due to the Gaussian beam divergence. Comparison with existing optical multicast switches shows that the proposed switch provides multicast capability with lower hardware complexity and a comparable performance. Cost analysis shows that, for $N = 4$, the overall cost of the new design is lower than that of existing

SNB switches even if the T-SE is 4 to 10 times the cost of typical MEMS mirrors.

8.1 Future Work

In this section, we discuss future research directions in the domain of OWC technology and its applications, development of wireless DCNs, and future research on FSO multicast optical switches.

8.1.1 Research Directions and Open Problems for OWC systems

We discussed different OWC link configurations and systems throughout this chapter. As we discuss the applications for the OWC links and systems, we pointed out future directions of research related to each OWC subdomain, system, and application. From previous sections, we can see that researchers are continuously finding new applications for OWC technology. This continuous expansion of OWC technology application portfolio makes the task of predicting the future of OWC technology challenging. In this section, we will shed the light on a few of the future OWC technology research directions and applications.

OWC and the Internet of Things (IoT)

To realize the IoT vision, in which 34 billion things (people, devices, and objects) will be connected to the Internet by 2020, different types of networks forming the infrastructure of the IoT paradigm must evolve to accommodate the data volume and transmission speed requirements. Moreover, the emerging practical deployments for the IoT trigger a need to integrate and inter-operate a variety of hybrid connectivity technologies to realize real business values. Several applications require the

integration of technologies, such as Wireless Sensor Networks (WSNs) and RFID, using WiFi, Bluetooth, and/or ZigBee connectivity technologies into one single hybrid network. As the RF spectrum gets more congested, there is a need to explore other connectivity technologies to be used in such networks. One of the key candidate technologies to complement RF is OWC since it does not interfere with the RF technology. Moreover, the possibility of developing a communication module that is small in size and weight, consumes lower power, has low cost, and on top of that, operates in an unregulated spectrum, leads us to envision that OWC will play a key role in the future of IoT.

In addition to connecting things in the IoT network, an indoor VLC network can also serve as a backbone of the OWC-enabled IoT network [442]. In [443], Hussein and Elgala a lightweight OFDM modulation scheme that is convenient for the OWC-enabled objects in the IoT network. Another research direction that can help pave the way for OWC in IoT domain is the use of OWC to recharge the battery of a an object in the IoT network [444, 445]. Such a technology can help extend the network lifetime, and also enables the objects in the network to transmit at higher power extending their reach and make them more discoverable.

Optical Scattering Communication

Modeling T/CC/NLOS/x OSC channel is more challenging as compared to modeling traditional LOS links [194]. The reason is that as the link range increases, so does the complexity of jointly modeling atmospheric turbulence and the multiple scattering [70]. Furthermore, the performance of the link highly depends on the geometry of the link with respect to the transmitter and receiver angles and beam shape. Developing channel and system models that capture the variables affecting the performance of OSC is of great interest especially that this link configuration can be viable for

connecting distributed nodes and objects in future IoT networks.

Relay-Assisted FSO Networks

As mentioned earlier in Section 2.6.2, relay transmission can be used to overcome the atmospheric turbulence by allowing the transmitted data to use a relay node and avoid a direct link to the destination that is severely impaired by the atmospheric turbulence. There are two types of relaying configurations, namely; serial (i.e., multi-hop transmission) and parallel (i.e., cooperative diversity) relaying [446]. Multi-hop relaying is usually used to extend the range of a transmitted with limited transmission range. In this approach, the signal moves from one relay node to the other in a serial fashion. In parallel relaying, the sending node transmits the data to the receiving node and a relay node which in turn retransmits the date to the receiving node. This form of transmission acts as a distributed array of antennas and is considered as a cooperative diversity approach [81].

Since the concept of relay-assisted networks is mature when it comes to RF technology, researchers in FSO are adopting the techniques and approached used in RF relay-assisted networks. For example, for the protocols used to forward the data using the relay nodes, researchers utilized amplify-and-forward (AF) [447–450], decode-and-forward (DF) [451, 452], and detect-and-forward (DetF) [453] protocols. All-optical AF relaying is introduced to avoid the requirement of optical-electro-optical (OEO) conversion at relay stations eliminating the need for high-speed circuits and delay associated with the conversion [454–458].

There are common assumptions among the aforementioned approaches that relay nodes are buffer-less and stationary. In [336], Fawaz et al. utilize moving UAVs equipped with buffers to function as a relay node in the relay-assisted heterogenous network in which fixed and moving relay nodes are used.

Hybrid FSO/x Networks

We discussed the application of hybrid FSO/x systems in several scenarios such as future indoor LiFi-WiFi networks, backhaul networks, underwater sensing, and providing internet access for underdeveloped regions of the globe. There are, however, some challenges that must be addressed to fully utilize the advantages of hybrid FSO/x systems. One of the main challenges is the handover and the realization of a seamless mobility of the mobile users. For example, in the discussed LiFi-WiFi network, a user should be able to seamlessly move between LiFi cells (horizontal handover) and between LiFi and WiFi networks (vertical handover) [135, 459].

With the increasing number of deployed OWC cells for coverage, inter-cell interference is inevitable. Inter-cell interference coordination (ICIC) and mitigation techniques have been studied for a long time in the RF domain [60]. The researchers in the OWC domain are utilizing the successful approached used in the RF domain [460–462]. Since OWC technology is becoming part of the future hybrid networks in particular to alleviate the spectrum congestion due to the interference in RF, it is critical to understand how to manage the interference in the between OWC link.

WDM FSO Links

The success of the WDM techniques in fiber optics has led the FSO researchers to consider the WDM to expand the capacity of the FSO links [463–468] In [463], Chen et al. realize a 160 Gbps T/PC/LOS/F/Long WDM FSO link using sixteen 10 Gbps channels. The link uses OOK and has a distance of 2.16 km. Other T/PC/LOS/F/Long FSO link WDM FSO links were developed and experimented realizing 8×40 Gbps [464] and 32×40 Gbps [465] and using OOK modulation. Theoretical analysis and link performance of WDM FSO systems were also performed.

In [466], Mbah et al. analyze the outage probability in the presence of turbulence-accentuated inter-channel crosstalk. Most recently, Zhao et al. present a 200 Gbps FSO WDM communication system. The system features integrated modules and utilizes PAM-4 modulation scheme [469]. Despite the recent advances in the WDM FSO links, more research is required to realize integrated, low-cost, and high capacity WDM FSO links in all of the four environments discussed.

8.1.2 Future Research Directions in Wireless DCNs

To further improve the performance of the proposed OWCell DCNs, we will design a multi-layered OWCell, where each cell of racks has a base switch. Base switches are connected using OWC forming a coexisting network. This is expected to improve the graph-theoretic properties of the OWCell DCN by reducing the diameter and increasing the bisection width, and thus reduce latency and improve throughput.

We also envision that the integration of OWC and RF wireless communication technologies in DCNs to realize a *hybrid wireless DCN* is a promising research direction. It is, however, challenging to envision a hybrid wireless DCN. This is because current research has not yet explored all the potentials and challenges of deploying wireless communication in DCNs. In order to realize the best possible designs, we must first develop the best practices in wireless DCNs.

One approach to develop hybrid wireless DCN may be based on small clusters of RF operated racks. In each cluster the set of all available frequency channels is used. This prevents the intra-cluster interference problem. The DCN might be organized such that the clusters are distant enough to prevent inter-cluster interference. This is doable since the 60 GHz technology has a limited short range. Moreover, additional FSO links can be used safely for intra-cluster communication since FSO does not interfere with the RF. On the other hand, for inter-cluster communication, FSO

LOS links can be used. This concept is analogous to the *coverage cells* in mobile communication, except that there is no mobility or handover needed.

8.1.3 Future Research Directions in Optical Switches

The proposed algorithm used to configure the RNB multicast switch in Chapter 7 may lead to redundant configuration of T-SEs that are not used in the routing process. Therefore, the proposed algorithm is not optimal. Currently, we are optimizing the routing algorithms developed for the proposed rearrangeable subclass of switches. We will formulate the routing problem as an optimization problem. The objective is to find a routing configuration for the switch such that the number of T-SE state transitions is minimized, thus minimizing the total configuration power and latency.

Bibliography

[1] J. M. Kahn and J. R. Barry, "Wireless infrared communications," *Proc. IEEE*, vol. 85, no. 2, pp. 265–298, 1997.

[2] D. Heatley, D. Wisely, I. Neild, and P. Cochrane, "Optical wireless: the story so far," *IEEE Commun. Mag.*, vol. 36, no. 12, pp. 72–74, 1998.

[3] H. Kaushal and G. Kaddoum, "Optical communication in space: Challenges and mitigation techniques," *IEEE Communications Surveys Tutorials*, vol. 19, no. 1, pp. 57–96, Firstquarter 2017.

[4] K. Ramachandran, R. Kokku, R. Mahindra, and S. Rangarajan, "60 ghz data-center netw.: wireless => worry less?" NEC Laboratories America,, Tech. Rep., 2008.

[5] H. Vardhan, N. Thomas, S.-R. Ryu, B. Banerjee, and R. Prakash, "Wireless data center with millimeter wave network," *IEEE GLOBECOM*, pp. 1–6, Dec 2010.

[6] J. Shin, , E. Sirer, H. Weatherspoon, and D. Kirovski, "On the feasibility of completely wireless datacenters," *Proc. Archit. for Netw. and Commun. Sys.*, pp. 3–14, 2012.

[7] K. Suto, H. Nishiyama, N. Kato, T. Nakachi, T. Sakano, and A. Takahara, "A failure-tolerant and spectrum-efficient wireless data center network design for improving performance of Big Data mining," *IEEE Vehicular Technology Conference (VTC Spring)*, pp. 1–5, May 2015.

[8] N. Riza and P. Marraccini, "Power smart indoor optical wireless link applications," *Wireless Commun. and Mobile Comput.*, pp. 327–332, 2012.

[9] N. Hamedazimi, H. Gupta, V. Sekar, and S. Das, "Patch panels in the sky: A case for free-space optics in data centers," *ACM Hotnets*, pp. 23:1–23:7, 2013.

[10] J. Bao, D. Dong, B. Zhao, Z. Luo, C. Wu, and Z. Gong, "Flycast: Free-space optics accelerating multicast communications in physical layer," *SIGCOMM Comput. Commun. Rev.*, vol. 45, no. 5, pp. 97–98, Aug. 2015.

[11] S. Arnon, "Next-generation optical wireless communications for data centers," *Proc. SPIE*, vol. 9387, pp. 938 703–938 703–6, 2015.

[12] J. Joseph, K. Lear, and D. Abell, "High speed free-space optical communications," WO Patent App. PCT/US2012/052,397, Mar. 7 2013.

[13] W. Hu and Q. Zeng, "Multicasting optical cross connects employing splitter-and-delivery switch," *IEEE Photon. Technol. Lett.*, vol. 10, no. 7, pp. 970–972, 1998.

[14] C. Zhang and W. Hu, "Design and analysis of a multicast-capable optical cross-connect," *Proc. SPIE*, vol. 7136, pp. 71 364H–71 364H–8, 2008.

[15] L. Y. Lin, E. L. Goldstein, and R. W. Tkach., "Free-space micromachined optical switches for optical networking," *IEEE J. Sel. Topics Quantum Electron.*, vol. 5, no. 1, pp. 4–9, 1999.

[16] A. S. Hamza, J. Deogun, and D. Alexander, "Free space optical multicast crossbar switch with non-movable switching elements," *Advanced Photonics for Communications*, p. JT3A.13, 2014.

[17] D. Laney, "3D data management: Controlling data volume, velocity and variety," META Group (now Gartner), Tech. Rep. 949, February 2001. [Online]. Available: http://blogs.gartner.com/doug-laney/files/2012/01/ad949-3D-Data-Management-Controlling-Data-Volume-Velocity-and-Variety.pdf

[18] L. Atzori, A. Iera, and G. Morabito, "The internet of things: A survey," *Computer Networks*, vol. 54, no. 15, pp. 2787 – 2805, 2010. [Online]. Available: http://www.sciencedirect.com/science/article/pii/S1389128610001568

[19] D. P. Martin, B. Murrell, M. Golden, A. Khoosal, and B. Muhire, "Rdp4: Detection and analysis of recombination patterns in virus genomes," *Virus Evolution*, vol. 1, no. 1, p. vev003, 2015. [Online]. Available: +http://dx.doi.org/10.1093/ve/vev003

[20] A. Gandomi and M. Haider, "Beyond the hype: Big data concepts, methods, and analytics," *International Journal of Information Management*, vol. 35, no. 2, pp. 137 – 144, 2015.

[21] C. O. Hendren, G. V. Lowry, J. M. Unrine, and M. R. Wiesner, *Science of The Total Environment*, pp. –, 2015.

[22] Large Synoptic Survey Telescope - Data Management, 2015. [Online]. Available: http://www.lsst.org/about/dm

[23] International Data Corporation, 2015. [Online]. Available: https://www.idc.com/

[24] Z. Cao, R. Proietti, and S. J. B. Yoo, "Hi-lion: Hierarchical large-scale interconnection optical network with awgrs [invited]," *J. Opt. Commun. Netw.*, vol. 7, no. 1, pp. A97–A105, Jan 2015.

[25] J. Mudigonda, P. Yalagandula, and J. C. Mogul, "Taming the flying cable monster: A topology design and optimization framework for data-center networks," *USENIX Annual Technical Conf.*, pp. 8–8, 2011.

[26] A. Singla, "Fat-free topologies," *Proceedings of the 15th ACM Workshop on Hot Topics in Networks*, pp. 64–70, 2016. [Online]. Available: http://doi.acm.org/10.1145/3005745.3005747

[27] S. Kandula, J. Padhye, and P. Bahl, "Flyways to de-congest data center networks," 2009.

[28] S. Kandula, S. Sengupta, A. Greenberg, P. Patel, and R. Chaiken, "The nature of data center traffic: Measurements & analysis," *ACM SIGCOMM*, pp. 202–208, 2009.

[29] T. Benson, A. Akella, and D. A. Maltz, "Network traffic characteristics of data centers in the wild," *ACM SIGCOMM*, pp. 267–280, 2010.

[30] T. Benson, A. Anand, A. Akella, and M. Zhang, "Understanding data center traffic characteristics," *ACM SIGCOMM*, vol. 40, no. 1, pp. 92–99, Jan. 2010.

[31] N. Calabretta, R. Centelles, S. Di Lucente, and H. Dorren, "On the performance of a large-scale optical packet switch under realistic data center traffic," *IEEE/OSA J. of Opt. Commun. and Netw.*, vol. 5, no. 6, pp. 565–573, June 2013.

[32] H. Vardhan and R. Prakash, "Towards 60ghz wireless switching interconnect," pp. 594–598, Jan 2013.

[33] M. Armbrust, A. Fox, R. Griffith, A. D. Joseph, R. Katz, A. Konwinski, G. Lee, D. Patterson, A. Rabkin, I. Stoica, and M. Zaharia, "A view of cloud computing," *Commun. ACM*, vol. 53, no. 4, pp. 50–58, Apr. 2010.

[34] K. Bilal, S. U. R. Malik, O. Khalid, A. Hameed, E. Alvarez, V. Wijaysekara, R. Irfan, S. Shrestha, D. Dwivedy, M. Ali, U. S. Khan, A. Abbas, N. Jalil, and S. U. Khan, "A taxonomy and survey on green data center networks," *Future Generation Comput. Syst.*, vol. 36, no. 0, pp. 189 – 208, 2014.

[35] C. Guo and *et al.*, "Bcube: a high performance, server-centric network architecture for modular data centers," *Proceedings of the ACM SIGCOMM*, pp. 63–74, 2009.

[36] C. Guo, H. Wu, K. Tan, L. Shi, Y. Zhang, and S. Lu, "Dcell: a scalable and fault-tolerant network structure for data centers," *Proceedings of the ACM SIGCOMM*, pp. 75–86, 2008.

[37] Y. Liao, D. Yin, and L. Gao, "Dpillar: Scalable dual-port server interconnection for data center networks," *Proceedings of IEEE ICCCN*, pp. 1–6, Aug. 2010.

[38] D. Guo, T. Chen, D. Li, Y. Liu, X. Liu, and G. Chen, "BCN: Expansible network structures for data centers using hierarchical compound graphs," *Proceedings of IEEE INFOCOM*, pp. 61–65, April 2011.

[39] D. Li, C. Guo, H. Wu, K. Tan, Y. Zhang, S. Lu, and J. Wu, "Scalable and cost-effective interconnection of data-center servers using dual server ports," *IEEE/ACM Transactions on Networking*, vol. 19, no. 1, pp. 102–114, Feb 2011.

[40] M. Al-Fares, A. Loukissas, and A. Vahdat, "A scalable, commodity data center network architecture," *ACM SIGCOMM*, pp. 63–74, 2008.

[41] Y. Cui, H. Wang, X. Cheng, and B. Chen, "Wireless data center networking," *Wireless Communications, IEEE*, vol. 18, no. 6, pp. 46–53, December 2011.

[42] R. Niranjan Mysore and *et al.*, "Portland: a scalable fault-tolerant layer 2 data center network fabric," *Proceedings of the ACM SIGCOMM*, pp. 39–50, 2009.

[43] W. Zhang, X. Zhou, L. Yang, Z. Zhang, B. Y. Zhao, and H. Zheng, "3d beamforming for wireless data centers," *ACM HotNets-X*, pp. 4:1–4:6, 2011.

[44] D. Halperin, S. Kandula, J. Padhye, P. Bahl, and D. Wetherall, "Augmenting data center networks with multi-gigabit wireless links," *ACM SIGCOMM*, vol. 41, no. 4, pp. 38–49, 2011.

[45] X. Tie, K. Ramachandran, and R. Mahindra, "On 60 ghz wireless link performance in indoor environments," in *Passive and Active Measurement*, ser. Lecture Notes in Computer Science, N. Taft and F. Ricciato, Eds. Springer Berlin Heidelberg, 2012, vol. 7192, pp. 147–157.

[46] T. Yamane and Y. Katayama, "An effective initialization of interference cancellation algorithms for distributed mimo systems in wireless datacenters," pp. 4249–4254, Dec 2012.

[47] X. Zhou, Z. Zhang, Y. Zhu, Y. Li, S. Kumar, A. Vahdat, B. Zhao, and H. Zheng, "Mirror mirror on the ceiling: Flexible wireless links for data centers," *ACM SIGCOMM*, pp. 443–454, 2012.

[48] H. Vardhan, S.-R. Ryu, B. Banerjee, and R. Prakash, "60ghz wireless links in data center networks," *Computer Networks*, vol. 58, no. 0, pp. 192 – 205, 2014.

[49] H. Vardhan and R. Prakash, "Concurrency in polygonally arranged wireless data centers with all line-of-sight links," *Intl. Conf. on Comput., Netw. and Commun.*, pp. 716–720, Feb 2014.

[50] N. Hamedazimi, Z. Qazi, H. Gupta, V. Sekar, S. R. Das, J. P. Longtin, H. Shah, and A. Tanwer, "Firefly: A reconfigurable wireless data center fabric using free-space optics," *ACM Conf. on SIGCOMM*, pp. 319–330, 2014.

[51] Z. Ghassemlooy, W. Popoola, and S. Rajbhandari, *Optical Wireless Communications: System and Channel Modelling with MATLAB*, 1st ed. Taylor & Francis, 2012.

[52] A. S. Hamza, J. S. Deogun, and D. R. Alexander, "Free space optical data center architecture design with fully connected racks," *IEEE GLOBECOM*, pp. 2192–2197, Dec 2014.

[53] ——, "Free space optical multicast crossbar," *J. Opt. Commun. Netw.*, vol. 8, no. 1, pp. 1–10, Jan 2016.

[54] Z. Zhu, S. Zhong, L. Chen, and K. Chen, "Fully programmable and scalable optical switching fabric for petabyte data center," *Opt. Express*, vol. 23, no. 3, pp. 3563–3580, Feb 2015.

[55] J. Dean and S. Ghemawat, "Mapreduce: Simplified data processing on large clusters," *Commun. ACM*, vol. 51, no. 1, pp. 107–113, Jan. 2008.

[56] K. Shvachko, H. Kuang, S. Radia, and R. Chansler, "The hadoop distributed file system," *Symp. on Mass Storage Syst. and Technologies (MSST)*, pp. 1–10, 2010.

[57] H. Willebrand and B. Ghuman, *Free Space Optics: Enabling Optical Connectivity in Today's Networks*, ser. Sams Other Series. Sams, 2002.

[58] C. V. N. I. (VNI), "The zettabyte eratrends and analysis," Cisco, White Paper 1465272001812119, June 2016. [Online]. Available: http://www.cisco.com/c/en/us/solutions/collateral/service-provider/visual-networking-index-vni/vni-hyperconnectivity-wp.html

[59] O. W. Hennes Henniger, "An introduction to free-space optical communications." *Radioengineering*, vol. 19, no. 2, 2010.

[60] H. M. Abdelsalam, H. S. Hamza, A. M. Al-Shaa, and A. S. Hamza, "On the use of particle swarm optimization techniques for channel assignments in cognitive radio networks," *Multidisciplinary computational intelligence techniques: Applications in business, Engineering, and Medicine, Hershey, IGI Global*, p. 202, 2013.

[61] A. Shahpari, I. Alimi, A. Sousa, R. Ferreira, P. Monteiro, and A. Teixeira, "Challenges and opportunities of optical wireless communication technologies," in *Optical Communication Technology*, P. Pinho, Ed. Rijeka: InTech, 2017, ch. 2.

[62] I. Takai, T. Harada, M. Andoh, K. Yasutomi, K. Kagawa, and S. Kawahito, "Optical vehicle-to-vehicle communication system using LED transmitter and camera receiver," *IEEE Photonics Journal*, vol. 6, no. 5, pp. 1–14, Oct 2014.

[63] D. Han, X. Fan, K. Zhang, and R. Zhu, "Research on multiple-scattering channel with monte carlo model in uv atmosphere communication," *Appl. Opt.*, vol. 52, no. 22, pp. 5516–5522, Aug 2013. [Online]. Available: http://ao.osa.org/abstract.cfm?URI=ao-52-22-5516

[64] A. S. Hamza, J. S. Deogun, and D. R. Alexander, "Wireless communication in data centers: A survey," *IEEE Communications Surveys Tutorials*, vol. 18, no. 3, pp. 1572–1595, thirdquarter 2016.

[65] P. H. Pathak, X. Feng, P. Hu, and P. Mohapatra, "Visible light communication, networking, and sensing: A survey, potential and challenges," *IEEE Communications Surveys Tutorials*, vol. 17, no. 4, pp. 2047–2077, Fourthquarter 2015.

[66] I. E. Lee, Y. Guo, T. K. Ng, K.-H. Park, M.-S. Alouini, and B. S. Ooi, "Near-infrared wireless optical communication with particulates in-suspension over the underwater channel," *Conference on Lasers and Electro-Optics*, p. STh3O.4, 2017.

[67] Z. Zeng, S. Fu, H. Zhang, Y. Dong, and J. Cheng, "A survey of underwater optical wireless communications," *IEEE Communications Surveys Tutorials*, vol. 19, no. 1, pp. 204–238, Firstquarter 2017.

[68] A. K. Majumdar and J. C. Ricklin, Eds., *Free-Space Laser Communications*, ser. Optical and Fiber Communications Reports. Springer-Verlag New York, 2008, vol. 2, no. 1.

[69] Z. Ghassemlooy and W. O. Popoola, *Mobile and Wireless Communications*. IntechOpen, January 2010, no. 17, ch. Terrestrial Free-Space Optical Communications.

[70] Z. Ghassemlooy, S. Arnon, M. Uysal, Z. Xu, and J. Cheng, "Emerging optical wireless communications-advances and challenges," *IEEE Journal on Selected Areas in Communications*, vol. 33, no. 9, pp. 1738–1749, Sept 2015.

[71] Y. Kaymak, R. Rojas-Cessa, J. Feng, N. Ansari, M. Zhou, and T. Zhang, "A survey on acquisition, tracking, and pointing mechanisms for mobile free-space optical communications," *IEEE Communications Surveys & Tutorials*, vol. 20, no. 2, pp. 1104–1123, Secondquarter 2018.

[72] "Lightpointe wireless." [Online]. Available: http://lightpointe.com/freespaceoptics.html

[73] D. Borah, A. Boucouvalas, C. Davis, S. Hranilovic, and K. Yiannopoulos, "A review of communication-oriented optical wireless systems," *EURASIP J. on Wireless Commun. and Netw.*, no. 1, pp. 1–28, 2012.

[74] F. Demers, H. Yanikomeroglu, and M. St-Hilaire, "A survey of opportunities for free space optics in next generation cellular networks," in *Communication Networks and Services Research Conference (CNSR), 2011 Ninth Annual*, May 2011, pp. 210–216.

[75] S. Wu, H. Wang, and C.-H. Youn, "Visible light communications for 5G wireless networking systems: from fixed to mobile communications," *Network, IEEE*, vol. 28, no. 6, pp. 41–45, Nov 2014.

[76] "National space science data center (nssdc), gemini 7," 1965. [Online]. Available: http://nssdc.gsfc.nasa.gov/nmc/masterCatalog.do?sc=1965-100A

[77] J. M. Grimwood, B. C. Hacker, and P. J. Vorzimmer, "Project gemini technology and operations - a chronology," *NASA, NASA SP-4002*, 1969.

[78] E. Kube, "Information transmission by light beams through the atmosphere," *J. Nachrichtentechnik*, 1969.

[79] F. Gfeller and U. Bapst, "Wireless in-house data communication via diffuse infrared radiation," *Proceedings of the IEEE*, vol. 67, no. 11, pp. 1474–1486, Nov 1979.

[80] E. Leitgeb, M. Awan, P. Brandl, T. Plank, C. Capsoni, R. Nebuloni, T. Javornik, G. Kandus, S. Muhammad, F. Ghassemlooy, M. Loschnigg, and F. Nadeem, "Current optical technologies for wireless access," in *Telecommunications, 2009. ConTEL 2009. 10th International Conference on*, June 2009, pp. 7–17.

[81] M. Khalighi and M. Uysal, "Survey on free space optical communication: A communication theory perspective," *Communications Surveys Tutorials, IEEE*, vol. 16, no. 4, pp. 2231–2258, 2014.

[82] "Technology demonstration missions: Laser communications relay demonstration (LCRD)." [Online]. Available: http://www.nasa.gov/mission_pages/tdm/lcrd/index.html

[83] S. Tang, Y. Dong, and X. Zhang, "Impulse response modeling for underwater wireless optical communication links," *IEEE Trans. Commun.*, vol. 62, no. 1, pp. 226–234, 2014.

[84] M. Khalighi, C. Gabriel, T. Hamza, S. Bourennane, P. Leon, and V. Rigaud, "Underwater wireless optical communication; recent advances and remaining challenges," *Intl. Conf. on Transparent Optical Networks (ICTON)*, pp. 1–4, July 2014.

[85] M. I. Sakib Chowdhury, M. Kavehrad, and W. Zhang, "Cable television transmission over a 1550-nm infrared indoor optical wireless link," *Optical Engineering*, vol. 52, no. 10, pp. 100 503–100 503, 2013.

[86] M. I. S. Chowdhury, M. Kavehrad, W. Zhang, and P. Deng, "Combined catv and very-high-speed data transmission over a 1550-nm wavelength indoor optical wireless link," *Proc. SPIE*, vol. 9010, pp. 901 009–901 009–8, 2014.

[87] A. Street, P. Stavrinou, D. O'brien, and D. Edwards, "Indoor optical wireless systemsa review," *Opt. and Quantum Electron.*, vol. 29, no. 3, pp. 349–378, 1997.

[88] G. Yun and M. Kavehrad, "Spot-diffusing and fly-eye receivers for indoor infrared wireless communications," *Wireless Commun., Intl. Conf. on Selected Topics in*, pp. 262–265, 1992.

[89] ——, "Indoor infrared wireless communications using spot diffusing and fly-eye receivers," *Canadian J. Elect. Comput. Eng.*, vol. 18, no. 4, pp. 151–157, 1993.

[90] C. Y. W. J. Hou, R. and H. Zhang, "A brief survey of optical wireless communication," *Australasian Symposium on Parallel and Distributed Computing (AusPDC 2015)*, vol. 163, pp. 41–50, 2015.

[91] H. Elgala, R. Mesleh, and H. Haas, "Indoor optical wireless communication: potential and state-of-the-art," *Commun. Mag., IEEE*, vol. 49, no. 9, pp. 56–62, 2011.

[92] R. Ramirez-Iniguez and R. Green, "Indoor optical wireless communications," *IEE Colloq. on Opt.. Wireless Commun.*, pp. 14/1–14/7, 1999.

[93] C. Singh, J. John, Y. Singh, and K. Tripathi, "A review of indoor optical wireless systems," *IETE Technical Review,*, vol. 19, pp. 3–17, 2002.

[94] Z. Ghassemlooy and A. Hayes, "Indoor optical wireless communications systems - part i: Review," *School of Engineering, Northumbria University, Newcastle upon Tyne, UK*, 2003.

[95] A. Mahdy and J. Deogun, "Wireless optical communications: a survey," in *Wireless Commun. and Netw. Conf.*, vol. 4, 2004, pp. 2399–2404.

[96] A. Bergh and J. A. Copeland, "Optical sources for fiber transmission systems," *Proceedings of the IEEE*, vol. 68, no. 10, pp. 1240–1247, Oct 1980.

[97] W. van Etten and J. van der Plaats, *Fundamentals of optical fiber communications*, ser. Prentice-Hall international series in optoelectronics. Prentice Hall, 1991.

[98] J. Hecht, *Understanding fiber optics*. Prentice Hall, 1999.

[99] J. Miller, *Principles Of Infrared Technology: A Practical Guide to the State of the Art*. Springer, 1994.

[100] G. Keiser, *Optical fiber communications*, ser. McGraw-Hill series in electrical and computer engineering: Communications and signal processing. McGraw-Hill, 2000.

[101] R. Ramaswami, "Optical fiber communication: From transmission to networking," *Comm. Mag.*, vol. 40, no. 5, pp. 138–147, May 2002.

[102] D. O'Brien, G. Faulkner, K. Jim, E. Zyambo, D. Edwards, M. Whitehead, P. Stavrinou, G. Parry, J. Bellon, M. Sibley, V. Lalithambika, V. Joyner, R. Samsudin, D. Holburn, and R. Mears, "High-speed integrated transceivers for optical wireless," *Communications Magazine, IEEE*, vol. 41, no. 3, pp. 58–62, Mar 2003.

[103] S. Sze and K. Ng, *Physics of Semiconductor Devices*. Wiley, 2006.

[104] J. M. Senior and M. Y. Jamro, *Optical Fiber Communications: Principles and Practice*, ser. Prentice Hall Internacional series in optoelectronics. Financial Times/Prentice Hall, 2009.

[105] R. Valadas, A. Tavares, and A. Duarte, "Angle diversity to combat the ambient noise in indoor optical wireless communication systems," *International Journal of Wireless Information Networks*, vol. 4, no. 4, pp. 275–288, 1997.

[106] S. Bloom, E. Korevaar, J. Schuster, and H. Willebrand, "Understanding the performance of free-space optics [invited]," *J. Opt. Netw.*, vol. 2, no. 6, pp. 178–200, 2003.

[107] S. Hranilovic, *Wireless Optical Communication Systems*. Springer, 2006.

[108] O. Bouchet, H. Sizun, C. Boisrobert, F. de Fornel, and P. Favennec, *Free-Space Optics: Propagation and Communication*, ser. ISTE. Wiley, 2010.

[109] D. L. Begley, "Free-space laser communications: a historical perspective," *IEEE Lasers and Electro-Optics Society*, vol. 2, pp. 391–392, 2002.

[110] S. Liverman, Q. Wang, Y.-C. Chu, A. Borah, S. Wang, A. Natarajan, T. Nguyen, and A. X. Wang, "Indoor communications networks realized through hybrid free-space optical and Wi-Fi links," *Proc. SPIE*, vol. 10559, pp. 10 559 – 10 559 – 5, 2018.

[111] G. Giuliano, L. Laycock, D. Rowe, and A. E. Kelly, "Solar rejection in laser based underwater communication systems," *Opt. Express*, vol. 25, no. 26, pp. 33 066–33 077, Dec 2017.

[112] J.-C. Chang, Y.-C. Wang, D.-Y. Chen, C.-Y. Li, H.-H. Lu, X.-H. Huang, and W.-S. Tsai, "Optical-based underwater communications," *Optical Fiber Communication Conference*, p. Tu2I.3, 2018.

[113] A. E. Willner, Z. Zhao, Y. Ren, L. Li, G. Xie, H. Song, C. Liu, R. Zhang, C. Bao, and K. Pang, "Underwater optical communications using orbital angular momentum-based spatial division multiplexing," *Optics Communications*, vol. 408, pp. 21 – 25, 2018, optical Communications Exploiting the Space Domain.

[114] K.-D. Langer and J. Grubor, "Recent developments in optical wireless communications using infrared and visible light," *Transparent Opt. Netw.*, vol. 3, pp. 146–151, 2007.

[115] A. Khalid, G. Cossu, R. Corsini, P. Choudhury, and E. Ciaramella, "1-gb/s transmission over a phosphorescent white led by using rate-adaptive discrete multitone modulation," *Photonics Journal, IEEE*, vol. 4, no. 5, pp. 1465–1473, Oct 2012.

[116] D. Tsonev, H. Chun, S. Rajbhandari, J. McKendry, S. Videv, E. Gu, M. Haji, S. Watson, A. Kelly, G. Faulkner, M. Dawson, H. Haas, and D. O'Brien, "A 3-gb/s single-led ofdm-based wireless vlc link using a gallium nitride μled," *Photonics Technology Letters, IEEE*, vol. 26, no. 7, pp. 637–640, April 2014.

[117] C.-H. Liu, Y.-C. Chang, T. B. Norris, and Z. Zhong, "Graphene photodetectors with ultra-broadband and high responsivity at room temperature," *Nature Nanotechnology*, vol. 9, pp. 273–278, 2014.

[118] F. H. L. Koppens, T. Mueller, P. Avouris, A. C. Ferrari, M. S. Vitiello, and M. Polini, "Photodetectors based on graphene, other two-dimensional materials and hybrid systems," *Nature Nanotechnology*, vol. 9, pp. 780–793, Oct. 2014.

[119] C. Ferrante, A. Virga, L. Benfatto, M. Martinati, D. De Fazio, U. Sassi, C. Fasolato, A. K. Ott, P. Postorino, D. Yoon, G. Cerullo, F. Mauri, A. C. Ferrari, and T. Scopigno, "Raman spectroscopy of graphene under ultrafast laser excitation," *Nature Communications*, vol. 9, no. 308, 2018.

[120] A. Sevincer, A. Bhattarai, M. Bilgi, M. Yuksel, and N. Pala, "Lightnets: Smart lighting and mobile optical wireless networks a survey," *Communications Surveys Tutorials, IEEE*, vol. 15, no. 4, pp. 1620–1641, Fourth 2013.

[121] M. S. Islim and H. Haas, "Modulation techniques for Li-Fi," *ZTE Communications*, vol. 14, pp. 29–40, 2016.

[122] A. Bekkali, C. B. Naila, K. Kazaura, K. Wakamori, and M. Matsumoto, "Transmission analysis of OFDM-based wireless services over turbulent radio-on-FSO links modeled by Gamma-Gamma distribution," *IEEE Photonics Journal*, vol. 2, no. 3, pp. 510–520, June 2010.

[123] J. Li, J. Q. Liu, and D. P. Taylor, "Optical communication using subcarrier PSK intensity modulation through atmospheric turbulence channels," *IEEE Transactions on Communications*, vol. 55, no. 8, pp. 1598–1606, Aug 2007.

[124] M. Z. Hassan, M. J. Hossain, J. Cheng, and V. C. M. Leung, "Subcarrier intensity modulated opticalwireless communications: A survey from communication theory perspective," *ZTE COMMUNICATIONS*, April 2016.

[125] D. Tsonev, S. Sinanovic, and H. Haas, "Complete modeling of nonlinear distortion in OFDM-based optical wireless communication," *Journal of Lightwave Technology*, vol. 31, no. 18, pp. 3064–3076, Sept 2013.

[126] J. B. Carruthers and J. M. Kahn, "Multiple-subcarrier modulation for nondirected wireless infrared communication," *IEEE Journal on Selected Areas in Communications*, vol. 14, no. 3, pp. 538–546, Apr 1996.

[127] X. Yu, H. Gu, K. Wang, and G. Wu, "Enhancing performance of cloud computing data center networks by hybrid switching architecture," *IEEE JLT*, vol. 32, no. 10, pp. 1991–1998, May 2014.

[128] Z. Dong, X. Li, J. Yu, Z. Cao, and N. Chi, "8×9.95-Gb/s ultra-dense WDM-PON on a 12.5-GHz grid with digital pre-equalization," *IEEE Photonics Technology Letters*, vol. 25, no. 2, pp. 194–197, Jan 2013.

[129] J. Zhang, J. Yu, N. Chi, and H.-C. Chien, "Time-domain digital pre-equalization for band-limited signals based on receiver-side adaptive equalizers," *Opt. Express*, vol. 22, no. 17, pp. 20 515–20 529, Aug 2014.

[130] D. Wisely, "A 1 gbit/s optical wireless tracked architecture for atm delivery," *Optical Free Space Commun. Links, IEE Colloq. on*, pp. 14/1–14/7, 1996.

[131] D. Wisely and I. Neild, "A 100 mbit/s tracked optical wireless telepoint," *Personal, Indoor and Mobile Radio Commun., 1997. Waves of the Year 2000, The 8th IEEE Intl. Symp. on*, vol. 3, pp. 964–968 vol.3, Sep 1997.

[132] Z. Ghassemlooy, M. Uysal, M. A. Khalighi, V. Ribeiro, F. Moll, S. Zvanovec, and A. Belmonte, *An Overview of Optical Wireless Communications*. Cham: Springer International Publishing, 2016, ch. 1, pp. 1–23.

[133] L. J. Johnson, F. Jasman, R. J. Green, and M. S. Leeson, "Recent advances in underwater optical wireless communications," *Underwater Technology*, vol. 32, no. 3, pp. 167–175, 2014.

[134] H. Kaushal and G. Kaddoum, "Underwater optical wireless communication," *IEEE Access*, vol. 4, pp. 1518–1547, 2016.

[135] M. Z. Chowdhury, M. T. Hossan, A. Islam, and Y. M. Jang, "A comparative survey of optical wireless technologies: Architectures and applications," *IEEE Access*, vol. 6, pp. 9819–9840, 2018.

[136] Z. Zeng, "A survey of underwater wireless optical communication," Ph.D. dissertation, University of British Columbia, 2015. [Online]. Available: https://open.library.ubc.ca/cIRcle/collections/24/items/1.0220823

[137] R. Rachmani and S. Arnon, "Server backplane with optical wavelength diversity links," *J. Lightwave Technol.*, vol. 30, no. 9, pp. 1359–1365, May 2012. [Online]. Available: http://jlt.osa.org/abstract.cfm?URI=jlt-30-9-1359

[138] R. Rachmani, A. Zilberman, and S. Arnon, "Computer backplane with free space optical links: Air turbulence effects," *J. Lightwave Technol.*, vol. 30, no. 1, pp. 156–162, Jan 2012.

[139] D. Bykhovsky, D. Elmakias, and S. Arnon, "Experimental evaluation of free space links in the presence of turbulence for server backplane," *J. Lightwave Technol.*, vol. 33, no. 14, pp. 2923–2929, Jul 2015.

[140] D. Elmakias, D. Bykhovsky, and S. Arnon, "Air turbulence effects on performance of optical wireless communication with crosstalk in server backplane," *Chin. Opt. Lett.*, vol. 15, no. 2, p. 020602, Feb 2017.

[141] C. S. Yen and R. D. Crawford, "The use of directed optical beams in wireless computer communications," *in Proc. of IEEE Global Communications Conference*, pp. 1181–1184, Dec 1985.

[142] T.-S. Chu and M. Gans, "High speed infrared local wireless communication," *IEEE Commun. Mag.*, vol. 25, no. 8, pp. 4–10, 1987.

[143] L. Ribeiro, "Point-to-point optical wireless network for factory communications," *Industrial Electronics, 1997. ISIE '97., Proceedings of the IEEE International Symposium on*, vol. 1, pp. 103–105 vol.1, Jul 1997.

[144] J.-i. Matsuda, T. Nyu, T. Saito, and S. Yamazaki, "125 mpbs ir wireless link for ieee 1394 multimedia home network," in *Optical Communication, 1998. 24th European Conference on*, vol. 1, Sep 1998, pp. 343–344 vol.1.

[145] "Serial infrared physical layer specification, version 1.4, infrared data association." [Online]. Available: 2001

[146] A. Boucouvalas, P. Chatzimisios, Z. Ghassemlooy, M. Uysal, and K. Yiannopoulos, "Standards for indoor optical wireless communications," *IEEE Commun. Mag.*, vol. 53, no. 3, pp. 24–31, March 2015.

[147] B. Glushko, D. Kin, and A. Shar, "Gigabit optical wireless communication system for personal area networking," *Optical Memory and Neural Networks*, vol. 22, no. 2, pp. 73–80, 2013.

[148] A. S. Hamza, S. Yadav, S. Ketan, J. S. Deogun, and D. R. Alexander, "OWCell: Optical wireless cellular data center network architecture," *IEEE International Conference on Communications (ICC)*, pp. 1–6, May 2017.

[149] M. McCullagh, D. Wisely, P. Eardley, and P. Smyth, *A 50 Mbit/s optical wireless LAN link using novel optical and electronic enabling technologies*, ser. Lecture Notes in Computer Science, C. Gnther, Ed. Springer Berlin Heidelberg, 1994, vol. 783.

[150] A. Street, K. Samaras, D. O'Brien, and D. Edwards, "High speed wireless ir-lans using spatial addressing," vol. 3, pp. 969–973 vol.3, 1997.

[151] F. Parand, G. Faulkner, D. O'Brien, and D. Edwards, "A cellular optical wireless system demonstrator," *Optical Wireless Commun, IEE Colloq. on*, pp. 12/1–12/6, 1999.

[152] J. Bellon, M. J. N. Sibley, D. Wisely, and S. Greaves, "Hub architecture for infrared wireless networks in office environments," *Optoelectronics, IEE Proceedings -*, vol. 146, no. 2, pp. 78–82, 1999.

[153] E. B. Zyambo, D. C. O'Brien, G. E. Faulkner, and D. J. Edwards, "Design of a high-speed optical wireless lan at long wavelengths," *Proc. SPIE*, vol. 4214, pp. 115–123, 2001.

[154] V. Jungnickel, T. Haustein, A. Forck, and C. Von Helmolt, "155 mbit/s wireless transmission with imaging infrared receiver," *Electronics Letters*, vol. 37, no. 5, pp. 314–315, Mar 2001.

[155] V. Jungnickel, A. Forck, T. Haustein, U. Kruger, V. Pohl, and C. Von Helmolt, "Electronic tracking for wireless infrared communications," *Wireless Communications, IEEE Transactions on*, vol. 2, no. 5, pp. 989–999, Sept 2003.

[156] K. Liang, H. Shi, S. J. Sheard, and D. C. O"Brien, "Transparent optical wireless hubs using wavelength space division multiplexing," *Proc. SPIE*, vol. 5550, pp. 80–87, 2004.

[157] H. Shi, K. Liang, S. J. Sheard, D. C. O'Brien, and G. E. Faulkner, "Two-dimensional wavelength routing for transparent optical wireless networking," *Proc. SPIE*, vol. 5892, pp. 58 920Z–58 920Z–12, 2005.

[158] M. Feldman, S. Esener, C. Guest, and S. Lee, "Comparison between optical and electrical interconnects based on power and speed considerations," *Appl. Opt.*, vol. 27, pp. 1742–1751, 1988.

[159] X. Zheng, P. J. Marchand, D. Huang, and S. C. Esener, "Free-space parallel multichip interconnection system," *Appl. Opt.*, vol. 39, no. 20, pp. 3516–3524, Jul 2000.

[160] G. Li, D. Huang, E. Yuceturk, P. J. Marchand, S. C. Esener, V. H. Ozguz, and Y. Liu, "Three-dimensional optoelectronic stacked processor by use of free-space optical interconnection and three-dimensional vlsi chip stacks," *Appl. Opt.*, vol. 41, no. 2, pp. 348–360, Jan 2002.

[161] S. W. W. S. C. M. R. C. MG Bevan, MAG Darrin, "Freespace optical data bus for spacecraft," *in Proceedings of the 3rd annual Earth Science Technology Conference*, June 2003.

[162] J. Xue, A. Garg, B. Ciftcioglu, J. Hu, S. Wang, I. Savidis, M. Jain, R. Berman, P. Liu, M. Huang, H. Wu, E. Friedman, G. Wicks, and D. Moore, "An intra-chip free-space optical interconnect," *SIGARCH Comput. Archit. News*, vol. 38, no. 3, pp. 94–105, Jun. 2010. [Online]. Available: http://doi.acm.org/10.1145/1816038.1815975

[163] S. Sultana, F. Shahriar, and M. Hasan, "Chip-to-chip free-space optical interconnection using liquid-crystal-over-silicon spatial light modulator," in *Technological Developments in Networking, Education and Automation*, K. Elleithy, T. Sobh, M. Iskander, V. Kapila, M. A. Karim, and A. Mahmood, Eds. Springer Netherlands, 2010, pp. 507–510. [Online]. Available: http://dx.doi.org/10.1007/978-90-481-9151-2_88

[164] K. Wang, A. Nirmalathas, C. Lim, E. Skafidas, and K. Alameh, "Performance of high-speed reconfigurable free-space card-to-card optical interconnects under air turbulence," *J. Lightwave Technol.*, vol. 31, no. 11, pp. 1687–1693, Jun 2013.

[165] A. S. Hamza, J. S. Deogun, and D. Alexander, "Rearrangeable Non-Blocking multicast FSO switch using fixed switching elements," *IEEE Global Communications Conference*, Dec. 2015, to be published.

[166] J. Bao, D. Dong, B. Zhao, Z. Luo, C. Wu, and Z. Gong, "FlyCast: Free-space optics accelerating multicast communications in physical layer," *SIGCOMM Comput. Commun. Rev.*, vol. 45, no. 5, pp. 97–98, Aug. 2015.

[167] D. Tagliaferri and C. Capsoni, "High-speed wireless infrared uplink scheme for airplane passengers communications," *Electronics Letters*, vol. 53, pp. 887–888(1), June 2017.

[168] 2014. [Online]. Available: http://purelifi.com/

[169] J. Carruthers and J. Kahn, "Angle diversity for nondirected wireless infrared communication," *IEEE ICC*, vol. 3, pp. 1665–1670 vol.3, Jun 1998.

[170] S. Hashemi, Z. Ghassemlooy, L. Chao, and D. Benhaddou, "Channel estimation for indoor diffuse optical ofdm wireless communications," *BROADNETS*, pp. 431–434, Sept 2008.

[171] A. K. Majumdar, "Non-line-of-sight (nlos) ultraviolet and indoor free-space optical (fso) communications," in *Advanced Free Space Optics (FSO)*, ser. Springer Series in Optical Sciences. Springer New York, 2015, vol. 186, pp. 177–202. [Online]. Available: http://dx.doi.org/10.1007/978-1-4939-0918-6_5

[172] R. L. Phillips and L. C. Andrews, "Measured statistics of laser-light scattering in atmospheric turbulence," *J. Opt. Soc. Am.*, vol. 71, no. 12, pp. 1440–1445, Dec 1981. [Online]. Available: http://www.opticsinfobase.org/abstract.cfm?URI=josa-71-12-1440

[173] S. Karp, R. Gagliardi, S. Moran, and L. Stotts, *Optical Channels: Fibers, Clouds, Water and the Atmosphere*, ser. Applications of Communications Theory. Springer, 1988. [Online]. Available: http://books.google.com/books?id=vSfCsRC6f8oC

[174] X. Zhu and J. Kahn, "Free-space optical communication through atmospheric turbulence channels," *Communications, IEEE Transactions on*, vol. 50, no. 8, pp. 1293–1300, Aug 2002.

[175] E. Lee and V. W. S. Chan, "Part 1: optical communication over the clear turbulent atmospheric channel using diversity," *Selected Areas in Communications, IEEE Journal on*, vol. 22, no. 9, pp. 1896–1906, Nov 2004.

[176] R. Lange, B. Smutny, B. Wandernoth, R. Czichy, and D. Giggenbach, "142 km, 5.625 gbps free-space optical link based on homodyne bpsk modulation," vol. 6105, 2006, pp. 61 050A–61 050A–9.

[177] G. G. Ortiz, S. Lee, S. P. Monacos, M. W. Wright, and A. Biswas, "Design and development of robust atp subsystem for the altair uav-to-ground lasercomm 2.5-gbps demonstration," *Proc. SPIE*, vol. 4975, pp. 103–114, 2003. [Online]. Available: http://dx.doi.org/10.1117/12.478939

[178] R. Mahon, H. R. Burris, W. S. Rabinovich, G. C. Gilbreath, P. G. Goetz, C. I. Moore, T. J. Meehan, M. F. Stell, M. J. Vilcheck, J. L. Witkowsky, L. Swingen, M. R. Suite, E. Oh, and J. P. Koplow, "Free-space optical communication link at 1550 nm using multiple-quantum-well modulating retroreflectors in a marine environment," *Proc. SPIE*, vol. 5160, pp. 456–465, 2004.

[179] P. G. Goetz, W. S. Rabinovich, R. Mahon, M. S. Ferraro, J. L. Murphy, H. R. Burris, M. F. Stell, C. I. Moore, M. R. Suite, W. Freeman, G. C. Gilbreath, and S. C. Binari, "Modulating retro-reflector devices and current link performance at the naval research laboratory," *MILCOM 2007 - IEEE Military Communications Conference*, pp. 1–7, Oct 2007.

[180] M. Plett, W. S. Rabinovich, R. Mahon, M. S. Ferraro, P. G. Goetz, C. I. Moore, and W. Freeman, "Free-space optical communication link across 16 kilometers over the chesapeake bay to a modulated retroreflector array," *Optical Engineering*, vol. 47, no. 4, pp. 045 001–045 001–10, 2008.

[181] W. S. Rabinovich, J. L. Murphy, M. Suite, M. Ferraro, R. Mahon, P. Goetz, K. Hacker, W. Freeman, E. Saint Georges, S. Uecke, and J. Sender, "Free-space optical data link to a small robot using modulating retroreflectors," *Proc. SPIE*, vol. 7464, pp. 746 408–746 408–9, 2009.

[182] G. G. Peter, S. R. William, R. Mahon, L. M. James, S. F. Mike, R. S. Michele, R. S. Walter, B. X. Ben, R. B. Harris, I. M. Christopher, W. S. Warren, T. F. Wade, S. Frawley, M. Colbert, M. M. Barry, and K. H. S. Reese, "Modulating retro-reflector lasercom systems at the naval research laboratory," *MILITARY COMMUNICATIONS CONFERENCE, 2010 - MILCOM 2010*, pp. 1601–1606, Oct 2010.

[183] P. G. Goetz, W. S. Rabinovich, R. Mahon, J. L. Murphy, M. S. Ferraro, M. R. Suite, W. R. Smith, H. R. Burris, C. I. Moore, W. W. Schultz, W. T. Freeman, S. J. Frawley, B. M. Mathieu, K. Hacker, and S. Reese, "Modulating retro-reflector lasercom systems for small unmanned vehicles," *IEEE Journal on Selected Areas in Communications*, vol. 30, no. 5, pp. 986–992, June 2012.

[184] "Extreme test for the vialight laser communication terminal mlt-20 optical downlink from a jet aircraft at 800km/h," November 2013. [Online]. Available: http://vialight.de/index.php?id=180

[185] "Optical data link successfully demonstrated between fighter plane and ground station," December 2013. [Online]. Available: http://www.defenceandsecurity-airbusds.com/en_US/web/guest/optical-data-link-successfully-demonstrated

[186] M. S. Rahman, M. Curran, H. Gupta, K. Zheng, S. Das, J. Longtin, and T. Mohamed, "FSONet: A wireless backhaul for multi-gigabit picocells using steerable free space optics," *ACM Mobicom*, 2017.

[187] A. S. Hamza, "Optical wireless communications for airport surface operations: Opportunities and challenges," *2016 Integrated Communications Navigation and Surveillance (ICNS)*, pp. 2B3–1–2B3–7, April 2016.

[188] M. Taheri, N. Ansari, J. Feng, R. Rojas-Cessa, and M. Zhou, "Provisioning internet access using FSO in high-speed rail networks," *IEEE Network*, vol. 31, no. 4, pp. 96–101, July 2017.

[189] Q. Fan, M. Taheri, N. Ansari, J. Feng, R. Rojas-Cessa, M. Zhou, and T. Zhang, "Reducing the impact of handovers in ground-to-train free space optical communications," *IEEE Transactions on Vehicular Technology*, vol. 67, no. 2, pp. 1292–1301, Feb 2018.

[190] S. Fathi-Kazerooni, Y. Kaymak, R. Rojas-Cessa, J. Feng, N. Ansari, M. Zhou, and T. Zhang, "Optimal positioning of ground base stations in free-space optical communications for high-speed trains," *IEEE Transactions on Intelligent Transportation Systems*, vol. 19, no. 6, pp. 1940–1949, June 2018.

[191] D. Kedar and S. Arnon, "Non-line-of-sight optical wireless sensor network operating in multiscattering channel," *Appl. Opt.*, vol. 45, no. 33, pp. 8454–8461, 2006.

[192] Z. Xu, G. Chen, F. Abou-Galala, and M. Leonardi, "Experimental performance evaluation of non-line-of-sight ultraviolet communication systems," *Proc. SPIE*, vol. 6709, pp. 67 090Y–67 090Y–12, 2007.

[193] G. Chen, F. Abou-Galala, Z. Xu, and B. M. Sadler, "Experimental evaluation of led-based solar blind nlos communication links," *Opt. Express*, vol. 16, no. 19, pp. 15 059–15 068, Sep 2008.

[194] Z. Xu and B. Sadler, "Ultraviolet communications: Potential and state-of-the-art," *Communications Magazine, IEEE*, vol. 46, no. 5, pp. 67–73, May 2008.

[195] Z. Xu, H. Ding, B. M. Sadler, and G. Chen, "Analytical performance study of solar blind non-line-of-sight ultraviolet short-range communication links," *Opt. Lett.*, vol. 33, no. 16, pp. 1860–1862, Aug 2008.

[196] G. Chen, Z. Xu, H. Ding, and B. Sadler, "Path loss modeling and performance trade-off study for short-range non-line-of-sight ultraviolet communications," *Opt. Express*, vol. 17, no. 5, pp. 3929–3940, Mar 2009.

[197] H. Ding, G. Chen, A. K. Majumdar, B. Sadler, and Z. Xu, "Modeling of non-line-of-sight ultraviolet scattering channels for communication," *Selected Areas in Communications, IEEE Journal on*, vol. 27, no. 9, pp. 1535–1544, December 2009.

[198] R. Moncur, P. Edwards, L. N. Binh, and N. D. Nguyen, "Non-line-of-sight cloud-scatter communication," in *Conference on Lasers and Electro-Optics/International Quantum Electronics Conference*. Optical Society of America, 2009, p. CMO1. [Online]. Available: http://www.opticsinfobase.org/abstract.cfm?URI=CLEO-2009-CMO1

[199] H. Ding, Z. Xu, and B. M. Sadler, "A path loss model for non-line-of-sight ultraviolet multiple scattering channels," *EURASIP J. Wirel. Commun. Netw.*, vol. 2010, pp. 63:1–63:11, 2010.

[200] G. Chen, Z. Xu, and B. M. Sadler, "Experimental demonstration of ultraviolet pulse broadening in short-range non-line-of-sight communication channels," *Opt. Express*, vol. 18, no. 10, pp. 10 500–10 509, 2010.

[201] L. Wang, Z. Xu, and B. M. Sadler, "Non-line-of-sight ultraviolet link loss in noncoplanar geometry," *Opt. Lett.*, vol. 35, no. 8, pp. 1263–1265, Apr 2010.

[202] R. J. Drost, T. J. Moore, and B. M. Sadler, "Monte-carlo-based multiple-scattering channel modeling for non-line-of-sight ultraviolet communications," *Proc. SPIE*, vol. 8038, pp. 803 802–803 802–9, 2011.

[203] ——, "Uv communications channel modeling incorporating multiple scattering interactions," *J. Opt. Soc. Am. A*, vol. 28, no. 4, pp. 686–695, Apr 2011.

[204] M. Noshad and M. Brandt-Pearce, "Nlos uv communication systems using spectral amplitude coding," pp. 843–848, Dec 2011.

[205] A. Gupta, M. Noshad, and M. Brandt-Pearce, "Nlos uv channel modeling using numerical integration and an approximate closed-form path loss model," *Proc. SPIE*, vol. 8517, pp. 851 709–851 709–10, 2012.

[206] A. Gupta and M. Brandt-Pearce, "Receiver design for shot noise limited mimo fso/uv communication systems," *Globecom Workshops (GC Wkshps), 2012 IEEE*, pp. 1183–1187, Dec 2012.

[207] M. Noshad, M. Brandt-Pearce, and S. Wilson, "Nlos uv communications using m-ary spectral-amplitude-coding," *Communications, IEEE Transactions on*, vol. 61, no. 4, pp. 1544–1553, April 2013.

[208] N. Raptis, E. Roditi, and D. Syvridis, "Power-spectrum requirements in ultraviolet optical wireless networks," *Proc. SPIE*, vol. 9354, pp. 935 403–935 403–15, 2015.

[209] M. A. El-Shimy and S. Hranilovic, "Spatial-diversity imaging receivers for non-line-of-sight solar-blind uv communications," *J. Lightwave Technol.*, vol. 33, no. 11, pp. 2246–2255, Jun 2015.

[210] W. Liu, D. Zou, and Z. Xu, "Modeling of optical wireless scattering communication channels over broad spectra," *J. Opt. Soc. Am. A*, vol. 32, no. 3, pp. 486–490, Mar 2015.

[211] D.-y. Peng, J. Shi, G.-h. Peng, S.-l. Xiao, S.-h. Xu, S. Wang, and F. Liu, "An ultraviolet laser communication system using frequency-shift keying modulation scheme," *Optoelectronics Letters*, vol. 11, no. 1, pp. 65–68, 2015.

[212] Y. Sun and Y. Zhan, "Closed-form impulse response model of non-line-of-sight single-scatter propagation," *J. Opt. Soc. Am. A*, vol. 33, no. 4, pp. 752–757, Apr 2016.

[213] X. Sun, S. Li, W. Yan, R. Zhang, and C. Zhang, "Non-line-of-sight optical scattering communication based on atmospheric inhomogeneity," *Optics Communications*, vol. 382, pp. 318 – 323, January 2017.

[214] G. Fletcher, T. Hicks, and B. Laurent, "The silex optical interorbit link experiment," *J. Electron. & Commun. Eng.*, 1991.

[215] B. L. T. T. Nielsen, G. Oppenhaeuser and G. Planche, "In-orbit test results of the optical intersatellite link, silex. a milestone in satellite communication,," *53rd International Astronautical Congress*, 2002.

[216] S. A. Townes, "The mars laser communication demonstration," *Proc. Aerosp. Conf.*, 2004.

[217] "Dlr communicates with terrasar-x earth observation satellite via laser beam," November 2008. [Online]. Available: http://www.dlr.de/en/desktopdefault.aspx/tabid-78/7420_read-14120/

[218] F. Hanson and S. Radic, "High bandwidth underwater optical communication," *Appl. Opt.*, vol. 47, no. 2, pp. 277–283, 2008.

[219] B. Cochenour, L. Mullen, and A. Laux, "Spatial and temporal dispersion in high bandwidth underwater laser communication links," *MILCOM 2008 - 2008 IEEE Military Communications Conference*, pp. 1–7, Nov 2008.

[220] M. Doniec, I. Vasilescu, M. Chitre, C. Detweiler, M. Hoffmann-Kuhnt, and D. Rus, "Aquaoptical: A lightweight device for high-rate long-range underwater point-to-point communication," in *Marine Technology for Our Future: Global and Local Challenges*, 2009, pp. 1–6.

[221] M. Doniec, C. Detweiler, I. Vasilescu, and D. Rus, "Using optical communication for remote underwater robot operation," *Intelligent Robots and Systems (IROS), 2010 IEEE/RSJ International Conference on*, pp. 4017–4022, Oct 2010.

[222] J. Simpson, W. Cox, J. Krier, B. Cochenour, B. Hughes, and J. Muth, "5 mbps optical wireless communication with error correction coding for underwater sensor nodes," *OCEANS 2010*, pp. 1–4, Sept 2010.

[223] B. Tian, F. Zhang, and X. Tan, "Design and development of an LED-based optical communication system for autonomous underwater robots," *2013 IEEE/ASME International Conference on Advanced Intelligent Mechatronics*, pp. 1558–1563, July 2013.

[224] G. Cossu, R. Corsini, A. Khalid, S. Balestrino, A. Coppelli, A. Caiti, and E. Ciaramella, "Experimental demonstration of high speed underwater visible light communications," *Intl. Workshop on Optical Wireless Communications (IWOW)*, pp. 11–15, Oct 2013.

[225] K. Nakamura, I. Mizukoshi, and M. Hanawa, "Optical wireless transmission of 405 nm, 1.45 gbit/s optical im/dd-ofdm signals through a 4.8 m underwater channel," *Opt. Express*, vol. 23, no. 2, pp. 1558–1566, Jan 2015.

[226] H. M. Oubei, C. Li, K.-H. Park, T. K. Ng, M.-S. Alouini, and B. S. Ooi, "2.3 Gbit/s underwater wireless optical communications using directly modulated 520 nm laser diode," *Opt. Express*, vol. 23, no. 16, pp. 20 743–20 748, Aug 2015.

[227] H. M. Oubei, J. R. Duran, B. Janjua, H.-Y. Wang, C.-T. Tsai, Y.-C. Chi, T. K. Ng, H.-C. Kuo, J.-H. He, M.-S. Alouini, G.-R. Lin, and B. S. Ooi, "4.8 Gbit/s 16-QAM-OFDM transmission based on compact 450-nm laser for underwater wireless optical communication," *Opt. Express*, vol. 23, no. 18, pp. 23 302–23 309, Sep 2015.

[228] A. Lin, W. Lu, J. Xu, H. Song, F. Qu, J. Han, X. Gu, and J. Leng, "Underwater wireless optical communication using a directly modulated semiconductor laser," *OCEANS 2015*, pp. 1–4, May 2015.

[229] Y. Ren, L. Li, Z. Zhao, G. Xie, Z. Wang, N. Ahmed, Y. Yan, A. Willner, Y. Cao, C. Liu, N. Ashrafi, S. Ashrafi, M. Tur, and A. Willner, "4 Gbit/s underwater transmission using OAM multiplexing and directly modulated green laser," in *Conference on Lasers and Electro-Optics*. Optical Society of America, 2016, p. SW1F.4.

[230] J. Xu, Y. Song, X. Yu, A. Lin, M. Kong, J. Han, and N. Deng, "Underwater wireless transmission of high-speed QAM-OFDM signals using a compact red-light laser," *Opt. Express*, vol. 24, no. 8, pp. 8097–8109, Apr 2016.

[231] J. Baghdady, K. Miller, K. Morgan, M. Byrd, S. Osler, R. Ragusa, W. Li, B. M. Cochenour, and E. G. Johnson, "Multi-gigabit/s underwater optical communication link using orbital angular momentum multiplexing," *Opt. Express*, vol. 24, no. 9, pp. 9794–9805, May 2016.

[232] A. Al-Halafi, H. M. Oubei, B. S. Ooi, and B. Shihada, "Real-time video transmission over different underwater wireless optical channels using a directly modulated 520 nm laser diode," *IEEE/OSA Journal of Optical Communications and Networking*, vol. 9, no. 10, pp. 826–832, Oct 2017.

[233] J. B. Snow, J. P. Flatley, D. E. Freeman, M. A. Landry, C. E. Lindstrom, J. R. Longacre, and J. A. Schwartz, "Underwater propagation of high-data-rate laser communications pulses," *Proc. SPIE*, vol. 1750, pp. 419–427, 1992.

[234] J. Bales and C. Chryssostomidis, "High-bandwidth, low-power, short-range optical communication underwater," *Intl. Symp. on Unmanned Untethered Submersible Technol.*, 1995.

[235] N. Fair, A. Chave, L. Freitag, J. Preisig, S. White, D. Yoerger, and F. Sonnichsen, "Optical modem technology for seafloor observatories," *OCEANS 2006*, pp. 1–6, Sept 2006.

[236] C. Gabriel, A. Khalighi, S. Bourennane, P. Léon, and V. Rigaud, "Optical Communication System for an Underwater Wireless Sensor Network," *EGU General Assembly Conference Abstracts*, vol. 14, p. 2685, Apr. 2012.

[237] C. Shen, Y. Guo, H. M. Oubei, T. K. Ng, G. Liu, K.-H. Park, K.-T. Ho, M.-S. Alouini, and B. S. Ooi, "20-meter underwater wireless optical communication link with 1.5 Gbps data rate," *Opt. Express*, vol. 24, no. 22, pp. 25 502–25 509, Oct 2016.

[238] M. Kong, W. Lv, T. Ali, R. Sarwar, C. Yu, Y. Qiu, F. Qu, Z. Xu, J. Han, and J. Xu, "10-m 9.51-Gb/s RGB laser diodes-based WDM underwater wireless optical communication," *Opt. Express*, vol. 25, no. 17, pp. 20 829–20 834, Aug 2017.

[239] L. Mullen, B. Cochenour, W. Rabinovich, R. Mahon, and J. Muth, "Backscatter suppression for underwater modulating retroreflector links using polarization discrimination," *Appl. Opt.*, vol. 48, no. 2, pp. 328–337, 2009.

[240] B. Cochenour, L. Mullen, W. Rabinovich, and R. Mahon, "Underwater optical communications with a modulating retro-reflector," *Proc. SPIE*, vol. 7317, pp. 73 170G–73 170G–10, 2009.

[241] W. C. Cox, K. F. Gray, J. A. Simpson, B. Cochenour, B. L. Hughes, and J. F. Muth, "A MEMS blue/green retroreflecting modulator for underwater optical communications," *OCEANS 2010 MTS/IEEE SEATTLE*, pp. 1–4, Sept 2010.

[242] W. S. Rabinovich, R. Mahon, M. Ferraro, J. Murphy, L. Mullen, B. Cohenour, J. Muth, and L. Ziph-Schatzberg, "Underwater optical modulating retro-reflector links," in *Lasers, Sources and Related Photonic Devices*. Optical Society of America, 2010, p. LSTuB1.

[243] B. Cochenour and L. Mullen, "Channel response measurements for diffuse non-line-of-sight (nlos) optical communication links underwater," *OCEANS*, pp. 1–5, 2011.

[244] C. Pontbriand, N. Farr, J. Ware, J. Preisig, and H. Popenoe, "Diffuse high-bandwidth optical communications," *OCEANS 2008*, pp. 1–4, Sept 2008.

[245] D. Alley, L. Mullen, and A. Laux, "Compact, dual-wavelength, non-line-of-sight (NLOS) underwater imager," *OCEANS'11 MTS/IEEE KONA*, pp. 1–5, Sept 2011.

[246] J. Simpson, B. Hughes, and J. Muth, "Smart transmitters and receivers for underwater free-space optical communication," *Selected Areas in Communications, IEEE Journal on*, vol. 30, no. 5, pp. 964–974, 2012.

[247] B. Cochenour, L. Mullen, and J. Muth, "A modulated pulse laser for underwater detection, ranging, imaging, and communications," *Proc. SPIE*, vol. 8372, pp. 83 720S–83 720S–10, 2012.

[248] S. Arnon and D. Kedar, "Non-line-of-sight underwater optical wireless communication network," *J. Opt. Soc. Am. A*, vol. 26, no. 3, pp. 530–539, 2009. [Online]. Available: http://josaa.osa.org/abstract.cfm?URI=josaa-26-3-530

[249] S. S. D. Neo, "Free sp ace optics communication for mobile military platforms," Masters Thesis, Naval Postgraduate School, December 2003.

[250] M. Toyoshima, "Trends in satellite communications and the role of optical free-space communications [invited]," *J. Opt. Netw.*, vol. 4, no. 6, pp. 300–311, Jun 2005. [Online]. Available: http://jon.osa.org/abstract.cfm?URI=jon-4-6-300

[251] H. Hemmati, *Near-Earth Laser Communications*, ser. Optical Science and Engineering. Taylor & Francis, 2009.

[252] "Gogo inflight internet," 2015. [Online]. Available: https://www.gogoair.com/gogo/cms/work.do

[253] "Lufthansa flynet: limitless communication on long-haul flights," 2015. [Online]. Available: http://www.lufthansa.com/us/en/Fly-Net

[254] J. Maynard and M. Ross, "Airborne flight test system (afts)," October 1981. [Online]. Available: http://adsabs.harvard.edu/abs/1981mcdd.rept.....M

[255] "Global security organization: Relay mirror experiment (rme)." [Online]. Available: http://www.globalsecurity.org/space/systems/rme.htm

[256] N. Kadowaki, M. Tanaka, K. Araki, and Y. Suzuki, "Advanced satellite communications experiments using ets-vi," *Technol. Enabling Tomorrow : Comput., Commun. and Autom. towards the 21st Century*, pp. 695–699, 1992.

[257] K. Wilson and J. Lesh, "An overview of the galileo optical experiment (gopex)," JPL, Jet Propulsion Lab., California Institute of Technology, Pasadena, Telecommunications and Data Acquisition Report, 1993.

[258] H. Hemmati and A. Biswas, *Deep-Space Optical Communications: Future Perspectives and Applications*, 1st ed., H. Hemmati, Ed. Wiley, 2006.

[259] "Nasa beams mona lisa to lunar reconnaissance orbiter at the moon," January 2013. [Online]. Available: http://www.nasa.gov/mission_pages/LRO/news/mona-lisa.html#.VUXc-vlVhBc

[260] "The lunar laser communication demonstration (llcd)," October 2014. [Online]. Available: http://esc.gsfc.nasa.gov/267/271/335.html

[261] B. Oaida, M. Abrahamson, R. Witoff, J. Martinez, and D. Zayas, "Opals: An optical communications technology demonstration from the international space station," *Aerospace Conference, 2013 IEEE*, pp. 1–20, March 2013.

[262] M. J. Abrahamson, O. V. Sindiy, B. V. Oaida, S. Fregoso, J. N. Bowles-Martinez, M. Kokorowski, M. W. Wilkerson, and A. L. Konyha, "Opals: Mission system operations architecture for an optical communications demonstration on the iss," *SpaceOps Conferences*, 2014.

[263] H. Willebrand and B. Ghuman, "Fiber optics without fiber," *IEEE Spectr.*, vol. 38, no. 8, pp. 40–45, 2001.

[264] A. S. Hamza, J. S. Deogun, and D. R. Alexander, "New class of rearrangeable nonblocking multicast free-space optical switches," *J. Opt. Commun. Netw.*, vol. 8, no. 8, pp. 569–581, Aug 2016.

[265] P. Nicholls, S. D. Greaves, and R. T. Unwin, "Optical wireless telepoint," *IEE Colloq. Opt. Free Space Commun. Links*, 1996.

[266] G. Wang, D. G. Andersen, M. Kaminsky, K. Papagiannaki, T. E. Ng, M. Kozuch, and M. Ryan, "c-through: part-time optics in data centers," *Proc. of the ACM SIGCOMM*, pp. 327–338, 2010.

[267] D. Karunatilaka, F. Zafar, V. Kalavally, and R. Parthiban, "Led based indoor visible light communications: State of the art," *Communications Surveys Tutorials, IEEE*, vol. PP, no. 99, pp. 1–1, 2015.

[268] F. Zafar, M. Bakaul, and R. Parthiban, "Laser-diode-based visible light communication: Toward gigabit class communication," *IEEE Communications Magazine*, vol. 55, no. 2, pp. 144–151, February 2017.

[269] N. Saha, M. S. Ifthekhar, N. T. Le, and Y. M. Jang, "Survey on optical camera communications: challenges and opportunities," *IET Optoelectronics*, vol. 9, no. 5, pp. 172–183, 2015.

[270] N. T. Le, M. Hossain, and Y. M. Jang, "A survey of design and implementation for optical camera communication," *Signal Processing: Image Communication*, vol. 53, pp. 95 – 109, 2017.

[271] T. Nguyen, A. Islam, T. Hossan, and Y. M. Jang, "Current status and performance analysis of optical camera communication technologies for 5G networks," *IEEE Access*, vol. 5, pp. 4574–4594, 2017.

[272] Z. Ghassemlooy, P. Luo, and S. Zvanovec, *Optical Camera Communications*. Cham: Springer International Publishing, 2016, ch. 25, pp. 547–568.

[273] D. Takase and T. Ohtsuki, "Optical wireless MIMO (OMIMO) with backward spatial filter (BSF) in diffuse channels," *Intl. Conf. on Communications (ICC)*, pp. 2462–2467, 2007.

[274] Y. Xing, M. Zhang, D. Han, and Z. Ghassemlooy, "Experimental study of a 2×2 MIMO scheme for ultraviolet communications," *Intl. Conf. on Optical Communications and Networks (ICOCN)*, pp. 1–3, 2016.

[275] "Visible light communications association," 2015. [Online]. Available: http://vlca.net/standard/

[276] "Japan Electronics and Information Technology Industries Association (JEITA)." [Online]. Available: http://www.jeita.or.jp/english/

[277] R. Valadas, A. Tavares, A. Duarte, A. Moreira, and C. Lomba, "The infrared physical layer of the IEEE 802.11 standard for wireless local area networks," *IEEE Comm. Mag.*, vol. 36, no. 12, pp. 107–112, Dec 1998.

[278] S. Rajagopal, R. D. Roberts, and S. K. Lim, "IEEE 802.15.7 visible light communication: modulation schemes and dimming support," *IEEE Communications Magazine*, vol. 50, no. 3, pp. 72–82, March 2012.

[279] V. Jungnickel, M. Uysal, N. Serafimovski, T. Baykas, D. O'Brien, E. Ciaramella, Z. Ghassemlooy, R. Green, H. Haas, P. A. Haigh, V. P. G. Jimenez, F. Miramirkhani, M. Wolf, and S. Zvanovec, "A European view on the next generation optical wireless communication standard," *IEEE Conference on Standards for Communications and Networking (CSCN)*, pp. 106–111, 2015.

[280] M. Uysal, F. Miramirkhani, O. Narmanlioglu, T. Baykas, and E. Panayirci, "IEEE 802.15.7r1 reference channel models for visible light communications," *IEEE Communications Magazine*, vol. 55, no. 1, pp. 212–217, January 2017.

[281] J. Horwath, M. Knapek, B. Epple, M. Brechtelsbauer, and B. Wilkerson, "Broadband backhaul communication for stratospheric platforms: the stratospheric optical payload experiment (stropex)," *SPIE Optics+ Photonics*, pp. 63 041N–63 041N, 2006.

[282] L. Li, R. Zhang, Z. Zhao, G. Xie, P. Liao, K. Pang, H. Song, C. Liu, Y. Ren, G. Labroille, P. Jian, D. Starodubov, B. Lynn, R. Bock, M. Tur, and A. E. Willner, "High-capacity free-space optical communications between a ground transmitter and a ground receiver via a UAV using multiplexing of multiple orbital-angular-momentum beams," *Nature Scientific Reports*, vol. 7, no. 17427, Dec 2017.

[283] C. A. Wargo and J.-F. D'Arcy, "Performance of data link communications in surface management operations," *IEEE Aerospace Conference*, vol. 0, pp. 1–10, 2011.

[284] C. M. Zingale, B. Willems, and J. M. Ross, "Future en route workstation study (fews iii): Human-in-the-loop simulation of air traffic controller management of advanced aircraft concepts," Federal Aviation Administration (FAA), Tech. Rep. DOT/FAA/TC-08/14, I, 2010.

[285] S. Hah, B. Willems, and K. Schulz, "The evaluation of data communication for the future air traffic control system (nextgen)," *Proceedings of the Human Factors and Ergonomics Society Annual Meeting*, vol. 54, no. 1, pp. 99–103, 2010.

[286] B. Ai, X. Cheng, T. Krner, Z. D. Zhong, K. Guan, R. S. He, L. Xiong, D. W. Matolak, D. G. Michelson, and C. Briso-Rodriguez, "Challenges toward wireless communications for high-speed railway," *IEEE Transactions on Intelligent Transportation Systems*, vol. 15, no. 5, pp. 2143–2158, Oct 2014.

[287] Y. Zhou, Z. Pan, J. Hu, J. Shi, and X. Mo, "Broadband wireless communications on high speed trains," *2011 20th Annual Wireless and Optical Communications Conference (WOCC)*, pp. 1–6, April 2011.

[288] F. Kaltenberger, A. Byiringiro, G. Arvanitakis, R. Ghaddab, D. Nussbaum, R. Knopp, M. Bernineau, Y. Cocheril, H. Philippe, and E. Simon, "Broadband wireless channel measurements for high speed trains," *2015 IEEE International Conference on Communications (ICC)*, pp. 2620–2625, June 2015.

[289] I. Akyildiz, W. Su, Y. Sankarasubramaniam, and E. Cayirci, "Wireless sensor networks: a survey," *Comput. Netw.*, vol. 38, no. 4, pp. 393 – 422, 2002.

[290] G. A. Shaw, M. L. Nischan, M. A. Iyengar, S. Kaushik, and M. K. Griffin, "NLOS uv communication for distributed sensor systems," *Proc. SPIE*, vol. 4126, pp. 83–96, 2000.

[291] R. M. Lerner and A. E. Holland, "The optical scatter channel," *Proceedings of the IEEE*, vol. 58, no. 10, pp. 1547–1563, Oct 1970.

[292] R. S. Kennedy, "Communication through optical scattering channels: An introduction," *Proceedings of the IEEE*, vol. 58, no. 10, pp. 1651–1665, Oct 1970.

[293] D. M. Reilly, "Atmospheric optical communications in the middle ultraviolet," Master's thesis, Massachusetts Institute of Technology, 1976. [Online]. Available: http://dspace.mit.edu/handle/1721.1/27480

[294] Y. Zuo, H. Xiao, J. Wu, Y. Li, and J. Lin, "A single-scatter path loss model for non-line-of-sight ultraviolet channels," *Opt. Express*, vol. 20, no. 9, pp. 10 359–10 369, Apr 2012.

[295] R. J. Drost and B. M. Sadler, "Survey of ultraviolet non-line-of-sight communications," *Semiconductor Science and Technology*, vol. 29, no. 8, p. 084006, 2014.

[296] R. Yuan and J. Ma, "Review of ultraviolet non-line-of-sight communication," *China Communications*, vol. 13, no. 6, pp. 63–75, June 2016.

[297] S. Mori and F. S. Marzano, *Ultraviolet Scattering Communication Channels*. Cham: Springer International Publishing, 2016, ch. 8, pp. 145–170.

[298] A. Majumdar and J. Ricklin, *Free-Space Laser Communications: Principles and Advances*, ser. Optical and Fiber Communications Reports. Springer, 2010.

[299] *Fixed service applications using free-space optical links*, International Telecommunication Union Std. F.2106-1 (2010).

[300] Laser Diode Source, "Laser diode source," August 2018. [Online]. Available: https://www.laserdiodesource.com/laser-diode-wavelength/quantum-laser-ir-laser/2000nm-2760nm

[301] F. Capasso, R. Paiella, R. Martini, R. Colombelli, C. Gmachl, T. L. Myers, M. S. Taubman, R. M. Williams, C. G. Bethea, K. Unterrainer, H. Y. Hwang, D. L. Sivco, A. Y. Cho, A. M. Sergent, H. C. Liu, and E. A. Whittaker, "Quantum cascade lasers: ultrahigh-speed operation, optical wireless communication, narrow linewidth, and far-infrared emission," *IEEE Journal of Quantum Electronics*, vol. 38, no. 6, pp. 511–532, Jun 2002.

[302] L. Chuanwei, Z. Shenqiang, Z. Jinchuan, Z. Yuhong, J. Zhiwei, L. Fengqi, and W. Zhanguo, "Free-space communication based on quantum cascade laser," *Journal of Semiconductors*, vol. 36, no. 9, p. 094009, 2015.

[303] Laser Diode Source, "Laser diode source," August 2018. [Online]. Available: https://www.laserdiodesource.com/laser-diode-wavelength/quantum-cascade-laser-ir-laser/2800nm-15000nm

[304] J. Mikolajczyk, "An overview of free space optics with quantum cascade lasers," *International Journal of Electronics and Telecommunications*, vol. 60, no. 3, pp. 259–264, October 2014.

[305] E. Luzhansky, F.-S. Choa, S. Merritt, A. Yu, and M. Krainak, "Mid-IR free-space optical communication with quantum cascade lasers," *Proc. SPIE*, vol. 9465, pp. 9465 – 9465 – 7, 2015.

[306] "P.1814 : Prediction methods required for the design of terrestrial free-space optical links," August 2007. [Online]. Available: https://www.itu.int/rec/R-REC-P.1814-0-200708-I/en

[307] "P.1817 : Propagation data required for the design of terrestrial free-space optical links," February 2012. [Online]. Available: https://www.itu.int/rec/R-REC-P.1817/en

[308] D. Zou, S. B. Li, and Z. Xu, "Improving the NLOS optical scattering channel via beam reshaping," *2014 48th Asilomar Conference on Signals, Systems and Computers*, pp. 1372–1375, Nov 2014.

[309] "LOWTRAN manual," 2017. [Online]. Available: https://www.ontar.com/Software/ProductDetails.aspx?item=pub_LowTranManual

[310] R. Martini and E. A. Whittaker, *Quantum cascade laser-based free space optical communications*. New York, NY: Springer New York, 2008, ch. 9, pp. 393–406. [Online]. Available: https://doi.org/10.1007/978-0-387-28677-8_9

[311] D. P. Hutchinson and R. K. Richards, *All-weather long-wavelength infrared free space optical communications*. New York, NY: Springer New York, 2008, ch. 10, pp. 407–417. [Online]. Available: https://doi.org/10.1007/978-0-387-28677-8_10

[312] K. Wilson and M. Enoch, "Optical communications for deep space missions," *Communications Magazine, IEEE*, vol. 38, no. 8, pp. 134–139, Aug 2000.

[313] K. Shantha Lakshmi, M. Senthil Kumar, and K. Kavitha, "Inter-satellite laser communication system," *Computer and Communication Engineering*, pp. 522–527, May 2008.

[314] A. Ranjan and A. Ranjan, "Underwater wireless communication network," *Advance in Electron. and Electric Eng.*, vol. 3, no. 1, pp. 41–46, 2013.

[315] B. Li, S. Zhou, M. Stojanovic, L. Freitag, and P. Willett, "Multicarrier communication over underwater acoustic channels with nonuniform doppler shifts," *IEEE Journal of Oceanic Engineering*, vol. 33, no. 2, pp. 198–209, April 2008.

[316] M. Stojanovic, "OFDM for underwater acoustic communications: Adaptive synchronization and sparse channel estimation," *IEEE International Conference on Acoustics, Speech and Signal Processing*, pp. 5288–5291, March 2008.

[317] V. P. Fedosov, A. V. Lomakina, A. A. Legin, and V. V. Voronin, "Modeling of systems wireless data transmission based on antenna arrays in underwater acoustic channels," *Proc. SPIE*, vol. 9872, pp. 98 720G–98 720G–10, 2016.

[318] A. ElMoslimany, M. Zhou, T. M. Duman, and A. Papandreou-Suppappola, "An underwater acoustic communication scheme exploiting biological sounds," *Wireless Communications and Mobile Computing*, pp. n/a–n/a, 2016.

[319] N. Farr, A. Bowen, J. Ware, C. Pontbriand, and M. Tivey, "An integrated, underwater optical /acoustic communications system," in *OCEANS IEEE*, 2010, pp. 1–6.

[320] I. F. Akyildiz, D. Pompili, and T. Melodia, "Underwater acoustic sensor networks: Research challenges," *AD HOC Netw.*, vol. 3, pp. 257–279, 2005.

[321] D. Anguita, D. Brizzolara, and G. Parodi, "Building an underwater wireless sensor network based on optical: Communication: Research challenges and current results," *Sensor Technologies and Applications*, pp. 476–479, 2009.

[322] S. Q. DUNTLEY, "Light in the sea," *J. Opt. Soc. Am.*, vol. 53, no. 2, pp. 214–233, 1963.

[323] R. C. Smith and K. S. Baker, "Optical properties of the clearest natural waters (200–800 nm)," *Appl. Opt.*, vol. 20, no. 2, pp. 177–184, Jan 1981.

[324] C. Mobley, *Light and water: radiative transfer in natural waters*. Academic Press, 1994.

[325] ——, *Ocean Optics Web Book*, 2011. [Online]. Available: http://www.oceanopticsbook.info/

[326] W. Cox, *Simulation, Modeling, and Design of Underwater Optical Communication Systems*. North Carolina State University, 2012.

[327] J. Giles and I. N. Bankman, "Underwater optical communications systems. part 2: basic design considerations," pp. 1700–1705 Vol. 3, 2005.

[328] M. A. Chancey, "Short range underwater optical communication links." NCSU Libraries, 2005.

[329] N. Fair, A. Chave, L. Freitag, J. Preisig, S. White, D. Yoerger, and F. Sonnichsen, "Optical modem technology for seafloor observatories," in *OCEANS 2006*, 2006, pp. 1–6.

[330] B. Cochenour, L. Mullen, and J. Muth, "Effect of scattering albedo on attenuation and polarization of light underwater," *Opt. Lett.*, vol. 35, no. 12, pp. 2088–2090, 2010.

[331] X. Yi, Z. Li, and Z. Liu, "Underwater optical communication performance for laser beam propagation through weak oceanic turbulence," *Appl. Opt.*, vol. 54, no. 6, pp. 1273–1278, Feb 2015.

[332] F. Schill, U. R. Zimmer, and J. Trumpf, "Visible spectrum optical communication and distance sensing for underwater applications," in *In: Proc. of Australasian Conf. on Robotics and Automation*, 2004.

[333] Y. Jang, "Current status of IEEE 802.15.7r1 OWC standardization," October 2015. [Online]. Available: http://vlca.net/site/wp/wp-content/uploads/2016/01/2015_10_26_YeongMinJangICEVLC2015CC.pdf

[334] D. Aviv, *Laser space communications*, ser. Artech House space technology and applications library. Artech House, 2006.

[335] H. Urabe, S. Haruyama, T. Shogenji, S. Ishikawa, M. Hiruta, F. Teraoka, T. Arita, H. Matsubara, and S. Nakagawa, "High data rate ground-to-train free-space optical communication system," *Optical Engineering*, vol. 51, pp. 51 – 51 – 10, 2012.

[336] W. Fawaz, C. Abou-Rjeily, and C. Assi, "UAV-aided cooperation for FSO communication systems," *IEEE Communications Magazine*, vol. 56, no. 1, pp. 70–75, Jan 2018.

[337] K. Wang, A. Nirmalathas, C. Lim, E. Skafidas, and K. Alameh, "High-speed reconfigurable card-to-card optical interconnects based on hybrid free-space and multi-mode fiber propagations," *Opt. Express*, vol. 21, no. 25, pp. 31 166–31 175, Dec 2013.

[338] Loon, "Loon project," August 2018. [Online]. Available: https://loon.co/technology/

[339] Facebook, "Internet.org," August 2018. [Online]. Available: https://info.internet.org/en/

[340] K. Wang, A. Nirmalathas, C. Lim, and E. Skafidas, "High-speed indoor optical wireless communication system with single channel imaging receiver," *Opt. Express*, vol. 20, no. 8, pp. 8442–8456, Apr 2012. [Online]. Available: http://www.opticsexpress.org/abstract.cfm?URI=oe-20-8-8442

[341] ——, "High-speed duplex optical wireless communication system for indoor personal area networks," *Opt. Express*, vol. 18, no. 24, pp. 25 199–25 216, Nov 2010. [Online]. Available: http://www.opticsexpress.org/abstract.cfm?URI=oe-18-24-25199

[342] ——, "Indoor gigabit optical wireless communication system for personal area networks," in *IEEE Photonics Society, 2010 23rd Annual Meeting of the*, Nov 2010, pp. 224–225.

[343] ——, "Gigabit optical wireless communication system for indoor applications," in *Communications and Photonics Conference and Exhibition (ACP), 2010 Asia*, Dec 2010, pp. 453–454.

[344] B. Makki, T. Svensson, M. Brandt-Pearce, and M. S. Alouini, "On the performance of millimeter wave-based RF-FSO multi-hop and mesh networks," *IEEE Transactions on Wireless Communications*, vol. 16, no. 12, pp. 7746–7759, Dec 2017.

[345] M. Usman, H. C. Yang, and M. S. Alouini, "Practical switching-based hybrid FSO/RF transmission and its performance analysis," *IEEE Photonics Journal*, vol. 6, no. 5, pp. 1–13, 2014.

[346] M. A. Esmail, H. Fathallah, and M. S. Alouini, "Outage probability analysis of FSO links over foggy channel," *IEEE Photonics Journal*, vol. 9, no. 2, pp. 1–12, April 2017.

[347] M. I. Petkovic, A. M. Cvetkovic, and G. T. Djordjevic, *Mixed RF/FSO Relaying Systems*. Cham: Springer International Publishing, 2016, ch. Mixed RF/FSO Relaying Systems, pp. 387–407.

[348] I. Vasilescu, K. Kotay, D. Rus, M. Dunbabin, and P. Corke, "Data collection, storage, and retrieval with an underwater sensor network," in *Intl. Conf. Embedded Netw. Sensor Syst.*, ser. SenSys '05. New York, NY, USA: ACM, 2005, pp. 154–165.

[349] M. Dunbabin, P. Corke, I. Vasilescu, and D. Rus, "Data muling over underwater wireless sensor networks using an autonomous underwater vehicle," in *Robotics and Automation*, 2006, pp. 2091–2098.

[350] I. Vasilescu, C. Detweiler, and D. Rus, "Aquanodes: An underwater sensor network," in *Proc. of the Second Workshop on Underwater Netw.*, ser. WuWNet '07. New York, NY, USA: ACM, 2007, pp. 85–88.

[351] B. Moision, B. Erkmen, E. Keyes, T. Belt, O. Bowen, D. Brinkley, P. Csonka, M. Eglington, A. Kazmierski, N. hyong Kim, J. Moody, T. Tu, and W. Vermeer, "Demonstration of free-space optical communication for long-range data links between balloons on project loon," *Proc. SPIE*, vol. 10096, pp. 10 096 – 10 096 – 14, 2017.

[352] X Company, "Project loon," August 2018. [Online]. Available: https://x.company/projects/loon/

[353] M. Ayyash, H. Elgala, A. Khreishah, V. Jungnickel, T. Little, S. Shao, M. Rahaim, D. Schulz, J. Hilt, and R. Freund, "Coexistence of WiFi and LiFi toward 5G: concepts, opportunities, and challenges," *IEEE Communications Magazine*, vol. 54, no. 2, pp. 64–71, February 2016.

[354] K. Wu, J. Xiao, and L. Ni, "Rethinking the architecture design of data center networks," *Frontiers of Comput. Sci.*, vol. 6, no. 5, pp. 596–603, 2012.

[355] N. Farrington, "Optics in data center network architecture." UC San Diego, 2012. [Online]. Available: http://escholarship.org/uc/item/8nv683wc

[356] Y. Kiriha and M. Nishihara, "Survey on data center networking technologies," *IEICE Trans. on Commun.*, vol. 96, no. 3, pp. 713–721, 2013.

[357] E. Baccour, S. Foufou, R. Hamila, and M. Hamdi, "A survey of wireless data center networks," *Information Sciences and Systems (CISS), Annual Conference on*, pp. 1–6, March 2015.

[358] A. S. Hamza, J. S. Deogun, and D. Alexander, "Evolution of data centers: A critical analysis of standards and challenges for FSO links," *2015 IEEE Conference on Standards for Communications & Networking (CSCN'15)*, pp. 100–105, Oct. 2015.

[359] ——, "CSOWC: a unified classification framework for standardizing optical wireless communications," *2015 IEEE Conference on Standards for Communications & Networking (CSCN'15)*, pp. 112–117, Oct. 2015.

[360] S. Yi, Y. Pei, S. Kalyanaraman, and B. Azimi-Sadjadi, "How is the capacity of ad hoc networks improved with directional antennas?" *Wireless Networks*, vol. 13, no. 5, pp. 635–648, 2007.

[361] Wireless High-Definition (WirelessHD), "Wirelesshd consortium std." 2014. [Online]. Available: http://www.wirelesshd.org/

[362] W. Roh, J.-Y. Seol, J. Park, B. Lee, J. Lee, Y. Kim, J. Cho, K. Cheun, and F. Aryanfar, "Millimeter-wave beamforming as an enabling technology for 5g cellular communications: theoretical feasibility and prototype results," *Communications Magazine, IEEE*, vol. 52, no. 2, pp. 106–113, February 2014.

[363] F. Xia, T. Mueller, Y. ming Lin, A. Valdes-Garcia, and P. Avouris, "Ultrafast graphene photodetector," *Nature Nanotechnology*, vol. 4, pp. 839 – 843, 2009.

[364] T. Mueller, F. Xia, and P. Avouris, "Graphene photodetectors for high-speed optical communications," *Nature Photonics*, vol. 4, pp. 297–301, 2010.

[365] G. Konstantatos, M. Badioli, L. Gaudreau, J. Osmond, M. Bernechea, F. P. G. de Arquer, F. Gatti, and F. H. L. Koppens, "Hybrid graphenequantum dot phototransistors with ultrahigh gain," *Nature Nanotechnology*, vol. 7, pp. 363–368, 2012.

[366] A. Pospischil, M. Humer, M. M. Furchi, D. Bachmann, R. Guider, T. Fromherz, and T. Mueller, "Cmos-compatible graphene photodetector covering all optical communication bands," *Nature Photonics*, vol. 7, pp. 892–896, 2013.

[367] B. Dum, "On-chip graphene photodetector breaks responsivity record," September 27 2013. [Online]. Available: http://nanotechweb.org/cws/article/tech/54812

[368] X. Gan, R.-J. Shiue, Y. Gao, I. Meric, T. F. Heinz, K. Shepard, J. Hone, S. Assefa, and D. Englund, "Chip-integrated ultrafast graphene photodetector with high responsivity," *NATURE PHOTONICS*, vol. 7, pp. 883–887, 2013.

[369] H. Chen, H. van den Boom, E. Tangdiongga, and T. Koonen, "30-Gb/s bidirectional transparent optical transmission with an MMF access and an indoor optical wireless link," *IEEE Photon. Technol. Lett.*, vol. 24, no. 7, pp. 572–574, April 2012.

[370] P. Smulders, "Exploiting the 60 ghz band for local wireless multimedia access: prospects and future directions," *IEEE Commun. Mag.*, vol. 40, no. 1, pp. 140–147, Jan 2002.

[371] P. Smulders, H. Yang, and I. Akkermans, "On the design of low-cost 60-ghz radios for multigigabit-per-second transmission over short distances [topics in radio communications]," *IEEE Commun. Mag.*, vol. 45, no. 12, pp. 44–51, December 2007.

[372] T. Zwick, T. Beukema, and H. Nam, "Wideband channel sounder with measurements and model for the 60 ghz indoor radio channel," *IEEE Trans. Veh. Technol.*, vol. 54, no. 4, pp. 1266–1277, July 2005.

[373] J. Kaufmann, "Free space optical communications: An overview of applications and technologies," Boston IEEE Commun. Society Meeting, December 2011.

[374] The Fiber Optic Association, "User's guide to fiber optic system design and installation," 2015. [Online]. Available: http://www.thefoa.org/user/

[375] A. Greenberg, J. R. Hamilton, N. Jain, S. Kandula, C. Kim, P. Lahiri, D. A. Maltz, P. Patel, and S. Sengupta, "Vl2: A scalable and flexible data center network," *ACM SIGCOMM*, vol. 39, no. 4, pp. 51–62, Aug. 2009.

[376] K. Chen, C. Hu, X. Zhang, K. Zheng, Y. Chen, and A. Vasilakos, "Survey on routing in data centers: insights and future directions," *Network, IEEE*, vol. 25, no. 4, pp. 6–10, July 2011.

[377] C. Kachris and I. Tomkos, "A survey on optical interconnects for data centers," *Communications Surveys Tutorials, IEEE*, vol. 14, no. 4, pp. 1021–1036, Fourth 2012.

[378] K. Barker and *et al.*, "On the feasibility of optical circuit switching for high performance computing systems," *Proceedings of the ACM/IEEE Supercomputing Conference*, p. 16, Nov. 2005.

[379] N. Farrington and *et al.*, "Helios: a hybrid electrical/optical switch architecture for modular data centers," *Proceedings of the ACM SIGCOMM*, pp. 339–350, 2010.

[380] M. Glick, "Optical switching and routing for the data center," *IEEE Photonics Society Winter Topicals Meeting Series (WTM)*, pp. 109–110, Jan. 2010.

[381] A. Curtis, W. Kim, and P. Yalagandula, "Mahout: Low-overhead datacenter traffic management using end-host-based elephant detection," *Proceedings of IEEE INFOCOM*, pp. 1629–1637, April 2011.

[382] A. Vahdat, H. Liu, X. Zhao, and C. Johnson, "The emerging optical data center," *Optical Fiber Communication Conference/National Fiber Optic Engineers Conference 2011*, p. OTuH2, 2011.

[383] A. Singla, A. Singh, K. Ramachandran, L. Xu, and Y. Zhang, "Proteus: a topology malleable data center network," *ACM HotNets*, pp. 8:1–8:6, 2010.

[384] S. Saha, J. Deogun, and L. Xu, "Hyscale: A hybrid optical network based scalable, switch-centric architecture for data centers," *IEEE ICC*, pp. 2967–2971, 2012.

[385] A. Singla and *et al.*, "Feasibility study on topology malleable data center networks (dcn) using optical switching technologies," *Proceedings of OFC/NFOEC*, pp. 1–3, 2011.

[386] C. Qiao, M. Gonzalez-Ortega, A. Suarez-Gonzalez, X. Liu, and J.-C. Lopez-Ardao, "On the benefit of fast switching in optical networks," *Proceedings of OFC/NFOEC*, pp. 1–3, March 2010.

[387] L. Xu, S. Zhang, F. Yaman, T. Wang, G. Liao, K. Chen, A. Singla, A. Singh, K. Ramachandran, and Y. Zhang, "All-optical switching data center network supporting 100gbps upgrade and mixed-line-rate interoperability," *Proc. of OFC/NFOEC*, pp. 1–3, Mar. 2011.

[388] S. Di Lucente, N. Calabretta, J. Resing, and H. Dorren, "Scaling low-latency optical packet switches to a thousand ports," *IEEE/OSA J. of Optical Commun. and Networking*, vol. 4, no. 9, pp. A17–A28, Sept. 2012.

[389] C. Xin, C. Qiao, Y. Ye, and S. Dixit, "A hybrid optical switching approach," *IEEE GLOBECOM*, vol. 7, pp. 3808–3812, Dec. 2003.

[390] C. Chou, F. Safaei, P. Boustead, and I. Ouveysi, "A hybrid optical network architecture consisting of optical cross connects and optical burst switches," *Proceedings of IEEE ICCCN*, pp. 53–58, Oct. 2003.

[391] V. Vokkarane and Q. Zhang, "Reliable optical burst switching for next-generation grid networks," *Intl. Conf. on Broadband Networks (BroadNets)*, pp. 1428–1437, Oct. 2005.

[392] C. Gauger and *et al.*, "Hybrid optical network architectures: bringing packets and circuits together," *IEEE Communications Magazine*, vol. 44, no. 8, pp. 36–42, Aug. 2006.

[393] Y. Wang, S. Wang, S. Xu, and X. Wu, "A new hybrid optical network design consisting of lightpath and burst switching," *Intl. Conf. on Advanced Communication Technology (ICACT)*, vol. 03, pp. 1873–1876, Feb. 2009.

[394] J. Buysse, M. De Leenheer, C. Develder, B. Dhoedt, and P. Demeester, "Cost-effective burst-over-circuit-switching in a hybrid optical network," *Intl. Conf. on Networking and Services (ICNS)*, pp. 499–504, April 2009.

[395] S. Saha, J. Deogun, and L. Xu, "HyScaleII: A high performance hybrid optical network architecture for data centers," *IEEE Sarnoff Symposium*, pp. 1–5, 2012.

[396] X. Ye, Y. Yin, D. Ding, S. Johnson, V. Akella, and S. Yoo, "Assessment of optical switching in data center networks," *in Proc. of OFC/NFOEC*, pp. 1–3, March 2010.

[397] H. Wang, A. Garg, K. Bergman, and M. Glick, "Design and demonstration of an all-optical hybrid packet and circuit switched network platform for next generation data centers," *Optical Fiber Communication (OFC)*, pp. 1–3, March 2010.

[398] H. Wang and K. Bergman, "A bidirectional 2×2 photonic network building-block for high-performance data centers," *Optical Fiber Communication Conference/National Fiber Optic Engineers Conference 2011*, p. OTuH4, 2011.

[399] J. Perelló, S. Spadaro, S. Ricciardi, D. Careglio, S. Peng, R. Nejabati, G. Zervas, D. Simeonidou, A. Predieri, M. Biancani, H. Dorren, S. Lucente, J. Luo, N. Calabretta, G. Bernini, N. Ciulli, J. Sancho, S. Iordache, M. Farreras, Y. Becerra, C. Liou, I. Hussain, Y. Yin, L. Liu, and R. Proietti, "All-optical packet/circuit switching-based data center network for enhanced scalability, latency, and throughput," *Network, IEEE*, vol. 27, no. 6, pp. 14–22, November 2013.

[400] R. Takahashi, S. Ibrahim, T. Segawa, T. Nakahara, H. Ishikawa, Y. Suzaki, Y.-C. Huang, K. ichi Kitayama, and A. Hiramatsu, "A torus datacenter network based on ops/ocs/vocs enabled by smart flow management," *Optical Fiber Communication Conference*, p. W3D.4, 2015.

[401] Y. Cui, H. Wang, and X. Cheng, "Channel allocation in wireless data center networks," *INFOCOM, 2011 Proceedings IEEE*, pp. 1395–1403, April 2011.

[402] Y. Cui, H. Wang, X. Cheng, D. Li, and A. Yla-Jaaski, "Dynamic scheduling for wireless data center networks," *Parallel and Distributed Systems, IEEE Transactions on*, vol. 24, no. 12, pp. 2365–2374, Dec 2013.

[403] Y. Katayama, K. Takano, Y. Kohda, N. Ohba, and D. Nakano, "Wireless data center networking with steered-beam mmwave links," *Wireless Communications and Networking Conference (WCNC), IEEE*, pp. 2179–2184, March 2011.

[404] H. Vardhan and U. of Texas at Dallas. Graduate Program in Computer Science, *Polycell: A Wireless Data Center Design with Millimeter-wave Network*, 2014.

[405] Y. Zhu, X. Zhou, Z. Zhang, L. Zhou, A. Vahdat, B. Y. Zhao, and H. Zheng, "Cutting the cord: A robust wireless facilities network for data centers," *Proc. of the 20th Annual International Conference on Mobile Computing and Networking*, pp. 581–592, 2014.

[406] M. Zaaimia, R. Touhami, V. Fono, L. Talbi, and M. Nedil, "60 ghz wireless data center channel measurements: Initial results," *Ultra-WideBand (ICUWB), IEEE International Conference on*, pp. 57–61, Sept 2014.

[407] Y. Cui, H. Wang, and X. Cheng, "Wireless link scheduling for data center networks," pp. 44:1–44:9, 2011.

[408] M. Camelo, D. Papadimitriou, L. Fbrega, and P. Vil, "Efficient routing in data center with underlying cayley graph," *Complex Networks V*, vol. 549, pp. 189–197, 2014.

[409] M. Camelo, P. Vila, L. Fabrega, and D. Papadimitriou, "Cayley-graph-based data centers and space requirements of a routing scheme using automata," *Distributed Computing Systems Workshops (ICDCSW), Intl. Conf. on*, pp. 63–69, June 2014.

[410] T. Aktas, C.-H. Wang, and T. Javidi, "WiCOD: Wireless control plane serving an all-optical data center," pp. 299–306, May 2015.

[411] Y.-J. Yu, C.-C. Chuang, H.-P. Lin, and A.-C. Pang, "Efficient multicast delivery for wireless data center networks," pp. 228–235, Oct 2013.

[412] K. Kant, "Data center evolution: A tutorial on state of the art, issues, and challenges," *Comput. Netw.*, vol. 53, no. 17, pp. 2939–2965, 2009.

[413] I. Djordjevic, "Spatial-domain-based energy-efficient optical communications and networks," *IEEE Photon. Conf.*, pp. 363–364, 2011.

[414] V. W. S. Chan, "Free space optical wireless network," *Transparent Opt. Netw.*, pp. 1–6, 2011.

[415] H. Kuo and R. Walmsley, "Free space optical interconnect," US Patent App. 12/864,231, Nov. 25 2010.

[416] H. Davidson, J. Hamilton, R. Hyde, A. Josefsberg, E. Jung, J. Kare, R. Lord, K. Lustig, W. Mangione-Smith, M. Manos *et al.*, "Data center with free-space optical communications," US Patent 8,483,569, Jul. 9 2013.

[417] P. Marraccini and N. Riza, "Power smart in-door optical wireless link design," *J. of the European Optical Society - Rapid publications*, vol. 6, no. 0, 2011.

[418] H. S. Hamza, "On the design of multi-wavelength copy interconnects with reduced complexity," *Photon. Netw. Comm.*, vol. 19, no. 3, pp. 240–256, 2010.

[419] ——, "Convert-and-deliver: a scalable multicast optical cross-connect with reduced power splitting fan-out," *The J. of Supercomputing*, vol. 62, no. 3, pp. 1189–1212, 2012.

[420] J. Turner, "Effects of data center vibration on compute system performance," *USENIX conf. on Sustainable Information Technology*, 2010.

[421] E. Kresch and X. Wang, "An area-efficient hexagonal interconnection network for multi-core processors," *Intl. Conf. on High Performance Computing Simulation (HPCS)*, pp. 39–46, July 2014.

[422] I. Stojmenovic, "Honeycomb networks: Topological properties and communication algorithms," *IEEE Transactions on Parallel and Distributed Systems*, vol. 8, no. 10, pp. 1036–1042, Oct 1997.

[423] K. H. Heng, W.-D. Zhong, and T. H. Cheng, "Multipoint free-space optics system for short-range communications between flight platforms," *Appl. Opt.*, vol. 49, no. 2, pp. 258–266, Jan 2010.

[424] Y. Cui, S. Xiao, C. Liao, I. Stojmenovic, and M. Li, "Data centers as software defined networks: Traffic redundancy elimination with wireless cards at routers," *IEEE J. Sel. Areas Commun.*, vol. 31, no. 12, pp. 2658–2672, 2013.

[425] H. Du, W. Hu, H. He, C. Zhang, Y. Dong, W. Sun, W. Guo, Y. Jin, and S. Xiao, "Separated unicast/multicast splitter-and-delivery switch and its use in multicasting-capable optical cross-connect," *IEEE Photon. Technol. Lett.*, vol. 21, no. 6, pp. 368–370, 2009.

[426] S. Chua and B. Li, *Optical Switches: Materials and Design*, ser. Woodhead Publishing Series in Electronic and Optical Materials. Elsevier Science, 2010.

[427] M. Fiorani, M. Casoni, and S. Aleksic, "Performance and power consumption analysis of a hybrid optical core node," *IEEE/OSA J. Opt. Commun. Netw.*, vol. 3, no. 6, pp. 502–513, 2011.

[428] M. Fiorani, S. Aleksic, P. Monti, J. Chen, M. Casoni, and L. Wosinska, "Energy efficiency of an integrated intra-data-center and core network with edge caching," *IEEE/OSA J. Opt. Commun. Netw.*, vol. 6, no. 4, pp. 421–432, 2014.

[429] M. Imran, M. Collier, P. Landais, and K. Katrinis, "HOSA: Hybrid optical switch architecture for data center networks," *ACM Intl. Conf. on Computing Frontiers*, pp. 27:1–27:8, 2015.

[430] M. Imran, P. Landais, M. Collier, and K. Katrinis, "Performance analysis of optical burst switching with fast optical switches for data center networks," *Intl. Conf. on Transparent Optical Networks*, pp. 1–4, 2015.

[431] Y. Xin and G. Rouskas, "Multicast routing under optical layer constraints," *INFOCOM 2004*, vol. 4, pp. 2731–2742, 2004.

[432] L.-Y. Lin, E. Goldstein, and R. Tkach, "On the expandability of free-space micromachined optical cross connects," *J. Lightw. Technol.*, vol. 18, no. 4, pp. 482–489, 2000.

[433] K. Optronics, "Switchable mirrors/switchable glass," 2012. [Online]. Available: http://kentoptronics.com/switchable.html

[434] C. Li, G. Li, V. Li, P. Wai, H. Xie, and X. Yuan, "Using 2x2 switching modules to build large 2-D MEMS optical switches," *IEEE Global Communications Conference*, vol. 5, pp. 2798–2802, Dec 2003.

[435] O. Solgaard, *Photonic Microsystems: Micro and Nanotechnology Applied to Optical Devices and Systems*, ser. MEMS Reference Shelf. Springer, 2009.

[436] G. Shen, T. H. Cheng, S. K. Bose, C. Lu, and T. Y. Chai, "A novel rearrangeable non-blocking architecture for mems optical space switch," *Optical Network Magazine*, vol. 3, no. 6, pp. 70–79, 2002.

[437] V. Li, C. Y. Li, and P. K. A. Wai, "Alternative structures for two-dimensional mems optical switches [invited]," *J. Opt. Netw.*, vol. 3, no. 10, pp. 742–757, Oct 2004.

[438] K. Murata, T. Saida, K. Sano, I. Ogawa, H. Fukuyama, R. Kasahara, Y. Muramoto, H. Nosaka, S. Tsunashima, T. Mizuno, H. Tanobe, K. Hattori, T. Yoshimatsu, H. Kawakami, and E. Yoshida, "100-gbit/s pdm-qpsk coherent receiver with wide dynamic range and excellent common-mode rejection ratio," *Opt. Express*, vol. 19, no. 26, pp. B125–B130, Dec 2011.

[439] R. A. Spanke and V. E. Benes, "N-stage planar optical permutation network," *Appl. Opt.*, vol. 26, no. 7, pp. 1226–1229, Apr 1987.

[440] R. P. Stanley, *Enumerative Combinatorics: Volume 1*, 2nd ed., ser. Cambridge Studies in Advanced Mathematics. New York, NY, USA: Cambridge University Press, 2011.

[441] A. S. Hamza, J. S. Deogun, and D. R. Alexander, "Free space optical multicast crossbar," *J. Opt. Commun. Netw.*, vol. 8, no. 1, pp. 1–10, Jan 2016.

[442] Z. Tian, K. Wright, and X. Zhou, "Lighting up the internet of things with DarkVLC," pp. 33–38, 2016.

[443] H. E. Ahmed F. Hussein, "Lightweight multi-carrier modulation for IoT," *Proc.SPIE*, vol. 10559, pp. 10 559 – 10 559 – 10, 2018.

[444] M. I. Afzal, W. Mahmood, and A. H. Akbar, "A battery recharge model for WSNs using free-space optics (fso)," *2008 IEEE International Multitopic Conference*, pp. 272–277, Dec 2008.

[445] M. W. S. S. Afzal, M.I. and S. Seoyong, "Optical wireless communication and recharging mechanism of wireless sensor network by using CCRs," *International Journal of Advanced Science and Technology*, vol. 13, no. 1, pp. 49–69, 2009.

[446] M. Safari and M. Uysal, "Relay-assisted free-space optical communication," *Wireless Commun., IEEE Trans. on*, vol. 7, no. 12, pp. 5441–5449, 2008.

[447] G. K. Karagiannidis, T. A. Tsiftsis, and H. G. Sandalidis, "Outage probability of relayed free space optical communication systems," *Electronics Letters*, vol. 42, no. 17, pp. 994–995, August 2006.

[448] M. Karimi and M. Nasiri-Kenari, "Free space optical communications via optical amplify-and-forward relaying," *Journal of Lightwave Technology*, vol. 29, no. 2, pp. 242–248, Jan 2011.

[449] K. P. Peppas, A. N. Stassinakis, H. E. Nistazakis, and G. S. Tombras, "Capacity analysis of dual amplify-and-forward relayed free-space optical communication systems over turbulence channels with pointing errors," *IEEE/OSA Journal of Optical Communications and Networking*, vol. 5, no. 9, pp. 1032–1042, Sept 2013.

[450] R. Boluda-Ruiz, A. García-Zambrana, C. Castillo-Vázquez, B. Castillo-Vázquez, and S. Hranilovic, "Amplify-and-forward strategy using MRC reception over FSO channels with pointing errors," *J. Opt. Commun. Netw.*, vol. 10, no. 5, pp. 545–552, May 2018.

[451] C. Abou-Rjeily and A. Slim, "Cooperative diversity for free-space optical communications: Transceiver design and performance analysis," *IEEE Transactions on Communications*, vol. 59, no. 3, pp. 658–663, March 2011.

[452] M. R. Bhatnagar, "Performance analysis of decode-and-forward relaying in Gamma-Gamma fading channels," *IEEE Photonics Technology Letters*, vol. 24, no. 7, pp. 545–547, April 2012.

[453] M. Karimi and M. Nasiri-Kenari, "Ber analysis of cooperative systems in free-space optical networks," *Journal of Lightwave Technology*, vol. 27, no. 24, pp. 5639–5647, Dec 2009.

[454] S. Kazemlou, S. Hranilovic, and S. Kumar, "All-optical multihop free-space optical communication systems," *Journal of Lightwave Technology*, vol. 29, no. 18, pp. 2663–2669, Sept 2011.

[455] E. Bayaki, D. S. Michalopoulos, and R. Schober, "EDFA-based all-optical relaying in free-space optical systems," *IEEE Transactions on Communications*, vol. 60, no. 12, pp. 3797–3807, December 2012.

[456] M. A. Kashani, M. M. Rad, M. Safari, and M. Uysal, "All-optical amplify-and-forward relaying system for atmospheric channels," *IEEE Communications Letters*, vol. 16, no. 10, pp. 1684–1687, October 2012.

[457] M. T. Dabiri and S. M. S. Sadough, "Performance analysis of all-optical amplify and forward relaying over log-normal FSO channels," *J. Opt. Commun. Netw.*, vol. 10, no. 2, pp. 79–89, Feb 2018.

[458] X. Huang, X. Xie, J. Song, T. Duan, H. Hu, X. Xu, and Y. Su, "Performance comparison of all-optical amplify-and-forward relaying FSO communication systems with OOK and DPSK modulations," *IEEE Photonics Journal*, vol. 10, no. 4, pp. 1–11, Aug 2018.

[459] Y. Wang and H. Haas, "Dynamic load balancing with handover in hybrid Li-Fi and Wi-Fi networks," *J. Lightwave Technol.*, vol. 33, no. 22, pp. 4671–4682, Nov 2015.

[460] C. Chen, S. Videv, D. Tsonev, and H. Haas, "Fractional frequency reuse in DCO-OFDM-based optical attocell networks," *Journal of Lightwave Technology*, vol. 33, no. 19, pp. 3986–4000, Oct 2015.

[461] H. Kazemi and H. Haas, "Downlink cooperation with fractional frequency reuse in dco-ofdma optical attocell networks," *2016 IEEE International Conference on Communications (ICC)*, pp. 1–6, May 2016.

[462] H. Liu, P. Xia, Y. Chen, and L. Wu, "Interference graph-based dynamic frequency reuse in optical attocell networks," *Optics Communications*, vol. 402, pp. 527 – 534, 2017.

[463] P.-L. Chen, S.-T. Chang, S.-T. Ji, S.-C. Lin, H.-H. Lin, H.-L. Tsay, P.-H. Huang, W.-C. Chiang, W.-C. Lin, S.-L. Lee, H.-W. Tsao, J.-P. Wu, and J. Wu, "Demonstration of 16 channels 10 Gb/s WDM free space transmission over 2.16 km," *2008 Digest of the IEEE/LEOS Summer Topical Meetings*, pp. 235–236, July 2008.

[464] Y. Arimoto, M. Presi, V. Guarino, A. D'Errico, G. Contestabile, M. Matsumoto, and E. Ciaramella, "320 Gbit/s (840 gbit/s) double-pass terrestrial free-space optical link transparently connected to optical fibre lines," *2008 34th European Conference on Optical Communication*, pp. 1–2, Sept 2008.

[465] E. Ciaramella, Y. Arimoto, G. Contestabile, M. Presi, A. D'Errico, V. Guarino, and M. Matsumoto, "1.28 terabit/s (32x40 Gbit/s) wdm transmission system for free space optical communications," *IEEE Journal on Selected Areas in Communications*, vol. 27, no. 9, pp. 1639–1645, December 2009.

[466] A. M. Mbah, J. G. Walker, and A. J. Phillips, "Outage probability of WDM free-space optical systems affected by turbulence-accentuated interchannel crosstalk," *IET Optoelectronics*, vol. 11, pp. 91–97(6), June 2017.

[467] J. Lin, L. Xi, J. Li, J. Li, X. Tang, L. Sun, and X. Zhang, "High-quality frequency-locked optical frequency comb source for terabits optical communication system," *Optical Engineering*, vol. 53, pp. 53 – 53 – 10, 2014.

[468] J. Tan, Z. Zhao, Y. Wang, Z. Zhang, J. Liu, and N. Zhu, "12.5 Gb/s multichannel broadcasting transmission for free-space optical communication based on the optical frequency comb module," *Opt. Express*, vol. 26, no. 2, pp. 2099–2106, Jan 2018.

[469] Z. Zhao, Z. Zhang, J. Tan, Y. Liu, and J. Liu, "200 Gb/s FSO WDM communication system empowered by multiwavelength directly modulated TOSA for 5G wireless networks," *IEEE Photonics Journal*, vol. 10, no. 4, pp. 1–8, Aug 2018.